UNIVERSITY OF BIRMINGHAM

UNDERSTANDING THE INTERACTIONS BETWEEN MICROCAPSULES AND FABRIC SURFACES

by

YANPING HE

A thesis submitted to the University of Birmingham
for the degree of
DOCTOR OF PHILOSOPHY

School of Chemical Engineering

The University of Birmingham

July, 2013

Abstract

Perfume-filled microcapsules are intended to be incorporated in household products (e.g. detergents), and then provide a pleasant scent to consumers after laundry processes. To realise this, it is essential for the microcapsules to deposit and then remain on fabric surfaces during and after laundry processes. Therefore, microcapsules and model fabric surfaces were modified respectively with special chemicals in order to enhance the adhesion between them in this work; then the adhesion and retention of microcapsules on model fabric surfaces were investigated and adhesion mechanisms were explained; finally, the relationship between the adhesion and the removal/retention of particles from a model surface was established by a mathematical model.

Microcapsules were modified by polyelectrolytes (PEs) (polyvinyl formamide (PVF) and chitosan). It was found by atomic force microscopy (AFM) that the adhesion between single PE-modified microcapsules and a cellulose thin film were enhanced compared with non-modified microcapsules; however, the PE-modified microcapsules were observed to aggregate. Bridging interactions were considered to be the reason causing the increase in adhesion and the aggregation of microcapsules by the polyelectrolytes. Additionally, big variations in the value of adhesion between different microcapsules were observed, which was attributed to uneven attachment of PE molecules on the surface of microcapsules after modification; the difference in the structure of PE molecules may be the reason causing the difference in their performance.

A flow chamber technique was then introduced to measure the removal/retention of microcapsules on a model fabric surface to characterise adhesion. In order to avoid aggregation of microcapsules, a new protocol to modify model fabric surfaces with polyelectrolytes was developed. A cellulose thin film was modified by PVF, chitosan and poly (ethyleneimine) (PEI) respectively and both the adhesion and retention of microcapsules on the PE-modified cellulose were found to increase by AFM and the flow chamber technique compared with the non-modified cellulose. The order of the performance on enhancing adhesion and retention of the three PEs is PVF $\geq$ Chitosan > PEI. Electrostatic attractions, bridging interactions and hydrogen bonds were considered to be the possible mechanisms to enhance adhesion and the structure of the PE molecules was the main factor to determine their performance on adhesion and retention enhancement.

The flow chamber technique and AFM were extended to investigate the retention and adhesion of microcapsules on a polyester substrate (PET), which were found much higher than those on a cellulose thin film. This was mainly because the PET surface is much more hydrophobic than the cellulose surface. Additionally, adhesion was found to decrease after a PET surface was modified with the three PEs, while the retention of microcapsules on the three PE-modified PET surfaces increased, which seems inconsistent. No difference was observed on adhesion after a PET surface was modified with the three PEs, but the order of retention of microcapsules on the PE-modified PET surface is PVF> chitosan> PEI. The inconsistency was mainly because adhesion determined by AFM is influenced by the surface properties; while the retention of particles on a surface can be influenced by the attached PE molecules on the side wall of microcapsules which extended from the PE-modified PET surface. A model was developed based on the displacement of microcapsules from a substrate in a flow chamber to establish the relationship between the removal/retention of microcapsules

exposed to a fluid flow and their adhesion to the substrate. The model predictions of adhesion and thermodynamic work of adhesion agree well with the results obtained by AFM and the flow chamber experiments for microcapsules interacting with glass and PET surfaces after considering possible microcapsule-substrate contacts in aqueous solution. Moreover, the model predicts that the sum of thermodynamic work of adhesion is the main parameter to determine the removal of particle, which has interpreted the inconsistency of the increase of retention but the observed decrease of adhesion between microcapsules and PET surfaces after modification with PEs.

It is believed that this study has enhanced fundamental understanding of the various interactions between microcapsules and fabric surfaces relevant to industrial applications and has laid a solid foundation to effectively develop new formulations to improve the performance of various consumer products.

Acknowledgements

I would like to sincerely thank my first supervisor Prof Zhibing Zhang for his excellent supervision and continuous support to my PhD study. His knowledge, his rigorous scientific spirit and his patience have influenced me and I have indeed benefited a lot. I also would like to thank my second supervisor Prof. Jon Preece, School of Chemistry at Birmingham, and Prof. Colin Thomas for their guidance, advice and help.

Thanks also go to Dr. James Bowen for his invaluable technical assistance, helpful advice, and insightful comments on my research work and writing of this thesis; I really appreciate his encouragements and support when I encountered difficulties. Also I would like to express my gratitude to James W. Andrews for his help on the modelling work, Dr. Artur Majewski for his assistance on building the flow chamber device and Dr. Marc Walker in Warwick University for his help on XPS analysis. I am very grateful to Dr. Johan Smets and Mrs Pascal Vansteenwinckel from Procter & Gamble for their support to this project.

Financial support from Proctor & Gamble, Belgium, School of Chemical Engineering, University of Birmingham and China Scholarship Council are greatly appreciated. An acknowledgement should also be made to Birmingham Science City: Innovative Uses for Advanced Materials in the Modern World (West Midlands Centre for Advanced Materials Project 2), with support from Advantage West Midlands (AWM) and part funded by the European Regional Development Fund (ERDF) for the using of AFM and Interferometer.

I would also like to thank members in Manipulation Group and staff in the School of Chemical Engineering for their help and friendship.

Last but not least, I would like to express my deepest gratitude towards my parents, my grandmother, my sister and brother for their unconditional support and love. I also would like to appreciate my boyfriend for his love, support and motivation.

Contents

List of Figures

List of Tables

Nomenclature

a_i	The normalised area ratio of microcapsules remaining after removal on i position
$\dot{a}$	The average normalised area ratio
A	Total area occupied by microcapsules, m^2
$A^{'}$	The effective area of the particle perpendicular to the flow direction, m^2
$A_{afterremoval}$	Total area occupied by microcapsules after using a water flow, m^2
$A_{beforeremoval}$	Total area occupied by microcapsules before using a water flow, m^2
A_i	Surface area occupied by a single microcapsule, m^2
A_H	Hamaker constant, J
b	The half lengths of the cross section of the rectangular channel in y direction, m
c	The half lengths of the cross section of the rectangular channel in z direction, m
C_D	The drag coefficient
D	The distance between two surfaces, m
$D^{'}$	The width or the height of the channel, m
$D_{4,3}$	The volume mean diameter, m
E	Young's modulus of each material, Pa
E_B	The binding energy, J
E_k	The energy of the core electron which excited from the atom, J
E_C	Young's modulus of the wall of microcapsule, Pa
E_S	Young's modulus of the substrate, Pa
E^*	The equivalent Young's modulus, Pa
F	The applied load, N
$F_{adhesion}$	The adhesion force, N
F_B	The sum of buoyancy force and gravity force, N
$F_{bouyancy}$	The buoyancy force, N

F_c	The pull-off/adhesion force, N
F_D/F_{drag}	The drag force, N
$F_f/F_{friction}$	The friction force, N
$F_{gravity}$	The gravity force, N
F_{lift}	The lift force, N
F_{SA}	The Saffman lift force, N
g	The gravity, m s^{-2}
h	The vertical distance between the contact point and the surface, m
$h\upsilon$	The incident energy of X-ray photon, J
l	is equal to (h/tan(θ)), m
L	The development length, m
M_D	The moment of the surface stress, Nm
N	The number of microcapsules
N_{DP}	The degree of polymerization
q	The net charge on the particle, C
R	Radius of microparticle, m
$R_{chain\text{-}size}$	The polyelectrolyte chain size
Re_p	The Reynolds number of the flow chamber system
U_f	The velocity of the fluid, m s^{-1}
U_m	The maximum velocity in the velocity profile, m s^{-1}
U_P	The velocity of the particle, m s^{-1}
V	The volume of the particle, m^3
y	The distance from the centre line to the particle, m
z	The location of the particle orthogonal to the direction of flow, m
z_0	The equilibrium separation, m

Greek Symbol

α	The contact radius, m
$\in$	The relative permittivity
$\in_0$	Permittivity of free space, $C^2\ m^{-2}\ N^{-1}$
γ_C	The surface energy of microcapsule per unit area, $J\ m^{-2}$
γ_S	The surface energy of substrate per unit area, $J\ m^{-2}$
γ_{CS}	The interfacial adhesion energy between microcapsule and substrate per unit area, $J\ m^{-2}$
$\Delta\gamma$	The thermodynamic work of adhesion per unit area, $J\ m^{-2}$
$\gamma(y,z)$	The shear stress in the position (y, z), $N\ m^{-2}$
$\dot{\gamma}$	The shear rate, s^{-1}
ν	The kinematic viscosity $m^2\ s^{-1}$
$\phi_{analyser}$	The work function of the electron analyser, J
κ_C	Coulomb's constant, $m^2\ N\ C^{-2}$
θ	Contact angle, °
κ	The static friction coefficient
υ	Poisson's ratio
υ_c	Poisson's ratio of microcapsule
υ_s	Poisson's ratio of substrate
ρ_p	The density of the particle, $kg\ m^{-3}$
ρ_f	The density of the fluid, $kg\ m^{-3}$
τ_f	The torque due to the flow, Nm

Abbreviations

AFM	Atomic Force Microscopy
DLVO	Derjaguin–Landau–Verweij–Overbeek Theory
DMSO	Dimethyl Sulfoxide
DMT	Derjaguin-Muller-Toporov Theory
ESEM	Environmental Scanning Electron Microscopy
HPLC	High Performance Liquid Chromatography
JKR	Johnson-Kendall-Roberts Theory
MF	Melamine Formaldehyde
NMMO	N-methylmorpholine-N-oxide
PE (s)	Polyelectrolyte(s)
PEI	Poly(ethyleneimine)
PET	Polyethylene terephthalate
PMMA	Poly(methyl methacrylate)
PVF	Polyvinyl formaldehyde
RH	Relative Humidity
RMS	Root Mean Square
SDBS	Sodium Dodecylbenzenesulfonate
SEM	Scanning Electron Microscopy
SFA	Surface Forces Apparatus
TEM	Transmission Electron Microscopy
XPS	X-ray Photoelectron Microscopy

Chapter 1: Introduction

1.1 General background of the project

The delivery of particles to surfaces and the removal of them from surfaces have attracted much attention in a wide range of fields such as personal and household care (Rodrigues *et al.*, 2009, Liu, 2010), drug delivery (Fischer *et al.*, 2009), biomaterials (Shin *et al.*, 2003), particle filtration and fouling (Oliveria, 1997), drying and cleaning industries (Zhang *et al.*, 1999, Zhang, 1999) and so on. Adhesion behaviour is fundamentally important for these processes and it can be favourable or undesirable depending on the system of interest. Particles containing active ingredients such as perfume oil (Rodrigues *et al.*, 2008, Rodrigues *et al.*, 2009), moisturizers (Ghosh, 2006), and vitamins (Yao *et al.*, 2011) are expected to be delivered to human surfaces such as skin and hair or to textiles to provide designated performances during the application process, in which the adhesive behaviour is favourable. However, in some other cases, like particle filtration, fouling and cleaning processes, one wishes particles to be removed from the surfaces, in which case adhesion should be avoided. Therefore, it is fundamentally important to understand the adhesion between particles and surfaces in order to either increase or avoid adhesion for different systems. In this project, the application of perfume-filled microcapsules to liquid detergent and their adhesion and retention on fabric surfaces are of special interest. It is expected that understanding of the adhesion behaviour between perfume-filled microcapsules and fabric surfaces can provide useful guidance on development of new formulations of detergents with perfume-filled microcapsules.

Perfume oil has been encapsulated into polymer walls to make perfume-filled microcapsules in order to reduce its evaporation, decrease the reaction with other substances in the surrounding environment and achieve a long-lasting release of the fragrance during applications (Hong and Park, 1999, Hong and Park, 2000, Long *et al.*, 2010). The features of perfume-filled microcapsules have attracted great attention in personal care and household-care industries, especially those leading companies such as Procter & Gamble. They are expected to add perfume-filled microcapsules into personal care and household-care products, including washing powders (Brown and Bowman, 1985), liquid detergents (Broeckx *et al.*, 2004), bleach (Bianchetti *et al.*, 2010), and personal cleaner (Ouali and Benczedi, 2008), to provide a long-lasting release of pleasant scent to consumers to improve the product image. The application of perfume-filled microcapsules into liquid detergents becomes one of the main focuses among the various kinds of products. Such microcapsules should ideally have a number of desirable properties, including no oil leakage in liquid detergents during storage, optimum mechanical strength not only to resist the external mechanical forces during the laundry process to avoid breakage but also to deliver the perfume oil through breakage resulting from friction with the cleaned fabrics, and certain surface properties to enhance their retention on the targeted fabric substrates after laundry processes.

The mechanical strength of melamine-formaldehyde perfume-filled microcapsules was systematically investigated by Liu (2010) and it was concluded that the mechanical strength of perfume-filled microcapsules can be adjusted by changing the formulation conditions including reaction time, temperature or adding a layer of coating. Additionally, the interaction between melamine formaldehyde (MF) microparticles which were used to mimic MF perfume-filled microcapsules and a cotton film used to mimic the cotton fabric surface was investigated (Liu *et al.*, 2013) and their adhesion

was detected in ambient air and no significant adhesive force could be measured in water and detergent solutions. From this, it was envisaged that the retention of microcapsules on fabric surfaces after laundry processes would be low, which needs to be improved.

1.2 Objective of the project

The low retention of perfume-filled microcapsules on fabric surfaces causes a product cost and financial loss. Therefore, the main objective of the project is to understand the adhesion and retention behaviour of perfume-filled microcapsules on fabric surfaces so that guidance can be provided to develop better product formulation which can enhance the retention of microcapsules on fabric surfaces in laundry processes.

1.3 Layout of the thesis

Chapter 2: This chapter aims to provide basic knowledge from previous research which could be used in the project. Firstly, knowledge of perfume-filled microcapsules, including the formulation methodology, wall materials and the applications is reviewed; and then general information about the fabric is introduced. Secondly, research work on enhancing adhesion between surfaces via surface treatment is reviewed. Finally, the adhesion behaviour of micro-particles on surfaces, especially the adhesion mechanisms in ambient air and liquid environments, the techniques (Atomic force microscopy (AFM) and flow chamber technique used for characterizing adhesion, the influencing factors and the methodology to calculate adhesion energy between surfaces are introduced.

Chapter 3: This chapter presents the materials, the techniques and the experimental methodologies including their principle and operation procedures that were used in the project.

Chapter 4: Melamine formaldehyde (MF) perfume-filled microcapsules were modified with functional polyelectrolytes and then the adhesion between single microcapsules and a cellulose film was investigated by AFM, which had been created to mimic a cotton fabric surface. MF perfume-filled microcapsules were then modified with chitosan and polyvinyl formamide (PVF) and their surface properties were characterized by an ESEM, particle sizer, zeta Master. Finally, the interactions between microcapsules and cellulose thin films were investigated by an AFM colloidal probe technique, and the effects of operation parameters including the compression load and contact time were investigated; and then the adhesion between microcapsules and cellulose films in ambient air, High Performance Liquid Chromatography (HPLC) grade H_2O water and sodium dodecylbenzenesulfonate (SDBS) solutions were studied; additionally, the factors influencing the adhesion results, including the particle size and surface roughness of both microcapsules and cellulose films were interpreted.

Chapter 5: The retention and adhesion behaviour of microcapsules on a cellulose film were investigated by a parallel-plate flow chamber device and AFM, which is presented in this chapter. Cellulose films were modified with the functional polyelectrolytes (i) polyvinyl formamide (PVF), (ii) chitosan, and (iii) poly(ethyleneimine) (PEI), to

increase the attraction to microcapsules. The surface properties were characterized by AFM imaging and XPS. The retention of microcapsules on modified cellulose surfaces was investigated by the flow chamber technique and then the interactions between single microcapsules and cellulose surfaces were investigated by an AFM colloidal probe technique. The results from both flow chamber experiments and the AFM technique were compared and the adhesion mechanism was proposed.

Chapter 6: The investigation of the retention and adhesion behaviours of MF microcapsules was further extended to polyester surfaces in this chapter. Functional polyelectrolytes (PVF, chitosan and PEI) were used to modify polyester surfaces and the retention and adhesion of microcapsules were investigated by the flow chamber technique and AFM. The performances of adhesion and retention enhancement resulting from using the three chemicals were compared and the adhesion mechanism was elucidated.

Chapter 7: A theoretical model was proposed based on the flow chamber experiments, to predict the adhesion and the thermodynamic work of adhesion between microcapsules and a glass surface used as a model substrate. The minimum sizes of microcapsules which can be removed by lift, sliding and rolling were calculated to investigate the removal mechanism. The influence factors such as the particle radius, flow rate, density of the particle, coefficient of friction and the distance of the central position of the settled particle to the centre line of the channel and their influence on adhesion behaviour were interpreted. The adhesion and thermodynamic work of adhesion between a microcapsule and a glass were then predicted by incorporating the

experimental results including the critical flow rate, particle size and particle location in the flow chamber to the model. Additionally, the thermodynamic work of adhesion was calculated from AFM adhesion results. The results of adhesion and thermodynamic work of adhesion from the flow chamber model and AFM were compared. The influence of the contact issue between the microcapsule and the substrate in aqueous solution on the adhesion and thermodynamic work of adhesion was further discussed. Finally, the model was used to interpret the relationship between the adhesion and the removal of particles as presented in Chapter 5 and Chapter 6.

Chapter 8: This chapter presents the overall conclusions of the project and recommendations for future work are proposed.

Chapter 2: Literature Review

2.1 Perfume

Perfume is a mixture of fragrant essential oils and aroma compounds, fixatives, and solvents, which is used to give the human body, animals, objects, and living spaces a pleasant scent (Ohloff *et al.*, 1994, Sell, 2006). It has been used in many diverse consumer products such as cosmetic, soaps, detergents, household cleansers, air fresheners (Herman, 2002). In fact, perfume itself has no effect on the functionality of the personal care and household products, but it plays an important role in promoting the product image and attracting consumers' attention for its aesthetic attributes.

However, the direct incorporation of perfume into personal care and household products has drawbacks. Most perfume ingredients are unsaturated hydrocarbons, alcohols, esters, aldehydes ketones, phenols or terpenes (Jellinek, 1975, Sell, 2006, Nivaldo, 2007) and these ingredients evaporate quickly during packaging, storage and application processes; they are sensitive to heat, light, oxygen and extraneous organic materials; additionally, they may also react with some ingredients such as oxidizing agents, strong acids, strong bases and also proteins and polypeptides from the surrounding environments (Jellinek, 1975); some perfume components themselves may undergo slow chemical changes by reacting with the air and container materials during storage (Ishikawa *et al.*, 1971); besides, surfactants are mean to solubilise perfume oils which can affect the performance of the detergent; Additionally, perfume oil is hydrophobic and it has poor solubility in the emulsion products; the incomplete solubility of perfume in consumer products often causes haziness or cloud and visible precipitation in the

products, and even worse cases such as clogging the valve orifices. All the issues were mentioned above not only cause perfume loss but also affect the performance of the products and break down the product image. Therefore, using perfume in detergent with a high efficiency and without causing problems has become an urgent business need.

2.2 Encapsulation

2.2.1 Encapsulation methodology

The encapsulation technique is one of the possible ways to achieve the goal to use perfume efficiently without causing problems in consumer products. Using the technique, different core materials, including particles, droplets and even gases can be coated or encapsulated into solid wall/shell to separate them from the outside environments and then to achieve some unique performances such as protecting the core materials and their slow release (Karsa and Stephenson, 1993).

Perfume oil, as a core material, has been captured with different encapsulation techniques in the past three decades or so. The most common techniques used are in-situ polymerization (Hong and Park, 1999, Sun and Zhang, 2002, Long et al., 2010, Pan et al., 2012), interfacial polymerization (Han et al., 2009, Rodrigues et al., 2008 and 2009), and complex coacervation (Michael, 1990, Meyer, 1992). It was found that the complex coacervation generally produced a microcapsule wall from polymers with low molecular mass, leading to a weak mechanical resistance (Rodrigues et al., 2008). Therefore, in-situ polymerization and interfacial polymerization have been the two main methods to prepare perfume microcapsules recently (Sun and Zhang, 2001 and 2002, Long et al., 2010, Pan et al., 2012).

2.2.2 Wall materials

The choice of wall material is extremely important to produce perfume-filled microcapsules with desirable properties. Until now, perfume oil was most commonly entrapped into polymers such as urea formaldehyde (Sun and Zhang, 2002, Rodrigues *et al.*, 2008, Rodrigues *et al.*, 2009) and melamine formaldehyde (Sun and Zhang, 2001, Hong and Park, 1999). Preparation of perfume-filled microcapsules with these polymers not only enhanced the stability and extended the release of the perfume oil (Hong and Park, 1999), but also produced microcapsules with desirable mechanical strength (Sun and Zhang, 2001, Sun and Zhang, 2002). Recently, an additional layer of inorganic materials, such as silica and nanoparticule $CaCO_3$ (Long *et al.*, 2010), was formulated on the inner organic shell to make double shell microcapsules, which significantly reduced the leakage of perfume oil in an aqueous environment.

2.2.3 Application and performance

Perfume-filled microcapsules (Figure 2.1) have been prepared to be incorporated in a wide range of consumer products. The release of the perfume on the cleaned fabric surfaces has been extended after incorporating the formulated perfume-filled microcapsules into the granular washing powders and liquid detergents, and then applying the detergents into laundry processes; some cationic fabric softener has been found to facilitate the attachment of microcapsules to the fabric surfaces during a pre-soaking and washing process (Michael, 1990, Broeckx *et al.*, 2004, Ouali and Benczedi, 2008). The extended release of perfume has also been achieved by direct incorporation of perfume-filled microcapsules to the textile with adding adhesive bonding materials to

the suspension of microcapsules at the curing stage. However, the percentage of the perfume-filled microcapsules which have been attached to the fabric surface during laundry process was still quite low (approximately 30% on artificial fabrics), leading to a waste of resource and low efficiency of using perfume-filled microcapsules in laundry processes; the direct impregnation of perfume-filled microcapsules to the textile can only be achieved at the final stage of fabric curing in industrial process and it cannot satisfy consumers' needs to have fresh scent after each laundry process; additionally, the attachment of the microcapsules to the fabric surfaces and then their retention during the complex washing process haven't been fully understood so far. Therefore, more study is required to evaluate the adhesion of perfume-filled microcapsules to fabric surfaces, to investigate the performances of adding special chemicals as bonding agent to enhance the retention of perfume-filled microcapsules on fabric surface, and to understand fundamental interactions between microcapsules and fabric surfaces linking to the real laundry process.

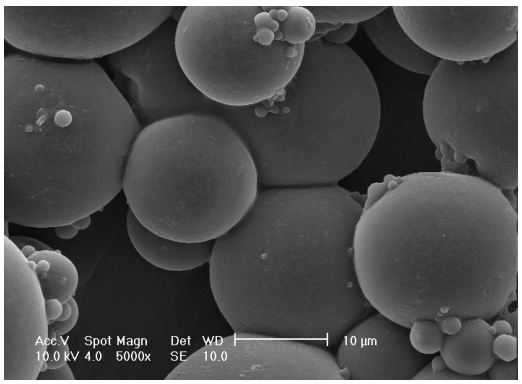

Figure 2.1 SEM image of MF microcapsules provided by P&G.

Perfume-filled microcapsules are desired to release perfume oil in the final stage of using cleaned fabric via diffusion from their shell or breakage via friction and rubbing

with the fabric. Therefore, the release rate in air and the mechanical strength are the two dominant factors to achieve the targeted goal. Firstly, perfume release is expected to sustain. The continuous release of perfume was effectively sustained when perfume-filled microcapsules were used in a series of household products (Brown and Bowman, 1985). Rodrigues *et al.* (2008, 2009) found that the impregnated perfume-filled microcapsules into textiles continued to release pleasant scent after 9000 abrasion cycles and 5 dry cleaning washing cycles. The perfume loss from the finished cotton fabric was effectively decreased from 69% to 52% with perfume nanocapsules compared with free fragrance, which (Hu *et al.*, 2011). Perfume microcapsules were formulated and their release rate can be adjusted by changing the formulation conditions like the content of medium and the stirring time (Hong and Park, 2000) or introducing an additional inorganic outer shell on the organic inner shell to make double shell microcapsules (Long *et al.*, 2010).

Secondly, perfume microcapsules should have optimum mechanical strength. They should be able to resist mechanical forces generated in mixing, packing and washing processes, but should be ruptured via friction and rubbing between human body and fabric if mechanical rupture is used as a main mechanism to release perfume. The mechanical properties (rupture force, nominal rupture stress, and deformation at rupture) and the elastic-plastic behaviours of melamine/urea-formaldehyde microcapsules were investigated by a manipulation rig (Sun and Zhang, 2001). A schematic diagram of the manipulation rig and a force versus probe displacement curve to compress a microcapsule to break are presented in Figure 2.2. The typical rupture force of melamine/urea-formaldehyde microcapsules is from a few μN to few mN and the microcapsules behaved as elastic at a small deformation (about 10% to 20%) (Hu *et al.*, 2009, Liu, 2010). The mechanical properties of perfume microcapsules can be

adjusted by changing the formulation and also adding an additional coating such as starch and silica (Liu, 2010).

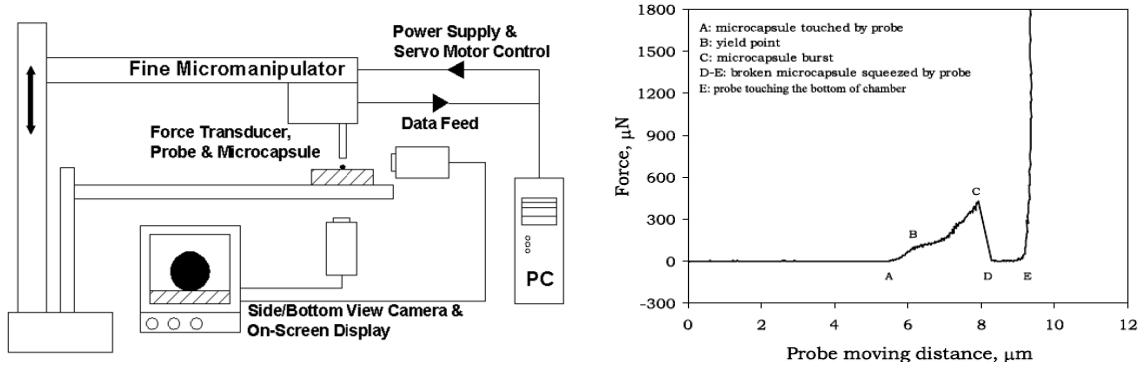

(a) (b)

Figure 2.2 A schematic representation of micromanipulation rig (Liu, 2010) (a) and a typical force versus probe displacement curve obtained from compressing a melamine formaldehyde microcapsule to rupture (Sun and Zhang, 2001) (b).

When perfume-filled microcapsules are used in household and personal care products, their adhesion and retention behaviours on substrates are crucial to effective usage. So far, investigation of the adhesion and retention of perfume-filled microcapsules on related surfaces has been very limited, except a few reports about impregnation of perfume-filled microcapsules into textiles with adhesives (Rodrigues *et al.*, 2008, Rodrigues *et al.*, 2009, Monllor *et al.*, 2010). Based on the author's knowledge, only Liu *et al.* (2013) reported the adhesion of perfume-filled microcapsules to cotton fabric surfaces. She used a MF microsphere instead of a MF perfume microcapsule to measure its adhesion to a cotton film which was used to mimic the cotton fabric surface in ambient air and liquid environments. Adhesion was only detected in ambient air which

was mainly due to the capillary force. However, in liquid environment, no adhesion was detected in most of the cases since both the particle and cotton fabric were negatively charged, and the occasional detected adhesion was attributed to bridging forces because of the extension of cellulose chains. The presence of perfume-filled microcapsules on a cotton fabric in an experiment to mimic the laundry process (Figure 2.3) was attributed to physical entrapments of the microcapsules by the fabric fibres rather than their adhesion.

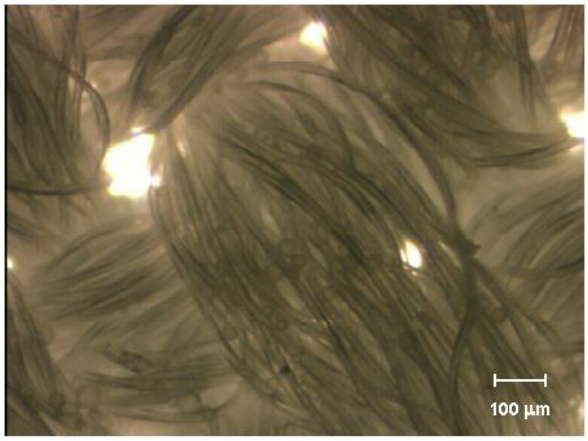

Figure 2.3 A woven fabric immersed into an aqueous suspension of MF microcapsules (Liu, 2010).

2.3 Fabric

The most common natural fabric materials used for the cloth industry are cotton, wool, silk and linen. Among them, cotton is widely used and its main component is cellulose. Cotton used for fabric is usually made of yarn and the surface is too rough (Liu *et al.*, 2013) for direct measurement of the adhesion of microcapsules to it. Therefore, attempts had been made to dissolve raw cotton materials in organic solvents and then flat cotton films (see Figure 2.4 (a)) were made on silicon wafers by a spin-coating technique

(Notley and Wågberg, 2005, Sczech and Riegler, 2006). The cotton films were successfully used to mimic cotton fabrics to study the adhesion of microcapsules based on AFM in Liu's work (2013).

Other than the natural fabric, synthetic fabrics such as nylon, acrylic, and polyester (Kadolph, 2010) account for a large percentage of usage in cloth industry. Among them, polyethylene terephthalate (PET) is the most commonly used and it accounts for approximate 50% of all polyester fibre materials (Takke *et al.*, 2011). Compared with cotton containing a large amount of carboxyl and hydroxyl groups on the molecular structure, PET is a linear and aromatic polymer which lacks of polar groups and is much more hydrophobic (Yang *et al.*, 2009, Nina *et al.*, 2011). Therefore many researchers have focused on treating PET surfaces by various methods to increase their hydrophilicity for different applications (Wang *et al.*, 2004, Li *et al.*, 2007, Navaneetha *et al.*, 2008). PET in flat sheet (Figure 2.4 (b)) is commercially available. Therefore it can be used directly for investigation of microcapsule adhesion.

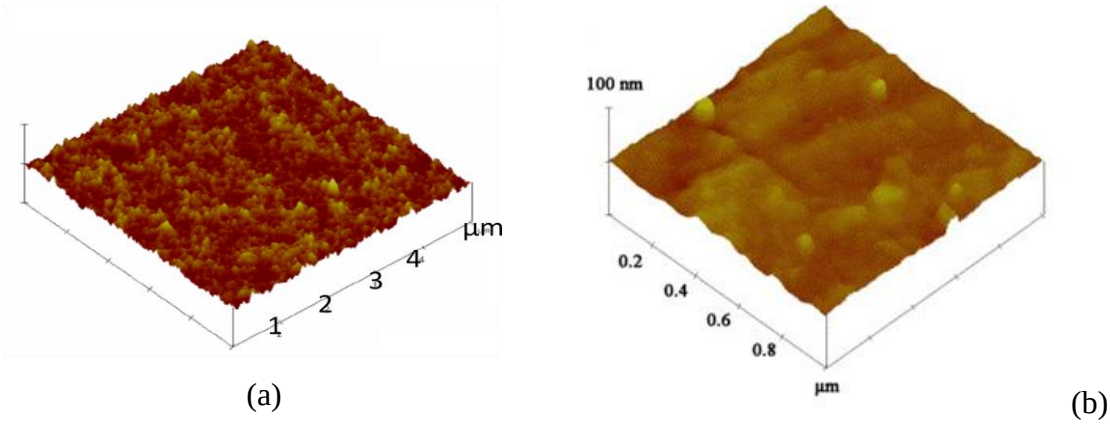

(a) (b)

Figure 2.4 AFM topography image of cellulose film over a scan area of 5 µm × 5 µm made from cotton powder (Liu, 2010) (a); and polyethylene terephthalate surface over a scan area of 1 µm × 1 µm (Hsieh *et al.*, 2006).

2.4 Surface treatment with functional chemicals to enhance adhesion and deposition

So far, the quantity of microcapsules deposited on the cleaned fabric surface after laundry processes has been quite low (personal communication with Dr Johan Smets, Procter & Gamble (P&G) Belgium; approximately 30% on the artificial fabrics). In order to increase the adhesion and retention of microcapsules on fabric surface, it is essential to understand possible interaction mechanisms between them. Adhesion between two surfaces originates from the van der Waals force and the electrostatic force (Bowling, 1985). However, the main reason causing adhesion is quite different for different systems. In ambient air, the capillary force (Butt *et al.*, 2010) was found to be the main contribution. While in liquid environment, the combination of van der Waals forces and the electrostatic double layer force (Radtchenko *et al.*, 2005) which can be described by DLVO theory (Israelachvili, 2011), ionic-bonds, H-bonds (Douglas *et al.*, 2008), bridging forces (Biggs, 1996), hydrophobic interactions (Ishida *et al.*, 2012) and some specific interactions (Giesbersa *et al.*, 2002, Altobelli *et al.*, 2010) were attributed to cause adhesion. The adhesion fundamentals will be further introduced in § 2.5.1. Here, based on the understanding of the adhesion mechanisms, adhesion can be adjusted by introducing chemicals such as adhesives, polyelectrolytes, and specific functional groups to change the surface properties.

2.4.1 Adhesive

Adhesive was used to bind objects together to enhance their adhesion. Fabric surfaces were impregnated into a suspension of perfume microcapsules by adding adhesives such

as self-crossing linking agents (Rodrigues, 2008; 2009) and an acrylic binder (Hong and Park, 1999; 2000), and the percentage of the perfume microcapsules remaining on the fabric surface was increased after curing and finishing. However, these adhesives can only work after the solvents evaporate. Additionally, they can react with the constitutes of liquid detergent (Onusseit *et al.*, 2000). Therefore, the application of the adhesives in laundry processes is limited.

2.4.2 Polyelectrolyte

Modifying surfaces with polyelectrolytes is another common method which was used to enhance adhesion between two surfaces (Claesson *et al.*, 2003, Christendat *et al.*, 2005, Che *et al.*, 2008, Orelma *et al.*, 2011). Polyelectrolyte is one kind of polymer with long molecular chains bearing electrolyte charges on each repeat unit (Podgornik and Ličer, 2006). Normally, opposite charged polyelectrolyte has been chosen to modify one of the contacted surfaces, and then adhesion was enhanced either through electrostatic attraction, or bridging forces, or even their combination that may lead to the entanglement of charged long polyelectrolyte molecular chains (Podgornik and Ličer, 2006). A schematic diagram in Figure 2.5 illustrates the polyelectrolyte bridging interaction between two single macro ions.

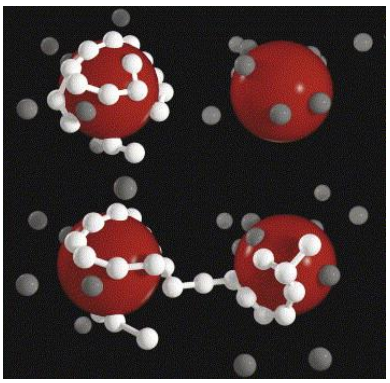

Figure 2.5 Schematic diagram of the mechanism of adhesion enhancement by polyelectrolyte bridging interaction (Podgornik and Ličer, 2006).

Using polyelectrolyte to enhance adhesion between surfaces has been applied in many systems. Immobilization of concanavalin A (FL-Con A) on a PANCAA nanofibrous surface was enhanced by treating the surface with chitosan through electrostatic attraction and also the specific recognition of Con A on chitosan (Che *et al.*, 2008). Opposite charged polyelectrolyte was used to modify a mica surface, and the adhesion between the modified surface and unmodified surface was increased; the main reason for the adhesion enhancement was due to the presence of electrostatic attraction for the high charge density polyelectrolyte and bridging forces for the low density charge polyelectrolyte (Claessona *et al.*, 2003). Sczech (2006) investigated the adhesion between cellulose powders and a cellulose film based on sticking experiments; modifying of either the cellulose film or the particles with positively charged polyelectrolytes increased the number of stuck cellulose particles. Nolte (2004) also found that adhesion of PSS-terminated polyelectrolyte capsules were blocked on a substrate with the same charge sign and enhanced to another substrate with the opposite charge sign. Therefore, polyelecteolyte is a favorable chemical to modify surfaces in order to enhance adhesion either through electrostatic attraction or bridging forces and it may be possible to enhance adhesion in a microcapsule - fabric system via modifying one of their surfaces using polyelectrolytes.

2.4.3 Specific chemicals with functional groups

Some other chemicals with special functional groups which can form special linkages or react with other groups on the surface, have been chosen to modify surface to enhance adhesion in many fields, such as papermaking industry and specific recognition between certain molecules in biomedical applications. PVAm-PBA (polyvinylamine derivatized with phenylboronic acid) is the most common chemical used to form strong adhesion joints between celluloses in papermaking industries and the adhesion was enhanced because boronic acid groups can form ester linkage with the *cis diol* groups on the cellulose surface (Chen *et al.*, 2009, Notley, 2009, Zhang *et al.*, 2010). Additionally, the specific recognition of cell and proteins such as fibronectin, collagen, laminin or peptides like arginine, glycine, and aspartic acid were investigated and the proteins and peptides were used to modify the synthetic polymeric materials to enhance adhesion for medical applications (Chen and Moy, 2000, Hersel *et al.*, 2003). Besides, these chemicals with hydroxyl, carboxyl and amine groups were used to modify surface to enhance adhesion through hydrogen bonds (Orelma *et al.*, 2011) and acid-base interaction (Giesbersa *et al.*, 2002). Therefore, treatment of surface with functional chemicals was demonstrated to be another possible way to enhance the adhesion between two surfaces.

2.5 Adhesion

Adhesion is the attractive interaction at the interface when two surfaces are brought into an intimate contact and it is a complex physicochemical process. The presence of adhesion either offers a favourable or an undesired effect in many industries. For

example adhesion is favourable in compacting process, enhancing interactions between cells and viruses in biological systems (Martines *et al.*, 2004), printing of toner particles on the photoreceptor and the targeted copy paper in electro photography (Rimai *et al.*, 2010) and particle deposition to fabric (Liu, 2010); whilst in particle filtration, (Oliveria, 1997), drying and cleaning processes (Zhang *et al.*, 1999, Zhang, 1999), particle-surface or particle-particle adhesion should be avoided. Therefore, it is fundamentally important to understand the basic mechanisms of adhesion in order to either increase or avoid adhesion for different systems.

2.5.1 Adhesion at molecular scale

2.5.1.1 Adhesion in ambient air

van der Waals force is the sum of the attractive or repulsive forces between molecules which refers to the interaction between dipoles (including permanent dipoles and induced diploes). It widely exists and has been reported to be the main mechanism to cause powder agglomeration (Hartley *et al.*, 1985) and the ability of geckos to hang on a glass surface using only one toe or to climb on a sheer surface (Autumn *et al.*, 2002). Additionally, it has been suggested to play an important role between surfaces and molecules when they are close enough (Eastman and Zhu, 1996, Pakarinen *et al.*, 2009, Aradhya *et al.*, 2012). van der Waals force is determined by the material properties, which is expressed as the Hamaker constant in Equation (2.1); additionally, it is inversely proportional to the squared distance between two surfaces (D) (see Table 2.1), therefore other than the material itself, the presence of any surface asperities will decrease the van der Waals force effectively in ambient air (Katainen *et al.*, 2006). van der Waals force may be negligible when the contact surfaces are quite rough.

Electrostatic interaction (see Table 2.1) exists between two electrically charged surfaces and it can be either attractive or repulsive. Electrostatic force is a function of the surface charge of the two contacted surfaces, the properties of the medium and the distance between them (Equation (2.2)). However, the presence of water in ambient air with moderate or high relative humidity (generally RH $\geq$ 40%) always dissipates the surface charges (Karner and Urbanetz, 2012), causing the electrostatic force to vanish. Therefore, electrostatic forces can be only observed under dry condition with less humidity or in some processes which can generate charges such as triboelectric charge arising when pharmaceutical powders are mixed (Karner and Urbanetz, 2012). Hence, the electrostatic force may not be the dominant factor to influence adhesion in laundry processes.

Compared with van-der Waals forces and electrostatic forces, capillary forces (see Table 2.1) have been considered as the main mechanism for the adhesion between two contacted surfaces in ambient air when the relative humidity is above 40% (Jones *et al.*, 2002, Liu, 2010). The water vapour condenses on the surface to form a thin water layer and then a small liquid capillary bridge forms between two surfaces. Capillary force is not only a function of the surface chemical state, but also a function of the relative humidity (RH). It has been validated to be the main mechanism of adhesion between two contacted surfaces in ambient air condition (Jones *et al.*, 2002, Grobelny *et al.*, 2006, Butt *et al.*, 2010, Liu, 2010).

Table 2.1 The schematic diagram and equations to describe van der Waals, electrostatic and capillary forces (Israelachvili, 2011)

	Schematic diagram	Equation
van der Waals force	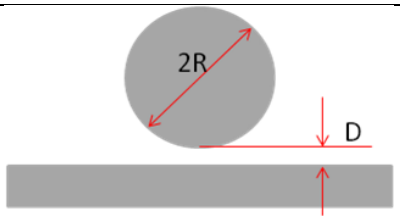	$F = -\frac{A_H R}{6D^2}$ (2.1) A_H is the Hamaker constant.
Electrostatic force	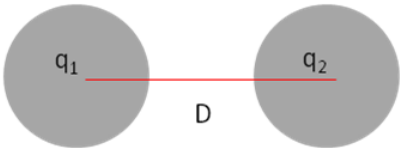	$F = \frac{\kappa_C \times q_1 \times q_2}{D^2}$ (2.2) $\kappa_C \equiv \frac{1}{4\pi \in_0 \in} = 8.9896 \times 10^9 \, N \cdot m^2 \cdot C^{-2}$ q is the net charge on the particle; κ_C is the Coulomb's constant and $\in_0$ is the permittivity of free space; $\in$ is the relative permittivity.
Capillary force	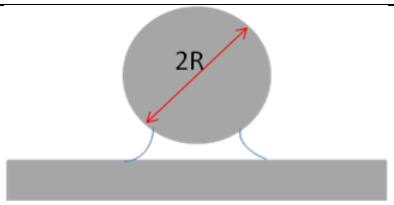	$F = 4\pi R\gamma_S \cos\theta$ (2.3) γ_S is the liquid-vapour surface tension and θ is the solid-liquid contact angle.

2.5.1.2 Adhesion in liquid environment

In liquid environment, adhesion is much more complicated. Besides van der Waals force, the electrostatic double layer force is another important parameter to influence the interaction between two surfaces. The surface which is immersed into a liquid generates charges either through dissociation or ionization of surface groups from the surrounding medium, or adsorption or binding charged ions or molecules to the previous uncharged or oppositely charged surface; the charged surface attracts counterions from the surrounding liquid environment and repels co-ion; therefore, an extended layer of

counterions is developed on the original surface which is called the electrical double layer (EDL) (Hunter, 2001); the wall charge is screened by the counterions. Electrostatic double layer force is a function of the surface charge, the properties of the medium, the concentration of the counterions and the distance between two surfaces. Two similarly charged surfaces usually repel each other electrostatically in solution (Israelachvili, 2011). The combination of van der Waals force and electrostatic double layer force is described by the DLVO theory (Israelachvili, 2011). A schematic diagram of the variation of free energy with particle separation according to DLVO theory is illustrated in Figure 2.6.

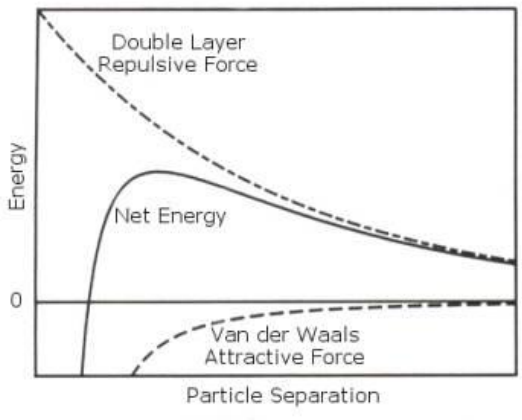

Figure 2.6 Schematic diagram of the variation of free energy with particle separation according to DLVO theory. The net energy is given by the sum of the double layer repulsion and the van der Waals attractive forces that the particles experience as they approach one another. (Malvern_Instruments, 2007).

Electrostatic attraction happens between two oppositely charged surfaces. It was reported to be the main reason to increase adhesion between cellulose beads and a cellulose surface (Sczech and Riegler, 2006), dye and cotton fibres (Janhom *et al.*,

2006), mica surfaces (Claessona *et al.*, 2003) after modifying one of the surfaces with a positive polyelectrolyte to alter the sign of the surface charge.

However, some inconsistency was observed which showed the classic DLVO theory underestimated the interaction in colloidal system (Grasso *et al.*, 2002). The reason for the failure is that when two surfaces are close enough to the molecule scale, some other non-DLVO forces come into play (Israelachvili, 2011), such as solvation, structural and hydration forces. The solvation or structure force can arise from the reordering of the solvent molecule at a small separation between two surfaces or a limited space. It is geometrically original and depends on the molecular shape. The solvent force in aqueous solution becomes hydration force. There are two kinds of common hydration force: one is the repulsion between the solid hydrophilic surfaces (Pashley, 1981a, Pashley, 1981b) and another is the attractive force between two hydrophobic surfaces (Meyer *et al.*, 2006, Thormann *et al.*, 2008, Israelachvili, 2011). The repulsive interaction between hydrophilic surfaces can be recognized as the propensity of certain molecules and groups to be water-soluble and to strongly repel each other in water; the groups prefer to be in contact with water rather than with each other, therefore the repulsive force can be observed when two surfaces containing the hydrophilic groups approach each other in water. The attractive force between two hydrophobic surfaces arises primarily from the rearrangement of the H-bond configurations in the overlapping solvation zones as two surfaces come together; and it favours adhesion enhancement. It has been observed in many systems, such as the interaction between silicone oil and hydrophobic Teflon and paraffin surfaces in water (Zbik and Frost, 2010), octadecyltrichlorosilane treated glass and silicon surfaces (Ishida *et al.*, 2012) and polyester surfaces (Faghihnejad and Zeng, 2012), micelle formation (Gao and Dubin, 1999), and protein folding (Lins and Brasseur, 1995). The reported range of

hydrophobic attraction was reviewed by Meyer (2006), and is from a few nanometres to hundreds of nanometres and it was concluded that the only short range attractive force (< 10 nm) is the true hydrophobic force. Hydrophobic attraction was found to be stronger than the van der Waals forces at separation less than 10-15 nm.

In addition to the hydration force, the diffusive force is another kind of non-DLVO force and refers to the diffusion of the polymer chains at the interface, which is also called the bridging force (Biggs, 1996). Diffusive adhesion is somewhat like mechanical interlocking at the molecular level. The adhesion occurs because of the entanglement and tethering of molecule chains and it is quite commonly observed in the systems involving with polymers. The range of the bridging force is a function of the effective length of the molecule chain, which was reported from dozens of nm (Liu, 2010) to a few μm (Notley, 2009, Kocuna *et al.*, 2011). Adhesion due to diffusive interaction was observed for many polymer molecules such as cellulose (Nigmatullin *et al.*, 2004, Notley, 2009), chitosan (Xu *et al.*, 2007, Orelma *et al.*, 2011), and Poly(N-isopropylacrylamide) (Poly (NiPAAm)) (Zoppe *et al.*, 2011).

Besides, these hydrogen bonds are another important interaction at interfaces. It was first noticed for the extremely strong and orientation-dependent adhesion between water molecules (Israelachvili, 2011). Although the hydrogen bonding is believed to be a purely electrostatic and Coulomb like interaction (Coulson, 1961), it is still complicated; it not only exists between water molecules, but also exists between electronegative atoms such as O, N, F and Cl and H atoms which are bonded to similar electronegative atoms covalently (Israelachvili, 2011). Therefore, hydrogen bonding becomes to be another important parameter to cause adhesion between surfaces containing functional groups such as hydroxyl, carboxyl, and amine groups. Additionally, amine groups are positively charged, while carboxyl and hydroxyl groups

are negatively charged. Hence, both the electrostatic attraction and hydrogen bonding work together to improved adhesion (Giesbersa *et al.*, 2002).

2.5.2 Adhesion at the micro scale

Adhesion via mechanical interlocking between two surfaces at the microscale is another important adhesion mechanism. It causes adhesion by holding surfaces together through adding adhesive material or physical entrapment. Mechanical interlocking can occur both in ambient air and liquid environments. Perfume microcapsules were impregnated into fabric surface by binding with some adhesives such as self-crossing linking agents (Rodrigues *et al.*, 2008, Rodrigues *et al.*, 2009) and acrylic binders (Hong and Park, 1999, Hong and Park, 2000); the filtration of MF microcapsules in cotton fabric by the network structures of the cotton bundles was considered as the main reason for the deposition of melamine formaldehyde microcapsules (Liu, 2010).

2.5.3 Adhesion measurements

In order to understand the adhesion between microcapsules and fabric surfaces, it is essential to characterize the adhesion. Therefore, the techniques to characterise adhesion are reviewed in this section. Characterization of the adhesive force is normally based on the detachment of the candidate particles from a substrate with measurable external forces. The most common techniques used so far are based on population and individual analyses.

2.5.3.1 The flow chamber technique

A fluid flow in a chamber removes particles or cells from a surface through hydrodynamic force (Decuzzi *et al.*, 2007) and it can be adjusted by the choice of flow velocity and the fluid physical properties; the flow chamber technique is most commonly used, based on particle population to study adhesion in liquid environments (Renshaw *et al.*, 2005, Garrett *et al.*, 2008). Most of the research on adhesion using a flow chamber so far relied on counting the number of the particles on the substrate before and after the flow experiment (Brown and Larson, 2001, Decuzzi *et al.*, 2007), or calculating the surface area coverage by the particles (Renshaw *et al.*, 2005, Garrett *et al.*, 2008).

Martines *et al.* (2004) investigated the cell adhesion on flat and nanopatterned poly (methylmethacrylate) substrates using a parallel-plate flow chamber. A greater number of cells were removed from the nanopatterned surface than that from the flat surface, which correlates well with the previous study (Gallagher *et al.*, 2002) of cell adhesion to nano-patterned surfaces. Bacterial adhesion on stainless steel substrate under different culture time was studied by Garrett (2008) with a self-designed flow chamber. More bacteria remained on the stainless steel substrate after they were cultured longer, which indicates a stronger adhesion between biomass and the substrate; and the results are consistent with the study of bacterial adhesion with a micromanipulation technique. Renshaw (2005) developed a flow chamber to study the adhesion of different kinds of cells on synthetic materials with a live-dead assay and image capturing system. A higher deposition number of rat aortic smooth muscle cells (SMC) to PLL films rather than that of endothelial cells (EC) were found. The displacement of microspheres from a glass surface was investigated by a flow chamber and centrifuge technique in Sanjit's (1994) work. More polystyrene microspheres remained on the glass surface compared

with the glass microspheres after the same hydrodynamic force was applied; additionally, the glass spheres with a large diameter were found to be more difficult to be displaced compared with the small ones; more glass microspheres remained on the glass surface by decreasing pH and increasing the ionic strength of the intervening fluid. These results agree with the experimental results from the centrifuge technique (Sharma *et al.*, 1992, Sanjit *et al.*, 1994)

The principle of the flow chamber technique is to displace particles from a surface with hydrodynamic force. Particles can be displaced from the substrate either by lift (Saffman, 1965), sliding (Derksen and Larsen, 2011), or rolling (Zoeteweij *et al.*, 2009) motions or a combination (Figure 2.7). Particles are removed by lift motion when the lift force overcomes the adhesion in vertical direction (Zoeteweij *et al.*, 2009). If the lift is not sufficient enough, particles will possibly be displaced by drag force in lateral direction through sliding or rotation motion (Sanjit *et al.*, 1994, Zhang, 1999, Zoeteweij *et al.*, 2009). The balance on the forces and torques resulting in the removal of a particle from a surface is directly correlated with the adhesion between two surfaces. Therefore, the flow chamber experimental data may also be used to calculate adhesion of particles on a substrate.

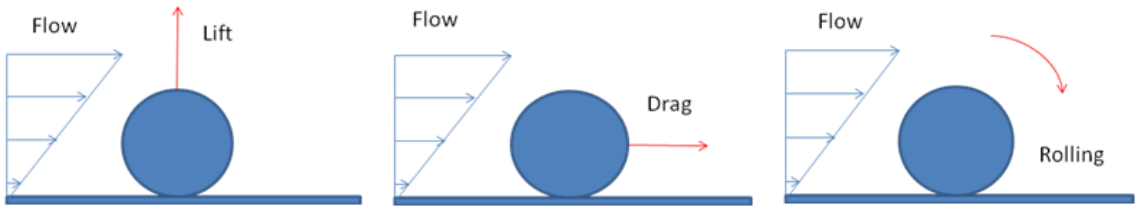

(a) (b) (c)

Figure 2.7 Schematic representation of displacement of micro particles by lift force (a), drag force (b) and rolling motion (c)

When a microparticle settles on a substrate in a flow chamber, adhesion (F_C), buoyancy force (F_B), lift force (F_{SA}), drag force (F_D), friction (F_f) are the possible interactions acting on the particle before it is removed or displaced (Figure 2.8). The buoyancy force is a constant value for a certain particle. However, adhesion in theory is influenced by the properties of the particle, including particle size (Lam and Newton, 1992, Katainen *et al.*, 2006), surface roughness (Chris S. Hodges, 2004, Katainen *et al.*, 2006), elastic properties of the contacted surfaces (Johnson *et al.*, 1971), and the properties of the fluid around such as the ionic strength and pH (Vakarelski *et al.*, 2000). Consequently, the force balance in the vertical direction will be affected by changing these parameters. The lift and sliding force are each a function of shear stress, which is dominated by the flow velocity, particle location and flow properties (Saffman, 1965, Decuzzi *et al.*, 2007, Derksen and Larsen, 2011). A given shear stress can lead to a complete removal of particle from surface or no removal at all. Additionally, the surface roughness of the contacted region influences the friction force corresponding to the on-set of displacement of a particle if it is displaced by sliding. Additionally, the settling time is important. The settling time should be long enough for the particle to fully interact with the substrate. If it is less than a critical settling time (Lamb, 1994), poor contact is achieved between the two surfaces and the particles will be removed easily compared with those well settled particles. Other than the theoretical prediction, the influence of these parameters on particle removal in a flow chamber was also validated by experiment results which have been reported in many publications. The increase in the surface roughness of the nanopatterned poly(methylmethacrylate) substrates caused more cell retention on them (Martines *et al.*, 2004). The fraction of micro particles on surface and the critical hydrodynamic force which is the minimum hydrodynamic force required to remove microspheres from the surface, is found to be a function of the particle size, elastic properties of the particle, surface roughness and the medium

properties (Sharma *et al.*, 1992, Sanjit *et al.*, 1994). A higher hydrodynamic force was needed to displace microspheres from a glass substrate if the microparticle became softer and the surface roughness decreased. The size effect of sphere particles on their removal behaviour in a flow chamber system was also observed by Decuzzi (2007) and it was concluded that the normalized number (number per unit area) of spherical micro- and nano-particles attached on surface of cells surface, which was prepared by plating human umbilical vein endothelial cells (HUVECs) on a borosilicate dish, decreased with the particle size for a given flow rate. Therefore, either the properties of the micro particles or the contacted substrate or the operation conditions can influence the deposition and removal behaviours of microparticles on a substrate in a flow chamber.

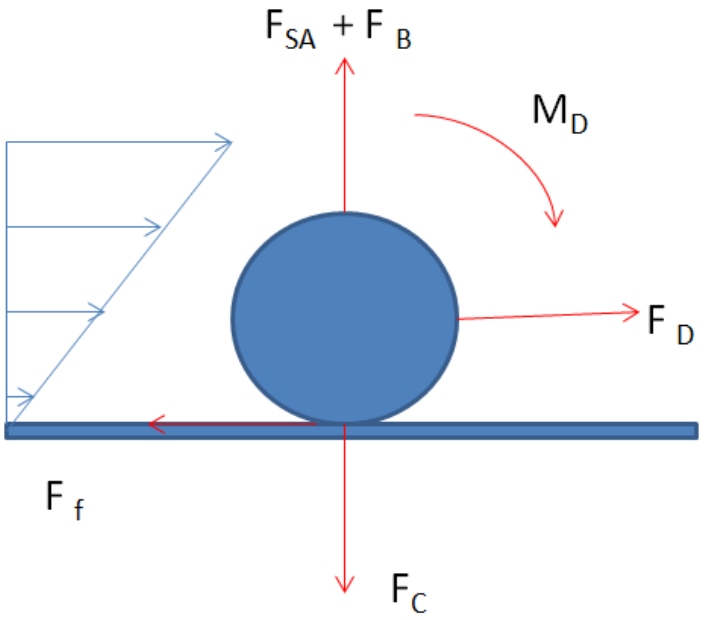

Figure 2.8 Schematic diagram of forces on a microparticle.

The above previous studies suggest that the flow chamber technique is a reliable technique to study microparticle or cell adhesion to a substrate. It is sensitive enough to detect the effects of the material properties, and the properties of the intervening fluid on particle removal. Moreover, it is possible that the adhesion between a particle and a

substrate can be predicted by the flow chamber technique if the removal mechanism of the particle is well understood. Therefore, the flow chamber technique may be used to characterize the remaining of microcapsules on fabric surfaces and to study the adhesion behaviours between single microcapsules and fabric surfaces.

2.5.3.2 Atomic force microscope (AFM)

AFM with a colloid probe has been used to measure micro- and nanoscale forces between particles and surfaces (Binnig *et al.*, 1986, Ducker *et al.*, 1992, Kappl and Butt, 2002). A candidate particle can be attached to the end of a cantilever and then the force between the particle and a surface in different environments can be measured with AFM. Figure 2.9 shows a SEM image of a single MF microsphere attached to the end of a tipless cantilever. The adhesion has been investigated either by comparison of adhesive forces directly or interpretation of the detailed information of the force curves: the difference in the adhesive force between surfaces with different chemical compositions (Eastman and Zhu, 1996, Żbik and Frost, 2010) and surface roughness (Cooper *et al.*, 2001, Katainen *et al.*, 2006); force curves were acquired by varying relativity humidity, ionic strength, pH, hydrophobic or hydrophilic nature etc to investigate adhesion mechanisms including capillary force, electrostatic interaction, hydrophobic interaction and bridging interaction (Vakarelski *et al.*, 2000, Jones *et al.*, 2002, Notley, 2009, Żbik and Frost, 2010, Kocuna *et al.*, 2011).

Bowen *et al.* (1998a; 1998b; 2001; 2002)) carried out a series of studies on cell adhesion using AFM with a colloidal probe, including the adhesion between single cell probes, which were prepared by immobilizing a single cell at the apex of a tipless AFM cantilever, and mica and synthetic membranes (Bowen *et al.*, 2001), *Bacillus mycoides* spores and glass substrates with hydrophilic and hydrophobic properties (Bowen *et al.*,

2002) to generate understanding of cell adhesion on surfaces relevant to bio-applications. The adhesion between a silica sphere and a mica plate ((Vakarelski *et al.*, 2000, Vakarelski and Higashitani, 2001) and a cellulose surface (Holmberg *et al.*, 1997) in water and electrolyte solutions was measured to investigate the adhesion mechanism at molecule level by AFM. AFM with a colloidal probe was also used to investigate the interaction between polystyrene particles as a function of particle size (Hodges *et al.*, 2002), surface roughness, relative humidity and compression load (Cleaver and Looi, 2007) to study their influences on adhesion. Besides the solid spheres, single perfume microcapsules with a core shell structure were successfully attached to the end of an AFM cantilever, to study their adhesion on a cotton film which was used to mimic fabric surface in Liu's (2010) work and to explore the application of the microcapsules in household products. Besides measuring the forces between microparticles and surfaces directly, AFM was also adopted to study the stretching of the molecule chains like cellulose (Notley *et al.*, 2009) and chitosan (Xu *et al.*, 2007, Kocuna *et al.*, 2011) to get information of molecule structure.

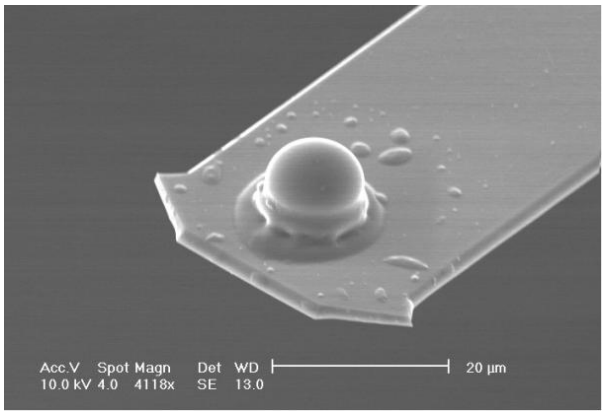

Figure 2.9 SEM image of a MF microsphere attached to the end of a tipless cantilever (Liu, 2010).

AFM is a very sensitive technique, and the force measured between a particle and surface is influenced by many factors, including compression load, contact time, and extending speed for non-perfectly elastic materials, particle size, surface roughness of the contact surfaces and the environmental conditions such as the relative humidity in ambient air and ionic concentration and pH value in liquid. Adhesion is also influenced by contact area and vice versa. The extra compression load can cause a significant deformation of the contact bodies to generate a contact area. Stegeman *et al.* (2007) investigated the influence of compression load on the pull-off force between sphere silicon probes and a Ag surface and the adhesion was found to be independent of compression load from 90 nN to 200 nN; a further increase of the compression load to 350 nN caused an increase in adhesion; the transmission of elastic deformation to plastic deformation by compressing silicon sphere was considered to be the main reason for the adhesion increase. Cleaver (2007) studied the adhesion between polystyrene particles as a function of humidity and applied load; there is no obvious variation in adhesion by increasing the applied load in low and moderate humidity environments; however, the adhesion increased steadily with compression load after it reached a threshold value of 1200 nN in high humidity condition; the enhancement of adhesion was also attributed to the plastic deformation of particle and the adsorption of water in high humidity environment, which acted as a plasticizer. The dependence of adhesion on contact time and compression load was observed when investigating the adhesion between a polymer sphere and a silicon surface; adhesion was increased by either increasing contact time or applied load, which was attributed to the viscous-elastic nature of the polymer and its elastic-plastic deformation through contact (Reitsma *et al.*, 2000). McNamee *et al.* (2006) investigated the influence of compression load and contact time on the adhesion between a colloid probe and cell; it was found that there is no obvious variation in adhesion by increasing the applied load to 10 nN, indicating that

cell will not be damaged under this compression load; however, adhesion increased with the contact time because of the visco-elastic property of the cells. Vakarelski et al. (2000, 2001) found that the adhesion between a silica sphere and a mica plate in water and electrolyte solutions increased by increasing the contact time and it was concluded that the adhesion is related to the structure of the layer of cations and water molecules adsorbed on the outside surface: a thin but firm primary inside layer and a thick but fragile secondary outside layer were suggested to be present on the surface in liquid environment.

Hodges *et al.* (2002, 2004) investigated the influence of particle size on the pull-off force between polystyrene particles; the average pull-off forces were quite scattered and there was no obvious trend between particle size and adhesion; surface roughness was attributed to the reason for adhesion variation. The interplay of surface roughness and particle size was investigated in Katainen *et al.*'s (2006) work, the dependence of the adhesion on particle size was observed when the asperities are much smaller than the particle dimension, otherwise the adhesion was dominated by the shape and size of the asperities. The dependence of adhesion between micro-particles and surfaces on the environmental condition such as relative humidity in air (Liu, 2010), and ionic strength and pH of the intervening medium was observed (Giesbersa *et al.*, 2002, Christendat *et al.*, 2005, Xu *et al.*, 2005).

It is suggested that AFM with a colloidal probe is a proven technique to measure adhesion between a single microparticle and a substrate both in dry and liquid environments. The technique is sensitive to the change in the properties of the particle and the substrate, the properties of the surrounding environments and the operation parameters. Therefore, it can be used to investigate adhesion between microcapsules and fabric surfaces both in dry and liquid environments.

2.5.4 Adhesion energy

Adhesion is a complex function of both adhesion energy and contact area. The surface energy of a solid surface is commonly determined by measuring the contact angle of a droplet with known surface energy and then calculated by fitting the contact angle data to the Young's equation; additionally, the surface energy of a solid surface can be evaluated according to semi-empirical analytical models such as Fowkes, Owens-Wendt, and Van Oss-Chaudhury-Good equations by knowing the contact angle (Medendorp, 2011). The methodology makes it possible to calculate adhesion energy on a flat and homogeneous surface at the macroscale; however, it is not desirable to determine adhesion energy on a substrate which is unstable to the probing liquid or a substrate with a small dimension (Drelich *et al.*, 2004). Alternatively, the thermodynamic work of adhesion or adhesion energy of an unstable substrate or a surface with microscopic dimension can be obtained by acquiring the contact area from the well established contact mechanics such as the JKR model (Johnson *et al.*, 1971) or the DMT model (Derjaguin *et al.*1975) or by direct measurement with a high-resolution reflection interference contrast microscopy (Liu *et al.*, 2002a, Liu *et al.*, 2002b, Elsner *et al.*, 2004) since the adhesion can be determined by an AFM colloidal probe technique.

2.5.4.1 Calculation of interfacial adhesion energy with contact mechanics models

Contact mechanics such as the Hertz model (Johnson, 1985), the Bradley model (Johnson, 1985), JKR (Johnson *et al.*, 1971) and DMT (Derjaguin *et al.*1975) have been well established to describe the contact between two objects. Except the Bradley model,

which has been applied to calculate the contact area between two rigid objects, the other models are applicable to elastic bodies. The Hertz model is used to describe non-adhesive elastic contact. Adhesive interaction was incorporated into the Hertz model to develop JKR and DMT models, which have been successfully used to predict the contact area and adhesion energy in many systems (Hodges *et al.*, 2004, Han *et al.*, 2009, Lamprou *et al.*, 2010). The JKR model considered the adhesion effect within the contact zone; while the DMT model took consideration of the long range attractive interaction outside of the Hertz contact area (Johnson, 1985). Generally, the JKR model is more appropriate for softer materials having higher surface energy and larger radius of particle curvature; the DMT model applies better to harder materials with low surface energy interacting with small particles (Drelich *et al.*, 2004). The Tabor number (Johnson and Greenwood, 1997, Tabor, 1977) has been used as the criteria to determine the applications of the JKR and DMT models to avoid the generalization. The contact radius (α) and the pull-off forces (F_c) when the two surfaces are separated for JKR and DMT models are listed in Table 2.2.

Table 2.2 JKR model and DMT model (Israelachvili, 2011).

	Tabor Number $\mu = \left(\frac{R\Delta\gamma^2}{E^{*2} Z_0^3} \right)^{1/3}$	Contact radius	Pull-force
JKR model	>5	$\alpha^3 = \frac{3R}{4E^*}\left(F + 3\Delta\gamma\pi R + \sqrt{6\Delta\gamma\pi RF + (3\Delta\gamma\pi R)^2}\right)$	$F_C = -\frac{3}{2}\Delta\gamma\pi R$
DMT model	<5	$\alpha^3 = \frac{3R}{4E^*}\left(F + 2\Delta\gamma\pi R\right)$	$F_C = -2\Delta\gamma\pi R$

where R is the radius of microparticle; $E^* = (\mathrm{k_C} + k_S)^{-1}$ ($\mathrm{k_C} = \frac{1-\upsilon_C^2}{\pi E_C}$ and $k_S = \frac{1-\upsilon_S^2}{\pi E_S}$); υ is the Poisson's ratio and E is the Young's modulus of each material; $\Delta\gamma = \gamma_C + \gamma_S - \gamma_{CS}$, is the work of adhesion per unit area (γ_C is the surface energy per unit area for the microparticle; γ_S is the surface energy per unit area for the substrate; γ_{CS} is the interfacial adhesion energy per unit area); Z_0 is the equilibrium separation; and F is the applied load.

The two contact models have been successfully used to calculate surface energy. The JKR and DMT models were used to calculate surface energy between a gold-coated tip and a modified glass surface with functional groups of $–CH_3$, –OH, $–CO_2H$, and $–CF_3$ from the adhesion force acquired by AFM and the results correlate well with the adhesion energy obtained from contact angle measurements (Lamprou *et al.*, 2010). C_4F_8 was used to treat polyimide (PI) and Si surface, and then interfacial adhesion energy of PI/Si, PI-F/Si, PI/Si-F and PI-F/Si-F were investigated by contact angle measurements and AFM pull-off data in conjunction with–JKR/DMT models. Both results indicate that the incorporation of fluorine decreased interfacial adhesion energy and the inconsistency in the absolute value of interfacial adhesion energy from two

techniques was attributed to the lack of the consideration of the meniscus forces in the contact angle methodology (Han *et al.*, 2009). Brunner *et al.* (Brunner *et al.*, 2010) investigated the adhesion between two surfaces separated by a thin layer of liquid and compared the adhesion results with surface energy from contact angle measurement; the observed decrease of the surface energy with the thickness of the liquid is in agreement with the decrease of adhesion; the JKR and DMT models were used to predict the linear relationship between interfacial adhesion energy and adhesion force, and a modified model by considering the total excess adhesion energy was proposed.

Although the agreement on surface energy was observed by using contact angle methodology and adhesion-contact models (JKR/DMT), the application of the contact mechanics models to calculate the surface energy was still challenging. Drelich et al (2004) reviewed those previous publications using JKR or DMT models to predict the surface energy and found that JKR model had been used most frequently without justifications; additionally, important parameters such as mechanical properties of the contact surfaces and the applied load which affects the interaction between the tip or the probe and the substrate were not always clearly reported; besides, the main reason for the scatter of the adhesion data from AFM is the surface roughness and heterogeneity. Therefore, determination of the surface energy according to the classic contact mechanics needs to be treated with caution and an investigation of the properties of the contact surfaces remains to be carried out.

2.5.4.2 Calculation of adhesion energy from contact area and energy balance

There was a query on the applicability of the classic contact mechanics such as JKR and DMT model to microspheres with a core-shell structure such as microcapsules and cells

(Liu *et al.*, 2002a, Liu *et al.*, 2002b); the contact area determined was much larger than the prediction from JKR model, which is probably because the stress distribution in the contact zone no longer obeys the Hertzian stress field and the large contact area resulted from a change in the geometry of the core shell structure.

Theoretical models based on energy balance of a microcapsule adhered to a substrate were proposed to calculate the adhesion energy (Liu *et al.*, 2002a, Liu *et al.*, 2002b, Elsner *et al.*, 2004). Liu *et al.* (2002a, 2002b) worked out a theoretical model to calculate the interfacial adhesion energy based on the balance of strain energy release rate and adhesion strength. The strain energy release rate is altered by changing the microcapsule volume caused by the osmotic inflation. With a fixed osmotic pressure, adhesion energy is a function of contact area and it was measured through a high-resolution reflection interference contrast microscopy. The interfacial adhesion energy between microcapsules and a glass surface is estimated from approximately 10 $\mu N\ m^{-1}$ to about 500 $\mu N\ m^{-1}$ under different buffer concentrations for urea-formaldehyde microcapsules (Liu *et al.*, 2002a) and 60 $mN\ m^{-1}$, 113 $mN\ m^{-1}$ and 257 $mN\ m^{-1}$ for three types of urea-formaldehyde microcapsules (Liu *et al.*, 2002b). Another model proposed in Elsner *et al.*'s (2004) research was used to calculate the adhesion energy based on the balance of the energy cost due to the deformation of microcapsules to establish the contact zone and the energy gain due to the work of adhesion. Contacts corresponding to different deformations were considered separately. However, the adhesion energy regardless of the extent of deformation is a function of the contact radius and wall thickness of microcapsules. The contact radius and wall thickness data were obtained using a reflection interference contrast microscope and AFM imaging system. The obtained interfacial adhesion energy by the small deformation model and large deformation model for microcapsules with 12 layers of PAH/PSS are 280.0±20.0

μN m^{-1} and 26.0±2.0 μN m^{-1} (according to radius dependency fit), 260.0±70.0 μN m^{-1} and 27.0±3.0 μN m^{-1} (according to thickness dependency fit) respectively; the interfacial adhesion energy was also estimated by an independent measurement using an AFM colloidal probe technique and it was from 200 to 500 μN m^{-1}, which indicates that the small deformation model was much more applicable. However, a further discussion indicates that the behaviour of the thin shell was described well by the large deformation model while the behaviour of the thick shell was described better by the small deformation model. Graf *et al.*, (2006) built a theoretical model by considering the deformed shape of microcapsule to calculate the adhesion energy; besides the elastic energy and adhesion energy, the bending effect of the membrane was also considered in this work. Experimental data in Elsner *et al.*'s (2004) work were fitted into Graf *et al.*'s (2006) model and the adhesion energy values are of the same order as the values obtained from Elsner *et al.*'s (2004) model. These theoretical models are adaptable to calculate the adhesion energy of microcapsules bound to substrate when the deformation (especially the contact radius) can be measured. Therefore, techniques which can be used to acquire the contact area between two surfaces at microscopic level are needed.

2.5.4.3 No real contact between two surfaces

In both the classic JKR/ DMT contact models and models based on the energy balance (Elsner *et al.*, 2004, Liu *et al.*, 2002b), it has been assumed that real contact is achieved between two surfaces. However, the assumption may not hold in aqueous solution, if the external force applied is not enough to squeeze out the water molecule layer (Rossetto *et al.*, 2012, Vakarelski and Higashitani, 2001) between two surfaces. (Vakarelski and Higashitani, 2001, Vakarelski *et al.*, 2000) investigated the short-range

interaction of a silica sphere on a mica surface and proposed that a thin and firm layer of water molecules existed on the surface. Kendall *et al.* (2010) simulated the interaction between magnesium oxide (MgO) surfaces contaminated with water and it was found that it is impossible to squeeze out the last water monolayer even at a pressure that causes the MgO deformation plastically. The presence of the confined water molecules on the surfaces in aqueous solution was also investigated in Rossetto *et al.*'s work (2012) and it was concluded that the behaviour of the confined water molecules is different from the bulk water solution because of the reordering of the water molecules between two surfaces at the nanoscale.

2.6 Conclusions

The literature review in this chapter has identified that perfume oil can be entrapped into a polymer wall such as UF and MF to make perfume-filled microcapsules through in-situ polymerization or interfacial polymerization processes in order to improve the efficiency of perfume usage and eliminate the issues of direct incorporation of perfume into fabric care products, such as liquid detergents. For such applications, it has been found that perfume-filled microcapsules should possess desirable properties, including long-lasting release of perfume, optimum mechanical properties and the ability to be kept on fabric surfaces. The release and the mechanical properties have been researched and they can be adjusted according to the requirement by altering the formulation and adding additional outer layers (Liu, 2010, Long *et al.*, 2010). However, the retention of microcapsules on a fabric surface in laundry process is comparably quite low at this stage and there is lack of good understanding of microcapsule-fabric interactions. Therefore, how to increase the retention of microcapsules on the fabric surface during

laundry processes via fundamental understanding of their interactions becomes a very important task, which is the final objective of this project.

The retention of microcapsules on the fabric surface is directly related to the adhesion behaviour; therefore fundamental interactions between surfaces, the methodology to enhance adhesion between two surfaces, techniques to characterise adhesion and retention of microparticles on a substrate, and adhesion energy at interfaces were reviewed. It has been found that special chemicals such as polyelectrolytes can be applied to modify the surfaces of microcapsules and fabric surfaces to enhance adhesion and retention between them through either electrostatic attraction or bridging forces, or even their combination; additionally, a flow chamber technique can be applied to investigate particle retention on a substrate in the liquid environment and AFM with a colloidal probe can measure adhesion between single microparticles and surfaces in order to understand possible adhesion mechanisms; Moreover, the relationship between adhesion obtained from AFM and the removal of particles from a substrate in a flow chamber has been qualitatively interpreted by considering possible mechanisms of displacing a particle from a substrate and the contact issue at the interface.

Chapter 3: Materials and Methods

Introduction

In order to understand molecular interactions between perfume-filled microcapsules and fabric surfaces, it was intended to measure their adhesion by AFM and the removal of the former on the latter by shear forces generated in a flow chamber, i.e. the flow chamber technique. However, the surface of fabric fibres, particularly cotton, is too rough, which makes it difficult to do direct measurements of adhesion by AFM. Therefore, a cellulose film was first created by dissolving cellulose powders in an organic solvent and then the cellulose solution was spin-coated on the pre-treated Si wafer. Then perfume-filled microcapsules, and the cellulose surface were treated with different polyelectrolytes respectively in order to modify their surface properties, the adhesion of the microcapsules to and removal from the model cellulose surface was investigated. The same approach has been taken to study molecular interactions between perfume-filled microcapsules and a model synthetic fabric polyethylene terephthalate (PET) film. In each case, the properties of microcapsules, model fabric surface and polyelectrolytes relevant to the adhesion and removal of the microcapsules from the model fabric surface were characterised. Moreover, in order to understand possible mechanisms of removal of microcapsules from fabric surfaces, a membrane to mimic the wall of microcapsules was also produced in order to determine the friction coefficient for the surface of microcapsules and that of model fabrics. The details of these experimental works are described in this chapter.

3.1 Materials

The main materials used in this work were melamine-formaldehyde perfume-filled microcapsules, model fabric surfaces and the chemicals used to do surface treatment, and they are introduced as follows.

3.1.1 Melamine-formaldehyde (MF) perfume microcapsules

Perfume-filled MF microcapsules were supplied by Procter & Gamble (P&G), Belgium. The details of their chemical compositions and preparation methods are not known due to commercial sensitivity. Typically, MF microcapsules are produced by in-situ polymerization (Pan *et al.*, 2012) of MF precondensate and formaldehyde with poly-(acrylamide-acrylic acid, sodium salt) at a temperature range of 55-85 ℃. The core oil is a typical perfume blend of various components (Long *et al.*, 2010), all of which have a relatively low solubility in water, and are used in consumer products. The mean diameter of the perfume microcapsules was approximately 20 μm, measured with a Malvern particle sizer (APA2000, Malvern Instruments Ltd., UK). Two kinds of MF microcapsules with the same wall material but different core oils of varying density were used in this work. The density of the MF microcapsules for the study presented in Chapter 4 was less than water and the density of the perfume microcapsules used for adhesion measurements and retention test in Chapter 5, 6, 7 was greater than water.

An example protocol of preparing MF microcapsules by in-situ polymerization is as follows (Pan *et al.*, 2012): 2.5 g Melamine formaldehyde (precondensate), 0.3 g formaldehyde solution (37% (w/v)) and 0.78 g acryl amide/acrylic acid were mixed with 70 g deionised H_2O; adjusted pH to 4.3 with acetic acid and then the solution was stirred (400 rpm) with a Rushton turbine impeller (Ø 32 mm), in a 250 mL standard

stirred vessel (Ø 65 mm) with 4 baffles for 105 min at a temperature of 23 ℃. Then 10.5 g oil, used as core material, was added and emulsified at 2500 rpm for 30 min at 15 ℃. After that, the dispersion was stirred continuously at 400 rpm for 30 min at 15 ℃. The dispersion temperature was then increased to 65 ℃ and allowed to polymerize for 4 h at 400 rpm in order to form microcapsule walls. Finally, microcapsules were formed, and the solution pH was raised to pH 10 by the addition of 20 wt% NaOH solution. Microcapsules with different properties can be fabricated by changing some parameters, including core/capsule ratios (the relative content of core and wall materials in microcapsules) or polymerisation time.

3.1.2 Model fabric surfaces

3.1.2.1 Cellulose thin films

Cellulose thin films were prepared according to a methodology reported by Notley and Wågberg (2005) and Liu *et al.* (2013) to mimic cotton fabric (Chapter 4 and Chapter 5).

Materials: cotton powder with a mean particle size of 20 μm (Sigma-Aldrich, UK) was used directly without any further purification. 50 wt% N-methylmorpholine-N-oxide (NMMO) in water solution (Sigma-Aldrich, UK) was used as received as a solvent to dissolve the cotton powder (Sigma-Aldrich, UK). Dimethyl sulfoxide (DMSO) (ACS spectrophotometric grade, ≥99.9%, Sigma-Aldrich, UK) was used as a viscosity modifier. 50% (w/v) poly(ethyleneimine) (PEI) in aqueous solution (Sigma-Aldrich, UK) was used as an anchoring polymer promoting adhesion of cellulose to the Si surface (single side polish Si wafers, 76 mm diameter, n <100>, resistivity 1-10 ohm cm, 381 μm thickness, IDB Technologies, UK). High Performance Liquid

Chromatography (HPLC) grade H_2O (Fisher Scientific, UK) was used throughout. General purpose grade NaOH powder (Sigma-Aldrich, UK) was used to make 10 wt% NaOH solutions.

Procedures (Figure 3.1): (a) 0.5 g cotton powder was added into 25 g 50 wt% NMMO solution in a 200 mL beaker, which was placed in a paraffin oil bath, and the temperature of the oil was increased to 115℃ to dissolve the cotton powders. 75 g DMSO was added into the cellulose/NMMO solution once the cotton powder was dissolved completely, visualised by the appearance of the cotton powder suspension turning to a dark yellow transparent liquid. (b) Si wafers were pre-treated with 10 wt % NaOH solution for 30 s, then washed with HPLC grade water and dried with N_2 afterwards. Si wafers were then treated with PEI solution for 10 min, then rinsed with HPLC grade H_2O and dried with N_2. (c) The cellulose solution obtained from procedures (a) was deposited on a pre-treated Si wafer obtained from procedure (b) with a Ø150 mm spinning processor (WS-400B-6NPP/LITE, Laurell Technologies Corporation, US) at 3500 rpm for 30 s, and then the cellulose thin film on the Si wafer was immersed in a batch of fresh HPLC grade H_2O for 1 h and afterwards immersed into another batch of fresh HPLC grade H_2O for 3 h. Finally, the cellulose thin film was dried and stored in a desiccator in the presence of silica gel.

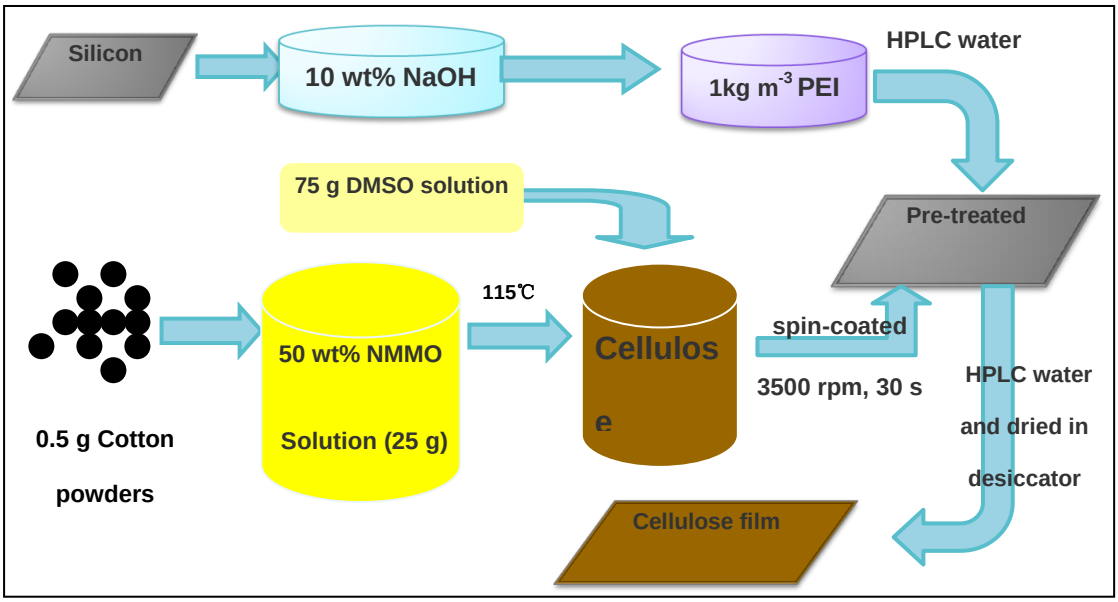

Figure 3.1 Schematic illustrating the protocol to prepare a cellulose thin film.

3.1.2.2 Polyethylene terephthalate (PET) films

A flat polyethylene terephthalate (PET) film was used to mimic an artificial fabric surface in Chapter 6 and it was provided by Goodfellow, UK. The PET film is amorphous with a thickness of 0.25 mm. The film was cut into small pieces (3 cm × 1 cm) and they were used directly for further investigation.

3.1.2.3 Glass slides

Fisherfinest premium plain glass microscope slides (Fisher Scientific, UK) were used as model substrates in Chapter 7.

3.1.3 Chemicals used to modify microcapsules and model fabric surfaces

Polyvinyl formamide (PVF): PVF in water solution with 20% hydrolysis was provided by P&G (Belgium). It is a long linear cationic polymer with a high molecular weight (1000 kg mol^{-1}). The structure of the PVF is shown in Figure 3.2(a).

Chitosan: chitosan was purchased from Sigma-Aldrich, UK with a molecule weight of 400 kg mol^{-1}; it is a positive polysaccharide containing D-glucosamine groups (Che *et al.*, 2008) and it bears a long linear structure with spiral planes (Figure 3.2(b)).

Poly (ethyleneimine) (PEI): 50% (w/v) PEI in water solution with a molecule weight of 750 kg mol^{-1} was provided by Sigma-Aldrich, UK. PEI is a branched cationic polymer bearing amine groups and the structure is presented in Figure 3.3 (c).

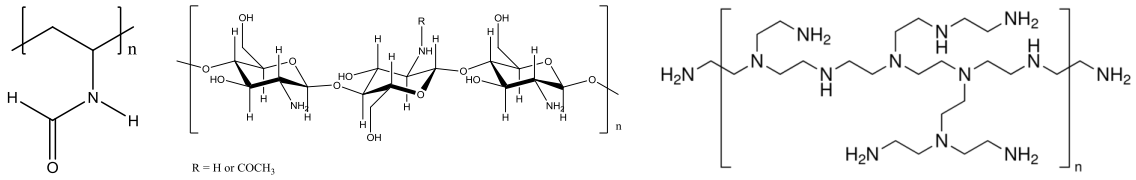

(a) (b) (c)

Figure 3. 2 The structure of PVF (a), Chitosan (b) and PEI (c) drawn with ChemDraw Software.

3.2 Modification of microcapsules and model fabric surfaces with PEs

3.2.1 Treatment on surface of microcapsules

3.2.1.1 Preparation of polyelectrolyte (PE) solution

PVF solution with 20% activity (1000 kg mol^{-1}, P&G, Brussels) and perfume-filled microcapsules (P&G, Brussels) were used as received, and they were diluted into 0.1 wt% and 1.0 wt% respectively. Chitosan (Sigma-Aldrich, UK) was dissolved into 10 wt% acetic acid (Sigma-Aldrich, UK) solution and then diluted to 0.1 wt% with HPLC grade H_2O. 10 wt% NaOH solutions were used to adjust polyelectrolyte (PE) solutions to pH 6.

3.2.1.2 Modification of MF microcapsules with PE solution

PVF and chitosan solutions were used to modify perfume microcapsules respectively. 0.1 wt% PVF and 0.1 wt% chitosan solutions each was added into a suspension of 1.0 wt% perfume microcapsules, which were then agitated with a Vortex mixer (FB15012 TopMix, Fisher Scientific) at 3000 rpm for 5 min. Then the modified microcapsules were used for further investigation.

3.2.2 Treatment on surface of model fabric surfaces

3.2.2.1 Preparation of polyelectrolyte (PE) solutions

0.1 wt% PVF and 0.1 wt% chitosan solutions prepared as described in § 3.2.1 each was further diluted to 0.01 wt% and 0.001 wt% with HPLC grade H_2O. 50% (w/v) poly

(ethyleneimine) (PEI) in water solution (Sigma-Aldrich, UK) was diluted into 0.1 wt%, 0.01 wt% and 0.001 wt% solution respectively with HPLC grade H_2O. 10 wt% NaOH solution was used to adjust PE solutions to pH 6.

3.2.2.2 Modification of model fabric surfaces for flow chamber experiment

Flow chamber experiment: to modify the model fabric surfaces (cellulose thin film/ PET surface in Chapter 5 and Chapter 6), 0.1 mL of PVF/chitosan/PEI solution with a prepared concentration was injected to the flow chamber, full details of which are given in § 3.4.1, using a model fabric substrate of lateral dimensions 1.5 mm × 24 mm; the substrate dimensions were chosen to match the internal dimensions of the flow chamber. The solution and substrate were left in contact for 30 minutes. A continuous flow of distilled H_2O at 10 mL h^{-1} was subsequently used to remove any unabsorbed PE molecules and wash the PE-modified cellulose thin film for 5 minutes. The modified substrate was further used for investigating the removal behaviour of microcapsules on it in the flow chamber (§ 3.4.1).

3.2.2.3 Modification of model fabric surfaces for AFM measurement

AFM measurement: 140 µL of PE solution was deposited on a model fabric surface (cellulose thin film/ PET surface) of dimensions 10 mm × 10 mm and left in contact for 30 min, in order to maintain the same concentration of PE per unit area as used in the flow chamber experiment. The PE-modified model fabric surface was then spun for 30 s at 1000 rpm using a spin processor (WS-400-6NPP, Laurell Technologies, USA). The PE-modified model fabric surface was then immersed in HPLC grade H_2O for 5 min, before being used as the substrate in the AFM measurement.

3.3 Characterization of microcapsules and substrate surfaces

3.3.1 Optical microscopy

The basic principle of optical microscopy is to magnify small samples or objects by using visible light and a serious of lenses. Firstly, an optical microscope (Leica DM RBE, Leica Microsystems GmbH, and Germany) equipped with Leica QWin Pro V2.8 software (Leica Microsystems Imaging Solutions Ltd., UK) was used to capture the image of microcapsules remaining on a transparent substrate (PET surface or glass substrate). Another optical camera (Navitar; with a light source on top (LLS - LED Light Source)) with Leica QWin Pro V2.8 software (Leica Microsystems Imaging Solutions Ltd., UK) was used to capture the images of microcapsules remaining on opaque substrates (cellulose film) for flow chamber experiments (§ 3.4.1).

The optical microscope (Leica DM RBE, Leica Microsystems GmbH, and Germany) equipped with Leica QWin Pro V2.8 software (Leica Microsystems Imaging Solutions Ltd., UK) was also used to capture the image of a microcapsule colloidal probe to ensure the single microcapsules were properly attached to the end of a tipples cantilever for adhesion measurements by AFM; the captured image was further analysed to calculate the diameter of the microcapsule and the distance between the end of the cantilever and the centre of microcapsule, which were used to calculate the spring constant of the cantilever with an attached microcapsule (Bowen *et al.*, 2010).

3.3.2 Particle size

The size distribution of microcapsules was characterized by a Malvern Mastersizer (APA2000, Malvern Instruments Ltd., UK) which connects with a small volume entry level wet dispersion unit (Hydro 2000SM) constituting of a continuously variable single shaft pump and a stirrer dispersion unit (Hydro 2000SM). The size range (diameter) which can be measured is from 200 nm to about 2000 μm. The principle of the measurement is based on Dynamic Light Scattering (Malvern, 2007): microparticles in a stable aqueous dispersion with a suitable concentration were delivered to the optical measurement area (optical bench) with the continuously variable single shaft pump which is contained in Hydro 2000SM dispersion unit and then a laser beam was applied to illuminate these microparticles. The intensity of the light scattered by the microparticles within the sample over a wide range of angles were collected by a series of detectors (Figure 3.3 (a)). The particles scattered light at an angle which is inversely proportional to their size (Malvern, 2007) (Figure 3.3 (a)). Then the mean diameter and the distribution of particles can be obtained by analysing the intensity of light scattered according to Mie Theory (Merkus, 2009). In order to use Mie Theory, the optical property (the refractive index) of the particle and the medium should be provided. The refractive index values of the MF microcapsules and the water are 1.65 (Brydson, 1999) and 1.333 (Hecht, 2003) respectively.

Procedures: A suspension of 0.1 wt% MF perfume-filled microcapsules was added to the sample unit with a 2000 rpm agitation speed until the concentration of microcapsules reached an optimum concentration range indicated by the software. 5

separate samples from the same batch were measured and data were averaged in order to obtain a mean value of the particle size and error bar.

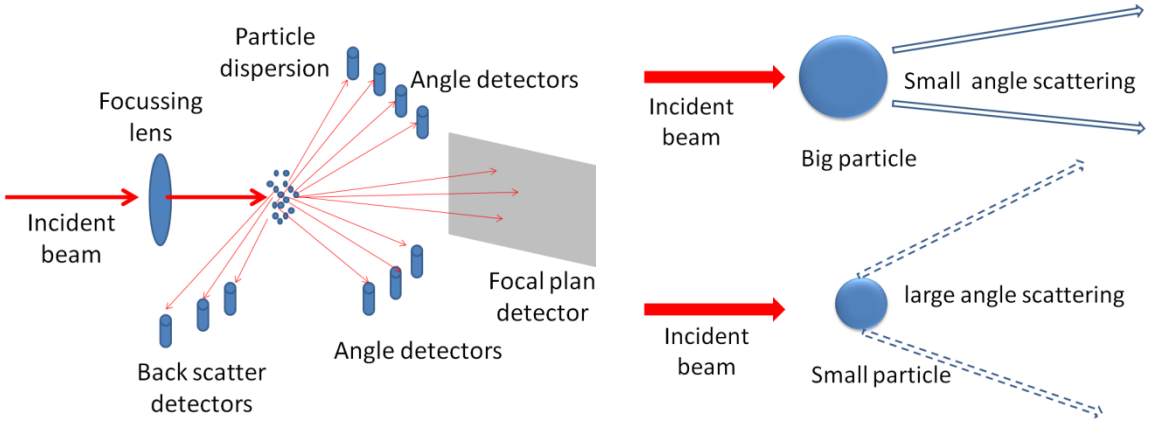

(a) (b)

Figure 3.3 Schematic representation of particle size measurement by the dynamic light scattering (a); the relationship between particle size and the scattering angle (a).

3.3.3 Zeta potential

A Zetasizer Nano Series (Malvern Instruments Ltd, UK) with disposable folded capillary cells was employed for determining the zeta potential of perfume-filled microcapsules, cotton powders in aqueous solution, and PVF/chitosan/ PEI solution. A Zetasizer Nano ZS is capable of determining the zeta potential of particles with a diameter of 3.8 nm to 100 μm. A dispersed particle or big molecule in a medium may bear surface charges and these charges affect the ionic distribution in the surrounding medium; some opposite charged ions will gather at the surface of the particle and form a strong bond, which is knowing as the Stern layer; and then more ions will bond the particle next to the stern layer loosely but work as a part of the whole when the particle

moves, which is called the slipping layer; zeta potential is the charge difference between the slipping layer and the bulk solution (Hunter, 1981, Myers, 1991, Hunter, 2001). A structure diagram of a negative charged particle in a medium is presented in Figure 3.4 to illustrate the concept of surface charge, stern charge and zeta potential. Therefore, zeta potential, which represents the effective charge on the particle, is a function of surface charge and the properties of the surrounding medium and it is always different from stern charge and surface charge (Malvern_Instruments, 2007). Zeta potential is usually, but not necessarily, of the same sign as the surface charge (Hunter, 1981) .

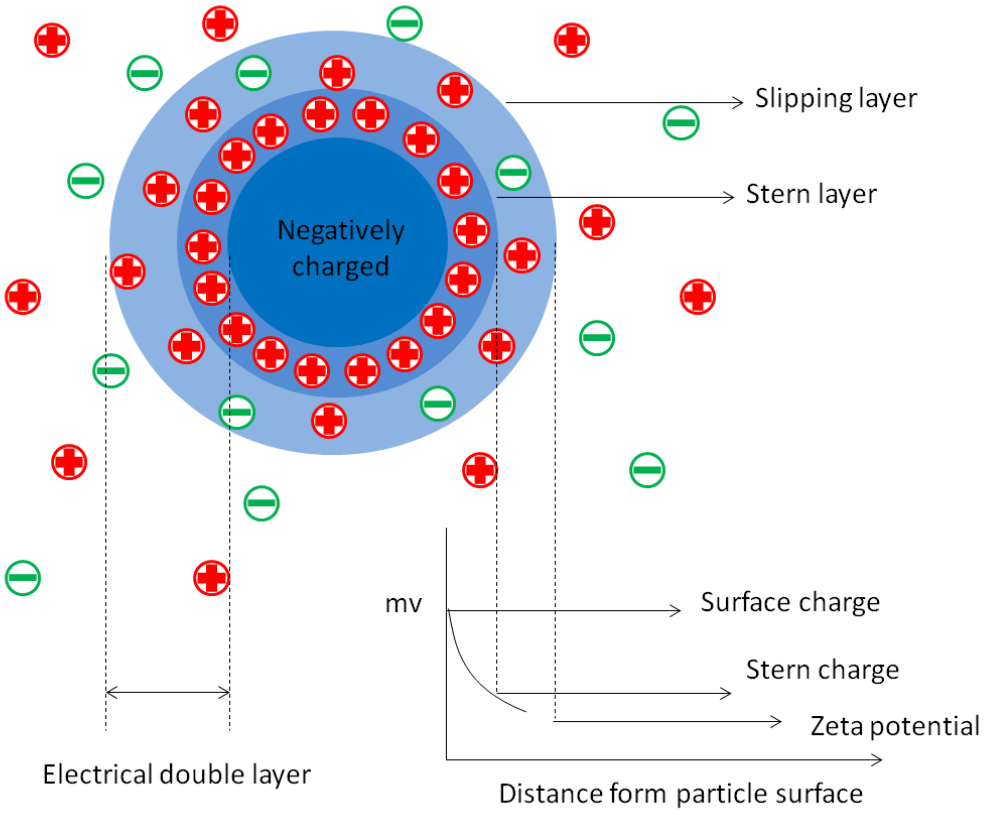

Figure 3.4 A schematic diagram to illustrate zeta potential (Malvern_Instruments, 2007).

The principle of the Zetasizer technique: the particle with a zeta potential is moved towards an oppositely charged electrode by applying an electric field across the dispersion. The velocity relevant to the electrophoretic mobility of the particle can be determined by a patented laser interferometric technique (M3-PALS, Phase analysis Light Scattering) (Malvern); and the electrophoretic mobility was converted to zeta potential by inputting the dispersant viscosity and dielectric permittivity, and the application of the Smoluchowski theories (Hunter, 1981, Sze *et al.*, 2003).

Perfume-filled microcapsules were diluted into deionised H_2O with a concentration of 0.1 wt%. 0.1 wt% PVF/Chitosan/PEI solution was prepared according to the protocol described in § 3.2. HCl and NaOH aqueous solution was used to adjust pH of the microcapsule suspension and polyelectrolyte solutions. 0.1 wt% microcapsule suspension and 0.1 wt% PVF/chitosan/PEI solutions with pH values of 3, 5, 7, 9 and 11 were formulated. Then, 3 separate samples from the same batch were measured and data were averaged in order to obtain a mean value for the zeta potential and error bar.

3.3.4 X-ray Photoelectron Spectroscopy (XPS)

X-ray Photoelectron Spectroscopy at the University of Warwick was used to do surface composition analysis. The principle of XPS is illustrated in Figure 3.5. An X-ray photon with energy of $h\upsilon$ is incident on the surface and the energy is absorbed by an atom with binding energy of E_B. When $h\upsilon > E_B$, the core electron with E_k is excited from the atom and then escapes into the surrounding environment. It is unique for each core electron bound to the atom; therefore XPS analysis can provide detailed information of the composition of a material. An ultra-high vacuum environment is often needed for XPS

analysis in order to maximise the free path of the electrons and increase the probability of detection. The binding energy can be calculated by equation (3.1)

$$E_B = h\upsilon - E_k - \phi_{analyser} \tag{3.1}$$

where $\phi_{analyser}$ is the work function of the electron analyser.

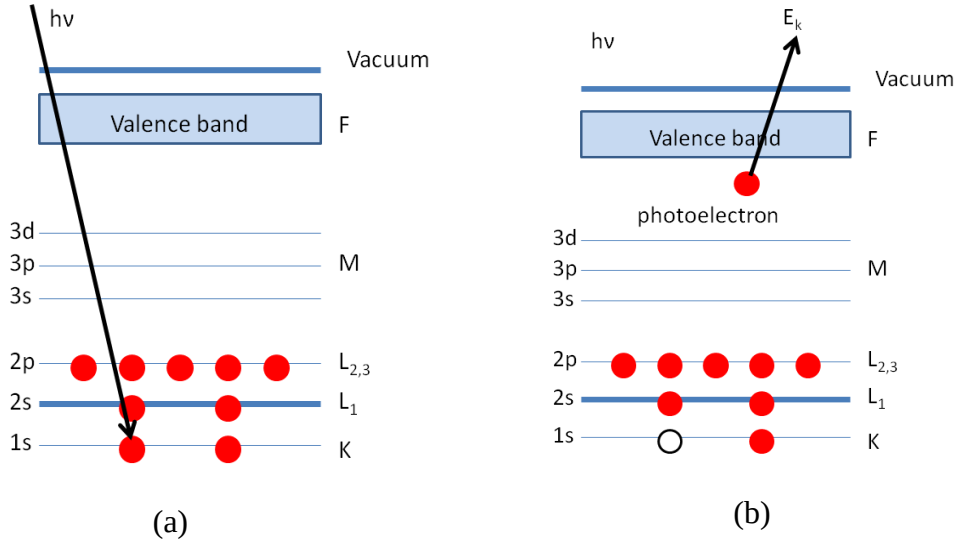

Figure 3.5 A schematic diagram showing the principle of the XPS technique: (a) the incidence of an X-ray photon with energy of $h\upsilon$ (b) the excitation of an electron with energy of E_k from the atom.

XPS was used to analyse the surface composition of the cellulose film to make sure there was no residual solvent on the surface. Additionally, both cellulose films and polyester surfaces were modified with PVF, chitosan and PEI respectively, and XPS was used to detect these chemicals attached on the surfaces. The unmodified cellulose film was used as manufactured and the PET surface was used as received. The PE-modified cellulose films/PET surfaces were prepared by applying 0.1 wt% a PE solution to an unmodified substrate for 30 min. In order to maintain the same concentration of

PE per unit area, the same volume/area ratio was maintained as described in § 3.2. Samples were gently washed with HPLC grade H_2O before drying under a stream of N_2. The substrates were analysed using a monochromated Al κα X-ray source (1486.6 eV) and the data acquired at normal emission with respect to the sample surface using a sampling spot size of diameter 1.2 mm. The analysis chamber base pressure was 2×10^{-11} mbar. The C 1s, O 1s, and N 1s photoelectron peaks were acquired using a pass energy of 20 eV, which gave an energy resolution of 0.69 eV. The cellulose film is insulating and can become positively charged as electrons leave the sample surface. Therefore a flux of 1 eV electrons was used to compensate. Data were analysed using the CasaXPS package using Voigt lineshapes, a mixture of Gaussian and Lorentzian lines.

3.3.5 Environmental Scanning Electron Microscope (ESEM)

The surface topography of microcapsules and MF membrane for the work presented in Chapter 4, Chapter 6 and Chapter 7 was scanned by an environmental scanning electron microscope (Philips XL30 ESEM-FEG fitting with an oxford Inca 300 EDS system, The Netherlands). ESEM is capable of collecting electron micrographs with high resolution at low vacuum and high temperature, which provided the capability to examine different kinds of samples such as wet, oily, and non-conductive surfaces in their original state without complex sample preparation and treatment (Danilatos, 1997). In this work, ESEM was used to scan the microcapsule surface and MF membrane in dry condition; therefore it functions in the same principle of scanning electron microscope (SEM) (Reimer, 1998, Goldstein *et al.*, 2003).

The principle of the technique: a focused beam of high-energy electrons is used to scan the sample surface and then the electrons interact with the atoms which will emit different types of electrons (Figure 3.6) as the signals to reveal the information of the sample, including secondary electrons (SE), backscattered electrons (BSE), and X-Rays (Reimer, 1998). These can be collected by different kinds of detectors and then analysed to get information of the sample. Normally, the SE and BSE are used to produce images; the characteristic X-rays of photons are used to analyse elements, which can be used to determine chemical compositions (energy-dispersive X-Ray Spectroscopy (EDS) (Goldstein *et al.*, 2003)). Compared with a conventional microscope, the size of the electron spot and the interaction volume are the critical parameters to determine the resolution of ESEM (SEM) (Goldstein *et al.*, 2003).

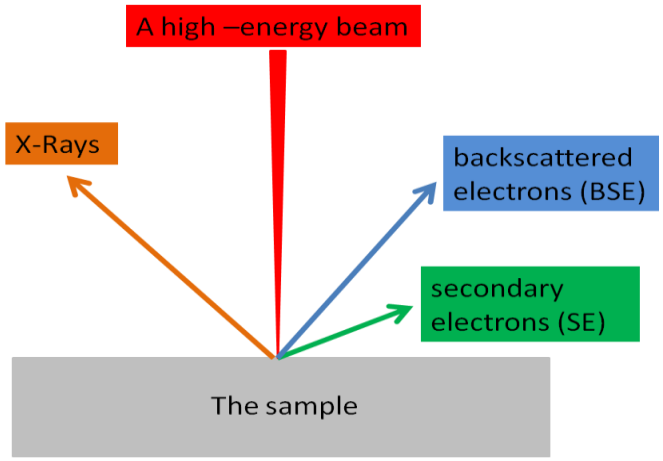

Figure 3.6 A schematic diagram to show the emitting of electrons.

0.1 wt% microcapsules in distilled water before and after their surfaces were modified with polyelectrolytes (PEs) were placed on double sided adhesive carbon filled conductive discs which were fixed on a pin mount stubs, and then they were dried in

ambient air; a MF membrane was placed on double sided adhesive carbon filled conductive discs which were fixed on a pin mount stub. A layer of gold with a thickness of about 5 to 6 nm was coated on the MF microcapsules or MF membrane in a sputter coater (Polaron S07640, Quorum Technologies Ltd, UK) in order to make the surface conductive. The beam energy and exposure time used in this work were controlled to be less than 20 kV and 1 minute to prevent damage to the microcapsules within 1 minute in dry environment (Ren 2007).

3.3.6 Interferometry

The surface topography of cellulose thin films and Si wafers was captured using a vertical scanning white light interferometer (MicroXAM2, Omniscan, UK), and the acquired data were analysed using Scanning Probe Image Processor software (Image Metrology, Denmark). The principle of the interferometer is to use the superposition of waves to combine them in a way in which some information about the sample properties and the original state of the waves can be diagnosed (Hariharan, 2007). In this work, the specimen was moved vertically over the full height range of the sample in order to find the position of maximum fringe contrast for each pixel. Then the analysis of nearby positions will produce an image of surface topography and information about surface roughness.

The cellulose thin films and Si wafers were used directly without any treatment by using a vertical scanning white light interferometer (MicroXAM2, Omniscan, UK). Samples were measured as prepared, and the acquired data were analysed using Scanning Probe Image Processor software (Image Metrology, Denmark). The scan area

was 839 μm x 639 μm and 3 separate images were acquired for each sample to calculate the root mean square (RMS) roughness and error bar.

3.3.7 Contact angle

The hydrophilic and hydrophobic nature of MF membranes in Chapter 6 and the PET surfaces before and after being treated with PE molecules were characterised using a contact angle measurement apparatus equipped with a Charge Coupled Device (CCD) camera (KP-M1E/K, Hitachi) (School of Chemistry, The University of Birmingham). The contact angle was used to indicate the affinity of a water droplet to the surface. The surface is considered to be hydrophobic with a larger contact angle (>90 °) and hydrophilic with a small contact angle (<90 °) (Kwok and Neumann, 1999).

A water droplet with a volume of approximately 1 μL was placed on a piece of PET surface and the profile of the water droplet was visualised with a side view camera within 30 seconds in order to obtain the equilibrium contact angle. FTA (First Ten Angstroms) video analysis software v1.96 was used to analyse the image subsequently to determine the contact angle; all the measurements were performed at room temperature of 20 ℃. At least 5 separate measurements were acquired for each sample to calculate the mean contact angle and error bar.

3.3.8 Viscosity

An AR-1000 Rheometer (TA Instrument, UK) with Rheology Advantage softerware (TA Instrument, UK) was used to measure the viscosity of the PE solutions. In

principle, the viscosity represents the resistance of a fluid to the gradual deformation by shear stress or tensile stress. It was used to indicate the information of the polymer molecule (Ofori-Kwakye *et al.*, 2006). The parallel plate system was chosen to do the measurement and an acrylic plate with a diameter of 40 mm (TA Instrument, UK) was used as the rotor. Approximately 2 mL of 0.1 wt% PE solution was placed on the sample stage and its temperature was maintained at 25℃ and the gap between the sample stage and the acrylic plate was 1000 μm. Then the experiment was performed to measure the viscosity by increasing the shear rate from 10 (s^{-1}) and 100 (s^{-1}). Each measurement was repeated twice to calculate the mean viscosity.

3.3.9 AFM imaging

A NanoWizard®II AFM with an attached CellHesion module (JPK Instruments, UK) was used for imaging cellulose films and polyester surfaces. The basic principle of AFM is that a cantilever with a sharp tip (probe) scans over the surface of the specimen and then the reflection of the light focusing on the back of the cantilever resulting from the interaction between the tip and the surface is recorded into an electrical signal of voltage, which is then used to produce image information (Binnig *et al.*, 1986, Nader and Karthik, 2004). Figure 3.7 shows the deflection of the cantilever and the signal recording in AFM. In order to get the topography information of a sample, the cantilever with a tip needs to be moved over the target surface. Therefore, the feedback and image control is significant. The most common used feedback control modes includes contact mode (Figure 3.8 (a)), intermittent contact mode (Figure 3.8 (b)), non-contact mode (Figure 3.8 (c)) and force modulation mode (Figure 3.8 (d)) (JPK Instruments, 2009). The tip never leaves the surface during the scanning process if

contact mode or the force modulation mode is used, which generates images with high resolutions, but it always causes large forces in the lateral direction, leading to the disruption of the surface (Nader and Karthik, 2004). Less or no contact between the tip and the surface can be achieved by applying the intermittent contact mode and non-contact mode, which decreases the lateral force significantly. However, the presence of the attractive force, especially the capillary force in the ambient environment, makes a jump of the cantilever to the surface possible, which can ruin the no-contact condition (García and Pérez, 2002).

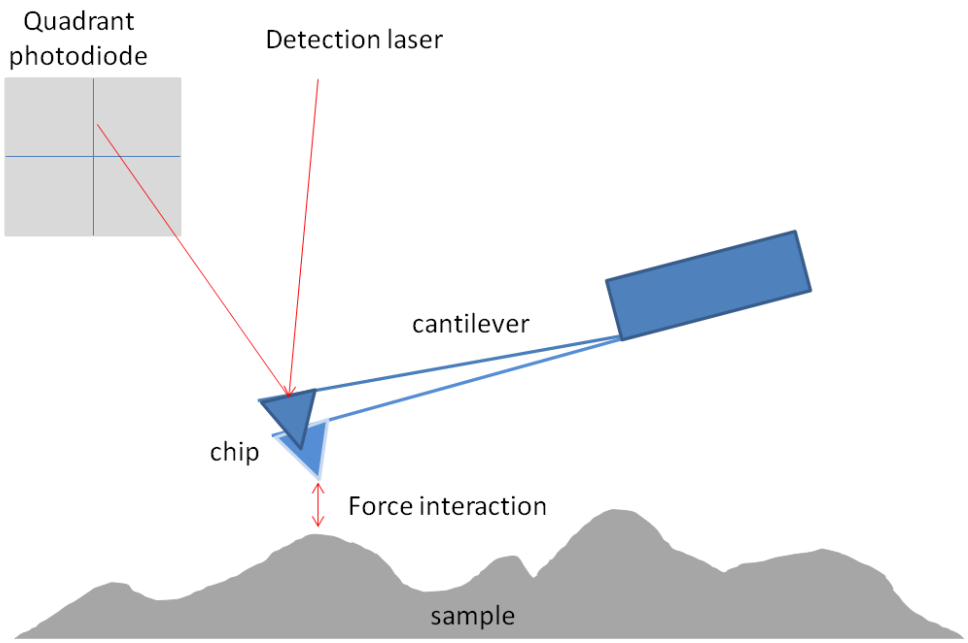

Figure 3.7 A schematic diagram to show the deflection and recording of the beam signals by AFM (JPK Instruments, 2009).

In this work, imaging was performed in intermittent contact mode using a pyramidal-tipped Si cantilever (RTESP, Veeco, France) with a nominal spring constant of 40 N m^{-}

[1] in ambient conditions. A scan rate of 1 Hz and a resolution of 1024 × 1024 pixels were set for all the scanning. At least 3 separate images were acquired for each sample to calculate the root mean square (RMS) roughness.

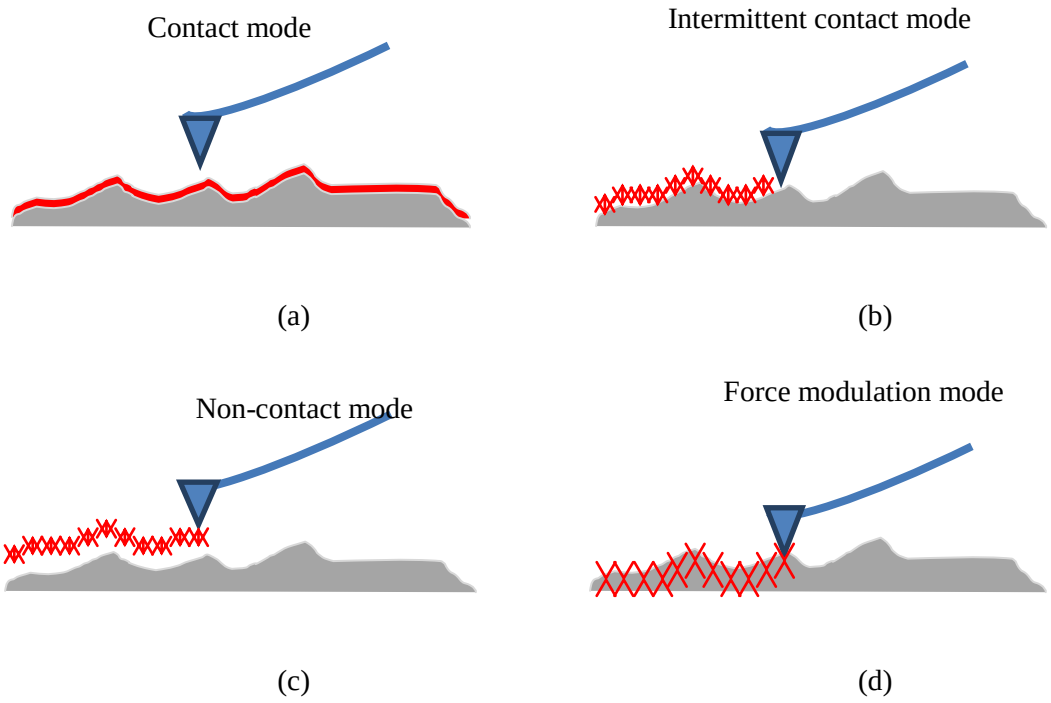

Figure 3.8 The control mode used for AFM imaging: contact mode (a); intermittent contact mode (b); non-contact mode (c) and force modulation mode (d) (JPK Instruments, 2009).

3.4 Characterization of microcapsule adhesion to and removal from surfaces

3.4.1 Flow chamber technique

A parallel-plate flow chamber was purposely built in order to measure the retention and removal behaviour of a population of microcapsules on a model fabric surface in an aqueous environment. The principle of the flow chamber technique is to displace particle from a substrate with hydrodynamic force (Decuzzi *et al.*, 2007).

3.4.1.1 Construction of the flow chamber system

The flow chamber (Figure 3.9 (a)) consisted of a top plate, a gasket with a rectangular channel, a cellulose film substrate, a piece of soft rubber, a bottom plate and suitable screws. Figure 3.9 (b) shows a schematic of the flow chamber: (1) a rectangular transparent plastic plate (PMMA, 70 mm × 30 mm × 5 mm) with an entrance, outlet port and sample injection port; (2) a gasket (70 mm × 30 mm × 5 mm) with a rectangular channel (24 mm × 1.5 mm × 1.5 mm) as the main body of the flow chamber; (3) a piece of model fabric surface with dimensions greater than those of the rectangular channel as the bottom substrate of the flow chamber; (4) a piece of soft rubber to ensure a well-defined seal between the cellulose film and the bottom plate; (5) a piece of transparent rectangular plastic plate (PMMA, 70 mm × 30 mm × 5 mm) as the bottom of plate. The flow chamber was fabricated by fixing the above pieces together with screws, which was then connected to a syringe pump (KD 100, KD Scientific Inc., USA) and a waste tank with rubber tubes, having an inner diameter of 2 mm. Figure 1 (b) shows a schematic of the visualisation and measurement system. The schematic diagram of the system can be seen in Figure 3.10.

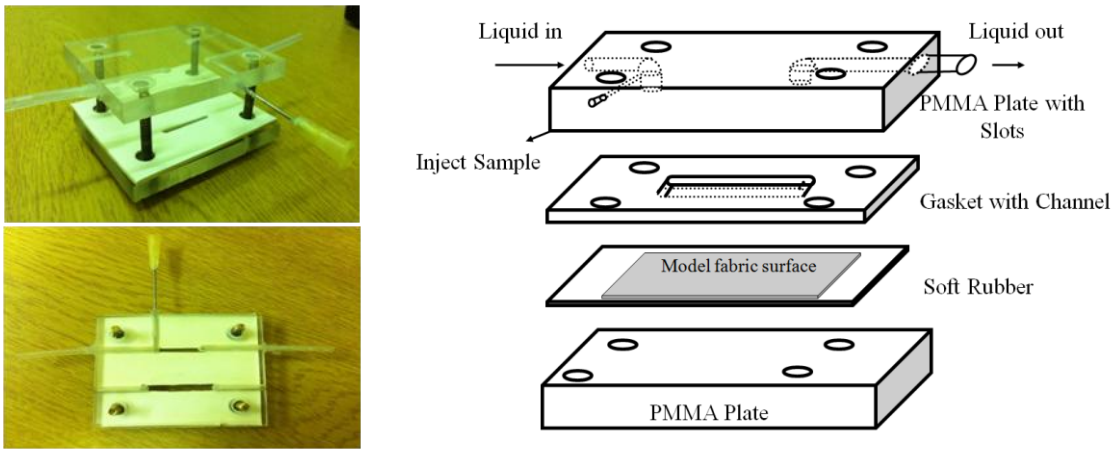

Figure 3.9 The image of the flow chamber (a); a schematic representation of the flow chamber (b).

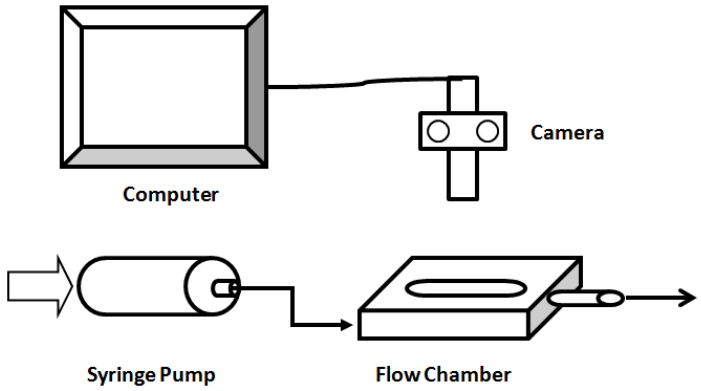

Figure 3.10 The schematic diagram of the flow chamber system.

3.4.1.2 Removal/retention measurement with the flow chamber device

(1) The retention of microcapsules to a model fabric surface for the experimental work presented in Chapter 5 and Chapter 6: Distilled H_2O was pumped through the system ensuring no air bubble was present. 0.2 mL microcapsule suspension (0.5 wt%) was then injected into the chamber through the sample injection port and these microcapsules were allowed to settle for 10 min. Subsequently, the system was subjected to a flow of 0.1 mL h^{-1} for 5 min in order to remove any suspended free oil

droplets introduced by occasional breakage of microcapsules and air bubbles imported by injection. A Navitar optical camera with an attached LED light source coupled with Leica QWin Pro V2.8 software (Leica Microsystems Imaging Solutions Ltd., UK) was used to capture the images of 6 positions in the flow chamber, as shown in Figure 3.11. Images of these six positions were recorded as the flow rate was increased, and continued to be taken until after removal of the microparticles deposited in these positions. All the experimental work was carried out at a flow rate which was equal or less than 200 mL h^{-1} and the Re number was far less than 2100; therefore the flow in the flow chamber system was in the laminar flow condition. A schematic diagram of the captured areas and an example of a series of 6 images before and after using water flow is presented in Figure 3.11.

(2) The removal of single microcapsules from a glass surface in the flow chamber for the experimental work presented in Chapter 7: Distilled H_2O was pumped through the system ensuring no air bubble was present. 0.1 mL microcapsule suspension (0.1 wt%) was injected into the chamber through the sample injection port and these microcapsules were allowed to settle under gravity for 10 min. Subsequently, the system was subjected to a flow of 0.1 mL h^{-1} for 5 min in order to remove any suspended air bubbles entrained by injection and unsettled microcapsules. Then a water flow of 10 mL h^{-1} was used to remove the microcapsules for 10 min. A video system was applied to monitor the fully developed flow region to ensure there is no suspended microcapsule in the region and the remaining microcapsules are far away from each other. The flow rate was then increased with an increment of 2 mL h^{-1}, and the removal of microcapsules was monitored by the video system.

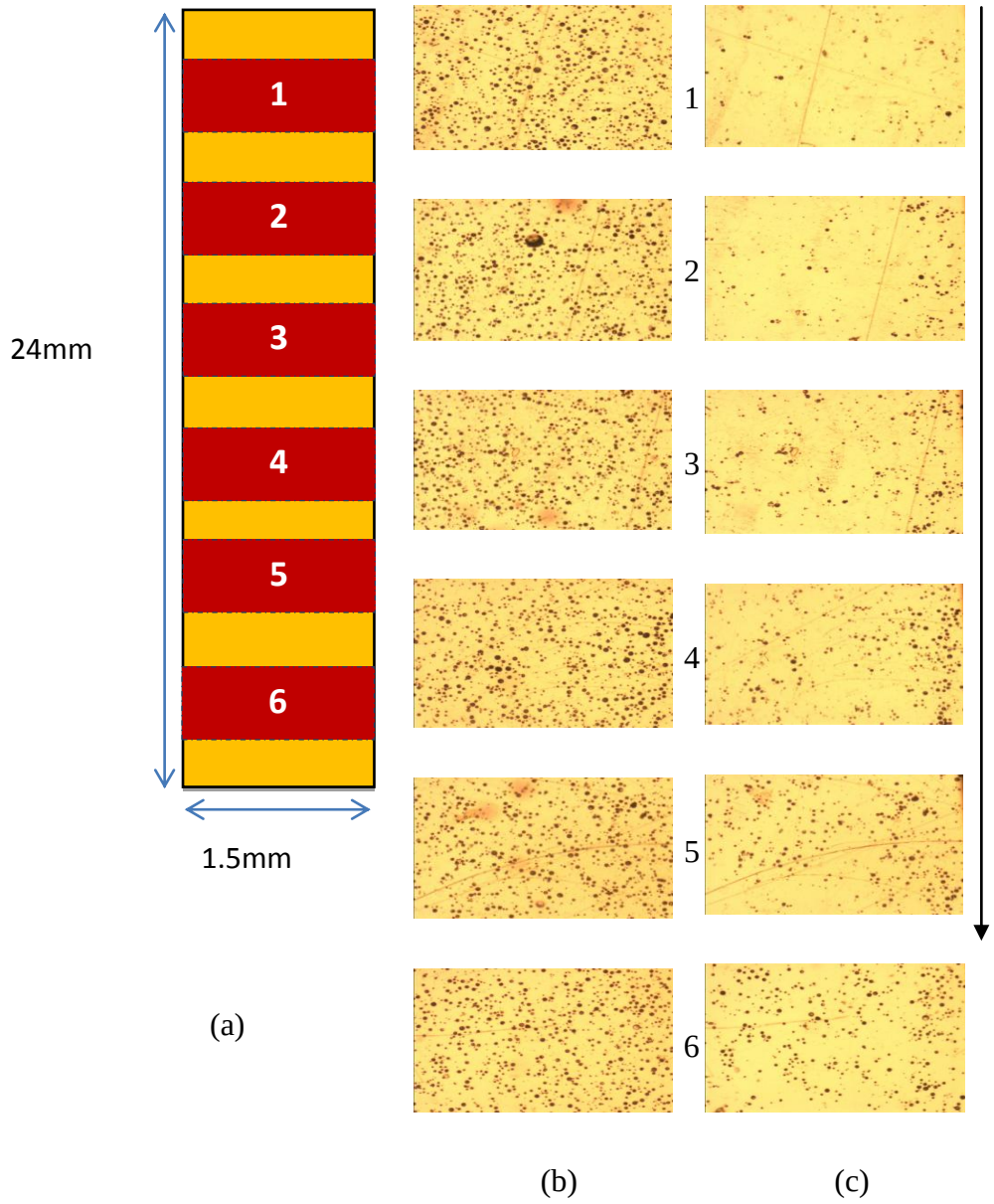

Figure 3.11 Images captured (6 red areas) in the channel (a); the images of microcapsules on PET surface before (b) and after (c) a water flow of 200 mL h^{-1} for 3 min. The black arrow indicates the flow direction.

3.4.1.3 Calculation of surface area occupied by microcapsules

A MATLAB code for calculating the surface area occupied by microcapsules for the experimental work presented in Chapter 5 and Chapter 6 was provided by Dr James W.

Andrews in the School of Chemical Engineering, University of Birmingham. The code was used to calculate the area ratio covered by microcapsules (the black spots in the original image) for each image (the red colour area in Figure 3.11). The original image (Figure 3.12 (a)) was converted into a grey-scale image (Figure 3.12 (b)), and then a black and white image (Figure 3.12 (c)) was generated to remove the shadow and fill the hollow holes with MATLAB. Then MATLAB was used to get the particle size distribution (Figure 3.12 (d)) and surface area covered by the microcapsules on the capture area. The MATLAB code was presented in Appendix I.

The surface area occupied by a single microcapsule was recorded as $A_{i,}$

the total area occupied by microcapsules is

$$A = \sum_{i=1}^{n} A_i \tag{3.2}$$

where n is the total number of microcapsules;

The normalised area ratio of microcapsules remaining after removal on one position was recorded as

$$a = \frac{A_{afterremoval}}{A_{beforeremoval}} \tag{3.3};$$

The average normalised area ratio in the six positions can be recorded as:

$$\dot{a} = \frac{\sum_{i=1}^{6} a_i}{6} \tag{3.4}.$$

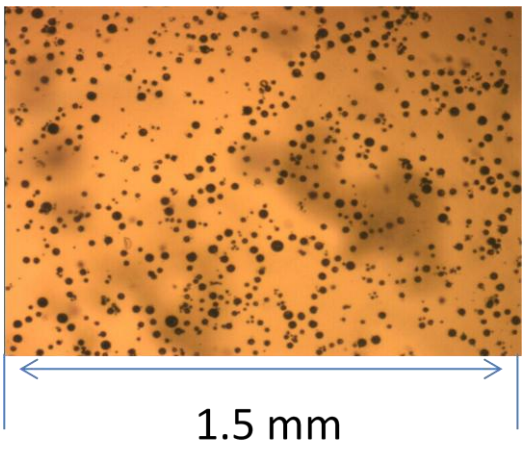

(a) The original image

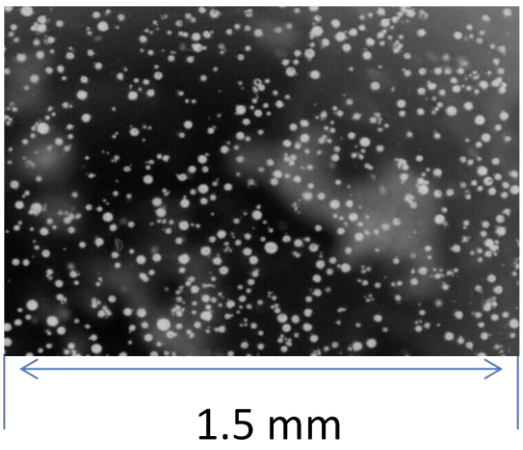

(b) Grey-scale image

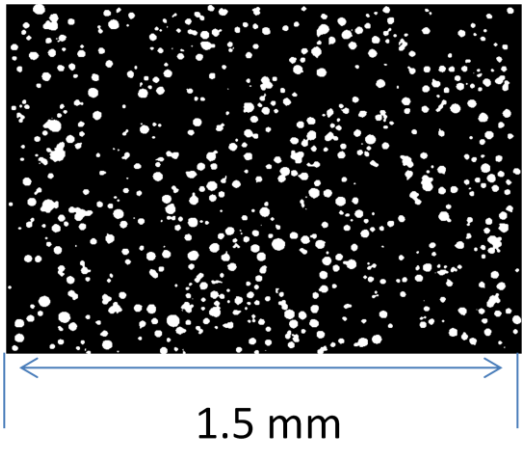

(c) Black & white image

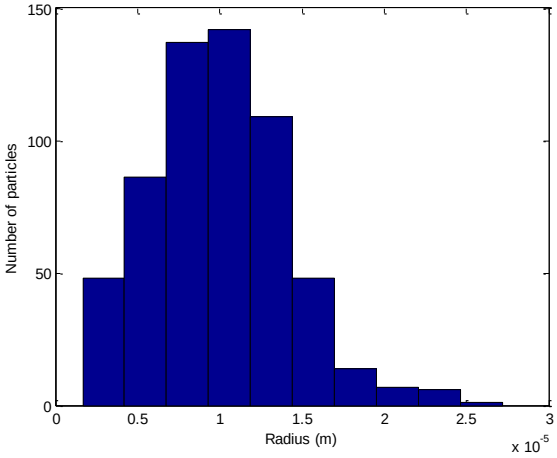

(d) Particle size distribution

Figure 3.12 Calculation of surface area covered by microcapsules using MATLAB.

The video which were used to record the removal of single microcapsules were analysed with the MATLAB code (provided by Dr James W. Andrew in University of Birmingham) to obtain the data of the displaced microcapsules, including the diameter of the microcapsules and the distance of the centre of each microcapsule from the central line of the flow channel before removal.

3.4.2 Measurement of microcapsule adhesion to a surface by AFM

3.4.2.1 The principle of AFM

The NanoWizard® Ⅱ AFM with an attached CellHesion module (JPK Instruments, UK) mentioned in § 3.2.7 was used for measuring the adhesive properties of microcapsules on different substrates in ambient air and aqueous solutions. The principle of the force measurements by AFM is the same as described in § 3.3.9. A tip of the cantilever was bought into contact with the sample directly without moving in the lateral direction, and then retracted from the surface (Binnig *et al.,* 1986). The bending of the cantilever because of the interaction was recorded in an electrical signal of voltage, which was then converted into force according to Hooke's law (JPK Instruments, 2009). In order to examine the interaction between single microparticles and a substrate, an AFM colloidal probe technique (Butt, 1991, Ducker *et al.*, 1992, Kappl and Butt, 2002) was applied. A single microparticle was glued to the free end of a tipless cantilever and the interaction between the particle and a surface could be determined. A schematic diagram in Figure 3.13 illustrates the interaction between a colloidal probe and a substrate on approach and retraction.

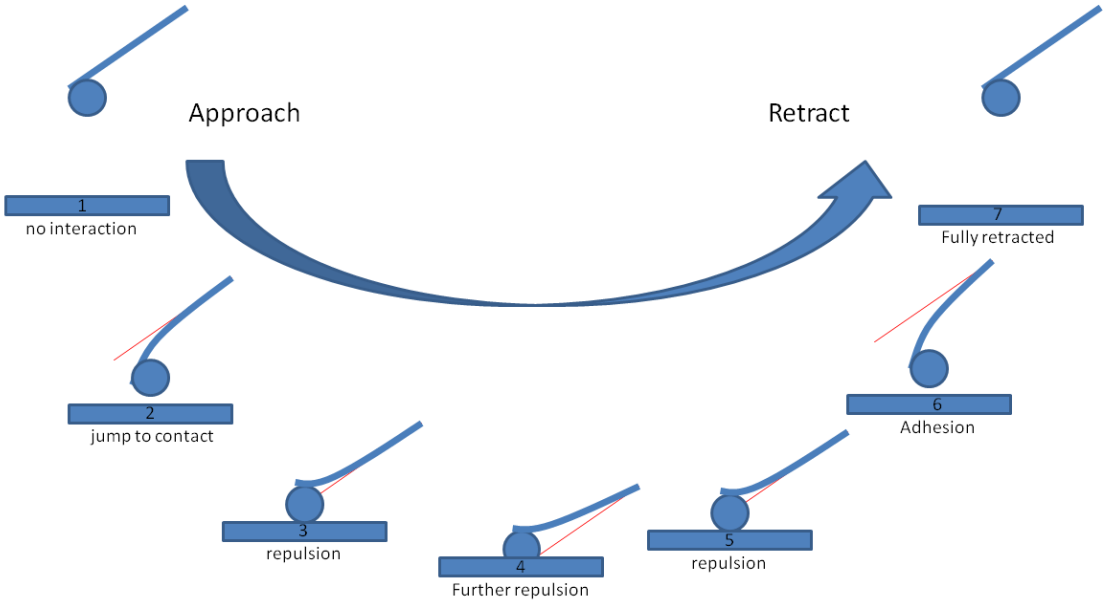

Figure 3.13 The blending of the cantilever with a sphere probe on approach and retraction (JPK Instruments, UK).

3.4.2.2 Preparation of colloidal probe

For measuring the adhesive force between single microcapsules and substrates, tipless rectangular Si cantilevers (NSC12, MikroMasch, Estonia) were used to attach single microcapsules. A schematic diagram of the procedures employed for the attachment of microcapsules to the free end of a tipless cantilever is presented in Figure 3.14, whereby a micromanipulation rig was used for precise displacement control (Zhang *et al.*, 1999). The procedures are listed as follows:

(1) A chip with tipless rectangular silicon cantilevers was reversely held on the micromanipulation rig with a fine glass tube and some Blu Tack, ensuring that the cantilevers were in focus and perpendicular to the incident beam of light.

(2) A droplet of suspension with diluted microcapsules was placed on a glass slide and dried at room temperature, and then the glass slide with microcapsules was

fixed on the sample stage; the glass slide with microcapsules was moved to the screen manually and a candidate microcapsule was focused.

(3) A small quantity of superglue was placed on the glass slide and then the cantilever was made to contact with superglue by moving the stage horizontally and cantilever vertically.

(4) After a fraction of the superglue was attached to the free end of the tipless cantilever, the sample stage was moved quickly to attach the candidate microcapsule; a gentle press on the microcapsule was maintained for a few minutes until the superglue was dried.

(5) At last the attached microcapsule colloid probe was moved upwards and taken away for further experiments.

The cantilever spring constant was calculated by measuring their width, length and resonant frequency according to the method described by Bowen *et al.* (2010).

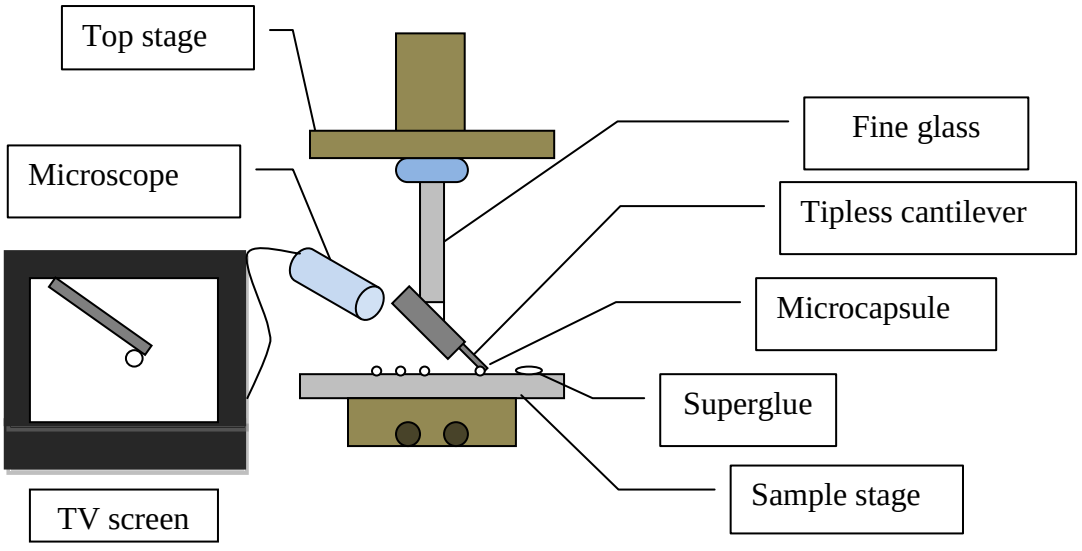

Figure 3.14 Schematic diagram of attaching a microcapsule onto a cantilever with micromanipulation.

3.4.2.3 AFM operation

A model fabric substrate was attached to a poly (styrene) Petri dish, of diameter 35 mm and height 4 mm, which was subsequently firmly secured with double sided carbon adhesive tape (SPI Supplies®) on the stage of AFM. Adhesion measurements were conducted in different environments. In dry conditions, the temperature and relative humidity of the surrounding environment were kept at 18 ℃ and 40%. In aqueous solution, the Petri dish with a substrate was filled to at least 2 mm height with H_2O (HPLC grade, Fisher Scientific, UK), ensuring there were no air bubble present. Upon immersion of the cantilever in the H_2O, the system was left to thermally equilibrate for 10 min. A minimum of 100 measurements were performed over an area of 10 μm × 10 μm for each microcapsule to calculate the mean value of adhesion for the experimental work presented in Chapter 4, 5, 6 and 7. A minimum of 25 measurements were performed over an area of 10 μm × 10 μm for each microcapsule to investigate the adhesion mechanism presented in Chapter 5 and 6. The approach velocity was 20 μm s^{-1}. The particle/surface contact time and the setpoint of compressive load were adjusted according to the requirement of the work described in each chapter. After each set of measurements, the cantilever with the attached microcapsule was washed gently with H_2O to remove any possible contamination on the microcapsule surface. The adhesive force between single microcapsules and substrates were measured in 10^{-3} M, 10^{-2} M and 0.1M NaCl solution to investigate the influence of ionic strength on adhesion; and then in 10^{-3} M NaCl solution, the pH of which was adjusted to the range 3 to 11 to investigate the influence of pH on adhesion.

3.5 Determination of friction coefficient

A model based on the displacement of a single microcapsule from a fabric substrate in the flow chamber was built to understand the mechanism of on-set removal and to interpret the relationship between adhesion and the retention of microcapsules on a surface. The parameter of friction coefficient between the microcapsule and the substrate was needed. Two methodologies based on AFM and a nano-tribometer were used to determine the friction coefficient as follows.

3.5.1 Determination of friction coefficient by AFM

Single microcapsules with a diameter of 8 μm to 25 μm were attached to the end of a tipless rectangular Si cantilever (NSC12, MikroMasch, Estonia), and then the microcapsule probe was used to make friction measurements on different substrates using AFM. The procedure of the calibration of the normal spring constant of the cantilever with an attached microcapsule is described in Bowen *et.al* (2010). The lateral spring constant was measured by using a microcapsule probe to scan a TGF11 silicon calibration grid (Figure 3.15) which consists of a 1-D array of trapezoidal steps with a 10 μm pitch and height of approximately 1.75 μm. The lateral faces of the steps have an inclination angle with respect to the horizontal plane of precisely arctan $\sqrt{2}$ (54°74'). The angle is defined by the crystallography of silicon and is maintained with high accuracy. Direct calibration of the lateral force can be obtained by analysing the contact response measured on the flat and sloped facet.

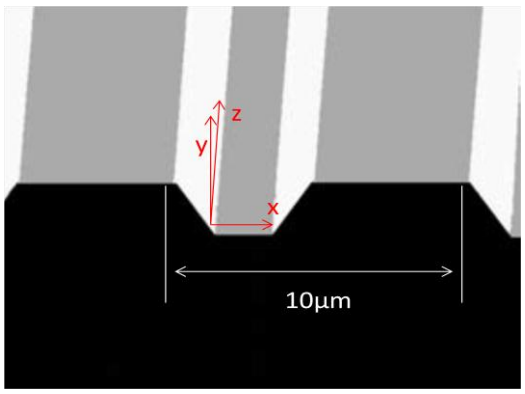

Figure 3.15 The TGF11 silicon calibration grid.

The TGF11 silicon calibration grid was attached to a glass slide, which was subsequently firmly secured on the stage of AFM. Calibration was performed by imaging the TGF11 silicon calibration grid using the microcapsule probe in ambient condition. The cantilever should be parallel to the z direction in Figure 3.15 to ensure that the cantilever scans over the flat and sloped surface. An applied load of 5 nN, a scan area of 50 µm × 2 µm, a scan velocity of 5 µm s^{-1} and a resolution of 512 × 512 pixels were set for all the scanning. The lateral deflection in voltage was recorded for further calculation of the calibration factor and the lateral spring constant of the cantilever (Varenberg *et al.*, 2003, Tocha *et al.*, 2006, Huang *et al.*, 2009).

Additionally, a microcapsule with a diameter of 25 µm was used to scan PET and glass surfaces in H_2O (HPLC grade, Fisher Scientific, UK) using the same scan area and scan velocity. The lateral deflection was recorded by increasing the applied load from 2 nN to 30 nN to investigate the contact issue between microcapsules and a substrate in HPLC grade H_2O.

3.5.2 Determination of friction coefficient by a nano-tribometer

A melamine formaldehyde membrane was prepared and the coefficient of friction between the membrane and a glass sphere which was made of the same material as the glass substrate was measured with a Nanovea Tribometer (Rotative Mode (ASTM G99), Nanovea, USA).

3.5.2.1 Preparation of melamine formaldehyde membrane

A melamine formaldehyde microparticle suspension was produced by in-situ polymerization of MF precondensate and formaldehyde with poly-(acrylamide-acrylic acid, sodium salt) as described in § 3.1.1 (Pan *et al.*, 2012) without adding perfume oil. And then the MF micro-particle suspension was deposited on a glass slide with a spinning disk (WS-400B-6NPP/LITE, Laurell Technologies Corporation, US) at 500 rpm for 30 s; finally, the MF membrane on a glass slide was dried in a desiccator.

3.5.2.2 Friction coefficient measurement

A Nanovea Tribometer (Rotative Mode (ASTM G99), Nanovea, USA) was used to measure the coefficient of static friction between a glass sphere with a diameter of 2 mm and the MF membrane in ambient air and HPLC H_2O. The glass sphere was loaded onto a MF membrane with a precisely known weight and at a specific position from the centre to create a circular wear track as the bottom plate rotated. The friction coefficient was determined from the experiment by measuring the deflection of the direct load cell. The applied force, the radius of the circular wear track and the rotation speed were set at

20 mN, 2 mm and 1mm s^{-1} respectively. For each experiment, the measurement was run for 10 cycles. Five replicated experiments were done for each sample. The Tribometer Friction Software (Nanovea, USA) was used to calculate the coefficient of friction.

Chapter 4: Adhesion of Single Perfume -filled Microcapsules on a Model Fabric Surface Investigated by AFM

4.1 Introduction

Perfume-filled microcapsules are intended to use in a wide range of personal care and household products, such as washing powders (Michael 1990), liquid detergents (Broeckx *et al.*, 2004), bleach (Bianchetti *et al.*, 2010), and personal cleaner (Ouali and Benczedi, 2008), to provide a long-lasting release of pleasant scent to consumers. Among them, the application of perfume-filled microcapsules into liquid detergents has drawn much attention recently (personal communication with Dr. Johan Smets from P&G, Belgium). The retention of perfume-filled microcapsules on fabric surfaces is the key factor to control their application to achieve a high efficiency of usage. However, not all the perfume-filled microcapsules can be kept on fabric surface during and after laundry processes. Therefore enhancement of the retention of perfume microcapsules on fabric surfaces has become an urgent objective which needs to be achieved.

Adhesion was reported in many publications to be enhanced by treating surfaces with functional chemicals such as polyelectrolyte (Biggs, 1996, Boura *et al.*, 2003, Claesson *et al.*, 2003, Borkovec and Papastavrou, 2008, Gurumoorthy and Khan, 2011). This approach has been widely adopted because adhesion can increase either by electrostatic interaction (Holmberg *et al.*, 1997, Claesson *et al.*, 2003) or bridging forces resulting from molecule chains' entanglement (Biggs, 1996, Suraya *et al.*, 2005, Gurumoorthy and Khan, 2011) or their combination (Podgornik and Ličer, 2006). Polyelectrolytes

such as chitosan (Che *et al.*, 2008, Da Róz *et al.*, 2010, Orelma *et al.*, 2011), polyvinyl amine and its derivative (Chen *et al.*, 2006, Notley *et al.*, 2009, Pinschmidt, 2010, Liu, 2012) have been found to enhance the adhesion between cellulose surfaces. Hence, they potentially may be used to enhance the deposition and retention of microcapsules on cotton fabrics.

So far, AFM with a collodial probe (Binnig *et al.*, 1986) is the most common and precise technique to measure adhesive forces between single particles and surfaces. A candidate particle is attached to the end of a microfabricated cantilever and the force between the particle and surface can be measured with AFM in different environments. It is accurate to atomic scale and has been successfully used to measure adhesion in various systems such as between protein layers (Bowen *et al.*, 1998), Saccharomyces cerevisiae cells and mica (Bowen *et al.*, 2001) or glass surfaces (Bowen *et al.*, 2002), a silicon sphere probe and mica surfaces (Vakarelski *et al.*, 2000, Vakarelski and Higashitani, 2001) and between polyester spheres (Hodges *et al.* 2002, Hodges *et al.* 2004) .

In this work, AFM with a colloidal probe was used to investigate adhesion between single microcapsules and a cellulose thin film. At first, cellulose thin films were prepared from cotton powders to mimic a cotton fabric surface. Then MF perfume-filled microcapsules were modified with polyvinyl formamide (PVF) and chitosan respectively and the aggregation of microcapsules and the surface topography were investigated. The adhesion was investigated under various conditions of AFM: compression load, contact time and particle size in order to study their influence on adhesion. After that, adhesion between unmodified and modified single microcapsules and cellulose thin films was investigated in both ambient air and aqueous environments. Finally, the mechanism of adhesion and the reason for the variation of adhesion data

were discussed. It is expected that the work can provide some guidance on further investigation of microcapsules' adhesion to fabric surfaces. Then a rational strategy for increasing the adhesion of perfume-filled microcapsules to fabric surfaces can be proposed in order to achieve the goal of effective delivery of perfume-filled microcapsules to fabric surfaces through laundry process.

4.2 Experimental

4.2.1 Perfume-filled MF microcapsules

Perfume-filled MF microcapsules were supplied by Procter & Gamble, Belgium, see §3.1.1 for more details.

4.2.2 Cellulose thin film

The materials and experimental procedures used to prepare a cellulose thin film were described in detail in §3.1.2.

4.2.3 Modification of microcapsules with chemicals

PVF and chitosan were used to modify the MF perfume-filled microcapsules and the details were described in §3.2.1.

4.2.4 Optical microscopy

The optical microscope described in § 3.3.1 was used to capture the image of a microcapsule colloidal probe to ensure the single microcapsules were properly attached to the free end of a tipples cantilever for adhesion measurements by AFM; the captured image was further analysed to calculate the diameter of the microcapsule and the distance between the end of the cantilever and the centre of microcapsule, which were used to calculate the spring constant of the cantilever with an attached microcapsule (Bowen *et al.* 2010).

4.2.5 Particle size

The mean volume particle size (D4,3) of perfume-filled MF microcapsules was characterized by a Malvern Mastersizer and the detailed information of the technique and the procedures to measure D4,3 were described in § 3.3.2.

4.2.6 Zeta potential

A Zetasizer Nano Series (Malvern Instruments Ltd, UK) with disposable folded capillary cells was employed to determine the zeta potential of perfume-filled microcapsules before and after they were modified with PVF and chitosan in aqueous solution. The details were described in § 3.3.3.

4.2.7 Surface topography by environmental scanning electron microscope (ESEM)

The aggregation, the surface topography of microcapsules before and after modification with PEs and the wall thickness of MF microcapsules were studied by an environmental scanning electron microscope (Philips XL30 ESEM-FEG fitting with an Oxford Inca 300 EDS system, The Netherlands). The detailed information was described in §3.3.4.

4.2.8 Interferometry

The surface topography of silicon wafers and cellulose thin films was captured using a vertical scanning white light interferometer described in §3.3.5.

4.2.9 Atomic force microscopy (AFM)

4.2.9.1 Imaging

The surface topography of silicon wafers and cellulose thin films was acquired by AFM as described in §3.3.9.

4.2.9.2 Force measurement

The adhesion between microcapsules and cellulose thin films in ambient air, HPLC water and 0.2 SDBS (pH 7) aqueous solutions was measured as described in §3.3.9.

4.3 Results

4.3.1 Cellulose thin films

Surface topography of a silicon wafer and cellulose thin film prepared from dissolving cellulose powders characterized by AFM (Figure 4.1) and interferometry (Figure 4.2) shows that a cellulose thin film was deposited on the Si wafer successfully. The RMS roughness of the cellulose thin film with a scan area of 5 μm × 5μm was 5.4 ± 0.4 nm, and the RMS roughness from the interferometer with a large scan area (639 μm × 839 μm) was 29.3 nm. The RMS roughness from AFM is comparable to the result obtained by Liu (2013), which was 5.2 nm over a scan area of 5 μm × 5 μm for a typical cotton film. Compared with a real cotton fibre (the root mean square (RMS) roughness was about 17.6 nm over an scan area of 4 μm^2 (Liu 2010)), the cellulose thin film was much smoother over a similar area.

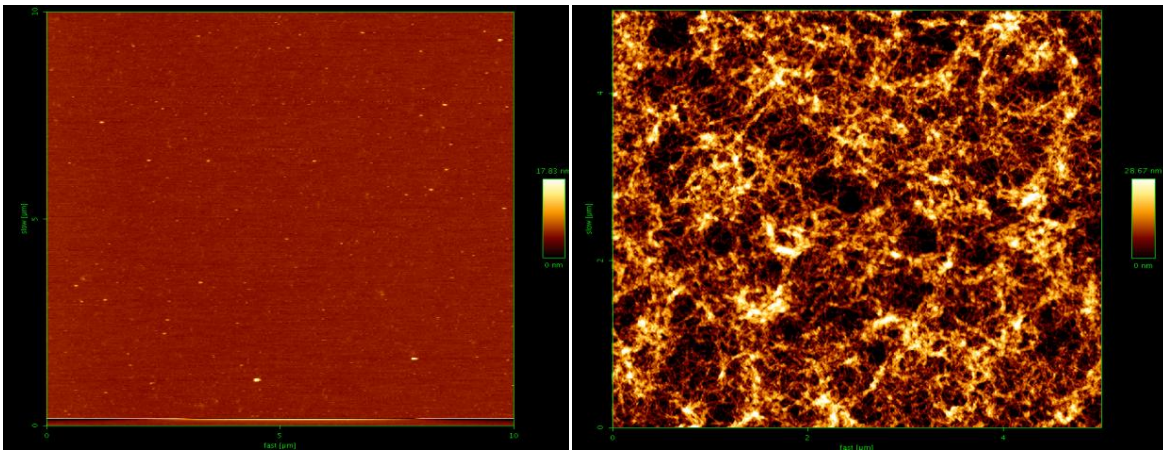

(a) (b)

Figure 4.1 AFM images of (a) bare silicon wafer (RMS = 0.3 nm); (b) dry cellulose thin film made of 0.5 wt% cotton powders (RMS = 5.4 ±0.4 nm). Both the scan areas are 5 μm ×5 μm.

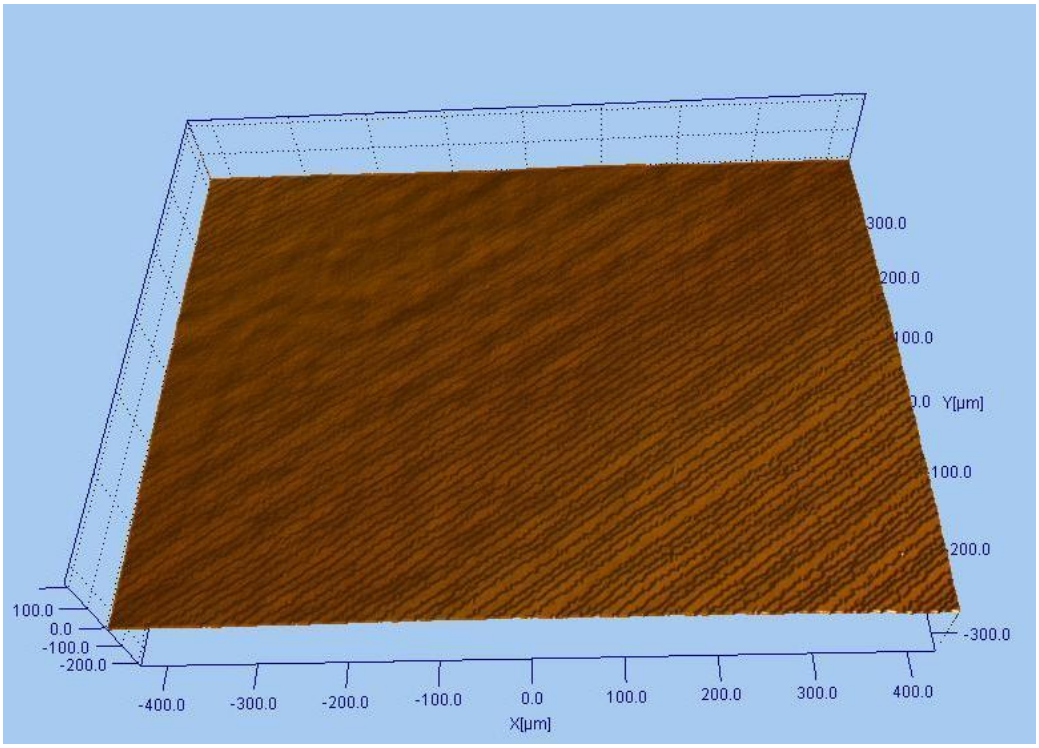

(a)

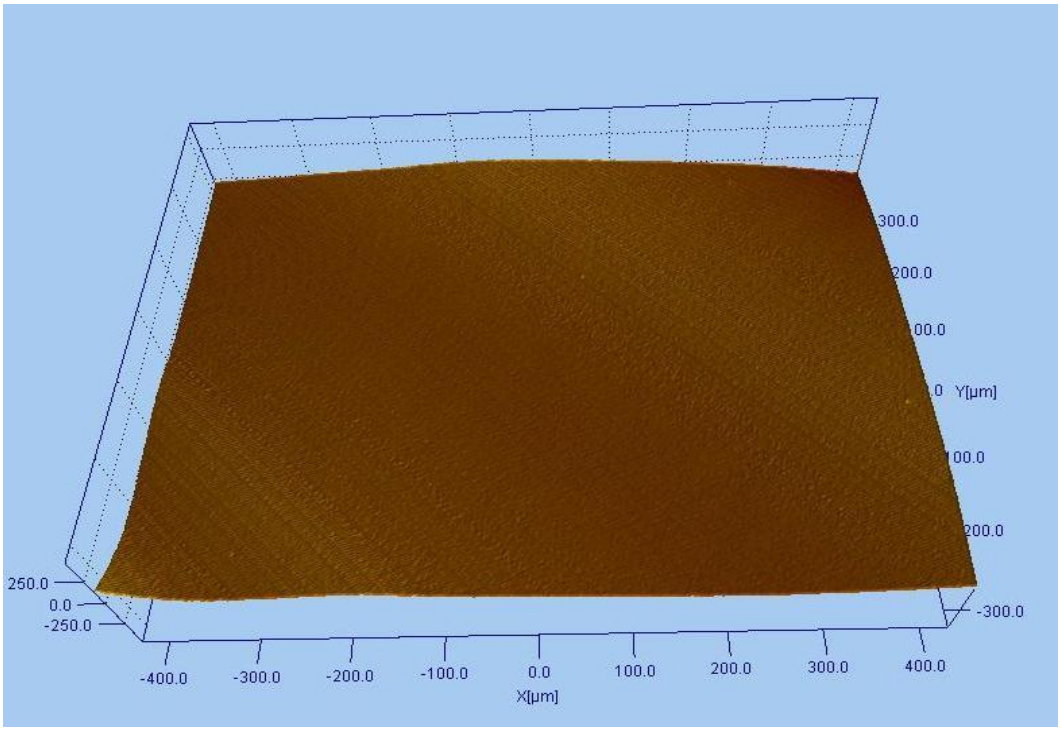

(b)

Figure 4.2 Interferometer images of (a) bare silicon wafer (RMS = 0.005 µm); (b) dry cellulose thin film made of 0.5 wt% cotton powders (RMS = 0.029 µm). Both scan areas are 639 µm ×839 µm.

4.3.2 Modification of perfume microcapsules with PVF and chitosan

4.3.2.1 Aggregation of microcapsules

The aggregation of microcapsules after their surfaces were modified with PVF and chitosan is shown in Figure 4.3 and 4.4. Most of non-modified microcapsules were dispersed and microcapsules aggregated after they were modified with PVF or chitosan solution with the increase of polyelectrolyte (PE) concentration. Obvious aggregation was observed when the concentration of PE to microcapsules approached to 0.3 wt% and 0.2 wt% for PVF and chitosan respectively, and the dimension of the aggregates increased from 20 μm to approximately 100 μm at 0.8 wt% and 0.5 wt% for PVF and chitosan respectively.

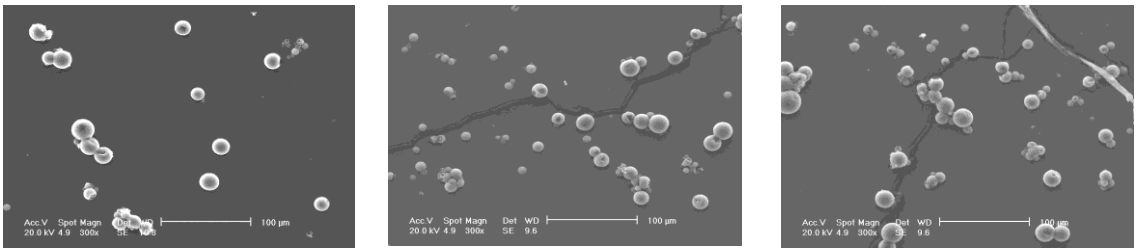

(a) 0 (d) 0.1% (e) 0.2%

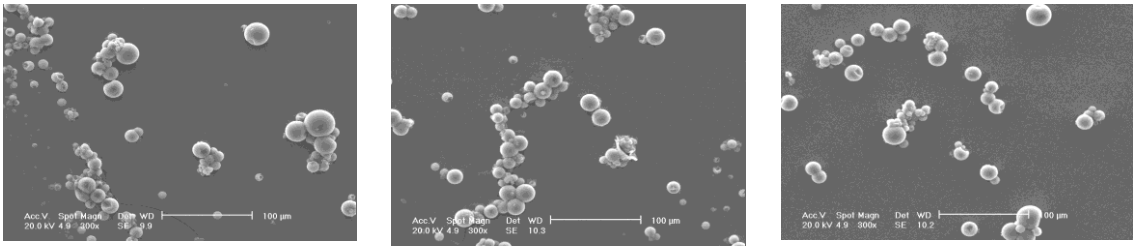

(f) 0.3% (g) 0.4% (h) 0.5%

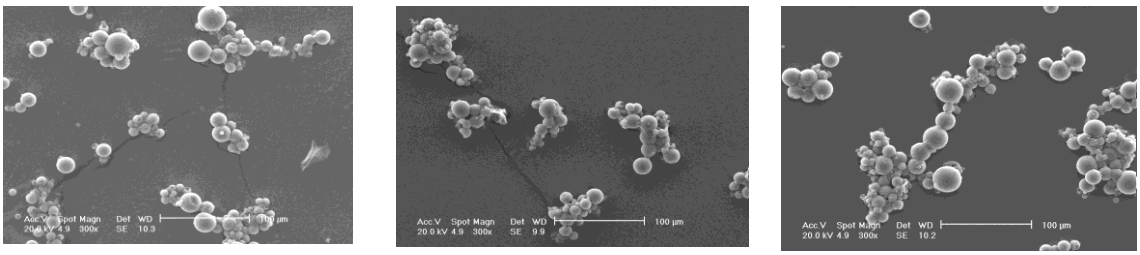

(i) 0.6% (j) 0.7% (k) 0.8%

Figure 4.3 ESEM images of microcapsule aggregates caused by PVF as a function of PVF concentration (wt %).

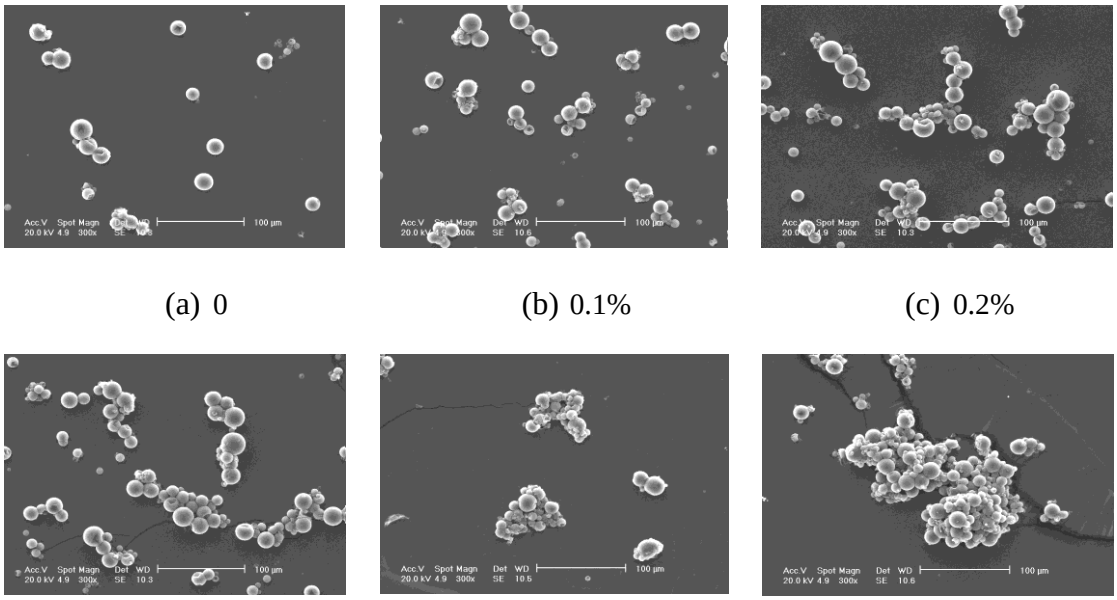

(a) 0 (b) 0.1% (c) 0.2%

(d) 0.3% (e) 0.4% (f) 0.5%

Figure 4.4 ESEM images of microcapsule aggregates caused by chitosan as a function of chitosan concentration (wt %).

The aggregation of microcapsules is also illustrated by the particle size analysis (Figure 4.5). The volume mean diameter ($D_{4,3}$) of microcapsules after being modified with PE solution began to increase at a concentration of 0.4 wt% and 0.3 wt% for PVF and chitosan respectively and then rapidly increased with each PE concentration. The concentration of PVF and chitosan at the onset of aggregation indicated by particle size

analysis is slightly higher than that by ESEM imaging. The mean reason can be that an agitation speed of 2000 rpm was used in a sampling cell for particle size measurement, which might reduce aggregation through mixing. Therefore the optimum concentration of PVF and chitosan to modify MF microcapsules is approximately 0.2 wt% and 0.1 wt% respectively in order to prevent aggregation.

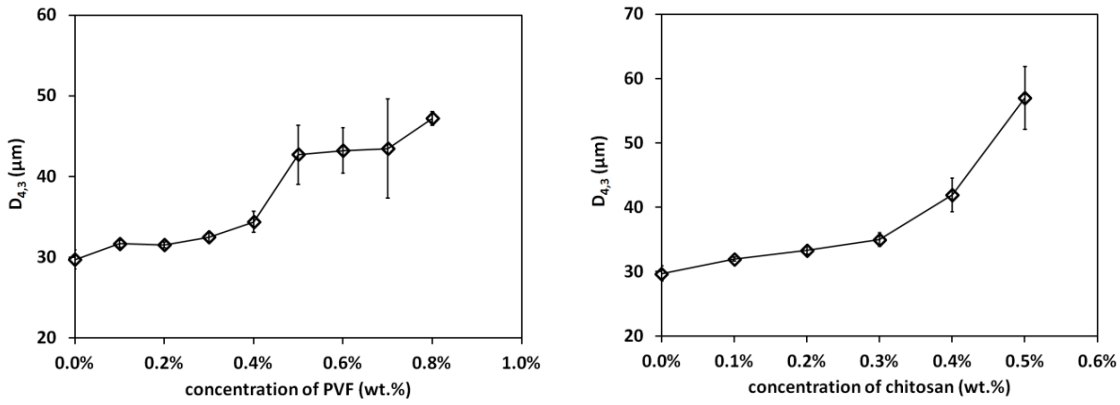

(a) (b)

Figure 4.5 The mean diameter ($D_{4,3}$) of microcapsules modified with PVF (a) and chitosan (b).

4.3.2.2 Surface topography

Figure 4.6 shows the surface topography of the MF microcapsules before and after modification with PVF and chitosan solution with a concentration of 1 wt%. The surfaces of the non-modified microcapsules are quite smooth, see Figure 4.6 (a). After MF microcapsules were modified with PE solution, there was a layer of filaments on the surface, particularly at the joint of two microcapsules. Additionally, the surface

roughness was increased. Therefore, PVF and chitosan are considered to have attached on the surfaces successfully.

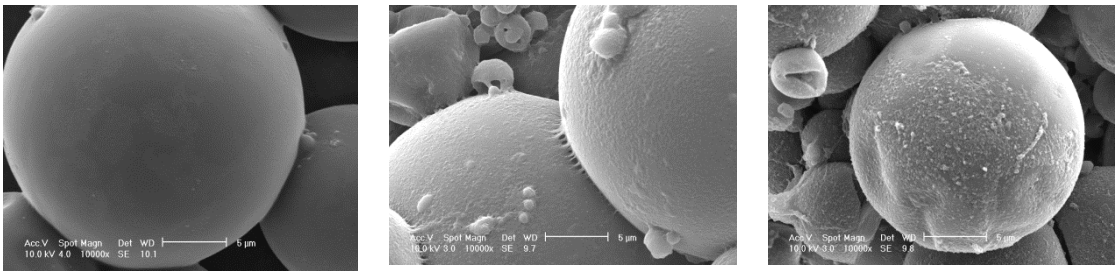

(a) (b) (c)

Figure 4.6 Surface topography of microcapsules before (a) and after being modified with PVF (b) and chitosan (c) with a concentration of 1 wt%.

4.3.3 Adhesion measured by AFM

4.3.3.1 Colloidal probe of single microcapsules

Single MF microcapsules were attached to the end of a tipless cantilever to prepare a colloidal probe of microcapsule. Figure 4.7 presents a typical top (a) and side (b) view image of a MF microcapsule with a diameter of 22 μm attached on the end of a tipless cantilever. The attached microcapsules were used to measure their adhesion to a cellulose thin film.

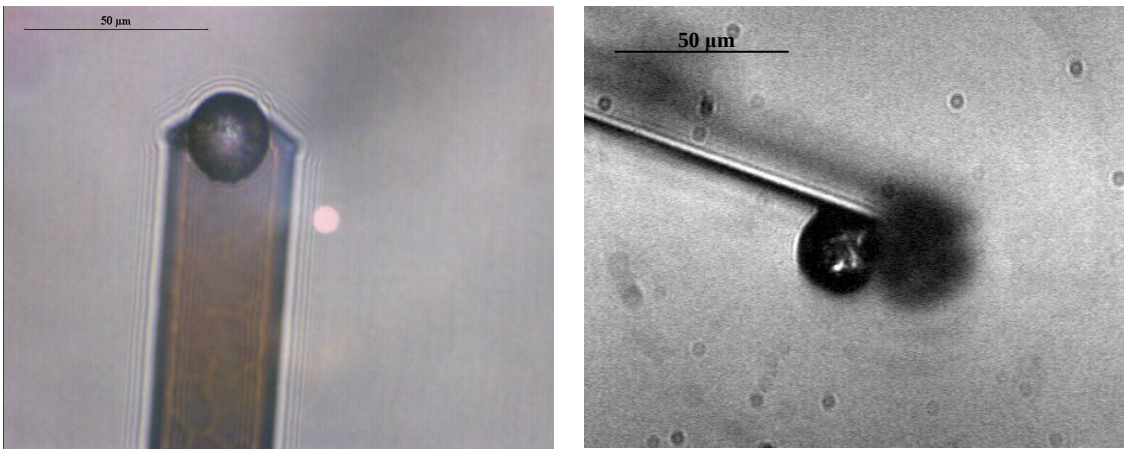

(a) Top view (b) Side view

Figure 4.7 Optical image of a single microcapsule (22 µm) on the end of the cantilever.

Figure 4.8 presents an approaching and retracting force curve to show interactions between a microcapsule and a cellulose thin film in HPLC H_2O. As can be seen, from point A to B, the microcapsule was approaching to the cellulose thin film and there was no extra force applied on the cantilever; from point B, a repulsion force was occurring between the two surfaces, leading to a bending of the cantilever against the substrate; when the repulsion force reached the pre-set compression load (point C), the microcapsule started to retract; at point D, the bending of the cantilever to the substrate approached to the maximum and the attractive interaction reached the peak value, then the microcapsule started to travel back from the surface; at point E, the cantilever recovered to zero position and then departed from the substrate. In Figure 4.8, there is no obvious "snap –in" on the approach curve when the microcapsule approached to the cellulose thin film. Bowen *et al.* (2002) studied the interactions between single *Bacillus mycoides* spores and hydrophobic-coated and hydrophilic glass surfaces in aqueous solution by AFM with a colloidal probe, a simple counting methodology and a spinning disk technique. It was found that the "snap-in" event on the approach curve indicates

that there is an attractive interaction between two surfaces. The attraction during the approach process can help the surface capture more *Bacillus mycoides* spores to the hydrophobic-coated glass surface (Bowen *et al.* 2002). Therefore, there is no attractive force when the microcapsule approached the cellulose thin film in HPLC H_2O. An obvious popup event on the retraction was observed, which is considered as the adhesion or the "pull-off" force between the microcapsule and the cellulose thin film. Adhesion on the retraction process is considered to relate to the remaining of the particles to a surface.

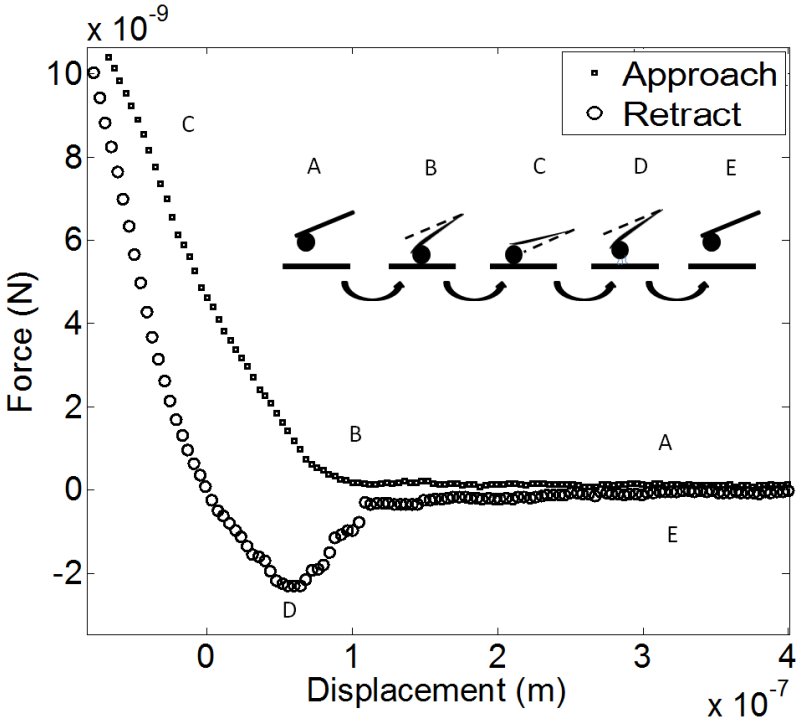

Figure 4.8 Schematic representations of steps during a typical force interaction between a non-modified microcapsule with a diameter of 22 μm and a cellulose thin film in HPLC H_2O.

4.3.3.2 Operation parameters for adhesion measurements by AFM

(1) The compression load

The compression load influences the adhesion of a particle on a substrate by causing the particle deformation to change the contact area. The adhesion of single MF microcapsules on a cellulose thin film was investigated as a function of the compression load in HPLC water. Four single microcapsules were measured (Figure 4.9). In general, adhesion of the single MF microcapsules on the cellulose thin film in HPLC H_2O increased with the compression load and then levelled off. However, slight difference in the shape of adhesion vs. compression load curve between microcapsules was seen, which may be attributed to the difference in the surface properties (such as wall thickness, surface roughness and porosities) between themselves. The difference in the wall thicknesses between perfume microcapsules from the same batch was noticed by the ESEM images shown in Figure 4.10, which varies from approximately 90 nm to about 120 nm. The dependence of the adhesion behaviour on the wall thickness of microcapsules was also observed in the work of Elsner *et al.* (2004) and the surface roughness was also shown to affect adhesion (Katainen 2006). The overall trend of adhesion increasing and then reaching a constant value by increasing the compression load correlates with previous publications (Bhushan 2003, Xu and Siedlecki 2009). However, other results are inconsistent with this. Stegemann *et al.* (2007) found that adhesion between a titanium sphere and metal single crystals was independent of compression load from 90 nN to 200 nN and then increased with the compression load to 350 nN. There was also a report showing no obvious varation in adhesion with the increase of the applied load in low and moderate humidity enviroments between polystyrene particles and then increase steadily with compression load after it reached a threshold value of 1200 nN (Cleaver and Looi 2007). The inconsistency may be

attributed to the transformation of elastic deformation to plastic deformation of particles at high compression load. In this work, the low compression load can generate low adhesion forces between microcapsules and a cellulose thin film in aqueous solution. Therefore in order to generate more an accurate measurement of adhesion force, an extremely low compression load should be avoided; additionally, the adhesion force of microcapsules to a cellulose thin film should be measured within the elastic limit of the microcapsules to avoid palstic deformation; The elastic limit of MF microcapsules was investigated in Sun and Zhang (2001) and Liu (2010) and the critical nominal deformation (ratio of displacement to diamter) to avoid plastic deformation was 15 ±1% (Liu 2010) and 19 ±1% (Sun and Zhang 2001) respectively. The rupture force of the MF microcapsules was reported to within a range of hundred of nN to few mN (Zhang *et al.* 1999, Liu 2010, Pan *et al.* 2012). In order to avoid plastic deformation, a comparable high compression load should be avoid. Comprehensively, a compression load of 10 nN was selected for application in the further experiments.

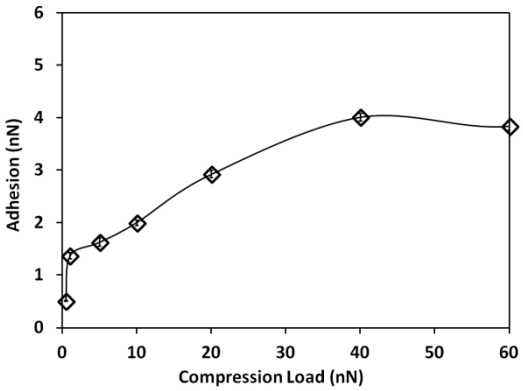

(a)

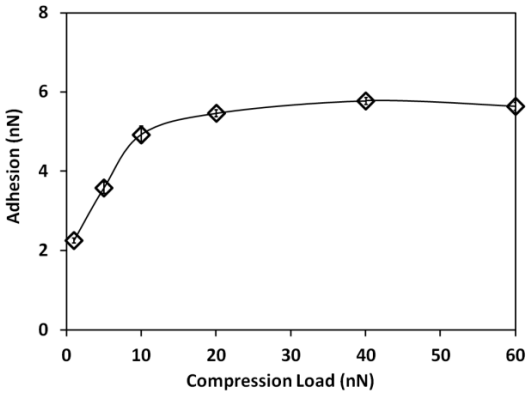

(b)

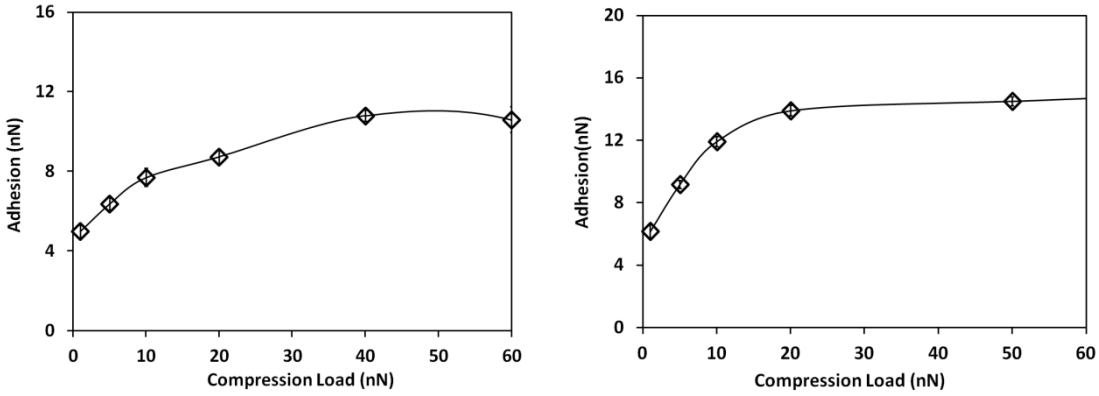

(c) (d)

Figure 4.9 The relationship between microcapsule adhesion and compression load in HPLC water. (a) diameter 23 μm, contact time 0.001 s; (b) diameter 17 μm, contact time 10 s; (c) diameter 19 μm, contact time 10 s; (d) diameter 23 μm, contact time 10 s.

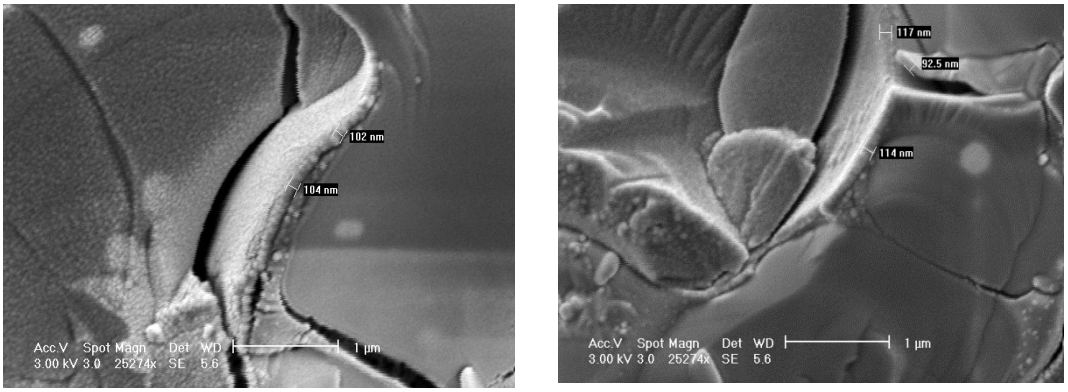

(a) (b)

Figure 4.10 ESEM images showing the wall thicknesses of MF microcapsules from the same sample.

(2) Contact time

Figure 4.11 shows a typical relationship between the adhesion and contact time. Generally, the adhesion increased with the contact time for the first few seconds, and then maintained a constant value with increasing the contact time (Figure 4.11); but there was one microcapsule (Figure 4.11 (d)), from which the adhesion started to decrease after a contact time of 20 s. When a certain compression load is placed on

microcapsules, it is suggested that there is a "stress transmission" effect resulting from slight viscoelasticity of the microcapsules (Zhang *et al.* 1999, Sun and Zhang 2001, Sun and Zhang 2002, Liu 2010), whereby the compressive load is transmitted through the particle with increasing time, resulting in the microcapsule deformation, and then the contact radius reaches a constant value. The required time to achieve the equilibrium contact radius is approximately 5 to 10 s. In the meantime, when two surfaces are brought together, cellulose molecular chains on each surface may penetrate and entangle with each other, leading to an increase in the pull-off force on separation (Poptoshev and Claesson 2002, Nordgren *et al.* 2009).

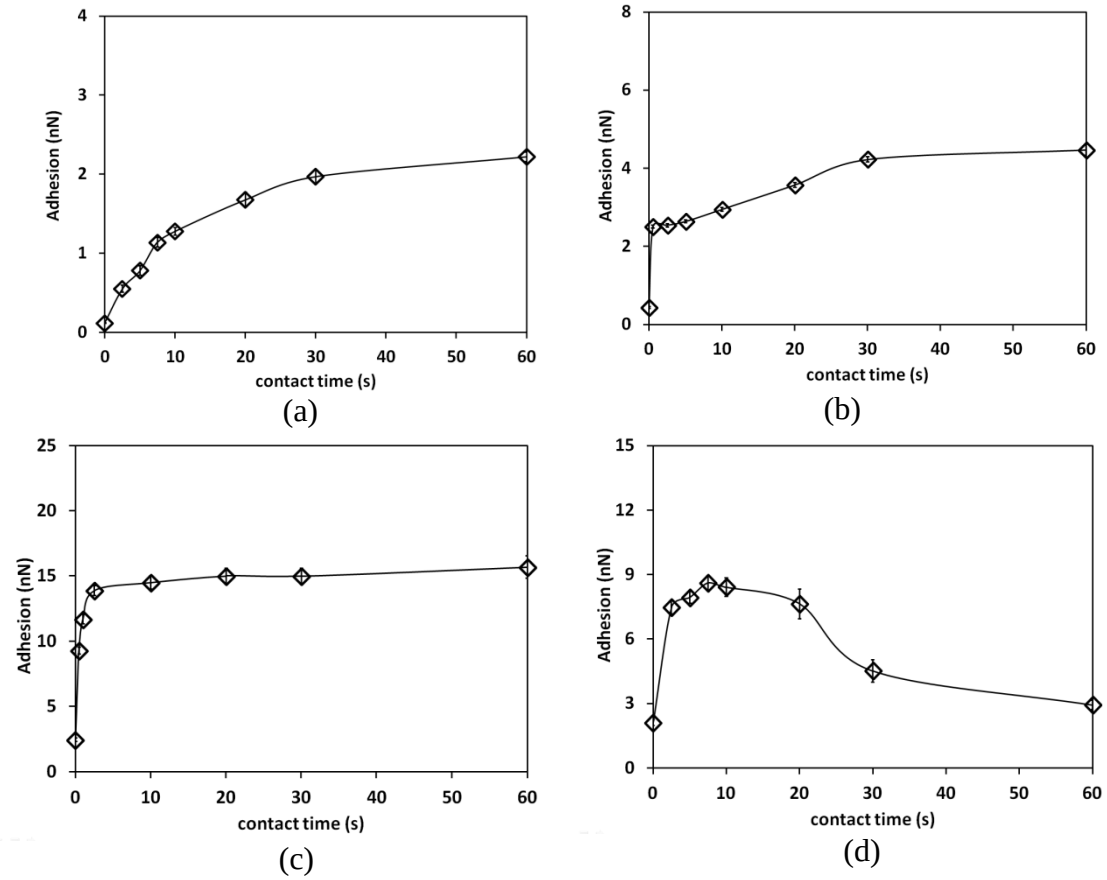

Figure 4.11 The relationship between microcapsule adhesion and contact time (compression load 10 nN). (a) diameter 17.0 μm; (b) diameter 19.0 μm; (c) diameter 23 μm; (d) diameter 14.5 μm.

However, for the microcapsule shown in Figure 4.11 (d), the adhesion started to decrease when the contact time increased to 20 s, which is probably because an increase in the holding time under a certain compression load caused the diffusion or even the leakage of the core material-perfume oil. With the presence of the perfume oil, the surface of microcapsules is much more hydrophobic (Liu 2010). The layer of perfume oil, with a high viscosity, can not only separate the two surfaces but also decrease the penetration speed of the molecular chains, which might suppress the adhesion between the microcapsule and the cellulose thin film. The breakage of the microcapsule after conducting the adhesion vs. contact time experiment in Figure 4.11 (d) was noticed, as shown in Figure 4.12. Therefore a contact time of 10 s for holding single microcapsules on the surface was chosen for application in the further experiments.

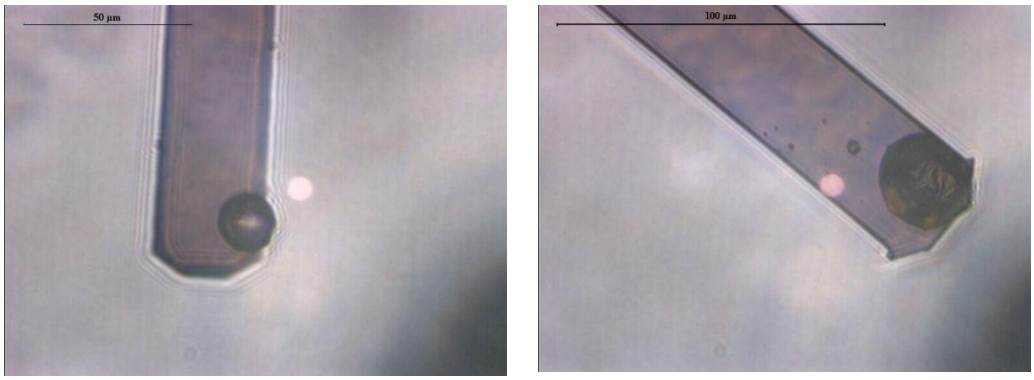

(a) (b)

Figure 4.12 Microscopy images of the microcapsule before (a) and after (b) conducting adhesion vs. contact time measurements; the microcapsule presented here is the same one as used in Figure 4.11 (d).

(3) Microcapsule size

The relationship between adhesion and microcapsule diameter is plotted in Figure 4.13. In HPLC H_2O, the adhesion of microcapsules is independent of their size. However, the pull-off forces were found to be proportional to the particle diameter according to continuum mechanics models (JKR (Johnson *et al.* 1971), DMT (Derjaguin *et al.* 1975) and Maugis-Pollock (Maugis and Pollock 1984). The independence may be due to the surface morphology of single microcapsules being different (Vakarelski *et al.* 2000, Hodges *et al.* 2002), leading to the variation in adhesion; the effects overcoming the influence from particle size (which will be explained in 4.4.2) in this work; additionally, in liquid environment the adhesion between microcapsules and the cellulose film is more likely to result from the entanglement of molecular loops or tails on the two surfaces to form "bridging forces" (Biggs 1996, Liu 2010). The intensity of the force depends on the number of the paired entangled molecular chains and also the strength of each entanglement. When the microcapsules were separated from the cellulose film, the adhesion depended on the entangled molecular chains other than the microcapsule diameter. Therefore, in this work the adhesion is not going to be normalized with the particle diameter in the analysis.

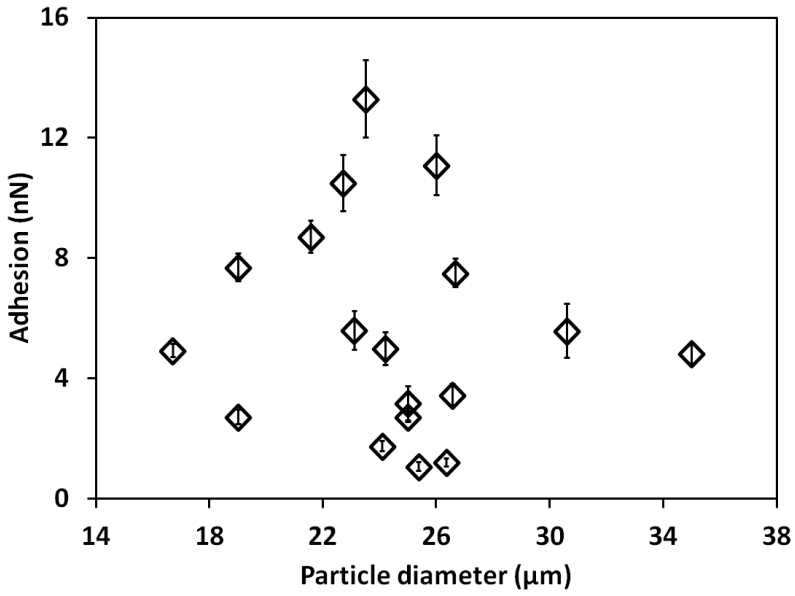

Figure 4.13 The relationship between microcapsules' adhesion on cellulose film in HPLC water and their diameter with a compression load of 10 nN and contact time of 10 s.

4.3.4 Adhesion between microcapsules and cellulose thin films in various environments

4.3.4.1 Adhesion between microcapsules and cellulose thin films in ambient air

Thirteen non-modified microcapsules, Ten modified microcapsules with PVF with a concentration of 0.25 wt% (provided by P&G) and eleven modified microcapsules with chitosan with 0.1 wt%, which had diameters of 15 μm to 30 μm, were used to measure adhesion on cellulose thin films in ambient air (18 ℃, 40% relative humidity (RH)) by AFM, and the results are shown in Figure 4.14. Only the data with a contact time of 10 ms are presented for comparison. The average adhesion force between non-modified MF microcapsules and the cellulose was 44±7 nN. The result of the adhesion between a MF microcapsule and a cellulose thin film in ambient air condition by Liu (2010) was

79.6 nN. The difference might result from the difference in the compression load and the relative humidity (RH) used in the AFM measurements. The RH in this work is 40%, and it is smaller than the value of 46% in Liu's work (2010). Additionally, the compression load used in this work was 10 nN, which is smaller than a force of a few hundreds of nano Newton used in her work. After modification with PVF and chitosan, the adhesion between MF microcapsules and the cellulose thin film increased to 90±27 nN and 61±21 nN respectively. An unpaired t-test (O'Rourke *et al.* 2005) was used to compare the results of the three groups of microcapsules by assuming no difference between them (the null hypothesis); the possibility (p-value) from the unpaired t-test between non-modified and PVF-modified microcapsules, non-modified and chitosan-modified microcapsules, and PVF-modified and chitosan-modified microcapsules is 0.07, 0.05 and 0.97 respectively, which indicates that after microcapsules were modified with PVF and chitosan, their adhesion increased significantly compared with non-modified microcapsules. However, no such difference was observed between PVF-modified microcapsules and chitosan-modified microcapsules. Capillary force is considered to be the reason causing adhesion between MF microcapsules and the cotton film in Liu's work (2010), which is not only determined by the properties of the condensed water layer but also the surface chemistry and roughness (Hodges *et al.* 2002, Jones 2002, Liu 2010). Modification of MF microcapsules with PVF and chitosan altered the surface properties of MF microcapsules, leading to the adhesion increase.

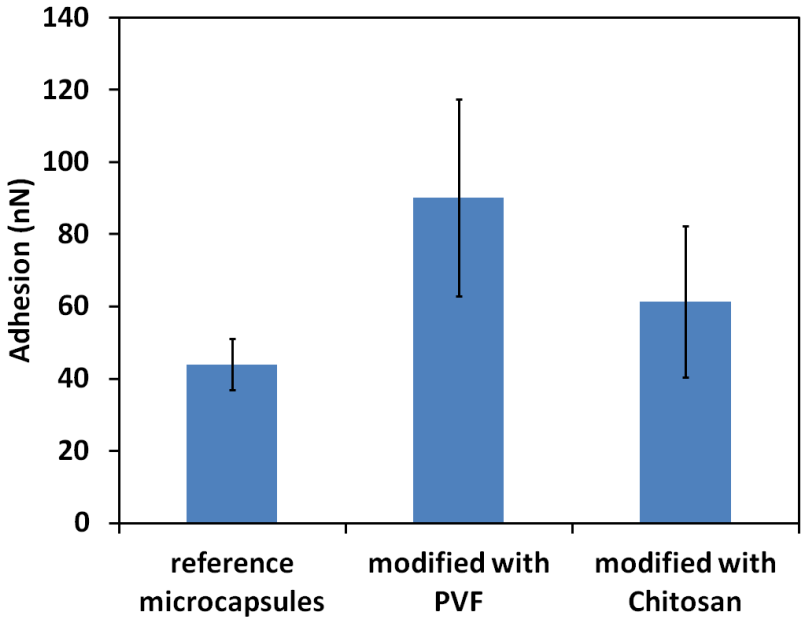

Figure 4.14 The average value of adhesion for non-modified (reference) microcapsules, modified microcapsules with PVF (0.25 wt%) and chitosan (0.1wt%) on cellulose films in ambient air with a contact time of 10 ms (the error bars represent the standard error of the mean).

4.3.4.2 Adhesion between microcapsules and cellulose thin films in HPLC water

In liquid environments, nine non-modified microcapsules, six PVF-modified microcapsules and five chitosan-modified microcapsules survived after adhesion measurements. The results are illustrated in Figure 4.15. Compared with the results in ambient air, adhesion in HPLC water dropped off dramatically. The significant decrease of adhesion in aqueous solution was attributed to the absence of capillary force (Weisenhorn *et al.* 1989), which was also observed in Liu *et al.* work (2013). She didn't detect obvious attractive interaction when a MF sphere and a cotton film were immersed in HPLC water. The MF microsphere used in her work was made of pure melamine formaldehyde without any surfactant (Liu *et al.*, 2013). However, the MF microcapsules

used in this work were likely made of melamine formaldehyde and copolymers (Long *et al.* 2010). The copolymers contain carboxyl and hydroxyl groups, which can form hydrogen bonding with the hydroxyl and carboxyl groups on cellulose (Claesson and Ninhami 1992). Additionally, the adhesion was observed to increase by modifying microcapsules with PVF and chitosan in HPLC water, in which the adhesion increased from 6.2 ± 1.7 nN to 19 ± 8 nN and 9.8 ± 0.5 nN respectively. The possibility of the adhesion to be the same between the non-modified and PVF-modified microcapsules, non-modified and chitosan-modified microcapsules, and PVF-modified and chitosan-modified microcapsules is 0.03, 0.30 and 0.22 respectively from the unpaired t-test. The p-value of adhesion between non-modified and PVF-modified microcapsules is much lower than between non-modified and chitosan-modified microcapsules, which indicates that the performance of PVF to enhance adhesion between microcapsules and cellulose thin films is better than that of chitosan in aqueous solution. Both PVF and chitosan are positively charged long molecules and were attached on the surface of microcapsules. When the modified microcapsules approached the negatively charged cellulose thin film, the positively PE molecules can stretch to the cellulose surface and then form entanglements between cellulose chains and PE molecular chains to enhance the adhesion. The difference in the performance of PVF and chitosan to enhance adhesion between microcapsules and cellulose thin films is possibly due to the difference in their molecule structures and this will be further discussed in § 4.4.1.

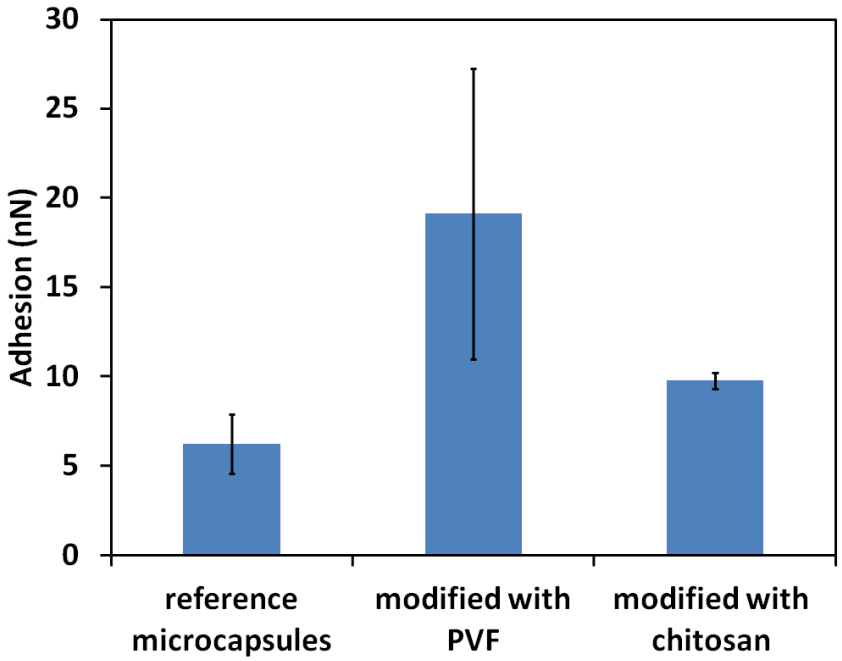

Figure 4.15 The average value of adhesion for non-modified (reference) microcapsules, modified microcapsules with PVF (0.25 wt%) and chitosan (0.1wt%) on cellulose films in HPLC water with a contact time of 10 s (the error bars represents the standard error of the mean).

4.3.4.3 Adhesion between microcapsules and cellulose films in SDBS solution

The interaction between single MF microcapsules and a cellulose thin film was also investigated in 0.2 mM SDBS solution which was used to mimic the detergent solution used in real laundry process (Liu 2010). 9 non-modified microcapsules, 6 PVF-modified microcapsules and 5 chitosan-modified microcapsules were measured and the results are shown in Figure 4.16. The p-value from the unpaired t-test on the adhesion results between non-modified and PVF-modified microcapsules, non-modified and chitosan-modified microcapsules, and PVF-modified and chitosan-modified microcapsules are 0.12, 0.08 and 0.30 respectively. Therefore, microcapsules modified with PEs still showed an increase in mean adhesion value in comparison with that of non-modified

microcapsules, as shown in Figure 4.16, but the extent of increase in adhesion in SDBS solution was less than that in HPLC water. This is also attributed to the PE molecules attached on MF microcapsules to enhance adhesion on the cellulose thin film. However, the presence of the negatively charged detergent molecules on the two contacted surfaces led to the reducing adhesion between surfaces (Holder and Keyhani 2005, Liu 2010) compared with the HPLC water.

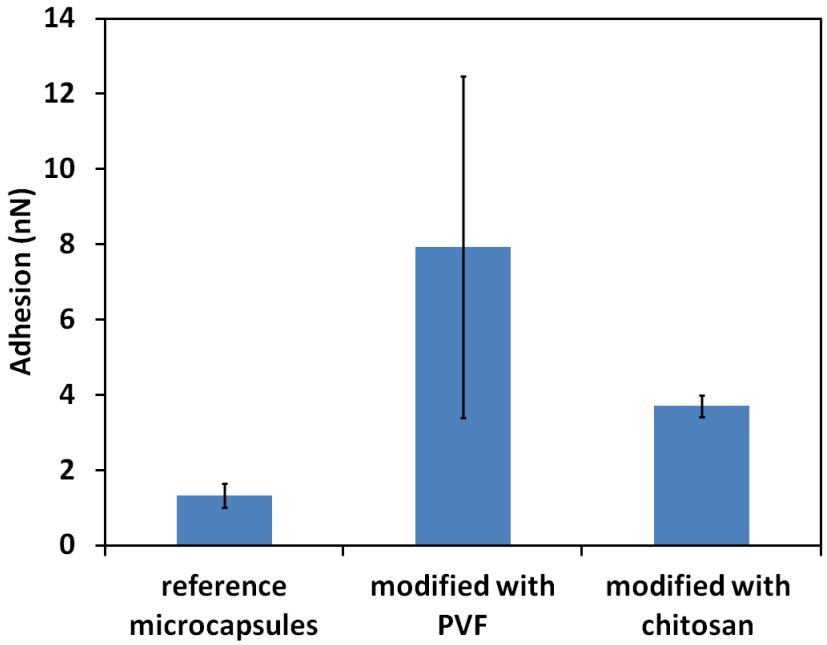

Figure 4.16 The average value of adhesion for non-modified microcapsules, modified microcapsules with PVF (0.25 wt%) and chitosan (0.1wt%) on cellulose films in 0.2 mM SDBS solution with a contact time of 10 s (the error bars represents the standard error of the mean).

4.4 Discussion

4.4.1 Adhesion mechanisms

Microcapsules turned to aggregate after modification with PVF and chitosan, which is either due to the compensation of surface charge or bridging interaction (Theodoly *et al.* 2001, Bordi *et al.* 2009). Zeta potential of the microcapsules before and after the modification was measured, and the results are presented in Figure 4.17. There was no significant change in the value of zeta potential when PVF and chitosan concentration increased to 0.9 wt% and 0.5 wt% respectively. This is possibly because the tiny amount of PEs used is not enough to alter the surface charge significantly, therefore the increase in adhesion between PEs-modified microcapsules and the negatively charged cellulose thin film (Notley 2006, Notley 2009, Da Róz *et al.* 2010) might not be due to electrostatic attraction. However, it might be big enough to cause formation of bridges between different MF microcapsules when they were close to each other, which agrees with the conclusion that bridging interactions are always observed in low polyelectrolyte concentration (Biggs 1996, Podgornik and Ličer 2006). Therefore, the increase in adhesion between the modified microcapsules and cellulose thin film is considered to mainly result from bridging interaction.

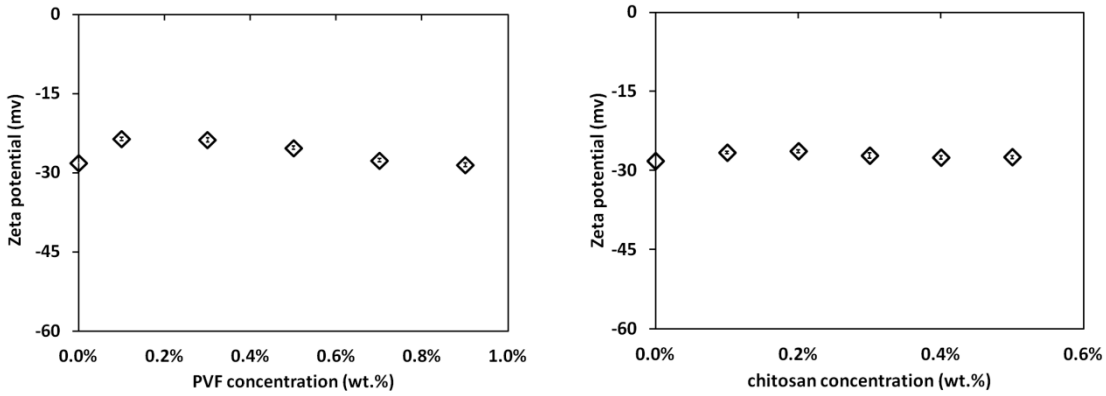

Figure 4.17 Zeta potential of microcapsules modified with PVF (a) and chitosan (b).

However, the performance of PVF to enhance the adhesion was better than that of chitosan. The main reason might be the difference in their properties, including molecule weight (400 kg mol^{-1} and 1000 kg mol^{-1} for chitosan and PVF respectively) and their structures (Figure 3.2). The molecular weight of the PVF is more than twice larger than that of chitosan; therefore the length of the PVF molecular chains is longer than that of chitosan. When the PE molecular chains encounter with the cellulose chains, the long molecular chains can form a longer bridges (Figure 4.18) with cellulose chains. Additionally, PVF is a long linear molecule, while chitosan has ring structures, and can be much fluffier if the molecule attached on the microcapsule surface. When PVF molecules are attached on the surface of microcapsules, they could be more flexible and the structure of their chains on the surface could possess more trains and loops other than tails (Gurumoorthy and Khan 2011) (Figure 4.18). However, the ring structures of chitosan can lead to the steric forces, which may form more tails on the surface. The entanglement of cellulose chains with loops may be much stronger than that between trails. Additionally, both chitosan and MF bear $–NH_2$ groups which will be protonated, and there will be a repulsive force between these functional groups if they approach each other. Compared with chitosan, the –NH- group on PVF is more stable

and less repulsive force can occur. Therefore modification with PVF led to a higher increase in adhesion than chitosan. The steric effect and protonation were much more often detected in liquid environments (Israelachvili and Wennerstroem 1990, Gurumoorthy and Khan 2011) than in air, which may explain why more increase in adhesion was observed in ambient air than in aqueous solution after MF microcapsules were modified with PVF and chitosan.

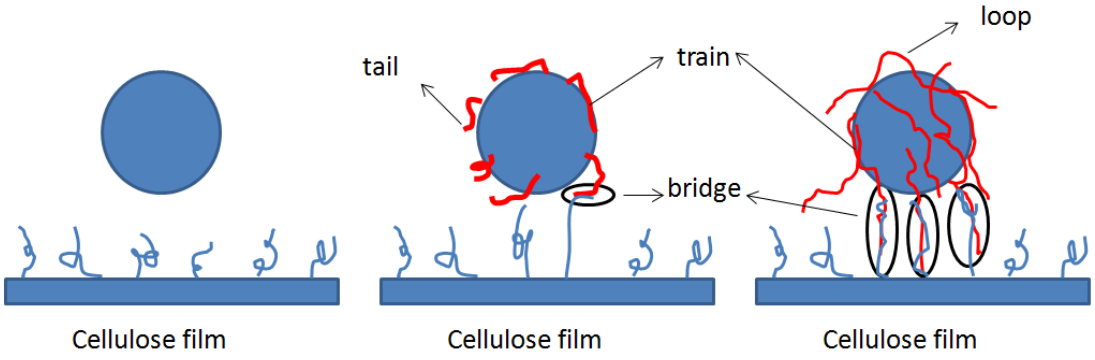

Figure 4.18 Schematic diagram showing possible interactions between microcapsules and a cellulose film before and after modification with chitosan and PVF.

4.4.2 The scattering of adhesion results

4.4.2.1 Surface properties of microcapsule

Big variations in the value of adhesion between different microcapsules were observed. One possibility is the limited number of the microcapsules measured in this work; another is that microcapsules were observed to aggregate after the modification in § 4.3.1, therefore for the single microcapsules used to measure adhesion, they were either

unmodified or less modified; the uneven coverage of PE and the increase of the surface roughness may be the main reasons causing the adhesion variation between difference microcapsules. The surface roughness of microcapsules in this work is shown in their ESEM images (Figure 4.19). The surface roughness of MF microcapsules from the same batch was quite different. The asperities on surface of the microcapsules varied from dozens of nanometers to hundreds of nanometers; these asperities covered the surface either as a monolayer of tiny particles or as particle aggregates. The presence of the asperities on the surface can decrease the actual interfacial contact area and the number of microscopic contact points between the microcapsule and the cellulose thin film, leading to the suppression on adhesion. The increase in the scatter of the pull-off force data (Tormoen and Drelich 2005, Tormoen *et al.* 2005, Drelich 2006) and the decrease of adhesion value (Hodges *et al.* 2004, Katainen *et al.* 2006) were noticed with the increase of the surface roughness.

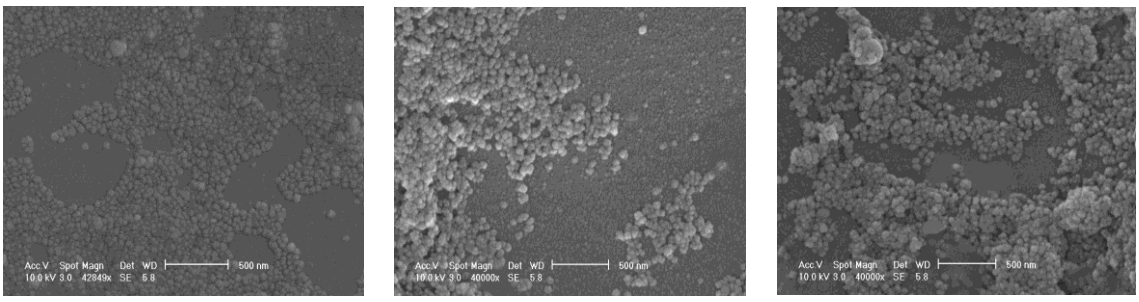

(a) Monolayer (b) Slight aggregation (c) Heavy aggregation

Figure 4.19 Asperities on the surface of microcapsules from the same batch.

4.4.2.2 Surface properties of cellulose thin films

In addition to the surface roughness of microcapsules, the network structure (see Figure 4.1) of the cellulose thin film may also influence the adhesion. The surface of the Si wafer is significantly smoother than that of the cellulose thin film from § 4.3.1, so the adhesion between different single microcapsules and the cellulose thin film and Si wafer was measured in ambient air (Figure 4.20) instead of the liquid environments to avoid the stretching of cellulose molecule chains in liquid (Liu 2010). In Figure 4.20 (a), the data of adhesion on the cellulose thin film at 100 positions are quite scattered, however for the Si wafer the adhesive forces are more consistent. For all the measured microcapsules, the standard errors from the Si wafer on 100 positions are much smaller than those from the cellulose thin film (Figure 4.20 (b)). These results indicate that the surface roughness of the cellulose thin film also caused the variation of the adhesion of microcapsules to it.

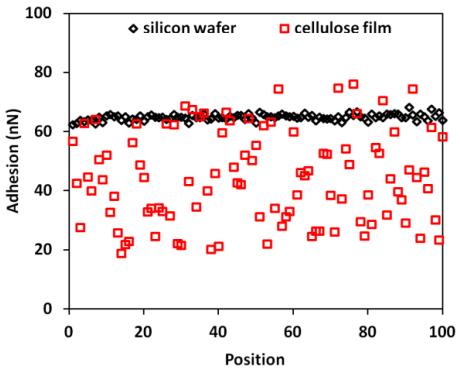

(a) The adhesion of one microcapsule at 100 positions

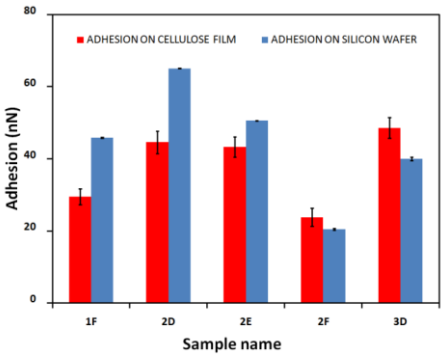

(b) Average results from five microcapsules (1F, 2D, 2E, 2F and 3D indicates the name of the microcapsule measured)

Figure 4.20 Adhesion of single microcapsules on a cellulose film (red) and silicon wafer (blue).

4.5 Conclusions

MF microcapsules were modified by PVF and chitosan successfully. However, microcapsules tended to aggregate after being modified with PEs. The adhesion between PE-modified microcapsules and cellulose thin films were found to increase compared with non-modified microcapsules in ambient air, HPLC water, and a SDBS solution. Bridging interactions because of the extension of long PE molecular chains between microcapsules and the entanglements of PE molecular chains with cellulose chains were considered to be the reason causing the aggregation of microcapsules by the polyelectrolytes and the increase in adhesion after microcapsules were modified with PEs. The difference in the structure of PE molecules was considered to be the reason causing the difference in their performance. The uneven coverage of PE on the surface of microcapsules and the difference in the surface roughness may be the reasons to cause the adhesion variation between difference microcapsules.

Chapter 5: Investigation of Adhesion of Perfume-filled Microcapsules to a Cellulose Thin Film by AFM and a Flow Chamber Technique

Part of the work presented in Chapter 5 has been submitted to Journal of Microencapsulation.

5.1 Introduction

The study presented in Chapter 4 indicates that modification of perfume-filled microcapsules with polyelectrolyte such as PVF and chitosan enhanced their adhesion to a model cotton fabric surface based on the results obtained using AFM with a colloidal probe. However, modification of microcapsules with the polyelectrolytes caused aggregation through bridging force; so for the single microcapsules used to measure adhesion, they were either unmodified or less modified; the uneven coverage of PE and the increase of the surface roughness may be the main reasons of adhesion variation between difference microcapsules. Additionally, the application of the AFM colloidal probe technique to investigate the adhesion of microparticles is restricted due to the low efficiency of attaching microparticles to the end of the cantilevers and some undesirable sample properties such as the easy breakage of the weak microcapsules. Therefore, a technique which can be used to investigate the adhesion based on a population of microcapsules is also desirable.

The adhesion of microparticles and cells on substrates has previously been investigated using shear flow in a flow chamber (Sanjit *et al.* 1994, Garrett *et al.* 2008). The removal of particles from a surface through hydrodynamic forces (Decuzzi *et al.* 2007) can be

adjusted by controlling flow velocity and the consequently shear stress imposed upon the particles; it is the most common technique used to study adhesion of particles on a surface in liquid environments (Martines *et al.* 2004, Renshaw *et al.* 2005, Garrett *et al.* 2008). Microparticles exposed to shear flow are expected to be displaced by lift, sliding, rolling or some combination thereof (Saffman 1965, Zhang *et al.* 1999a, Zoeteweij *et al.* 2009). Particles are removed by lift motion when the lift forces overcome the adhesion in direction normal to the surface (Zoeteweij *et al.* 2009). If the lift is not sufficient, particles can also be displaced by drag forces in the lateral direction through either sliding or rotating motion (Sanjit *et al.* 1994, Zhang *et al.* 1999a, Zoeteweij *et al.* 2009). The balance on the forces and torques resulting in particle removal from the surface is directly correlated with the adhesion between the two surfaces. Crucially, the technique provides adhesion for a population of particles, providing statistically significant information in a short period of time.

In contrast, atomic force microscopy (AFM) can be used to measure micro- and nanoscale forces between a single particle and a surface of interest via a colloid probe technique (Binnig *et al.* 1986, Ducker *et al.* 1992, Kappl and Butt 2002). Adhesion has been investigated either by comparison of adhesive forces on specimen with different chemical compositions (Eastman and Zhu 1996, Żbik and Frost 2010) and surface roughness (Cooper *et al.* 2001, Katainen *et al.* 2006), or through interpretation of the force-displacement data by varying relativity humidity, ionic strength, pH, hydrophobic or hydrophilic nature etc to explore adhesion mechanisms including capillary force (Jones *et al.* 2002), electrostatic interaction (Vakarelski *et al.* 2000), hydrophobic interaction (Zbik and Frost 2010) and bridging interaction (Notley 2009, Kocuna *et al.* 2011).

Therefore, in this study a custom-built flow chamber was employed in order to investigate the removal/retention of perfume-filled MF microcapsules from a cellulose thin film; and then AFM measurements to determine the adhesion were also performed in order to obtain information regarding the specific interactions which occur between individual particles and the surface. The cellulose thin film was modified with polyelectrolytes (PEs) (PVF, chitosan and PEI) to avoid the aggregation of microcapsules and then removal/retention of microcapsules on it was investigated. Finally, the adhesion between microcapsules and a cellulose thin film in different aqueous environments was quantified by AFM in order to elucidate the possible adhesion mechanisms.

5.2 Experimental

5.2.1 Perfume-filled MF microcapsules

Perfume-filled MF microcapsules were supplied by Procter & Gamble, Belgium. The detailed information was described in §3.1.1.

5.2.2 Cellulose films

The materials and experimental procedures used to prepare a cellulose thin film were described in detail in §3.1.2.

5.2.3 Surface treatments on cellulose films

The detailed procedures to modify cellulose film with PVF, chitosan and PET solutions for adhesion measurements by AFM and retention tests by a flow chamber technique were described in §3.2.2.

5.2.4 X-ray Photoelectron Spectroscopy (XPS)

X-ray Photoelectron Spectroscopy at the University of Warwick was used to do surface composition analysis of cellulose film before and after being modified with PVF, chitosan and PEI. The detailed information and the procedures were described in §.3.3.4.

5.2.5 Zeta potential

A Zetasizer Nano Series (Malvern Instruments Ltd, UK) was employed for determining the zeta potential of perfume-filled microcapsules and PVF, chitosan and PEI in aqueous solution. The detailed information was described in §3.3.3.

5.2.6 Interferometer

The surface topography of cellulose films was captured using a vertical scanning white light interferometer and the detailed information was described in §3.3.6

5.2.7 Atomic force microscopy

5.2.7.1 AFM imaging

The surface topography of cellulose thin films before and after modification with PEs was acquired by AFM as described in §3.3.9.

5.2.7.2 Force measurement

The adhesion of single microcapsules to cellulose thin films before and after modification with PEs, and the adhesion as a function of ionic concentration, pH were investigated by AFM as described in §3.4.2.

5.2.8 Flow chamber experiment

The detailed procedures to measure the retention of microcapsules on cellulose surfaces before and after being modified with PEs were illustrated in §3.4.1.

5.3 Results

5.3.1 Modification of cellulose thin films with PVF/chitosan/PEI

Cellulose films were modified with PEs (PVF/chitosan/PEI) in an attempt to enhance the adhesion of microcapsules on them. The surface properties of cellulose films before and after the modification were investigated by XPS and AFM to ensure that the modification was successful.

5.3.1.1 Surface composition

Cellulose is an organic compound with the formula of $(C_6H_{10}O_5)_n$ (Johansson and Campbell 2004); while the formula of PVF, chitosan and PEI is $(C_3H_5NO)_n$ (the information was provided by P&G, Brussels), $(C_6H_{11}O_4N)_n$ and $(N_{11}C_{22}H_{55})_n$ respectively. Therefore, the N 1s photoelectron peak was used to indicate the adsorption of the three kinds of PE to the cellulose surface, because nitrogen is absent in cellulose but present in PEs (Da Róz *et al.* 2010, Franca *et al.* 2011). Figure 5.1 shows the results of XPS analysis of both cellulose film and the PVF/chitosan/PEI-modified surface. The cellulose thin film does not display a N 1s photoelectron peak, found in the binding energy region 401 ± 5 eV. In contrast, the PEs-modified cellulose thin film exhibits a clear peak in this region, indicating the successful adsorption of PVF, chitosan and PEI to the cellulose thin film respectively. Similar results of adsorption of chitosan onto model cellulose thin films through electrostatic attraction were observed by Da Róz *et al.* (2010) and Orelma *et al.* (2011) with XPS.

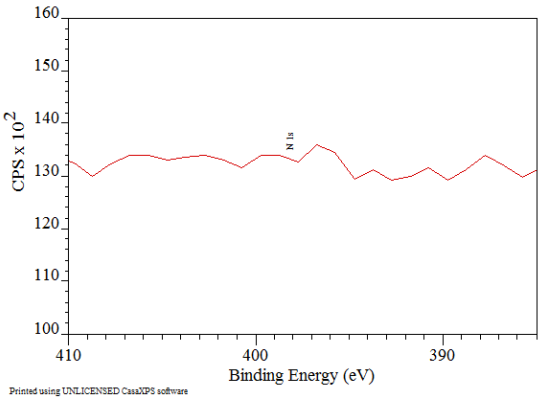

(a)

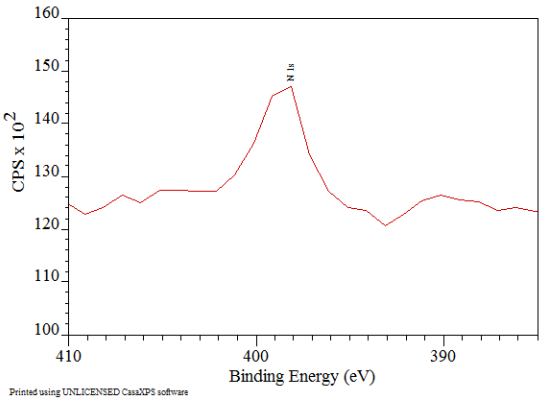

(b)

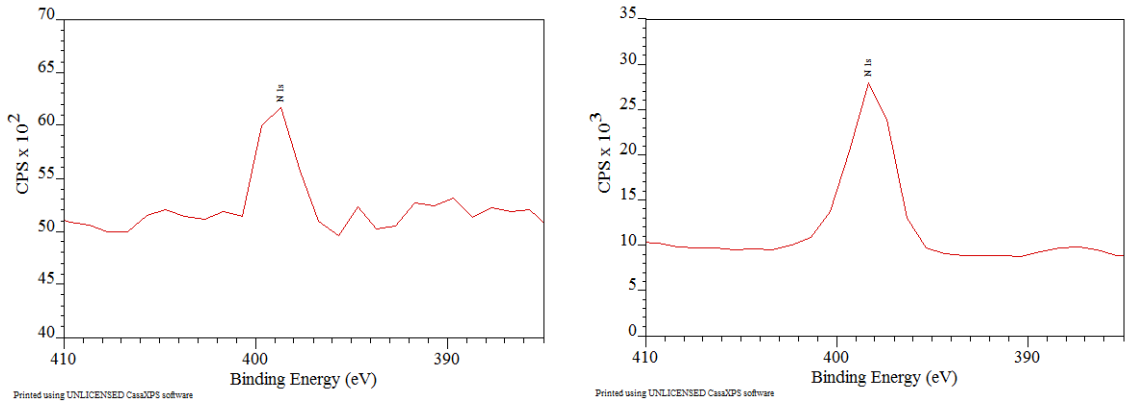

(c) (d)

Figure 5.1 XPS analysis of the N element of cellulose thin film (a); cellulose film modified with 0.1 wt % PVF (b); chitosan (c); and PEI (d) solution.

5.3.1.2 Surface topography

The surface topography of cellulose thin films was imaged using AFM. In Figure 5.2, the root mean square (RMS) roughness of a dry cellulose thin film measured over a scan area of 10 µm ×10 µm was 6.8±0.6 nm. After modification by PVF/chitosan/PEI, the surface roughness increased to 11.5±1.5 nm, 9.0±1.4 nm, and 8.8±0.3 nm respectively. An increase in surface roughness after modification was also observed in Da Róz *et al.*'s work (2010), in which the RMS roughness of cellulose films over a scan area of 2.5 µm x 2.5 µm was reported as 13 nm, which increased to 33 nm over a scan area of 5 µm x 5 µm after modification by chitosan. Therefore, the results presented here indicate that PEs were attached to the cellulose thin film successfully.

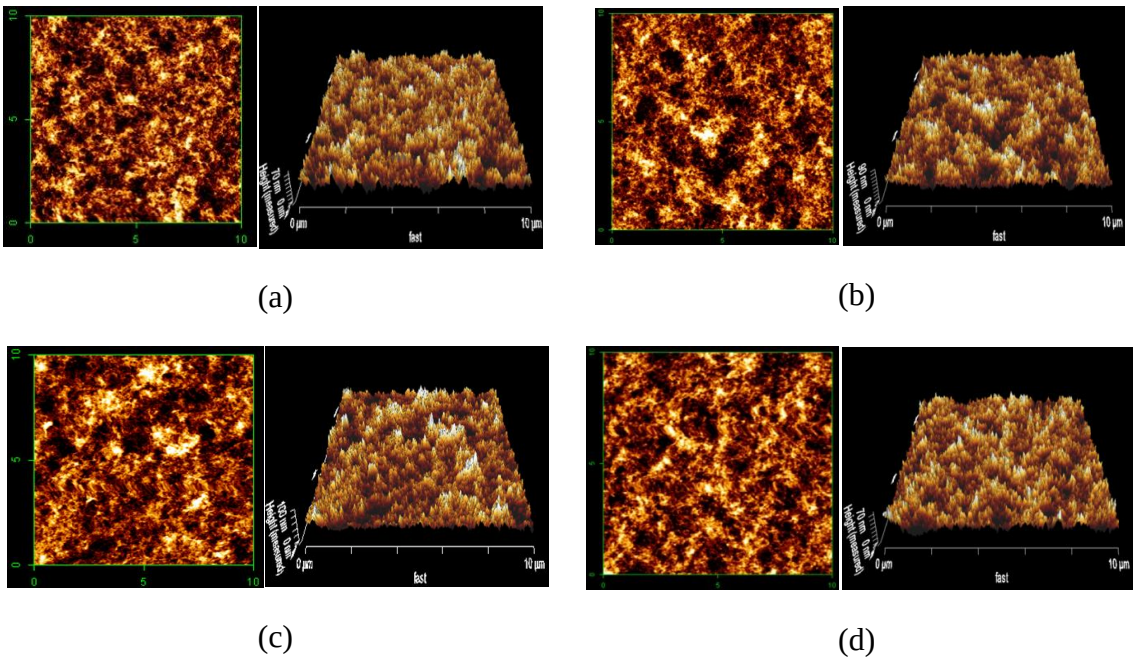

(a) (b)

(c) (d)

Figure 5.2 2D and 3D images of dry cellulose films (10 μm ×10 μm) made of 0.5 wt% cotton powders (a); after modification with 0.1wt% PVF (b)/chitosan (c)/PEI (d) (RMS: (a) 6.8 ±0.6 nm, (b) 11.5 ±1.5 nm, (c) 9.0 ±1.4 nm, (d) 8.8 ±0.3 nm).

5.3.2 Retention of microcapsules on cellulose thin films investigated by the flow chamber technique

5.3.2.1 The experimental parameters for flow chamber experiments

(1) Concentration of microcapsules

The concentration of microcapsules is important for the deposition experiments by a flow chamber. Either a high concentration or a low concentration of microcapsules results in uneven particle distributions (Sjollema and Busscher 1990). 0.2 ml of microcapsule solution with a concentration of 0.3 wt%, 0.5 wt%, and 0.7 wt% were injected into the flow chamber channel and they were allowed to settle for 10 min; and then the images were captured, as shown in Figure 5.3. When the concentration of 0.3

wt% was used, there were just few microcapsules settled on the surface unevenly, which is insufficient for statistical analysis. Conversely, a high concentration such as 0.7 wt% not only caused aggregates but also led to the overlapping (Derksen and Larsen 2011) of single microcapsules. The irregular structures of microcapsule aggregates and the overlapping of single microcapsules can decrease the effective contact area and increase the centre of gravity, which may cause the microcapsules to be removed from the surface more easily. Besides, the overlapping can cause error in the area calculation by considering a microcapsule aggregate as one microcapsule. Therefore, a medium concentration of 0.5 wt% was adopted in this work, in which microcapsules distributed uniformly without aggregation and overlapping.

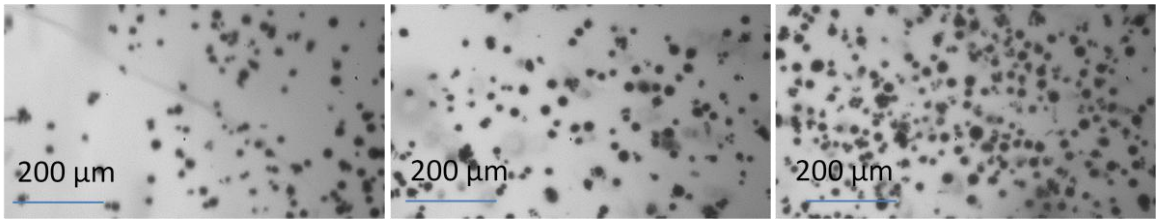

(a) (b) (c)

Figure 5.3 Images of microcapsule distribution as a function of microcapsules' concentration (a) 0.3 wt%, (b) 0.5 wt% and (c) 0.7 wt%.

(2) Settling time

The settling time of microcapsules in the flow chamber before removal was also characterized (Figure 5.4). As can be seen, the retention of microcapsules increased significantly by increasing the settling time from 5 min to 10 min and then the trend slowed down. The settling time was also calculated according to Stokes' law (Lamb 1994) and the settling time is approximately 136 s (the density of the microcapsule is

1.050 g cm^{-3}). Therefore, a settling of 10 min was deemed to be sufficient for all of the microcapsules to attach to the cellulose surface prior to commencing removal experiments.

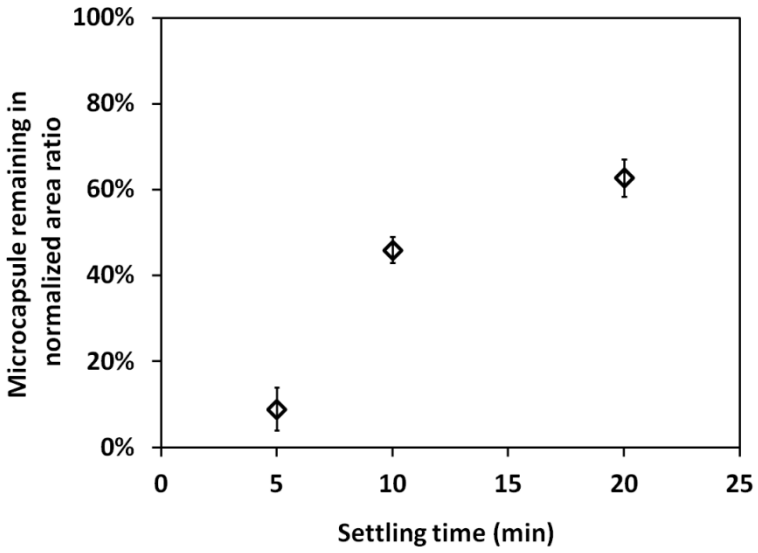

Figure 5.4 Microcapsules remaining in normalized area as a function of settling time (The concentration of microcapsules was 0.5 wt%; the flow rate was 20 mL h^{-1}; the removal time was 3 min).

(3) The running time of the flow used to remove microcapsules

The running time of the flow used to remove microcapsules from substrate is another important parameter to affect their retention. A short time may not be sufficient for the flow to go through the channel to remove all the loose attached microcapsules. The residence time for water passing through the flow channel is 19 seconds at a flow rate of 10 mL h^{-1}. With the increase of the flow rate, the residence time decreased. Therefore, the running time should be longer than the residence time. The retention of microcapsules on a cellulose film under different running time is illustrated in Figure

5.5. The microcapsules removed by the flow increased with the running time to about 150 s and then levelled off. An integral value of 3 min was chosen as the running time and used in the following experimental work.

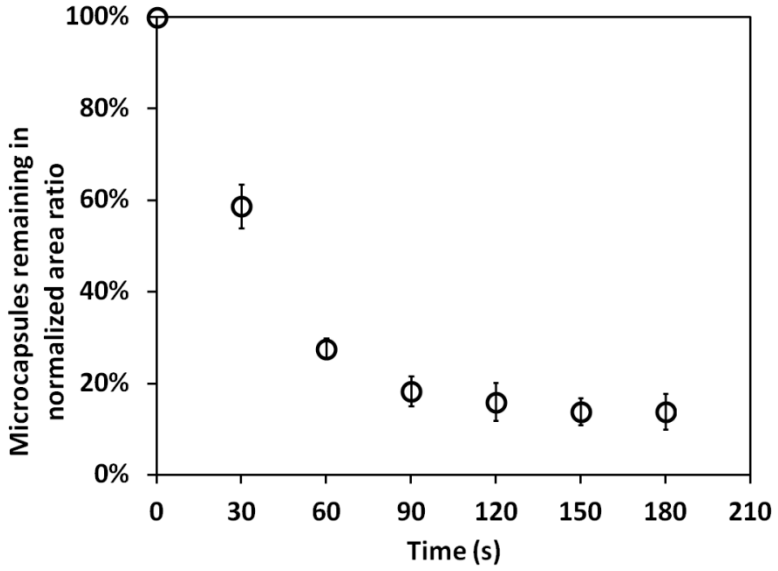

Figure 5.5 Microcapsules remaining in normalized area as a function of removal time. (The concentration of microcapsules was 0.5 wt%; the settling time was 10 min; the flow rate was 60 mL h^{-1}).

(4) Flow rate

The shear stress of a flow varies with the flow rate, which can influence the detachment of microcapsule from a substrate (Zoeteweij *et al.* 2009). A flow rate of 100 mL h^{-1} produced a Reynolds Number (Re) of 9.26 (the density of water at room temperature is taken to be 1000 kg m^{-3}), which is much less than the critical Re of 1400 (Bakker *et al.* 2003) for laminar flow conditions. The retention of microcapsules on a cellulose thin film was investigated as a function of flow rate (Figure 5.6). As can be seen, at 20 mL h^{-1}, more than 50% microcapsules still remained on a cellulose thin film after the water

flow was applied. It can be difficult to determine the effect of surface modification on a cellulose surface if the flow rate used is not able to remove a significant proportion of the microcapsules (Garrett *et al.* 2008). Therefore, higher flow rates were tested and more microcapsules were removed by increasing the flow rate. The microcapsules remaining only dropped marginally when the flow rate was increased from 80 mL h^{-1} to 100 mL h^{-1}. Therefore, a flow rate of 80 mL h^{-1} was used to remove MF microcapsules from a cellulose thin film in the flow chamber.

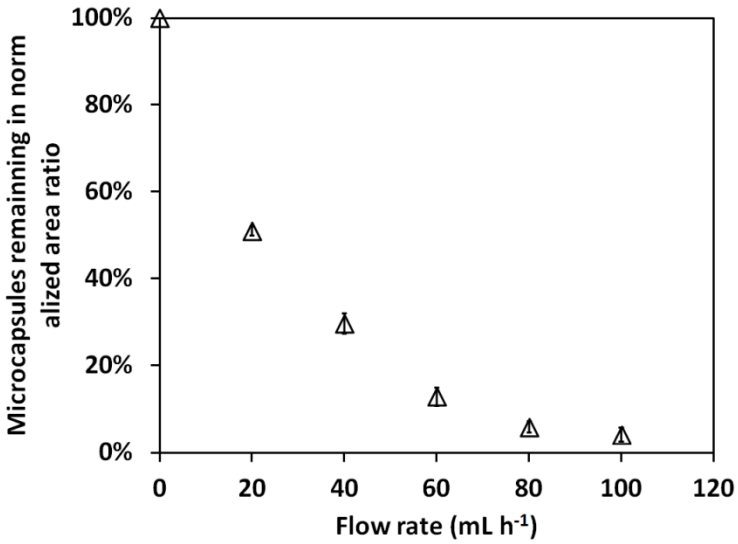

Figure 5.6 Microcapsules remaining in normalized area as a function of flow rate. The concentration of microcapsules was 0.1wt%; the settling time was 10 min; the removal time was 3 min.

5.3.2.2 Microcapsule distribution after removal

The removal of microcapsules from a cellulose thin film was investigated as a function of the distance from the entrance of the flow chamber (Figure 5.7). Microcapsules were evenly distributed before using the water flow (Figure 5.7 (a)). After using a H_2O flow

of 80 mL h^{-1} for 3 min to attempt removal of microcapsules from the cellulose thin film, a significant number of microcapsules were displaced from the cellulose thin film; more microcapsules were detached from the area near the entrance and exit than in the centre region of the chamber (Figure 5.7 (b)). It is suggested that the configuration of flow chamber is the main reason to cause the uneven distribution of velocity in the flow chamber (Bakker *et al.* 2003), in which the fluid velocity is found to be higher at the transition zones between the vertical inlet and outlet, and the parallel plate middle region.

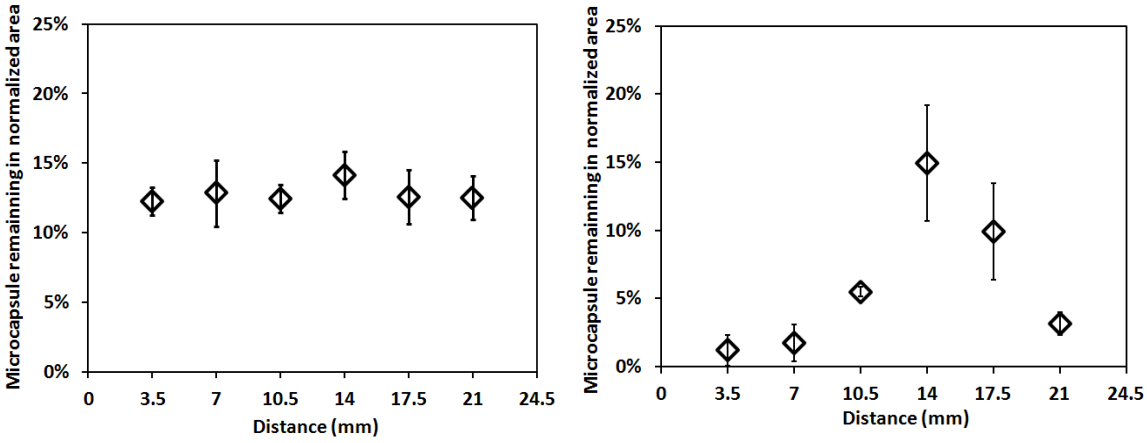

(a) (b)

Figure 5.7 Distribution of microcapsules as a function of the distance from the chamber entrance, before (a) and after (b) removal with a water flow of 80 mL h^{-1} for 3 min.

5.3.3 Retention of microcapsules on modified cellulose films with PEs in the flow chamber

Figure 5.8 shows the results of three repeated experiments of the removal of microcapsules from a cellulose thin film and PE-modified cellulose thin films with a

water flow of 80 mL h^{-1}, for different concentrations of PE solution. The shear stress was estimated to be 3.95 $\times 10^{-2}$ Pa, assuming the viscosity of water to be 10^{-3} Pa s at 20^{o}C (Bakker *et al.* 2003). The modification of the cellulose thin film by PEs promoted significant particle retention. For PVF and chitosan solutions of concentration 0.01 wt% and 0.1wt%, the retention of the microcapsules after exposure to the water flow for 3 min was in excess of 90 %, compared with retention of microcapsules to a non-modified cellulose thin film of less than 10%. In contrast, fewer microcapsules were found to remain on cellulose thin films after PEI solutions with a concentration of 0.01 wt% and 0.1 wt% respectively were applied on the cellulose thin films for 30 min, which was approximate 10% and 67% accordingly. Therefore, modification of cellulose thin films with PEs enhanced the retention of MF microcapsules to cellulose thin films and the performances of PVF and chitosan were better than that of PEI.

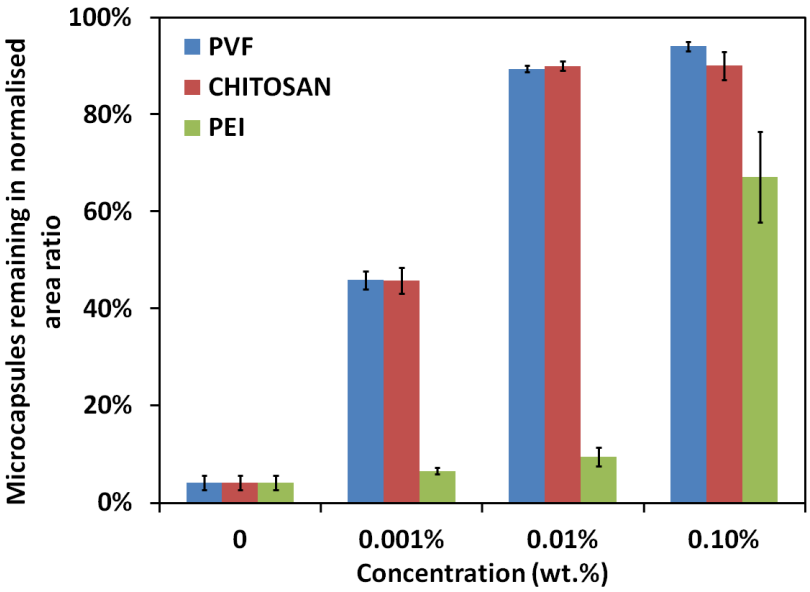

Figure 5.8 Effect of modification of cellulose thin film with PVF/chitosan/PEI solution on the removal of microcapsules from the corresponding surface. The error bars represent the standard error of the mean from three same measurements.

The removal of microcapsules adhered to a surface in a flow chamber was a dynamic process. The displacement of microparticles from surface was conventionally suggested to be via rotation (Sanjit *et al.* 1994, Zhang 1999, Zhang *et al.* 1999, Zoeteweij *et al.* 2009). Modification of the cellulose thin film with PEs altered the surface chemical moieties available for interaction with adhering species; furthermore the surface roughness was also altered. The three kinds of PE are cationic under the aqueous conditions employed here, and may adsorb to the anionic cellulose thin film through electrostatic attraction (Da Róz *et al.* 2010). The resultant adhesion between anionic MF microcapsules and the modified surfaces may be increased through electrostatic attraction and bridging forces (Fras Zemljič *et al.* 2009, Da Róz, *et al.* 2010). With increasing PE concentration used to treat the cellulose thin film there might be a greater polycationic surface charge, increasing the adhesion of MF microcapsules. Correspondingly, a greater shear stress was required in order to displace the adhered microparticles. Therefore, under conditions of constant shear stress but increasing PE concentration, a greater number of MF microcapsules remained adhered to the modified cellulose thin film.

5.3.4 Adhesion between single microcapsules and cellulose films investigated with AFM

The mean maximum adhesive force between single MF microcapsules and a cellulose thin film before (N=9) and after modification by PVF (N=5), chitosan (N=7) and PEI (N=6) are shown in Figure 5.9. Both the adhesion between microcapsules and the cellulose thin film with a short contact time (0.01 s) and a longer contact time (10 s) were measured. The mean maximum adhesive force between a single MF microcapsule

and the unmodified cellulose thin film was 2.3±1.0 nN for a contact time of 0.01s, which increased to 72±23 nN, 58±31 nN and 13±4 nN after modification using PVF, chitosan and PEI respectively each with a concentration of 0.1 wt%; the mean maximum value of adhesive force for a contact time of 10 s also increased from 4.0±0.9 nN to 80±15 nN, 69±33 nN and 32±11 nN after a cellulose thin film was modified with PVF, chitosan and PEI respectively each with a concentration of 0.1 wt%. The large standard error may be attributed to the small number of MF microcapsules investigated and the difference in the surface properties between microcapsules, in which the surface asperities appear to be the main reason to cause the variation of adhesion, following suggestions of Hodges *et al.* (2004) and Katainen *et al.* (2006) on similar systems. The adhesion was also found to increase when the contact time was increased from 0.01 s to 10 s, which is consistent with the results reported for adhesion between a PCL-grafted cellulose sphere and a neat cellulose sphere (Nordgren, *et al.* 2009). When the two surfaces were brought together, molecular chains on the surfaces might start to extend and then entangle with each other, leading to an increase of the pull-off force when separated (Poptoshev and Claesson 2002, Nordgren, *et al.* 2009). The adhesion results from AFM validate the flow chamber data that modification of the cellulose thin film with PEs enhanced adhesion between the MF microcapsules and the cellulose thin film, and also that the adhesion increased with increasing PE concentration, resulting in greater retention of MF microcapsules on the substrate in the flow chamber. The performances of PVF and chitosan to enhance adhesion were better than that of PEI.

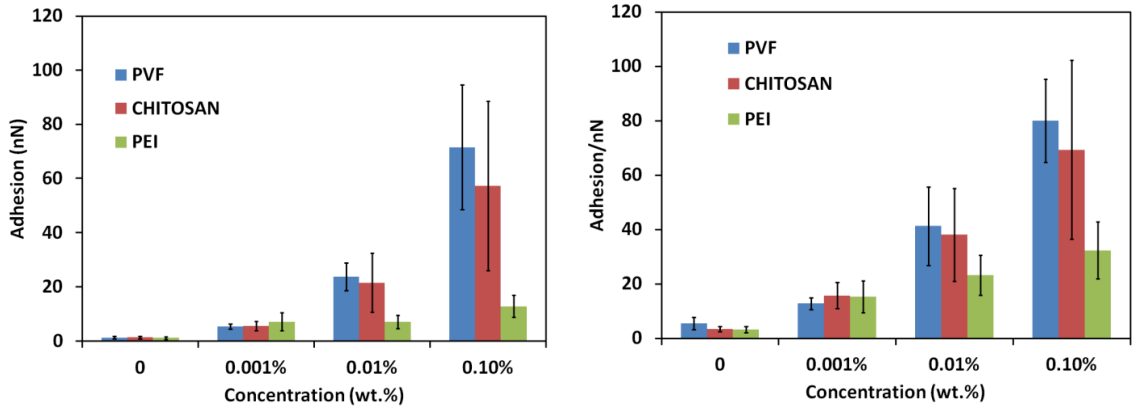

(a) (b)

Figure 5.9 adhesions between microcapsules and cellulose thin films modified with PVF/chitosan/PEI solution with a contact time of (a) 0.01 s and (b) 10 s. The error bars represent the standard error of the mean from 10, 5, 7, 6 microcapsules on no modified, modified cellulose thin films with PVF, chitosan and PEI respectively.

5.4 Discussions

The results from both the flow chamber experiments and AFM measurements indicate that the three kinds of PE enhanced the interaction between the MF microcapsules and the cellulose thin film. In order to understand the possible mechanisms, the zeta potential of the MF microcapsules in aqueous suspension was measured and their adhesion on a cellulose thin film exposed to different pH and ionic strength was further investigated.

5.4.1 Zeta Potential

The zeta potential of MF microcapsules in aqueous suspension and PVF, chitosan and PEI in solution are shown in Figure 5.10. MF microcapsules were negatively charged over a pH range of 3 to 11, which correlates with the results obtained by Liu (2010). PVF, chitosan and PEI were positively charged over the range of pH 3 to pH 9 and the

value of zeta potential decreased by increasing pH. PVF was provided as the partly hydrolysed polyvinylformamide (PVFA) and this contains both vinylformamide and vinylamine functional groups (Pinschmidt 2010). Chitosan is a positive polysaccharide containing D-glucosamine groups (Che *et al.* 2008). The branched PEI also contains amine groups on its molecular structure (Chibowski *et al.* 2009). The presence of amine groups is the main reason for the positive charge of PEs (Chen *et al.* 2009) and they will be protonated under low pH environment, leading to a high surface charge; amino groups will become deprotonated with increasing pH and the surface charge will become increasingly lower. The zeta potential of chitosan was much more influenced by the pH and the value drops off from 73±3 mv to -4±4 mv from pH 3 to pH 11; compared with chitosan, PEI and PVF were less influenced, decreased from 44±4 mv to -2±1 mv and 30±1 mv to 12±1 mv respectively. The reason might be because chitosan possesses more amino groups than PEI and then PVF.

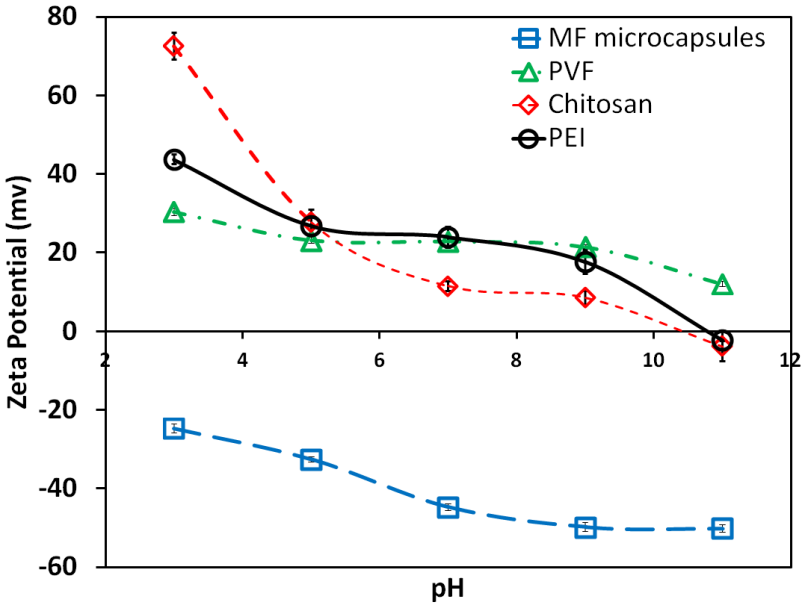

Figure 5.10 Zeta potential of MF microcapsules in aqueous suspension and PVF, chitosan and PEI in aqueous solution with pH 3-11.

5.4.2 Adhesion as a function of ionic strength

The interaction between single microcapsules and a cellulose thin film before and after modification with PEs (PVF, chitosan and PEI) was measured as a function of ionic strength of NaCl solution by AFM, and the data are shown in Figure 5.11, Figure 5.12 and Figure 5.13. Repulsive interactions can be observed when the microcapsule approached a non-modified cellulose thin film in HPLC water (Figure 5.11 (a)), and the increase of ionic concentration decreases the decay length (Israelachvili 2011). The repulsion force might originate from electrostatic repulsion because both MF microcapsules and the cellulose thin film are negatively charged (Liu 2010). The increase of the ionic strength decreases the thickness of the electrical double layer (Zoppe *et al.* 2011), which decreases the decay length. After the two surfaces contacted, adhesion was detected on separation (Figure 5.12 (a)).

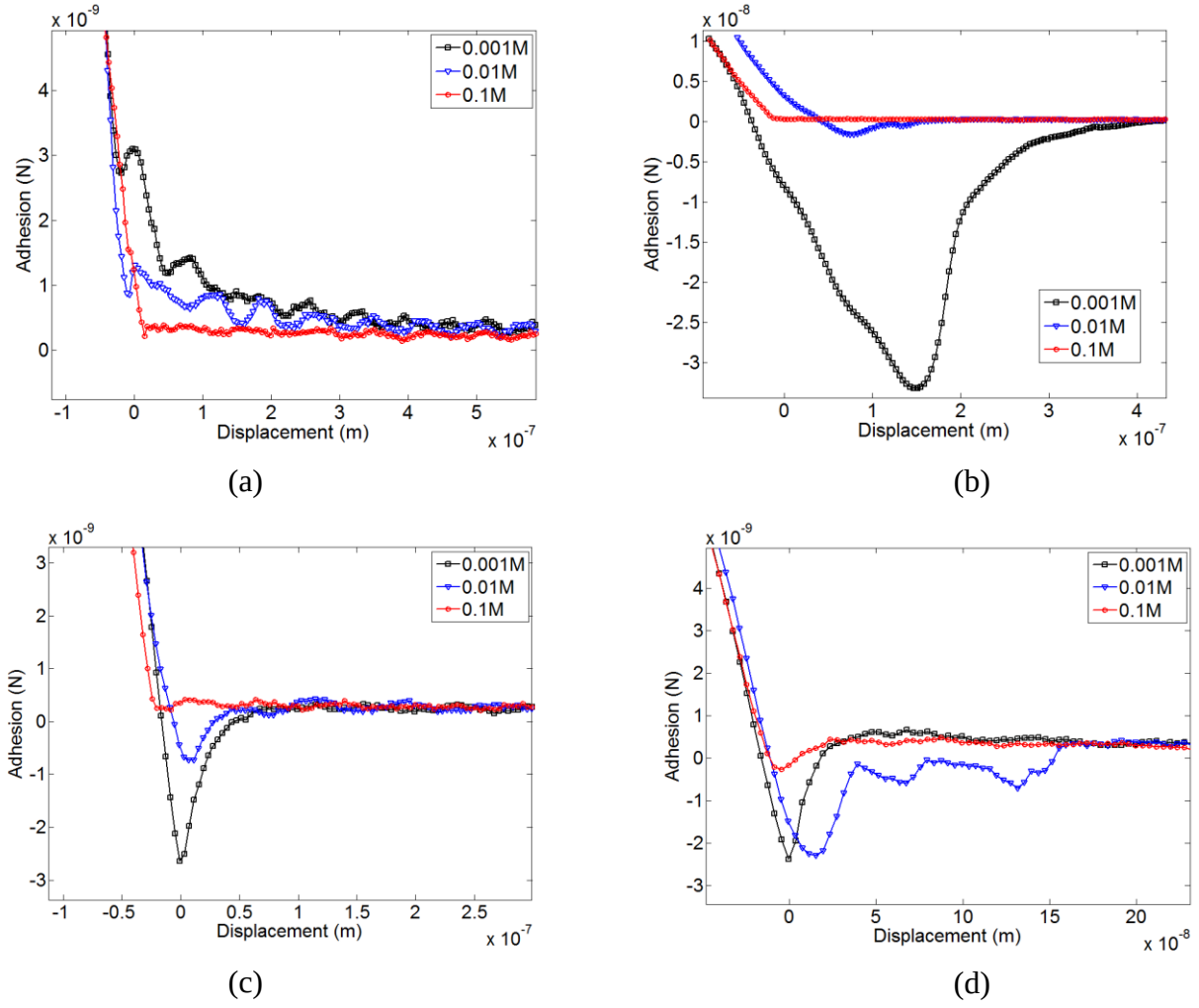

Figure 5.11 Typical force curves when the microcapsule was approaching to a non-modified cellulose film (a), modified cellulose film with PVF (b), chitosan (c) and PEI (d) with a contact time of 0.01s in NaCl solutions with different concentrations.

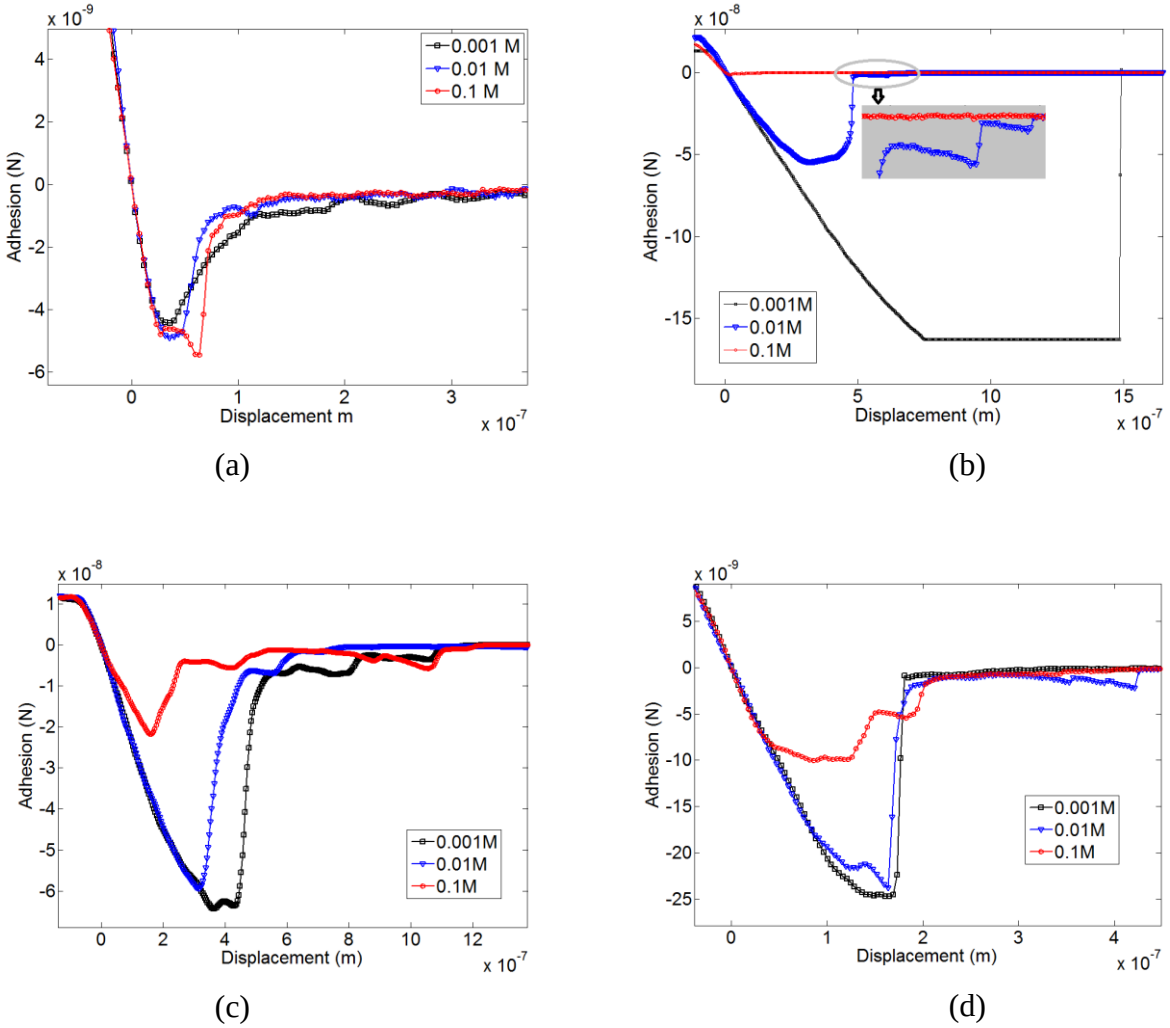

Figure 5.12 Typical force curves when the microcapsule was retracting from a non-modified cellulose film (a), modified cellulose film with PVF (b), chitosan (c) and PEI (d) with a contact time of 0.01s in NaCl solutions with different concentrations.

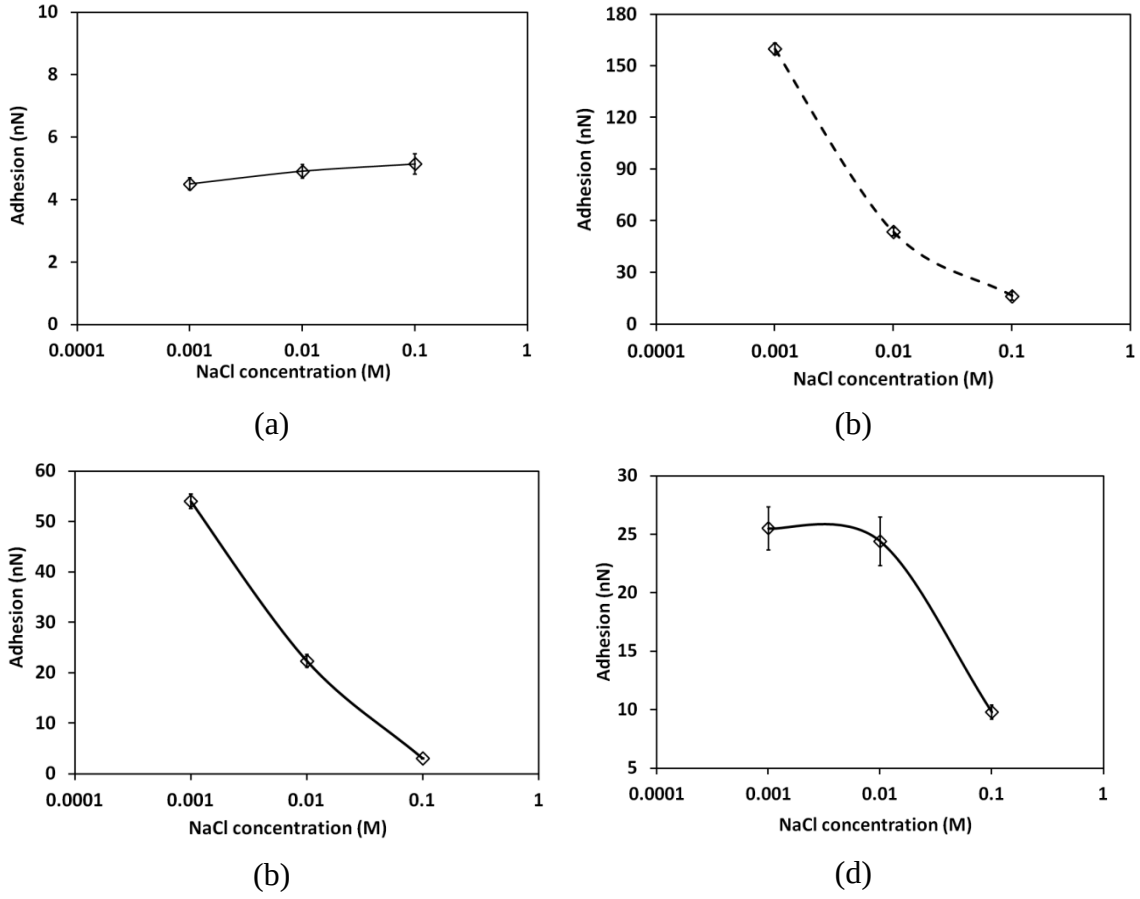

Figure 5.13 The average pull-off force between microcapsule and non-modified (a), PVF-modified (b), chitosan-modified (c) and PEI-modified (d) cellulose film with a contact time of 0.01s in NaCl solution with different concentrations, and the dotted line just indicates the trend. At 10^{-3} M NaCl solutions, some of the adhesion values are out of the scale in (b).

Furthermore, 25 approach curves were analysed. Among them, 11 curves show the "snap-in" valleys on approach for NaCl solutions of 10^{-3} M and 10^{-2} M as presented in Figure 5.11(a). This is possibly because of the loose extension of cellulose chains causing steric hindrance (Notley 2009) in the solution with low ionic concentration. When the microcapsule approached the surface, it probably met the loose cellulose chains at first. Then a repulsive force was generated from compressing cellulose chains. Whenever a group of cellulose chains were compressed, a "snap-in" event was

produced. The difference in the effective length of the cellulose chains might be the main reason to cause several "snap-in" valleys. However, in a solution with a high ionic concentration, the cellulose chains were folded and compressed into a dense layer (Zoppe *et al.* 2011). Therefore, no multiple "snap-in" events were detected as shown in Figure 5.11(a). Figure 5.14 presents a schematic of the interaction between a microcapsule and cellulose chains in a solution with different ionic concentrations.

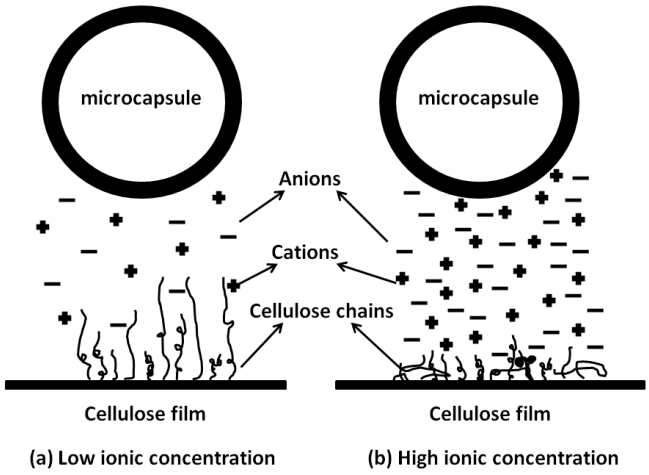

Figure 5.14 Schematic diagrams illustrating the configuration of cellulose molecule chains under different ionic concentration.

The extension of cellulose molecule chains to the surface of microcapsules can also be explained by the detailed information on separation: in a weak ionic environment, the microcapsule separated from the cellulose surface with plateau events before the force dropped to zero for a NaCl solution of 10^{-3} M in Figure 5.12 (a); while in an environment with high ionic strength, a sharp pop-up interaction before the microcapsule was really separated with the surface was observed because cellulose chains were folded (Notley 2009, Zoppe *et al.* 2011) and the microcapsule might meet a

pop-up with the folded cellulose chains before final separation with the attached extended cellulose chains. 25 retract curves were analysed and 16 cases exhibited obvious sharp pop-up interaction in 0.1 M NaCl solution as shown in Figure 5.12 (a), which means it was not an occasional case. Additionally, the mean adhesion force seemed to be independent of ionic concentration in Figure 5.13(a), which indicates that the interaction between MF microcapsules and the cellulose thin film may be irrelevant to electrostatic interaction. Therefore, the bridging force is considered to be one of the main mechanism of the adhesion in this case. The bridging interaction proposed here is consistent with Zoppe *et al.*'s work (2011) when they investigated the surface interaction between a silicon sphere probe and a cellulose nanocrystal surface modified with poly (NiPAAm) as brushes.

After the cellulose thin film was treated with PVF, chitosan and PEI, the attractive forces were observed on approach (Figure 5.11 (b), (c) and (d)), which is in direct contrast to comparable measurements with the unmodified cellulose film in Figure 5.11 (a). After the modification, the microcapsule and cellulose thin film surfaces had opposite charges. When a microcapsule approached the modified surface, electrostatic attraction occurred to capture the microcapsule to the surface, enhancing the adhesion. Therefore the increase of ionic strength screening the attractive interaction between the two surfaces was observed in NaCl solution of 0.1 M, see the mean value of the pull-off force as a function of ionic strength in Figure 5.13 (b), (c) and (d). The plateau in the force-separation curve is observed on retraction after cellulose thin film was modified with PVF, chitosan and PEI (Figure 5.12 (b), (c) and (d)). The tip-surface separation distance (the distance from the point of two surfaces contacted to the point where the microcapsule separated from the surface on the retraction curve, which will be explained in detail in Chapter 6) between the microcapsule and PE-modified cellulose

film is about 1500 nm, 1000 nm and approximately 200 nm to 400 nm in a 10^{-3} M NaCl solution for PVF, chitosan and PEI respectively (Figure 5.12 (b), (c) and (d)). The tip-surface separation distances may reflect the length of the polyelectrolyte molecules; the molecule weight of PVF, chitosan and PEI is 1000 kg mol^{-1}, 400 kg mol^{-1} and 750 kg mol^{-1} respectively. However, PEI is highly branched and this is possibly to be the reason that the tip-surface separation of PEI was much smaller than that of PVF and chitosan. The tip-surface distance between the microcapsule and chitosan-modified cellulose thin film was about 5 to 10 times of the contour length of single chitosan molecule (94 to 178 nm) measured in Kocuna *et al.*'s work (2011). It should be mentioned that the chitosan molecule used in this work (400 kg mol^{-1}) is about twice as big as the one used in Kocuna *et al.*'s work (220 kg mol^{-1}); and also the diameter of the microcapsule probe is much bigger than that of a tip of a cantilever, so there were more chitosan strands (Kocuna *et al.* 2011) attaching on the microcapsule surface, extending the tip-surface separation distance. Therefore, after contact positively charged PE acts as a "polyelectrolyte bridge" and "molecule chain bridge" connecting the negatively charged microcapsule and negatively charged cellulose film. When two surfaces were separated, a higher force was needed.

5.4.3 Adhesion as a function of pH

The adhesion between MF microcapsules and a non-modified cellulose film decreased with increasing pH of the suspension liquid, as shown in Figure 5.15 (a). However, the adhesion between microcapsules and the modified cellulose thin film with PVF, chitosan and PEI firstly increased and then decreased with pH (Figure 5.15 (b), (c) and (d)). The maximum value was observed approximately at pH 5 for PVF and chitosan

and pH 7 for PEI. Both non-modified cellulose thin film and MF microcapsules were negatively charged and their surfaces became more negative by increasing the pH, causing the decrease of adhesion between them. However, after PE molecules were attached on the cellulose film, amine groups of PVF, chitosan and PEI are totally protonated and deprotonated at pH 3 and pH 11 respectively. At pH 3 or pH 11, the carboxyl groups (Liu 2010) on the surface of the microcapsules are uncharged or negatively charged. So the attraction was weak between them at pH 3 or pH 11. Both functional groups on the surface of microcapsule and modified cellulose thin surfaces are of half-deprotonation in medium pH range. The pK_a value of charged carboxyl group on cellulose and glucosamine segments on chitosan molecule is 4-5 (Notley 2009) and 6.3-7.5 (Claesson and Ninhami 1992, Kocuna *et al.* 2011) respectively. Therefore, the attraction between the microcapsule and modified surface reached a maximum value under pH 5. No pK_a is provided for PVF, but it contains similar $-NH_2$ groups so the pK_a may be similar. The maximum adhesion shifted from pH 5 to 7 after treatment with PEI compared with PVF and chitosan, which is attributed to be the increase of the pK_a value (8-10) of PEI (Zander 2009). Besides electrostatic attraction at the medium pH, amine groups and carboxyl groups on two surfaces may form hydrogen bonding (Giesbersa, Kleijnb *et al.* 2002), which helps to promote the adhesion. Additionally, a shape of the plateau in the force -separation curve is observed in low pH environment (Figure 5.16). In low pH solution, the carboxyl group on cellulose molecule is fully protonated. Cellulose film under this condition extended into solution loosely, causing the plateau events on retraction (Notley 2009). Therefore, the bridging force, because of the extension of cellulose chains, dominated the interaction between the microcapsule and cellulose thin film. However, the interaction between the microcapsule and PE-modified surface is mainly due to electrostatic attraction on approach. The strong electrostatic attraction brings the two surfaces into close contact

and there will be charge neutralization on approach. Upon separation, extra force will be required (Giesbersa *et al.* 2002). Additionally, hydrogen bonding and PE molecules act as bridges (Kocuna *et al.* 2011) increasing the energy required to separate the two surfaces, which corresponds to an increase in the peak force on separation.

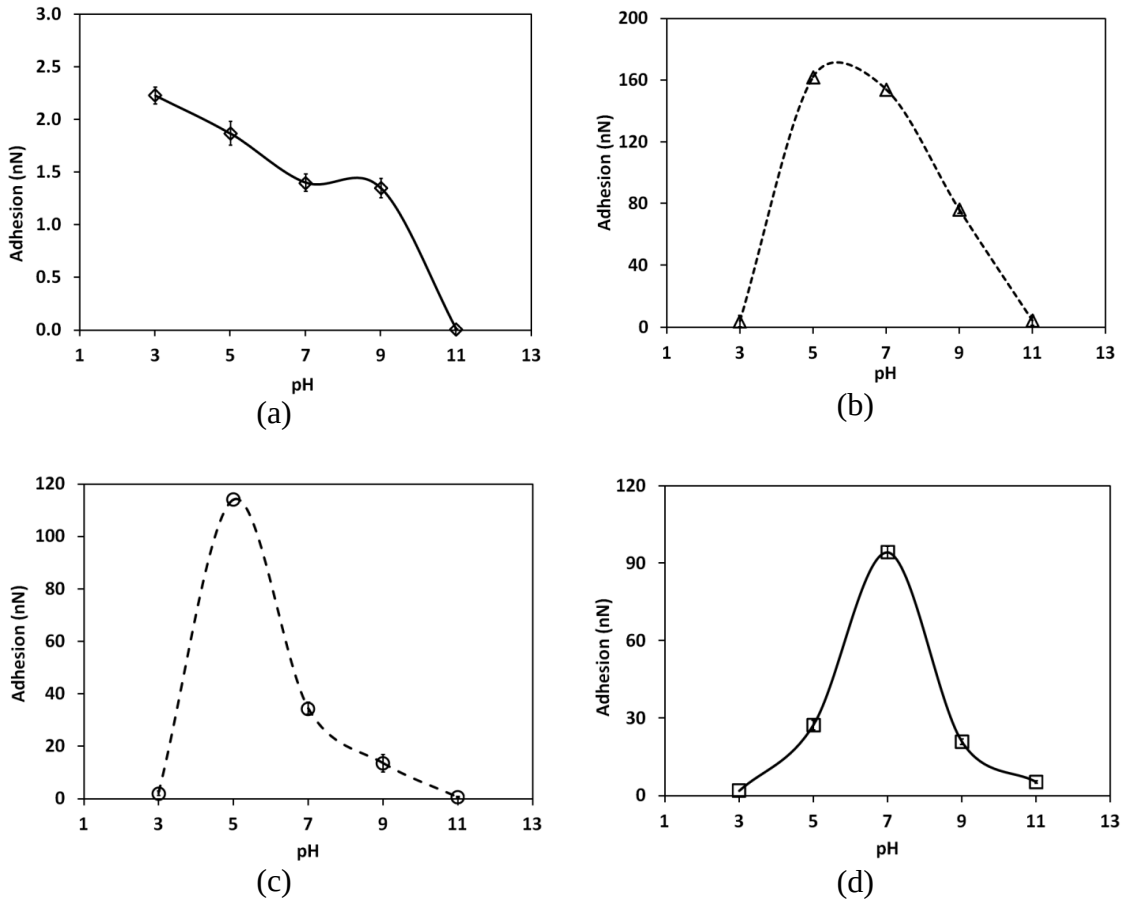

Figure 5.15 The average pull-off force between microcapsule and non-modified (a), PVF-modified (b), chitosan-modified (c) and PEI-modified (d) cellulose film in 10^{-3} M NaCl solution with different pH, and the dotted line just indicates the trend. At pH 5 some of the adhesion values are out of the scale in (b) and (c).

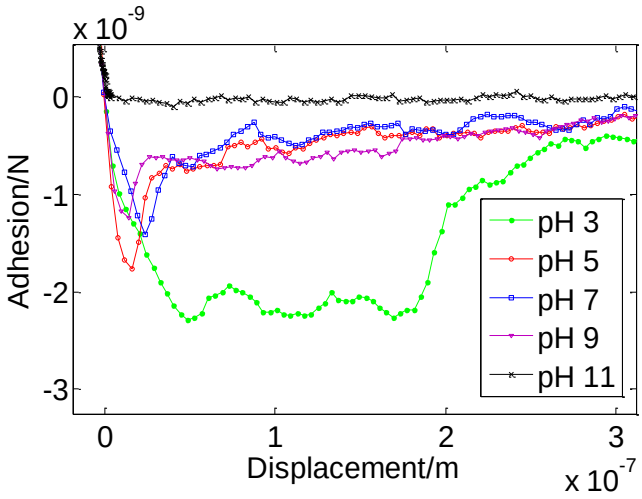

Figure 5.16 Typical force curves when single microcapsules were approaching to a non-modified cellulose film in 10^{-3} M NaCl solution with different pH.

5.4.4 Interpretation of the difference in the performance of PVF, chitosan and PEI

The main reason causing adhesion increase between MF microcapsules and PVF/chitosan/PEI-modified cellulose films was found to be electrostatic attraction, bridging force and hydrogen bonding. However, differences in the performance of different PEs were observed, in which the performances of PVF and chitosan were better than that of PEI. Since the similar functional amine groups are present on the three chemicals, the molecule structure and the surface charge of the chemicals may be the reason causing the difference and they are discussed as follows.

The zeta potentials of PVF, chitosan and PEI were investigated in §5.4.1 and the values at pH 5 were approximately the same; however, at pH 7 the zeta potential of chitosan was slightly lower than that of PVF and PEI. The retention test by a flow chamber technique and the adhesion measurement was conducted in aqueous solution, of which the pH value was about 5 to 6. Within the range, there was not much difference in the

value of zeta potential of the three chemicals and therefore the influence resulting from surface charge can be ignored.

Other than surface charge, the molecule structure is another possible reason causing the difference in the performance of the three chemicals. PVF is a kind of long linear molecule chains with repeated vinyl groups as the bone structure (Liu 2012); chitosan molecular chains in solution exist in a string-like conformation appearing as worm-like (spiral) single chains (Pedroni *et al.* 2003, Franca *et al.* 2011) and each repeat unit forms a spiral plane. Compared to PVF and chitosan, the PEI molecule is highly branched. Therefore, it is possible that when a microcapsule approaches to the surfaces modified with the three chemicals, molecules with long linear structures such as PVF and chitosan can be attracted to the microcapsule surface to form more trains and loops (Al-Hashmi and Luckham 2010); whilst it might be difficult for the steric effect from the highly branched molecules of PEI to form tight contact with the microcapsule surface. The spiral planes of chitosan also promote higher steric hindrance than PVF and it is expected that a higher adhesion between microcapsules and a modified cellulose thin film should be detected for PVF compared with chitosan. Therefore, the order of the performance of PEs to enhance adhesion and retention between microcapsules and cellulose thin films is PVF > chitosan > PEI.

5.5 Conclusions

PVF, chitosan and PEI were successfully introduced to the surface of a cellulose thin film respectively and the retention and adhesion of perfume-filled melamine formaldehyde microcapsules on the cellulose thin film was correspondingly enhanced. The surface area covered by remaining microcapsules increased from less than 10 % to

90 % at a shear stress of 3.95 $\times 10^{-2}$ Pa before and after PVF and chitosan solutions at a concentration of 0.1 wt% were applied to a cellulose film for 30 min. Less retention of microcapsules on the cellulose film modified by PEI for the same other conditions was observed, just 67%. Correspondingly, the average pull-off force between single microcapsules and the cellulose thin film increased from 2.3 ± 1.0 nN to 72 ± 23 nN, 58 ± 31 nN and 13 ± 4 nN after modification using PVF, chitosan and PEI respectively at a concentration solution of 0.1 wt%, as measured by AFM with a contact time of 0.01 s. The agreement between the adhesion results obtained using the two techniques indicates that the flow chamber technique can be potentially used as a tool for fast screening the effects of various chemicals on the adhesion of microcapsules on different fabric surfaces.

The mechanism of adhesion between the microcapsules and unmodified cellulose thin film was mainly attributed to the bridging force resulting from the extension of cellulose molecule chains. After the modification, chitosan molecules attached on the surface of the cellulose to capture microcapsules through electrostatic attraction and then the adhesion was enhanced by electrostatic attraction, bridging interaction and hydrogen bonding on separation. The difference in the molecular structure may be the main reason to cause the difference in the performance of adhesion enhancement between microcapsules and cellulose films, which is PVF > chitosan > PEI. The mechanisms proposed here suggest that the positively charged chemicals with long molecule chains can be potentially useful to modify the surface of microcapsules and enhance their retention on a fabric surface.

Chapter 6: Investigation of Adhesion of Perfume-filled Microcapsules to A Polyester Fabric Surface by AFM and a Flow Chamber Technique

6.1 Introduction

Polyethylene terephthalate (PET) is the most commonly used material to make polyester fabrics and it accounts for approximate 50% of all polyester fibre materials (Takke *et al.* 2011). Polyester is widely used in the clothes industry as an alternative to cotton. Polyethylene terephthalate (PET) is a linear and aromatic polymer which lacks polar and reactive functional groups such as hydroxyl, carboxyl and amine groups (Mohamed *et al.* 2012). It is hydrophobic in nature and the water contact angle on its surface was reported to be about 80 ° (Dadsetan *et al.* 2000, Liu *et al.* 2005, Yang *et al.* 2009, Nina *et al.* 2011). The surface hydrophobicity of PET has been decreased by various methods such as plasma treatment (Navaneetha *et al.* 2008, Yang *et al.* 2009), hydrolysis followed by adsorption of oppositely charged polymers (Liu *et al.* 2005), silver ion implantation (Li *et al.* 2007) and introducing a hydrophilic surface finishing agent to the surface (Zaman *et al.* 2013) to increase the wetting ability. Adhesion could be either enhanced between the modified-PET surface and surfaces or chemicals containing caboxyl, hydroxyl and amine groups through forming hydrogen bonds (Takke *et al.* 2011) or decreased between *Staphylococcus epidermis* and the Ag^+ modified PET surface because the release of the antibacterial Ag^+ (Li *et al.* 2007).

Polyelectrolytes are the most common chemicals reported to enhance adhesion (Claesson *et al.* 2003, Sczech and Riegler 2006, Che *et al.* 2008). Adhesion was

enhanced either through electrostatic attraction or bridging forces at the interface (Podgornik and Ličer 2006). Electrostatic attraction works between oppositely charged surfaces and it is most likely to occur after one of the surfaces was modified with polyelectrolyte of a high concentration (Che *et al.* 2008); conversely, bridging forces are more likely to occur at interfaces modified with a low concentration of PE, which is more dependent on the molecular structures (Roiter and Minko 2005, Podgornik and Ličer 2006, Notley 2009, Kocuna *et al.* 2011) and the dimension of single molecular chains of polyelectrolyte. Polyelectrolyte molecules such as chitosan (Kocuna *et al.* 2011), poly (2-vinylpyridine) (Roiter and Minko 2005) and PVAm-PBA (polyvinylamine derivatized with phenylboronic acid) (Chen *et al.* 2009, Notley 2009, Zhang *et al.* 2010) were reported to raise adhesion between a Si_3N_4 AFM cantilever tip and a mica surface, and cellulose surfaces through bridging forces by AFM. However, the work is still very limited on using polyelectrolytes to modify polyester surfaces, then investigating the adhesion and understanding the adhesion mechanism between microcapsules and polyester surfaces; furthermore, no work has been published on exploring the influence of the polyelectrolytes' molecular structures on the adhesion behaviour.

Therefore in this study, three polyelectrolytes (PEs): PVF, chitosan and PEI were introduced to modify a PET surface and then the adhesion between perfume-filled microcapsules and the PET surfaces before and after being modified with PEs were investigated by AFM and the retention of microcapsules on these surfaces under a shear flow by a flow chamber technique. Adhesion mechanisms between them were investigated based on the hydrophobic nature of the PET surfaces, the structures of the polyelectrolytes and the detailed information extracted from the force-displacement curves obtained by AFM. It is expected that a correlation between the data of adhesion

and those of retention using the polyelectrolytes with different molecular structures can be determined, which can provide guidance to propose a strategy to enhance the retention of microcapsules on the polyester surface according to the molecular structures of PEs.

6.2 Experimental

6.2.1 Perfume-filled MF microcapsules

Perfume-filled MF microcapsules were supplied by Procter & Gamble, Belgium. The detailed information was provided in §3.1.1.

6.2.2 Polyethylene terephthalate (PET) films

A flat polyethylene terephthalate (PET) film was used to mimic an artificial fabric surface and the information was described in 3.1.2.2.

6.2.3 Surface treatments on PET surfaces

The detailed procedures to modify PET surfaces with PVF, chitosan and PET solutions for adhesion measurements by AFM and retention tests by a flow chamber technique were described in §3.2.2.

6.2.4 X-ray Photoelectron Spectroscopy (XPS)

X-ray Photoelectron Spectroscopy at the University of Warwick was used to do surface composition analysis of PET before and after being modified with PEs. The experimental details were described in §3.3.4.

6.2.5 Contact angle

The contact angle of a water droplet on PET surface before and after being modified with PEs was characterised using a contact angle measurement apparatus equipped with a Charge Coupled Device (CCD) camera (KP-M1E/K, Hitachi). The detailed procedures were described in §3.3.7.

6.2.6 Viscosity

The viscosities of the PE solutions were measured as described in §3.3.8.

6.2.7 Environmental scanning electron microscope (ESEM)

The image of MF membrane which was used to mimic the wall of MF microcapsules and the shell of microcapsules were scanned by ESEM, and the experimental details were described in §3.3.5.

6.2.8 Atomic force microscopy

6.2.8.1 AFM imaging

The topography of PET surfaces before and after being modified with PEs, and also PET surfaces after being hydrolyzed with 10 wt% NaOH solution was analyzed by AFM. For the details, see §3.3.9.

6.2.8.2 Force measurement

The adhesion of microcapsules to PET surfaces before and after being modified with PEs in HPLC water was measured by AFM, see §3.4.2.

6.2.9 Flow chamber experiment

The detailed procedures to measure the retention of microcapsules on PET surface before and after being modified with PEs were illustrated in §3.4.1.

6.3 Results

6.3.1 Modification of PET surfaces with PVF/chitosan/PEI

6.3.1.1 Surface composition of PET before and after modification with PVF/chitosan/PEI

PET is a kind of polymer containing C, O, H elements (Wang *et al.* 2004, Eslami and Müller-Plathe 2009). Other than the three elements, N element is another component

present in PVF, chitosan and PEI molecules, which can be used as an indication of the attachment of PVF/chitosan/PEI molecules to the PEI surface. The results of XPS analyses of PET surfaces are illustrated in Figure 6.1. No peak was present at 400±5 eV for a bare PET surface (Figure 6.1 (a)). After PVF, chitosan and PEI solutions at a concentration of 0.1 wt% were applied to the PET surface for 30 min respectively; obvious peaks were observed at approximately 400 eV, which indicates the attachment of the PE molecules on the surface. The results are consistent with the validation of attachment of PE molecules to cellulosic fabrics in a previous publication (Fras Zemljič *et al.* 2009). The atomic concentration of N on the PET surface modified with PVF, chitosan and PEI was 1.94%, 1.43% and 3.90% respectively, of which N present on the PET surface modified by PEI was higher than that by PVF or chitosan, which may be attributed to a higher atomic concentration of N in a PEI $(N_{11}C_{22}H_{55})_n$ molecule than that of PVF $(C_3H_5NO)_n$ and chitosan $(C_6H_{11}O_4N)_n$.

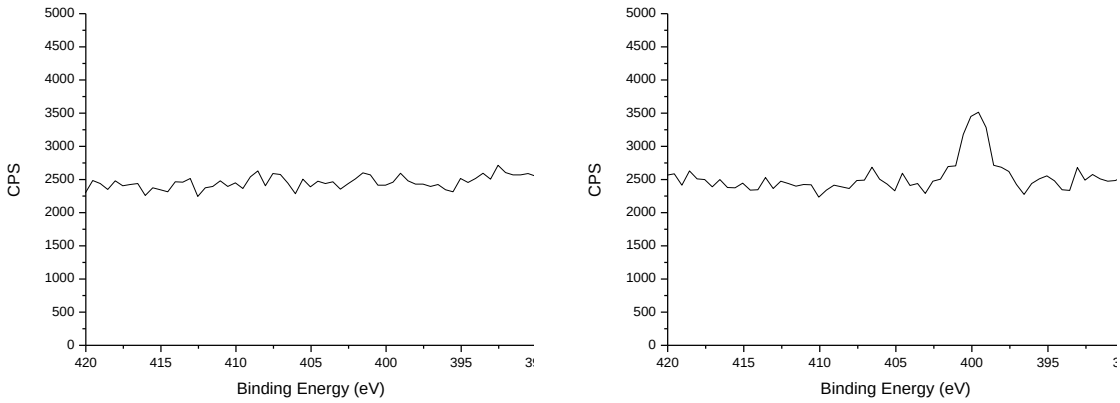

(a) (b)

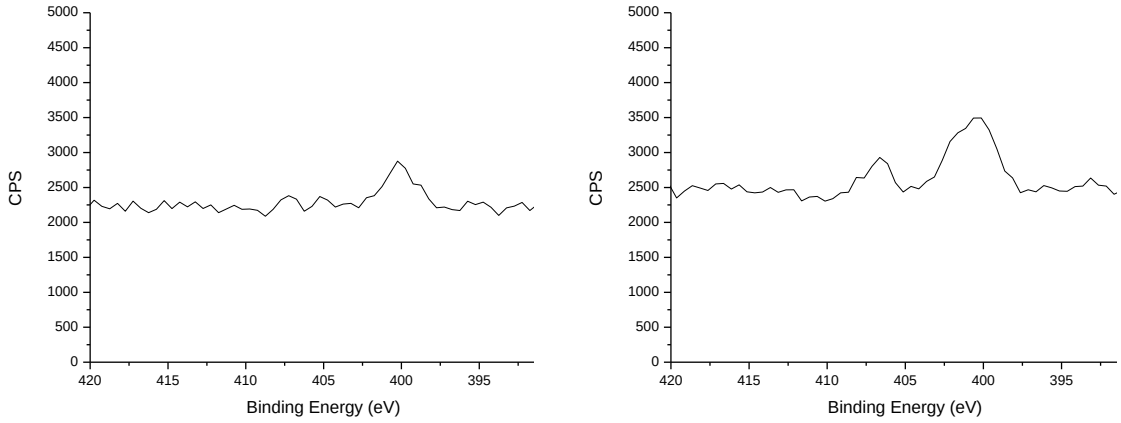

(c) (d)

Figure 6.1 XPS analyses of the N element of polyethylene terephthalate surface (a) and polyethylene terephthalate surface modified with 0.1% (wt. %) PVF (b) chitosan (c) PEI (d) solution.

6.3.1.2 Surface roughness

The surface topography and roughness of PET surfaces were investigated by AFM. As can been seen in Figure 6.2 (a), the PET surface was quite smooth and the RMS roughness was just 2.9±0.6 nm over a scan area of 10 μm × 10 μm. The results are comparable with those reported in previous publications (Fu *et al.* 2005, Liu *et al.* 2005, Yang *et al.* 2009). After the three PE solutions at a concentration of 0.1 wt% were applied to each PET surface for 30 min, some protuberances were present on the modified surfaces. The RMS roughness of the PET surface slightly increased by the surface treatment with PVF and PEI, which was 4.8±0.7 nm and 4.7±1.0 nm respectively; however, after being modified with chitosan solution, the PET surface became much rougher with a RMS roughness of 12.3±1.0 nm, see Figure 6.2 (c). The increase of surface roughness is attributed to the attachment of PVF, chitosan, PEI

molecules to the PET surface, which agrees with the observation of PEG deposition on untreated PET surfaces (Takke *et al.* 2011).

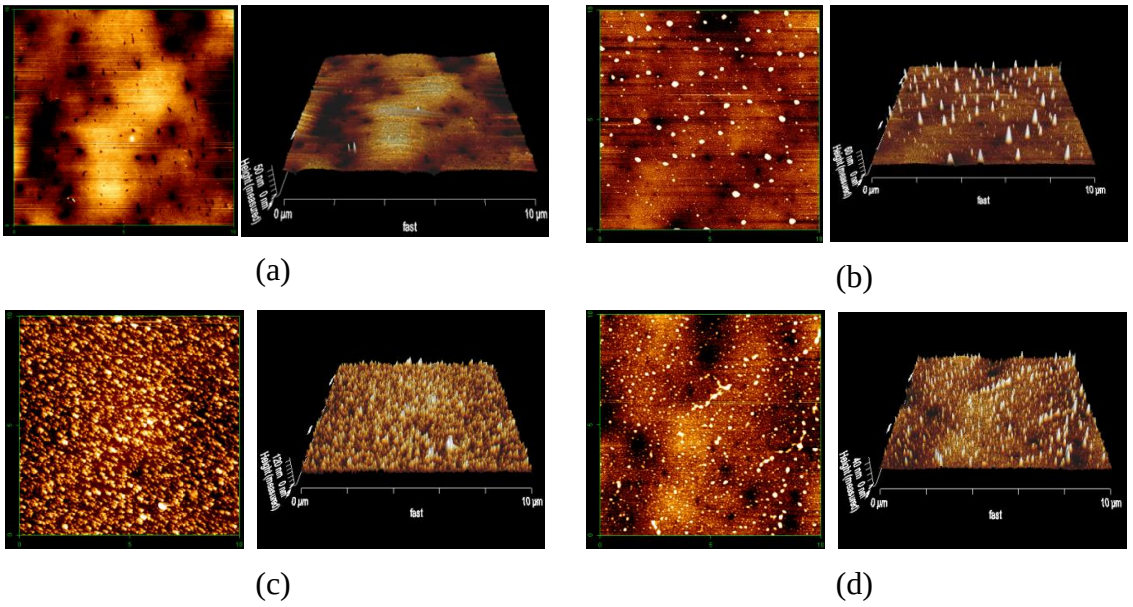

Figure 6.2 2D and 3D images of polyethylene terephthalate surfaces (10 μm ×10 μm) (a); after modification with 0.1wt% PVF (b)/chitosan (c)/PEI (d) (RMS: (a) 2.9 ±0.6 nm, (b) 4.8 ±0.7 nm, (c) 12.3 ±1.0 nm, (d) 4.7 ±1.0 nm).

6.3.2 Retention of microcapsules on PET surfaces investigated by the flow chamber technique

The retention of microcapsules on PET surfaces was investigated by the flow chamber technique. Water with a given flow rate of 80 mL h^{-1} as used to remove microcapsules from cellulose films was first used to remove microcapsules from PET surfaces, and it was found that more than 80% of microcapsules still remained on the PET surface. Compared with a retention ratio of less than 10% on the cellulose film under the same flow condition, the interaction between MF microcapsules and the PET surface is much

stronger than that on the cellulose film. The PET surface modified by the polyelectrolytes, was found to enhance the retention ratio of MF microcapsules on the surfaces. In order to show their effects, higher flow rates were used and the results for the non-modified surface are shown in Figure 6.3. The retention ratio of microcapsules decreases with the increase of the flow rate from 50 mL h^{-1} (shear stress of 2.47×10^{-2} Pa) to 200 mL h^{-1} (shear stress of 9.88×10^{-2} Pa). At 200 mL h^{-1}, more than 66% of microcapsules were removed; therefore a flow rate of 200 mL h^{-1} was used in further experiments on the modified PET surfaces.

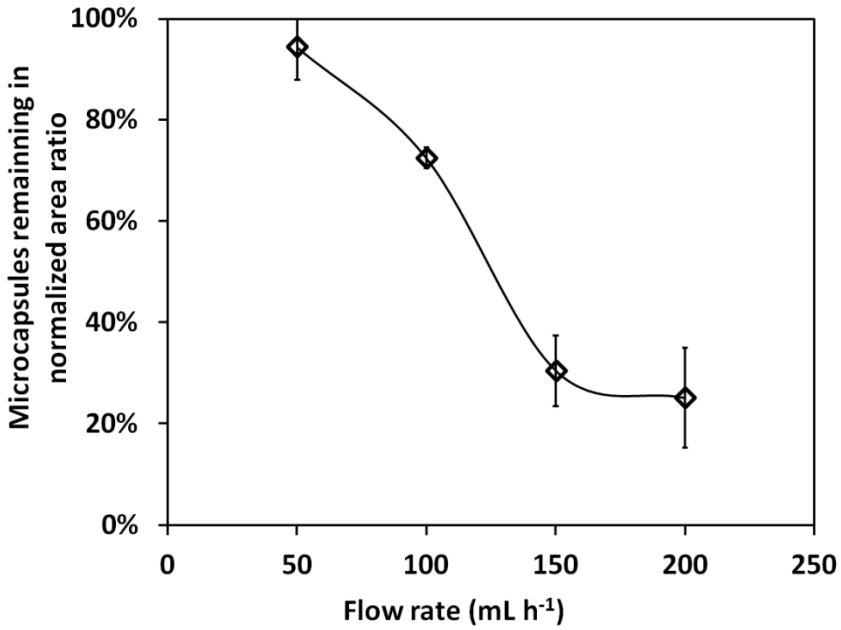

Figure 6.3 Microcapsules remaining on a non-modified PET surface in normalized area ratio as a function of flow rate.

Each PET surface was modified with PVF, chitosan and PEI respectively with a concentration of 0.1 wt% and 0.01 wt%. Without the modification, about 33% microcapsules remained on the PET surface after applying a shear stress of 9.88×10^{-2} Pa

to the microcapsules for 3 min. After each PVF, chitosan and PEI solution of a concentration of 0.1 wt% was applied on the PET surface for 30 min, more than 90% of microcapsules remained for all three chemicals (the blue columns in Figure 6.4). The order of the performance of the three chemicals was PVF > chitosan > PEI (Figure 6.4). In order to get a clear contrast, the concentration of PVF, chitosan and PEI was further diluted to 10^{-4} ppm, and then the results of microcapsules remaining on the modified PET surfaces are illustrated in Figure 6.4. As can be seen, after the modifications with the diluted PVF, chitosan and PEI solution, the retention ratio of microcapsules was 79%, 55% and 49% respectively (the red columns in Figure 6.4). A better contrast of the performance of the three chemicals (PVF> chitosan > PEI) has now been observed and more microcapsules remained on the modified PET surface compared with the non-modified surface, the retention ratio of which is 33%.

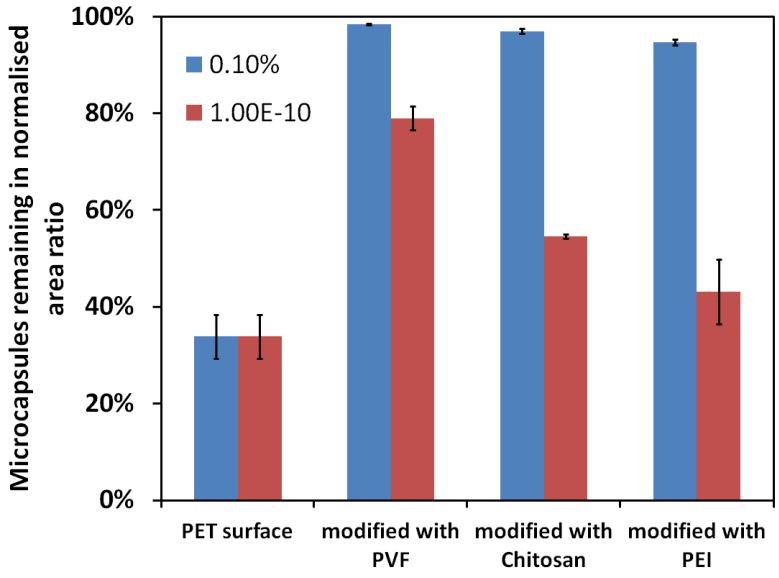

Figure 6.4 Effect of modification of each PET surface with PVF/chitosan/PEI solution on the removal of microcapsules from it. The errors bars represent the standard error of the mean based on at least 3 repeated measurements.

6.3.3 Adhesion between single microcapsules and PET surfaces investigated with AFM

The interaction between single microcapsules and a PET surface before and after being modified by PVF, chitosan and PEI respectively was also investigated by AFM with a colloidal probe. The average pull-off forces with a contact time of 0.01 s and 10s are presented in Figure 6.5. The average adhesion of single microcapsules (N=5) on a non-modified PET surface was 13±3 nN (0.01 s) and 35±3 nN (10 s) respectively. After the surface was modified with PVF (N=6), chitosan (N=5) and PEI (N=5) respectively, the average adhesion decreased to 7.2±3.6 nN (0.01 s) and 23±6 nN (10 s), 4.7 ±0.5 nN (0.01 s) and 21 ±4 nN (10 s) and 6.3±1.1 nN (0.01 s) and 23±4 nN (10 s) respectively. It is surprising that the adhesion decreased after the PET surface was modified with the three PEs, which seems to be inconsistent with the retention behaviour presented in 3.2. Additionally, there is no significant difference in the value of the adhesion between single microcapsules and the modified PET surface with the three kinds of PE. A further interpretation will be discussed in §6.4.

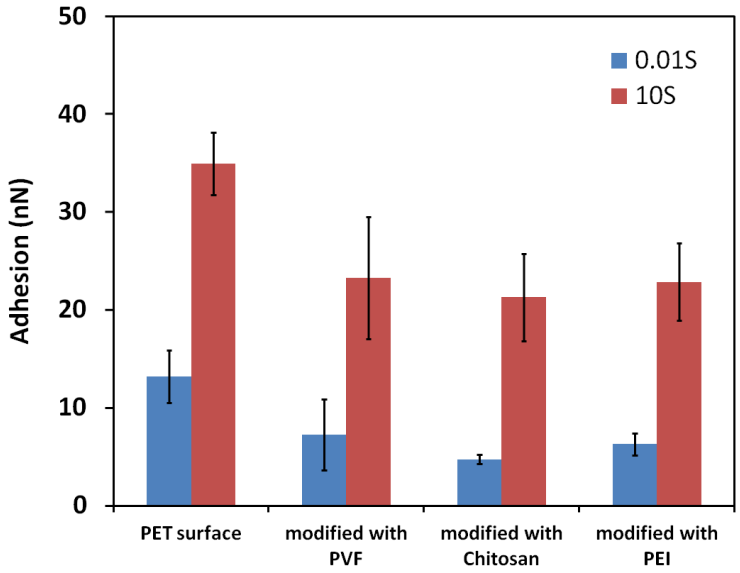

Figure 6.5 Adhesion between single microcapsules and a PET surface before and after being modified with PVF/chitosan/PEI solution. The error bars represent the standard error of mean pull-off force. The number of microcapsules (N) measured for non-modified, modified PET surface with PVF, chitosan and PEI are 5, 6, 5 and 5 respectively.

6.3.4 Summary of the adhesion behaviour on PET surfaces

The attachment of PVF, chitosan and PEI molecules on each polyethylene terephthalate surface was validated by XPS analyses and AFM mapping in this work. It was more difficult to remove microcapsules from a PET surface by a given fluid flow than from a cellulose film, and treatment of the PET surface with the three kinds of PE all showed an enhancement of retention of microcapsules. The performance of PVF was better than that of chitosan and PEI. It is surprising to note that the average adhesion force characterized by AFM presented a different trend, in which the average pull-off force decreased after each PET surface was modified with PVF, chitosan and PEI. The PET surface was reported to be much more hydrophilic after a polyelectrolyte was introduced on the surface (Huh *et al.* 2001, Nina *et al.* 2011, Takke *et al.* 2011) and a

decrease of adhesion of 3T3 fibroblast cell to the modified-PET surface (Nina *et al.* 2011) has been observed. To the author's knowledge, there has been no research work to date investigating the interaction between single micro-particles and a PET surface. It is supposed that the inconsistency indicates that the peak value of the pull-off force is not the only factor to determine the retention behaviour, especially when microcapsules are removed in the lateral direction. Possible mechanisms of the retention enhancement and the reason for the inconsistency of the results between AFM and the flow chamber technique observed on the modified PET surfaces will be discussed in §6.4.

6.4 Discussion

6.4.1 Mechanisms of adhesion between MF microcapsules and PET surfaces

The adhesion of single MF microcapsules on a un-modified PET surface was found to be greater compared with the corresponding result on a cellulose film, see Chapter 5, and the adhesion increased from a few nano-Newton on a cellulose film to about 13 to 35 nN on the PET substrate for contact times of 0.01s and 10 s measured by AFM. Additionally, a flow rate of 80 mL h^{-1} which was used to remove most of the microcapsules from the cellulose film was not sufficient to remove the microcapsules from the unmodified PET surface. Therefore, the mechanisms of adhesion between MF microcapsules and PET surfaces is supposed be different from those between MF microcapsules and cellulose thin films.

6.4.1.1 Hydrophilic and hydrophobic nature of MF microcapsules and PET surfaces

A MF membrane prepared according to a method proposed by a visiting scholar Professor Hong Huang from South China University of Technology (personal communication) was used to mimic the shell of MF microcapsules and the contact angle on the membrane was measured to determine the hydrophilic and hydrophobic nature of the surface of MF microcapsules. ESEM was used to determine the surface topography of both MF microcapsules and the MF membrane, and the images are shown in Figure 6.6. Although the thickness of the MF membrane, which was approximately 1.2 μm, was about 12 times larger as that of the shell of MF microcapsules of 100 nm, the morphologies of the MF membrane and MF microcapsules were nearly the same, which means that the MF membrane can be used to mimic the shell of MF microcapsules.

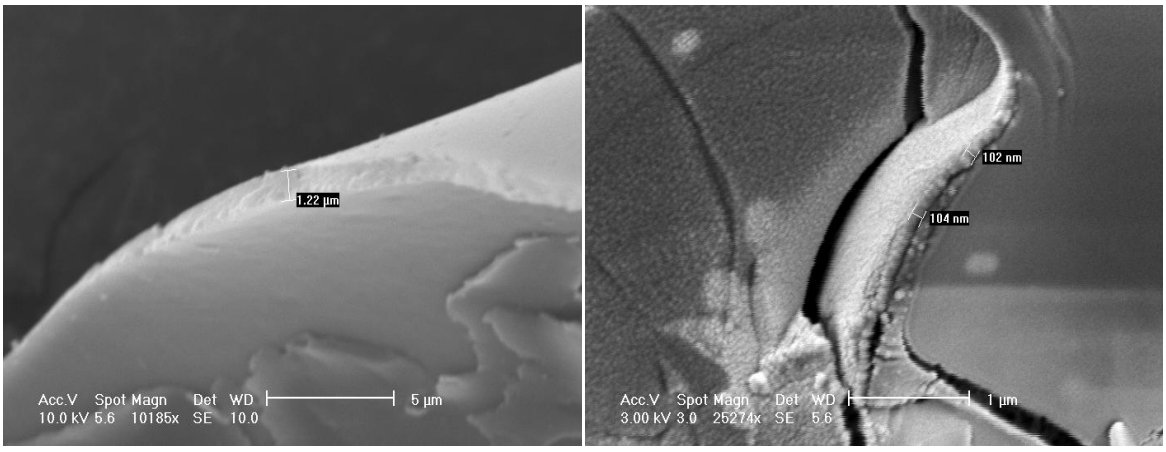

(a) (b)

Figure 6.6 ESEM images of a MF membrane (a) and shell of MF microcapsules (same image as used in Figure 4.10 (a)) (b).

The contact angles between water droplets and a MF membrane and PET surface were measured, which are 66 °±1 ° and 82 °±1 ° respectively. Although melamine-

formaldehyde is hydrophilic in nature with a contact angle of 34 ° (Crick and Parkin 2011), the hydrophilic and hydrophobic nature can be adjusted by their surface topography (Xu *et al.* 2007, Crick and Parkin 2011) because proper microstructures can trap air under the water droplet which can increase the hydrophobicity. The result of the contact angle on the MF membrane in this work is comparable with that measured in Crick and Parkin's work (2011). PET is synthesized from ethylene glycol and dimethyl terephthalate ($C_6H_4(CO_2CH_3)_2$) or terephthalic acid and it bears repeated units containing aromatic rings, ester and vinyl groups on the backbone of the molecules. The contact angle of a water droplet on the PET surface is consistent with that determined in the previous research works (Dadsetan *et al.* 2000, Liu *et al.* 2005, Yang *et al.* 2009, Nina *et al.* 2011). Therefore, compared with the cellulose thin film with a contact angle of about 30 ° (Liu 2010), the PET surface is much more hydrophobic and the hydrophobic interaction (Meyer *et al.* 2006, Thormann *et al.* 2008, Israelachvili 2011) between MF microcapsules and the PET might be one of the reasons for the adhesion.

6.4.1.2 Influence of the hydrophobic nature and surface roughness on adhesion

The adhesion of single MF microcapsules on a PET with varying hydrophobicity was investigated. The hydrophobicity of PET was adjusted by converting the ester groups into carboxyl and hydroxyl groups (Liu, He *et al.* 2005) by treating it with NaOH. Figure 6.7 presents the surface topography of the PET surface after being treated with NaOH and the RMS roughness is 176.4 ± 6.2 nm. The morphology of the surface is quite similar to that reported in Liu *et al.*'s work (2005). The contact angle of water droplets on the treated PET surface was 72 °±1 °, which was smaller compared with that on the untreated PET surface which was 82 °±1 °. Therefore the PET surface became

more hydrophilic and rougher after being treated with NaOH. The adhesion between a microcapsule with a diameter of about 20 μm and the PET surface before and after treatment with NaOH is presented in Figure 6.8. The adhesion decreased from 10.6 ± 0.3 nN and 34.1 ± 1.0 nN to 3.7 ± 0.3 nN and 10.3 ± 1.4 nN with a contact time of 0.01 s and 10 s. The adhesion decreased as expected from the increase of the hydrophilicity and surface roughness, in which the adhesion is further explained to be due to hydrophobic interaction.

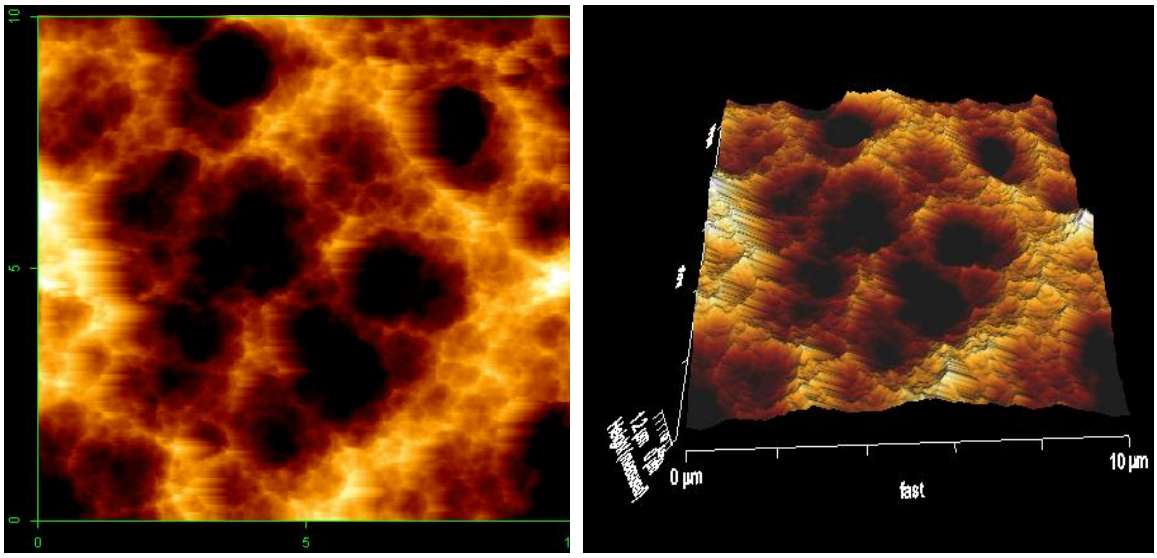

(a) (b)

Figure 6.7 AFM image of a PET surface treated with 10 wt% NaOH solutions at 80 ℃ for 12 hours, (a) 2D image and (b) 3D image.

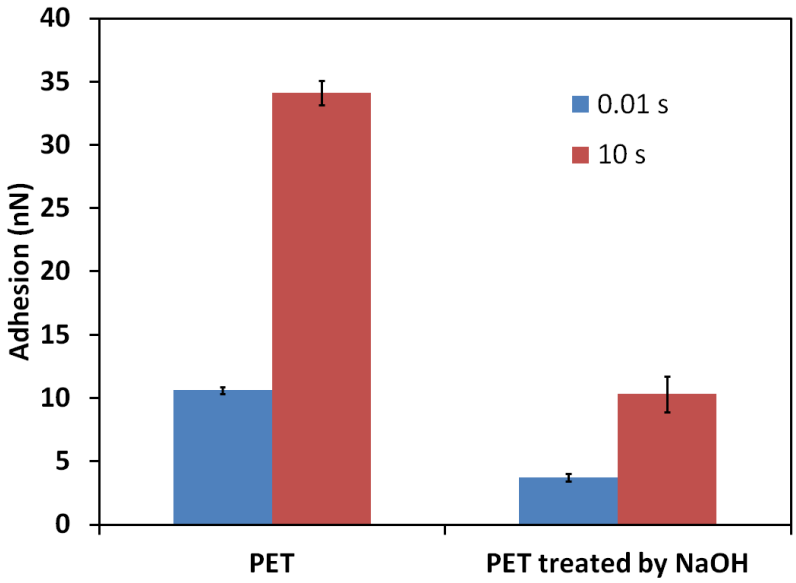

Figure 6.8 The mean value of adhesion between a MF microcapsule with a diameter of 20 μm and PET surface before and after being treated with NaOH in HPLC water with a contact time of 0.01 s and 10 s.

6.4.2 Adhesion between microcapsules and PET surface modified with polyelectrolytes

The mean value of adhesion was found to decrease after a PET surface was modified with the polyelectrolytes, which was unexpected. However, the retention ratio was enhanced. Therefore, it is fundamentally important to understand why there is such a discrepancy.

6.4.2.1 Surface hydrophilic properties of PET

Contact angle measurements were conducted to determine the hydrophilic and hydrophobic nature of PET surfaces before and after modification with PVF, chitosan and PEI. The contact angle θ, between a drop of water and a reference PET surface and

modified surfaces is listed in table 1. The contact angle of a water droplet on a non-modified PET surface was 82 °±1 °, which is comparable with that determined in the research works (Dadsetan *et al.* 2000, Liu *et al.* 2005, Yang, *et al.* 2009, Nina *et al.* 2011). After the PET surfaces was modified with PVF, chitosan and PEI, the contact angle decreased slightly to 65 °±2 °, 77 °±2 °, 70 °±1 ° respectively. The results of contact angle after the PET was modified with the polyelectrolytes are comparable with that on a PET surface deposited with a layer of chitosan in Liu *et al.*'s work (2005). The functional groups of PET are nonpolar and it is difficult for them to form hydrogen bonds with amine groups which presented in the three polyelectrolytes used to modify the PET surface. Therefore, it is suggested that the attachment of polyelectrolyte molecules on the surface of PET after modification altered the hydrophobic nature of the substrate, which caused the decrease of the adhesion between microcapsules and the PET surface. The adhesion measured by AFM with a hydrophobic probe coated with octyltrichlorosilane (OLTS) to a polystyrene (PS) surface was also reported to decrease due to increasing the hydropilicity of the PS surface by modifying it with poly(styrene-b-origoethylene glycol methyl ether methacrylate) (PS-PME NMA) in previous publication (Zhang *et al.* 2008)

Table 6.1 the contact angle of a water droplet on PET surfaces.

	polyester	modified with 0.1% PVF	modified with 0.1% chitosan	modified with 0.1% PEI
Contact angle	82 °±1 °	65 °±2 °	77 °±2 °	70 °±1 °

6.4.2.2 Surface topography analysis

Polyelectrolyte molecules were attached on the PET surfaces and their configuration was examined by AFM. PVF, chitosan and PEI molecules on the PET surface were found to be stretched because the PET surface is neutral and the positively charged PE molecules cannot have intimate contact compared with a negative surface such as cellulose, as shown in Figure 6.9, which is another factor causing the decrease in adhesion between microcapsules and the modified PET surface. Besides, after modification with the chemicals, some protuberances were observed on the PET surfaces. These were analysed. As can be seen in Figure 6.9, the protuberances distributed more densely on the surfaces modified with chitosan and PET compared with PVF. However, the dimension of the protuberances on the PVF-modified surface was bigger than that of chitosan and PEI. The height of the protuberances was about 60 nm, 30 nm and 15 nm for PVF, chitosan and PEI respectively; and the diameter of the protuberances was about 500 nm for PVF, while for chitosan and PEI it was much smaller, i.e. 100 nm to 300 nm and 50 nm to 200 nm respectively. The polyelectrolyte chain size $R_{chain\text{-}size}$ was reported to be dependent on the degree of polymerization N_{DP}, in which $R_{chain-size} \sim N_{DP}(\ln N_{DP})^{0.33}$ (Liao *et al.* 2003). The calculated polyelectrolyte size is presented in Table 6.2 and the size of PVF is much bigger than that of chitosan and PET; although the molecule weight of PEI is bigger than that of chitosan, but its size is still smaller because it is branched (Üzüm *et al.* 2012).

Considering the molecular structure of the polyelectrolytes gives a reasonable explanation of the difference in the protuberances on the PET surface caused by them. Single polyelectrolyte chains like poly(2-vinylpyridine) (P2VP) (Roiter and Minko 2005) and chitosan (Kocuna *et al.* 2011) on mica substrates have been imaged by AFM.

The length and width of a single molecule were reported to be around a few hundred nano-meters and less than 1 nm respectively, which are much smaller than the height value determined in this work. It was supposed that single positively charged molecular strands adsorbed on mica through electrostatic attraction and they were distributed in parallel to the surface at a very low concentration; however, the polyelectrolyte concentration used to modify the PET surface here was higher and therefore molecular chains were not presented as single strands; additionally, PET is naturally charged and a polyelectrolyte bearing positive charges is unlikely to form intimate parallel contacts with PET as with the negatively charged mica, and they possibly stretch from the surface to the solution and distribute vertically; moreover, the image in this work was captured in dry conditions, in which molecular chains are coiled and less extended than in liquid condition. Therefore, the stretching of the polyelectrolyte might not only increase the surface roughness, but also cause steric hindrance, which decreases the peak value of adhesion.

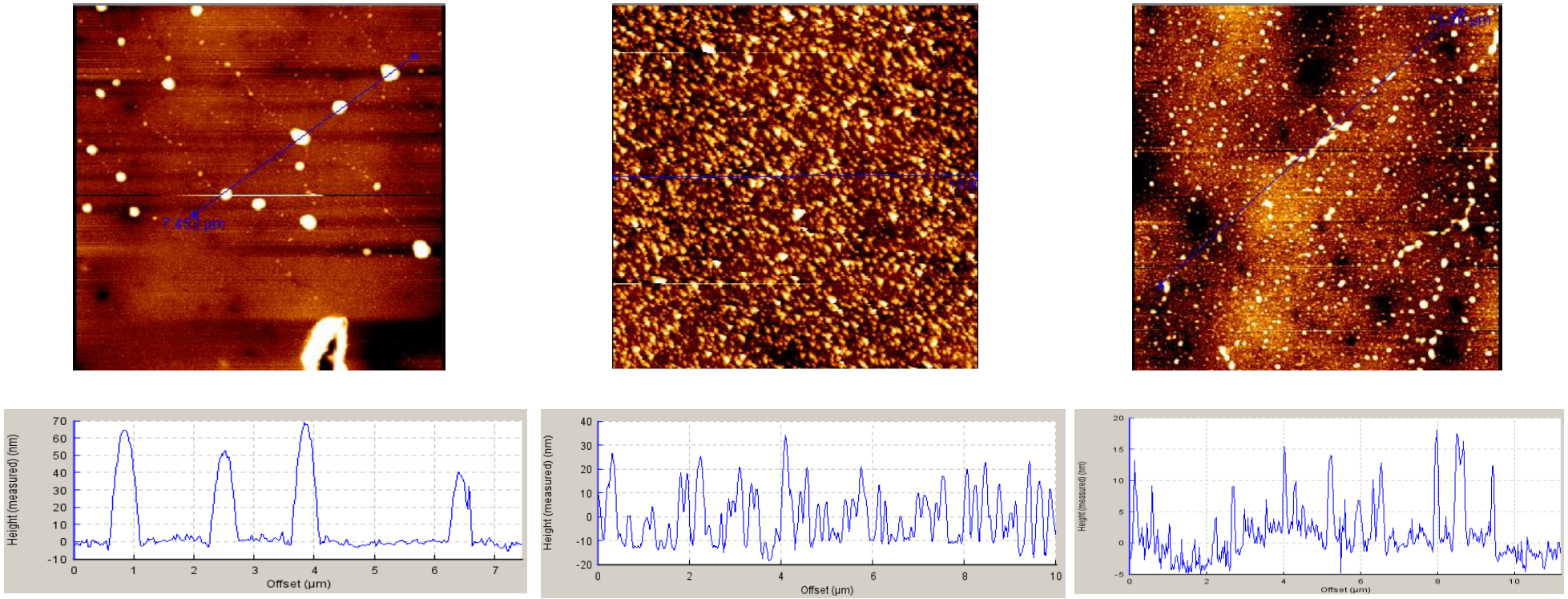

(a) (b) (c)

Figure 6.9 AFM analyses of the protuberances on the PET surface modified with PVF (a), chitosan (b) and PEI (c).

Table 6.2 Calculated polyelectrolyte size

	PVF	Chitosan	PEI
molecule weight (kg mol^{-1})	1000	400	750
molecule weight of each monomer(g mol^{-1})	71	161	473
the degree of polymerization N_{DP}	14085	2484	1586
The chain size $R_{chain-size}$	29661	4897	3065

6.4.2.3 Viscosity investigation

The viscosity of the three polyelectrolyte solutions was also investigated at 25^{o}C, and the results are given in Figure 6.10. The viscosity of water solution at 25^{o}C is 0.8902 × 10^{-4} Pa s^{-1} (Kestin *et al.* 1978). The viscosity of each polyelectrolyte solution decreases with the increase of shear rate from 10 (s^{-1}) to 100 (s^{-1}), which indicates the polyelectrolyte solutions are shear thinning liquids. The observation agrees well with conclusions of previous work (Wyatt and Liberatore 2009, El-Hefian *et al.* 2010, Wyatt *et al.* 2011) 0.1 wt% of PVF solution exhibited a higher viscosity than chitosan and PEI at a given shear rate, which indicates that the molecular chain of PVF is longer than that of chitosan and PEI (Ofori-Kwakye *et al.* 2006). This is consistent with the conclusion of §6.4.2.2. Therefore, the stretching of polyelectrolyte molecular chains is supposed here to be one of the reasons causing decrease in adhesion. Additionally, the molecular chains of PVF were found to be the longest and then chitosan and PEI was the shortest, which correlates well with the conclusion in §6.4.2.2.

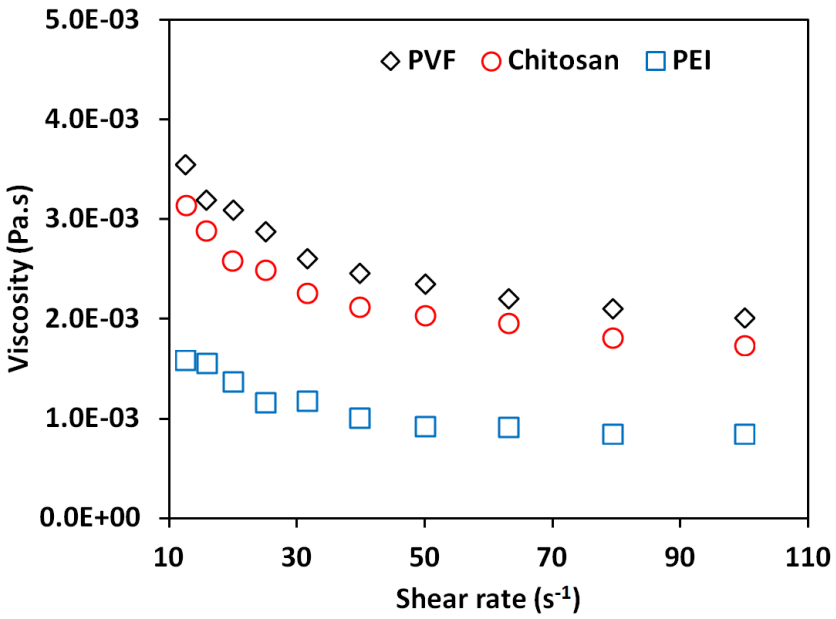

Figure 6.10 The viscosity of 0.1 wt% PVF, chitosan and PEI solution at pH 5.

6.4.2.4 Interpretation of forces curves obtained using AFM

Figure 6.11 shows typical force-displacement curves obtained by applying AFM to measure the adhesion between single MF microcapsules and PET surfaces before and after being modified by the three polyelectrolytes. Although the mean value of adhesion decreased after the surface modification, there are other features on the forces curves. The MF microcapsule retreated back sharply from the non-modified PET surface; see Figure 6.11 (a). However, multiple plateau events can be observed for the PET surface modified with PVF, chitosan and PEI (Figure 6.11 (b), (c) and (d)). The attachment of polyelectrolyte molecules to the surface was demonstrated in § 6.3.1. The presence of multiple events on the retraction curves is believed to be due to the extension of polyelectrolyte long molecular chains when the MF microcapsule was separated from the PE-modified PET surface. The results agree with the bridging interaction proposed in Chapter 4, which occurred between the cellulose film and the MF microcapsules modified with PVF and chitosan. Additionally, similar multiple events were observed

between a polystyrene sphere colloidal probe and a glass surface by AFM (Thormann *et al.* 2008), chitosan molecules (Kocuna *et al.* 2011) and a silica nitride tip and a cellulose film by AFM (Notley 2009), which was attributed to the extension of the long molecule chains.

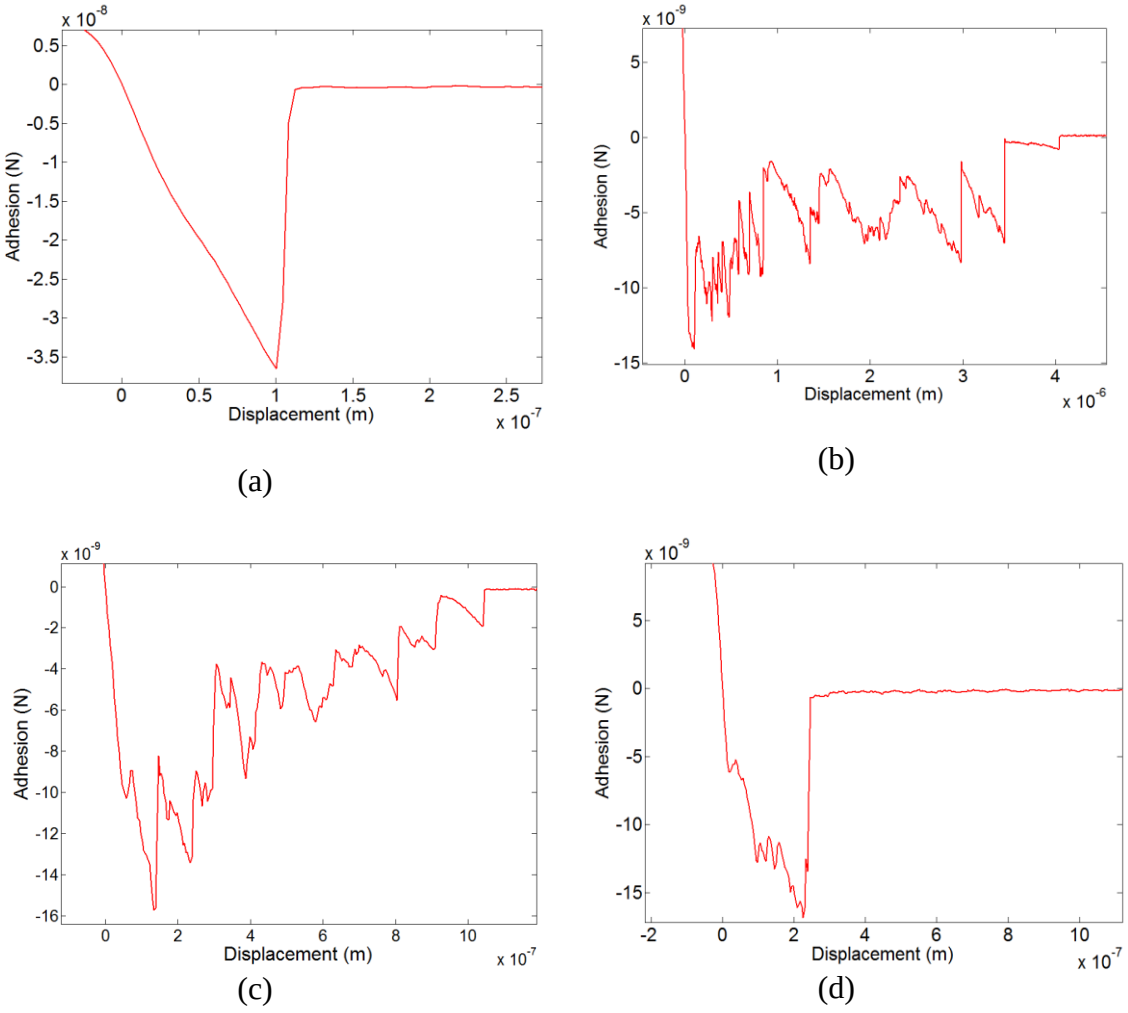

Figure 6.11 Typical force-displacement curves from AFM to measure the interactions between single MF microcapsules and a PET surface (a) and PET surface modified with PVF (b), chitosan (c) and PEI (d) at a concentration of 0.1 wt%.

A schematic diagram in Figure 6.12 illustrates how the multiple events might occur. Each polyelectrolyte with long molecular chains attached on the PET surface and they extended into water solution freely. When a microcapsule contacted the modified PET surface, the polyelectrolyte at the contact region might be folded and act as bridges to connect the two surfaces. Those chains beside the contacted area still extended to the side wall of the MF microcapsule and made contacts. Those connections were released gradually when the microcapsules was separated from the PET surface, causing multiple events. This interpretation is consistent with the previous research (Thormann *et al.* 2008). The "microcapsule-surface separation distance" as presented in Figure 6.13 is considered as one of the parameters to characterise the strength of bridging interactions. The values of the distance were determined from the force-displacement curves of AFM. The results are illustrated in Figure 6.14. Five microcapsules were used to investigate their adhesion on a polyelectrolyte-modified PET surface, and 10 typical force-displacement curves were analysed for each microcapsule. Figure 6.14 (a) presents the distribution of the "microcapsule-surface separation distance" for the PET surface modified with three chemicals and Figure 6.14 (b) shows the mean value. The values of the microcapsule-surface separation distance for PVF and chitosan were scattered and the mean values were 2130±120 nm and 1100±70 nm respectively. However, the microcapsule-surface separation distance distribution of PEI was less scattered and the mean value was just about 280±20 nm. There was no multiple event for the unmodified PET surface and the order of the separation distance after modification with three chemicals is PVF > chitosan > PEI. The values of "microcapsule-surface separation distance" are much bigger than the height dimension as shown in Figure 6.9. This may result from several molecular chains attaching to the side of a microcapsule wall and the gradual breakage of the connections from the side wall to the contact area causing the long plateau events (Kocuna *et al.* 2011);

additionally, the PE molecules may be much more stretched in aqueous solution than in dry environments. The value of the separation distance observed in this work is comparable with the approximate 1000 nm observed on the retraction curves in Kocuna *et al.*'s work (2011) by using a chitosan-modified tip to investigate adhesion to a glass surface. The separation distance may be used to reveal the length of the polyelectrolyte chains, which correlates well with the order of the length of the three chemicals suggested in §6.4.2.2 and §6.4.2.3.

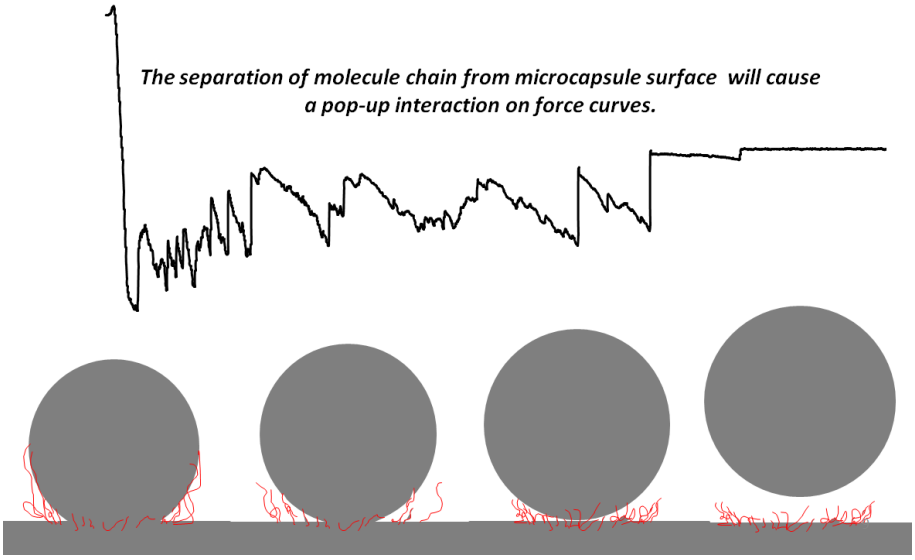

Figure 6.12 Schematic representation of the multiple events showing on retraction curves between single MF microcapsules and the PET surface modified with polyelectrolytes.

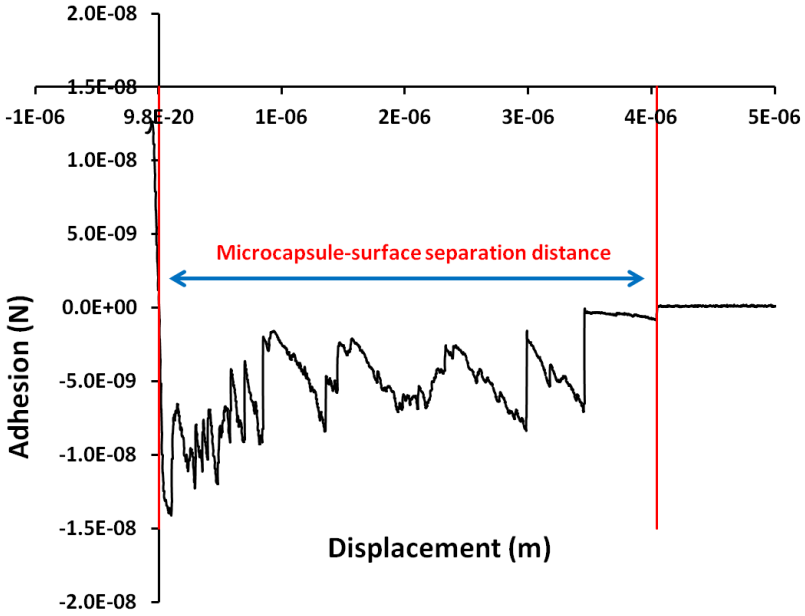

Figure 6.13 Definition of the "microcapsule- surface separation distance" from a typical force-displacement curve between a microcapsule and a PE-modified PET surface, obtained from using AFM.

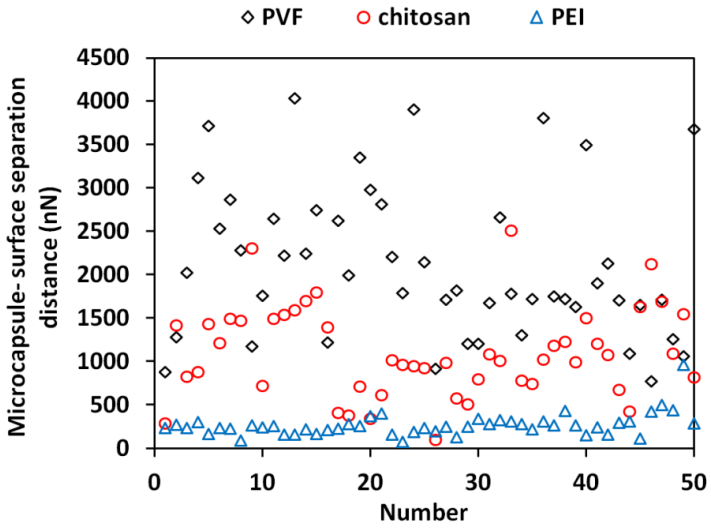

(a)

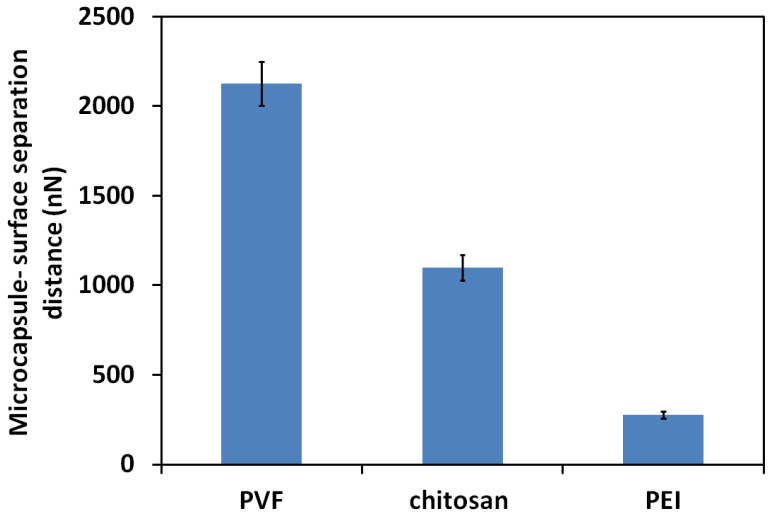

(b)

Figure 6.14 The distribution of the microcapsule-surface separation distance (a) for the modified PET surfaces and the mean value (b); the error bars represent the standard error of mean microcapsule-surface separation distance.

6.4.2.5 Adhesion Energy

The adhesion energy was calculated between single MF microcapsules to the PET surface before and after being modified by the three polyelectrolytes and the results are presented in Table 6.2. The average adhesion energy of single microcapsules (N=5) on a non-modified PET surface was $1.2\times10^{-15}\pm0.2\times10^{-15}$ J (0.01 s) and $3.7\times10^{-15}\pm1.0\times10^{-15}$ J (10 s) respectively. After the surface was modified with PVF (N=6), chitosan (N=5) and PEI (N=5) respectively, the average adhesion decreased to $1.7\times10^{-15}\pm0.9\times10^{-15}$ J (0.01 s) and $10.1\times10^{-15}\pm3.8\times10^{-15}$ J (10 s), $1.8\times10^{-15}\pm0.5\times10^{-15}$ J (0.01 s) and $7.9\times10^{-15}\pm2.9\times10^{-15}$ J (10 s) and $1.9\times10^{-15}\pm1.2\times10^{-15}$ J (0.01 s) and $6.0\times10^{-15}\pm2.1\times10^{-15}$ J (10 s) respectively. The adhesion energy between microcapsules and PET surfaces was increased after PET surfaces were modified with the three chemicals and the order is PVF > chitosan > PEI> non-modified PET surface. The trend of the increase of surface

energy after PET surface was modified with PEs is consistent with the retention of microcapsules to PET surface before and after being modified with PEs. Therefore, it is suggested that other than the net adhesion force, the adhesion energy is another important parameter to determine the retention of microcapsules to PET surface.

Table 6.2 Adhesion energy between single microcapsules and a PET surface before and after being modified with PVF/chitosan/PEI solution. The error bars represent the standard error of adhesion energy, the number of microcapsules (N) measured for non-modified, modified PET surface with PVF, chitosan and PEI are 5, 6, 5 and 5 respectively.

	Adhesion Energy ($\times 10^{-15}$ J)			
	non-modified PET	PVF-modified PET	chitosan-modified PET	PEI-modified PET
0.01 s	1.2 ±0.2	1.7 ±0.9	1.8 ±0.5	1.9 ±1.2
10 s	3.7 ±1.0	10.1 ±3.8	7.9 ±2.9	6.0 ±2.1

6.4.3 The retention of microcapsules on PET surfaces under a shear flow

In the above section it was proposed that polyelectrolyte molecular chains after attaching to a PET surface extended into the aqueous solution and the length of PVF is considered to be longer than that of chitosan and PEI. Additionally, the roughness of a PET surface increased after it was modified with PVF, chitosan and PEI, as presented in 6.3.1. The adhesion is measured by AFM based on popping-out a single microcapsule from a substrate in the vertical direction. However, the removal of microcapsules from a surface by a fluid flow is much more complex. Micro particles are theoretically removed or displaced by lift, sliding and rolling or even a combination (Saffman 1965,

Cherukat *et al.* 1994, Zoeteweij *et al.* 2009, Larsen *et al.* 2010, Derksen and Larsen 2011); rolling is reported to be the most likely motion when a micro particle is displaced in a flow chamber (Sharma *et al.* 1992, Zoeteweij *et al.* 2009, Zhang *et al.* 2010). Therefore, the removal of microcapsules from a PET surface may not be relevant to the friction between them because the friction only works when micro particles are displaced by sliding (Zoeteweij *et al.* 2009). However, the relationship between the retention behaviour and adhesion may be interpreted by considering the molecule structures of polyelectrolytes, and their long molecular chains beyond the contacted area are supposed to attach on the side of the microcapsule wall as presented in Figure 6.12. Without the surface modification, the microcapsule starts to rotate by overcoming the torque at point A as illustrated in Figure 6.16 (a); at this point, the displacement vector for friction is zero, therefore the friction has no influence on the torque balance. However, after the surface modification, the right position for the torque balance can be raised to each contacted point such as B, C and D (Figure 6.16 (b)); and then the displacement of the microcapsule from the PET surface is not a single motion anymore, which becomes to be a gradual process of breaking joints from the position far away from the substrate to the contact region. The strength and the number of the bonding of each joint become an important factor to influence the displacement. Those molecules with longer chains and less steric hindrance tend to form close and long distance contacts with the microcapsule wall easily and then it will be less easy for them to be released from the substrate, see Figure 6.11 in which more single plateaus are observed for PVF than those of chitosan and then PEI. This is supposed to be the main mechanism of the modified PET surface providing enhanced retention of microcapsules than a non-modified surface and the reason why the performance of PVF was better than chitosan and then PEI on improving the retention behaviour of MF microcapsules on a PET surface in flow chamber experiments.

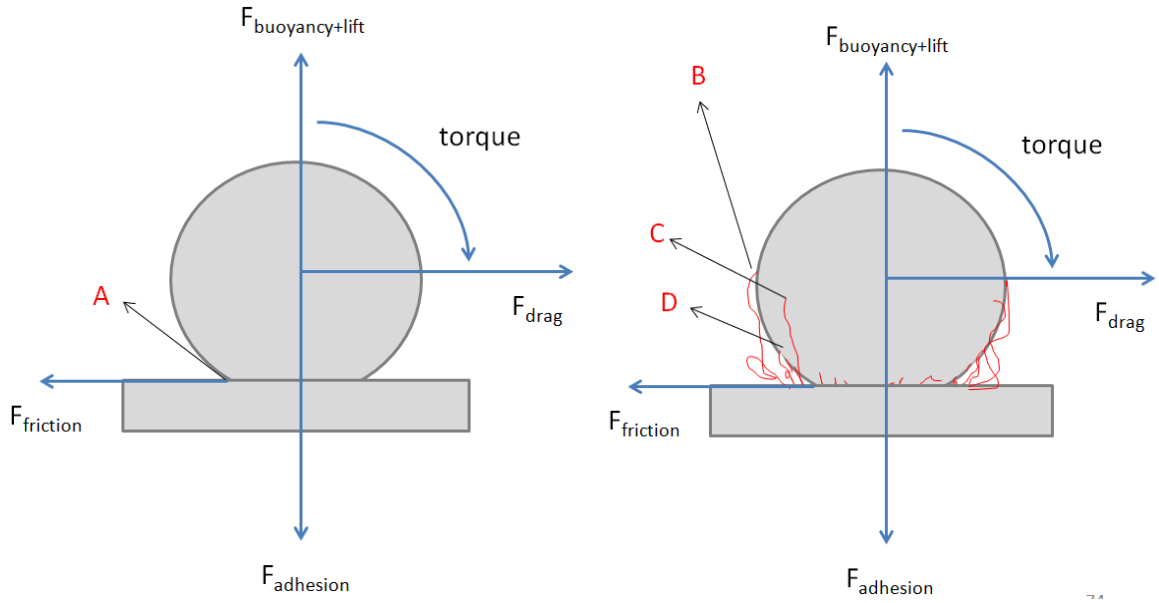

Figure 6.15 Schematic to illustrate the extension of molecule chains to the surface of a microcapsule wall and the influence on the displacement; (a) unmodified PET surface, (b) modified PET surface.

6.5 Conclusions

The investigation of the retention of microcapsules on fabric surfaces has been extended to PET surfaces. It is found that both the adhesion and retention behaviours of MF microcapsules on a PET surface are better than those on a cellulose film. This is because the PET surface is much more hydrophobic than the cellulose film and hydrophobic interaction is considered to be the main reason causing the difference.

Adhesion was found to decrease after the PET surface was modified with three polyelectrolytes by AFM. However, the retention behaviour of MF microcapsules on

the modified PET surfaces in the flow chamber was enhanced. All three polyelectrolytes on the PET surface might extend into aqueous solution, and the increase of its hydrophilicity, roughness and the steric hindrance are considered to be the main reasons for the decrease of the peak value of adhesion. Additionally, multiple plateau events on the retraction curves of AFM were found for the interactions between the microcapsules and the PET surface modified with all the three chemicals and the order of the microcapsule-surface separation distance correlates with length of the molecules calculated according to the molecule weight, the viscosity value and the dimension of the three chemicals on the PET surface in air. Bridging interactions are attributed to be the main mechanism of adhesion between microcapsules and the modified PET surface.

The inconsistency between the adhesion and retention results of microcapsules on the PET surface before and after modification with the polyelectrolytes was interpreted according to their molecular structure. The attachment of the long molecule chains which are beyond the contact region on the side of the microcapsule wall caused the change on the torque balance and the gradual breaking of the joints between microcapsules and single molecules led to more difficult displacements of microcapsules from the modified PET surface. The molecular chains of PVF are longer and cause less steric hindrance than chitosan and then PEI, therefore PVF provided the best performance on retention enhancement and then chitosan and then PEI. Until now, based on the author's knowledge, this is the first time to interpret the removal of micro particles from a substrate by considering the structure of the molecule chains in a flow chamber. It is expected that understanding the influence of molecular structures on retention will provide useful guidance in selecting proper chemicals to modify either perfume microcapsules or the fabric surface to enhance retention of the microcapsules on the fabric surface in laundry processes.

Chapter 7: Modelling Removal of Microcapsules from Model Fabric Surfaces in a Flow Chamber

7.1 Introduction

Adhesion is the attractive interaction at the interface when two surfaces are brought into an intimate contact and it is a complex physicochemical phenomenon. So far, the AFM colloidal probe technique (Butt, 1991, Ducker *et al.*, 1992) and flow chamber technique (Sanjit *et al.*, 1994, Decuzzi *et al.*, 2007, Haun and Hammer, 2008) are the most common techniques used to characterise the adhesion between microparticles and substrates. AFM detects adhesion (pull-off forces) when a single microparticle separates from a surface both in dry and wet conditions. The flow chamber technique characterizes adhesion by employing a large sample population, and it therefore based on statistical analysis by counting the number of particles remaining on a substrate (Brown and Larson, 2001, Decuzzi *et al.*, 2007), or calculating the surface area coverage (Renshaw *et al.*, 2005, Garrett *et al.*, 2008) after applying an air or a fluid flow. Microparticles exposed to shear flow are expected to be displaced/removed by lift, sliding, rolling or some combination thereof (Saffman, 1965, Zhang *et al.*, 1999, Zoeteweij *et al.*, 2009). The balance of the forces for lift and sliding motion and torques for rolling resulting in particle removal from the surface is directly correlated with the adhesion between the two surfaces by knowing the contact area. Therefore, it is generally considered that a greater adhesion force at the interface gives a higher retention of microparticle on the surface, which was also found in previous publications (Sanjit *et al.*, 1994, Garrett *et al.*, 2008, Zoeteweij *et al.*, 2009) and the author's work in Chapter 5. However, an inconsistency of adhesion decrease and retention enhancement

between microcapsules and PET surfaces after they were modified with polyelectrolytes were observed in Chapter 6.

Therefore, a model was developed by analysing the forces acting on the microcapsule adhered to the substrate when a liquid (water in this case) flowed through the flow chamber to displace the microcapsule to investigate the relationship between adhesion behaviour and the removal of particles in a flow chamber. The model began with a simple assumption of DMT contact between a microcapsule and a glass surface to calculate the adhesion and thermodynamic work of adhesion between them. Then a further consideration of the contact mechanics between microcapsules and a glass surface in aqueous solution was discussed. Additionally, the model predictions of adhesion and thermodynamic work of adhesion were compared with the data obtained by AFM. Finally, the model was used to interpret the inconsistency between the adhesion to and retention of microcapsules on PET surfaces after they were modified with PEs, observed in Chapter 6.

7.2 Theoretical background

The model was developed based on the following assumptions:

(1) The microcapsules are perfectly spherical;
(2) Real contact has been achieved between the microcapsules and the substrate in aqueous solution;
(3) The contact mechanics between the microcapsules and the substrate obeys the DMT model.

The onset removal of a particle bonded to a wall in a flow chamber is a dynamic process. Gravity force, buoyancy force, and adhesion between the particle and the substrate act on the particle in a static condition. The detachment of a particle from a surface in a linear shear flow will happen by lifting, sliding, rolling or their combination (Saffman, 1965, Sanjit *et al.*, 1994, Zoeteweij *et al.*, 2009). Figure 2.8 illustrates the possible forces and torques present on a microcapsule bound to a wall in a flow chamber; F_B and F_C represent the resultant force of buoyancy force and gravity force, and adhesion at the contact region, and the expression of each force is illustrated in § 7.2.2 and § 7.2.4. When a liquid flow (water) is applied, the particle will be removed by F_{SA} which is the lift force if it can overcome the balance of F_B and F_C. Otherwise, the particle is most likely to be displaced by F_D and a friction force F_f will be present in the opposite direction to the drag force. If the drag force is still not enough to exceed the friction force, the particle can be displaced by rolling when the torque M_D due to the flow overcomes the torque caused by these forces which are perpendicular to the contact area. The expression and the critical condition for the removal under the possible motion of lifting, sliding and rolling will be further interpreted in § 7.2.3.

7.2.1 The velocity profile

7.2.1.1 Reynolds Number

The Reynolds number of the flow chamber system is

$$\mathrm{Re}_p = \frac{2\left(U_f(y,z) - U_P\right)R}{\nu} \tag{7.1}$$

where, U_f is the velocity of the fluid which will be explained in 7.2.1.3; U_P is the velocity of the particle and is equal to zero before the particle is displaced; *R* is the radius of the microcapsule and *v* is the kinematic viscosity; *y* is the distance from the centre line to the particle and *z* is the location of the particle orthogonal to the direction of flow.

7.2.1.2 Development length

The development length (Durst *et al.*, 2005) is the distance between the entrance of the channel and the position where the flow reaches a parabolic velocity profile. It can be calculated by equation (7.2),

$$L / D^{'} = C_0 + C_1 \,\mathrm{Re} \tag{7.2}$$

where *L* is the development length; $D^{'}$ is the width or the height of the channel (the smaller value should be used into the calculation to make sure the flow reaches the parabolic velocity profile at both directions); Durst *et al.* (2005) suggests C_0=0.631; C_1=0.044.

7.2.1.3 Velocity profile in fully developed flow region

Figure 7.1 shows the velocity profile of a linear shear flow in a rectangular channel in the fully developed flow region and the velocity is given by equation (7.3),

$$U_f(y,z) = 4U_m(y,z)\left(1-\frac{y^2}{b^2}\right)\left(1-\frac{z^2}{c^2}\right) \tag{7.3}$$

where, U_m is the maximum velocity in the velocity profile, b and c are the half lengths of the cross section of the rectangular channel. The shear rate is given as,

$$\gamma(y,z)=\frac{\partial U_f}{\partial y}+\frac{\partial U_f}{\partial z}=8U_m\left(\frac{y}{b^2}\left(1-\frac{z^2}{c^2}\right)+\frac{z}{c^2}\left(1-\frac{y^2}{b^2}\right)\right) \tag{7.4}$$

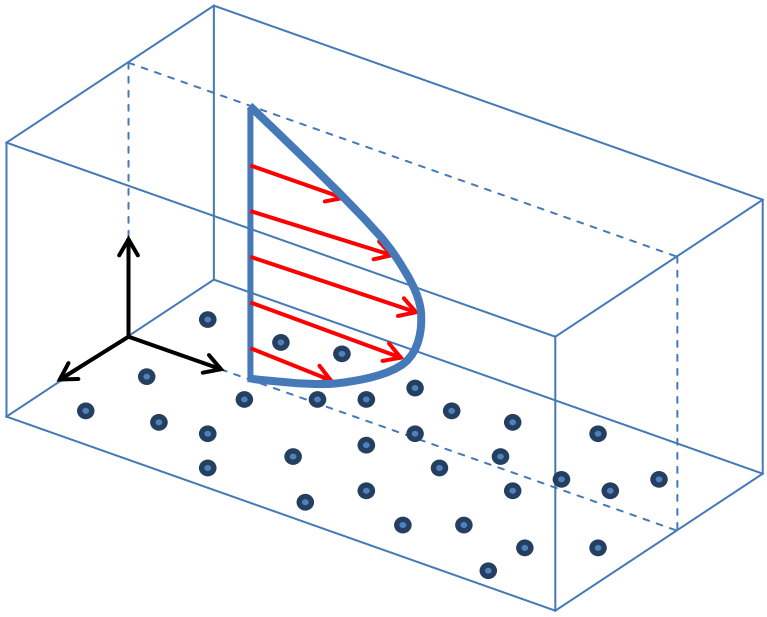

Figure 7.1 A fully developed flow over microcapsules settled on a wall and its velocity profile.

7.2.2 Buoyancy force and gravity force

When a particle adheres to a substrate in fluid environment, buoyancy and gravity will act orthogonally on the particle. The resultant force of buoyancy force and gravity force is given by

$$F_B = \frac{4}{3}\pi R^3 \left(\rho_p - \rho_f\right) g \tag{7.5}$$

where F_B is the buoyancy force, ρ_p is the density of the particle, ρ_f is the density of the fluid and g is gravity.

7.2.3 Removal forces and critical condition for each motion

The detachment of a particle from a surface in a linear shear flow will happen by lifting, sliding or rolling. The critical condition at which the microcapsule can be removed from the surface will be calculated by considering each removal motion.

7.2.3.1 Lift

Lift force represents a force which is perpendicular to the relative motion of the flow, and it is created by different pressure of opposite side of an object due to the fluid flow past the object. In this work, the lift force resultes from the gradient of the velocity placed on the particle. Other than the flow velocity, shear rate and the particle dimension, lift force is also a function of the viscosity. The lift force of a fluid with a very large viscosity (the Stokes fluid) is negligible. The lift force was firstly investigated by Saffman (1965), and it is expressed by

$$F_{SA} = 81.2\mu\left(U_f\left(y,z\right) - U_P\right)\left(\frac{\dot{\gamma}\left(y,z\right)}{\nu}\right)^{1/2} R^2 \tag{7.6}$$

where F_{SA} is the lift force on the particle, μ is the viscosity of the fluid, U_f is the velocity of the fluid, U_p is the velocity of the particle, and $\dot{\gamma}$ is the shear rate.

When the lift force exceeds the attraction force and the buoyancy force, the particle will be removed. The critical adhesion at which the microcapsule can be removed is calculated by

$$F_{SA} \geq F_C + F_B \tag{7.7}$$

The equation can be converted into,

$$F_C \leq F_{SA} - F_B \tag{7.8}$$

7.2.3.2 Sliding

The particle will slide over the surface because of the drag force generated by the shear stress of the flow in a direction of the relative flow velocity. It is a function of the fluid density, flow velocity and the effective area of the particle perpendicular to the flow direction. The drag force (Zoeteweij *et al.*, 2009) on a particle can be expressed as,

$$F_D = \frac{1}{2}\rho_f U_f^2 C_D A' \tag{7.9}$$

where F_D is the effective drag force; C_D is the drag coefficient and A' is the effective area of the particle perpendicular to the flow direction. The drag coefficient for a particle attached to a wall is given by (for $10^{-4} < \mathrm{Re}_p < 2$)

$$C_D = 1.7009\frac{24}{\mathrm{Re}_p} \tag{7.10}$$

Particle sliding will happen in a situation where the drag force is greater than the friction force which is in the opposite direction to the flow,

$$F_D \geq \kappa\left(F_B + F_C - F_{SA}\right) \tag{7.11}$$

where κ is the static friction of the system; if the condition provided by the equation is satisfied, the particle may slide over the surface. The critical condition of adhesion for sliding is,

$$F_C \leq \frac{F_D}{\kappa} + F_{SA} - F_B \tag{7.12}$$

7.2.3.3 Rolling

Particles will also experience another kind of complicated motion, which is rotation. A particle may be displaced from the surface by rolling. The rotation is related to the balance of the moment of the surface stresses on the particle.

The torque as a result of the vertical forces can be approximately calculated by,

$$\tau_\upsilon = \left(F_B + F_C - F_{SA}\right)\alpha \tag{7.13}$$

where α is the contact radius. The DMT model mentioned in the previous section is used to calculate the contact radius (it will be interpreted in §7.2.4),

$$a^3 = \frac{3R}{4E^*}\left(F + 2\Delta\gamma\pi R\right) \tag{7.14}$$

where $F = F_b + F_c - F_{SA}$ and E^* is the equivalent Young's modulus. The torque due to the flow can be calculated as

$$\tau_f = M_D + F_D R \tag{7.15}$$

where M_D is the moment of the surface stress. The torque due to the drag force does not take such a simple expression, and consideration of the shear stress on the sphere will correct for this. This simple approach enables the following condition; the particle will roll when,

$$M_D + F_D R + F_{SA}\alpha \geq (F_B + F_C)\alpha \tag{7.16}$$

This can be converted into equation,

$$F_C \leq \frac{M_D + F_D R}{\alpha} + F_{SA} - F_B \tag{7.17}$$

The moment of surface stresses (Batchelor, 1967) is given by,

$$M_D = \frac{1}{2}\rho_f U_f{}^2 C_M V \tag{7.18}$$

Where V is the volume of the particle,

$$C_M = 0.94339\frac{24}{\mathrm{Re}_p} \tag{7.19}$$

7.2.4 Adhesion

Adhesion between a particle and a surface is another vertical force acting on the particle. Until now, adhesion and the contact mechanism between two surfaces have been poorly understood. Microcapsules can be treated as the elastic spheres under small deformation (Liu, 2010) and DMT (Derjaguin *et al.*, 1975) contact was assumed to be the contact mechanism at the initial stage. Here, the Tabor number μ (Tabor, 1977) was calculated by equation (7.20):

$$\mu = \left(\frac{R\Delta\gamma^2}{E^{*^2} Z_0^3} \right)^{1/3} \tag{7.20}$$

Where $E^* = (k_1 + k_2)^{-1}$ ($k_1 = \frac{1-\upsilon_1^2}{\pi E_1}$ and $k_2 = \frac{1-\upsilon_2^2}{\pi E_2}$); υ is the Poisson's ratio and E is the Young's modulus of each material, $\Delta\gamma$ is the thermodynamic work of adhesion per unit area; Z_0 is the equilibrium separation.

The Young's modulus and Poisson's ratio of glass are 70 GPa and 0.23 (Akhtar *et al.*, 2009) respectively. The diameter of microcapsules was assumed to be 20 μm and their Young's modulus is 1.8 GPa (Mercade-Prieto *et al.*, 2011) and their Poisson's ratio is assumed to be 0.5 (Liu, 2010). The thermodynamic work of adhesion between microcapsule and a glass surface in aqueous solution is assumed to be 100 μJ/m^2 (Liu *et al.*, 2002a, Liu *et al.*, 2002b). The equilibrium separation is assumed to be 3Å (Tabor, 1977). Then the calculated Tabor number is 0.04, which is smaller than 5 (Table 2.2). So DMT model has been used to calculate thermodynamic work of adhesion, which is given as

$$F_c = 2\Delta\gamma\pi R \quad (7.21)$$

7.3 Experimental

7.3.1 Perfume-filled microcapsules

Perfume-filled MF microcapsules were supplied by Procter & Gamble, Belgium, described in §3.1.1.

7.3.2 Glass slides

Fisherfinest premium plain glass microscope slides (Fisher Scientific, UK) were used as substrates in this work.

7.3.3 Determination of friction coefficient by AFM

AFM was used to determine the friction coefficient between microcapsules and glass surfaces in H_2O (HPLC grade, Fisher Scientific, UK). It was also used to investigate the contact mechanics between microcapsules and a glass surface in aqueous solution by varying the compression load. The detailed procedures were described in §3.5.1.

7.3.4 Determination of friction coefficient by a Nanovea Tribometer

A melamine formaldehyde (MF) membrane was prepared according to a protocol described in § 3.5.2.1; and then the static coefficient of friction between a glass sphere and the MF membrane was measured with a Nanovea Tribometer in dry condition. The detailed information was described in § 3.5.2.2.

7.3.5 Prediction of adhesion behaviour by the model

7.3.5.1 Flow chamber experiment

The displacement of single microcapsules from a glass surface by a fluid flow in the flow chamber was recorded. The video was analysed by a Matlab code to determine the radius of the microcapsules and its location (the distance to the centre line of the channel). The detailed methodology was described in § 3.4.2.2 and § 3.4.2.3.

7.5.3.2 Adhesion and the thermodynamic work of adhesion

Adhesion and the thermodynamic work of adhesion was calculated by incorporating the corresponding flow rate to remove the microcapsule, the particle radius and particle location acquired in § 7.5.3.1 in equation (7.17).

7.3.4 Adhesion behaviour by AFM

The adhesion between single MF microcapsules and a glass surface was measured by the AFM colloidal probe technique according to the procedures described in § 3.4.1. The mean value of the pull-off force was calculated and the DMT model (Derjaguin *et*

al., 1975) was used to predict the thermodynamic work of adhesion between a microcapsule and the glass surface according to equation (7.21).

7.4 Results

7.4.1 Friction coefficient

7.4.4.1 Measurement of friction coefficient by AFM

The coefficient of friction between a microcapsule and a glass surface was measured according to a methodology proposed in previous publications (Varenberg *et al.*, 2003, Tocha *et al.*, 2006, Huang *et al.*, 2009) by applying a AFM microcapsule probe to scan a TGF11 silicon calibration grid described in § 3.5.1. Several microcapsules with diameters of 8 μm to 25 μm were applied to do the measurements. Unfortunately, all the experiments failed either due to dropping of microcapsules during the scanning process or unstable result. The main reason may be that the particle sizes of the microcapsules used in this work were so big compared with the dimension of the calibration grid that it was easy for the particle to get stuck or they couldn't contact the slopped plane. Until now, no proper calibration grid has been found to do the calibration. Therefore, an alternative methodology to measure the friction coefficient was chosen.

7.4.1.2 Measurement of friction coefficient by a Nanovea Tribometer

(1) MF membrane

A MF membrane was prepared to mimic the surface of MF microcapsules to measure the coefficient of friction. AFM and SEM were used to determine the surface topography and the thickness of the MF membrane (Figure 7.2). It was dense and compact, which formed with small MF particles. Over a scan area of 100 μm × 100 μm, the RMS roughness was 243.8 nm (Figure 7.3 (a)). Liu (2010) studied the surface roughness of MF microcapsules over a scan area of 500 nm×500 nm and she found that the RMS roughness was 3.4 nm. The captured area of the MF membrane in this work and that of the MF microcapsule in Liu's (2010) work are not in the same order of magnitude; therefore it is difficult to make the direct comparison. Figure 7.3 (b) and (d) show the surface topography of a piece of MF membrane and the surface of a MF microcapsule by SEM. The tiny particles over a size range of nanometres to micrometres were observed on both surfaces. MF particles with a diameter of few nanometres to about 1 micrometre were observed on the MF membrane; while the diameter of the circular MF particles observed on the surface of the microcapsule is much smaller than that on the MF membrane, most of which was approximately several micrometres to hundreds of micrometres in dimension. However, the MF material is elastic at small deformations (Liu, 2010) and an applied load of 20 mN was used in the friction measurement. The applied load might be large enough to overcome the heterogeneity on the two surfaces. The MF membrane had a thickness of about 2 μm (Figure 7.3 (c)), which is about ten times larger than that of the wall thickness of MF microcapsules (Long *et al.*, 2010, Mercade-Prieto *et al.*, 2011). It was used to measure friction coefficient in this work.

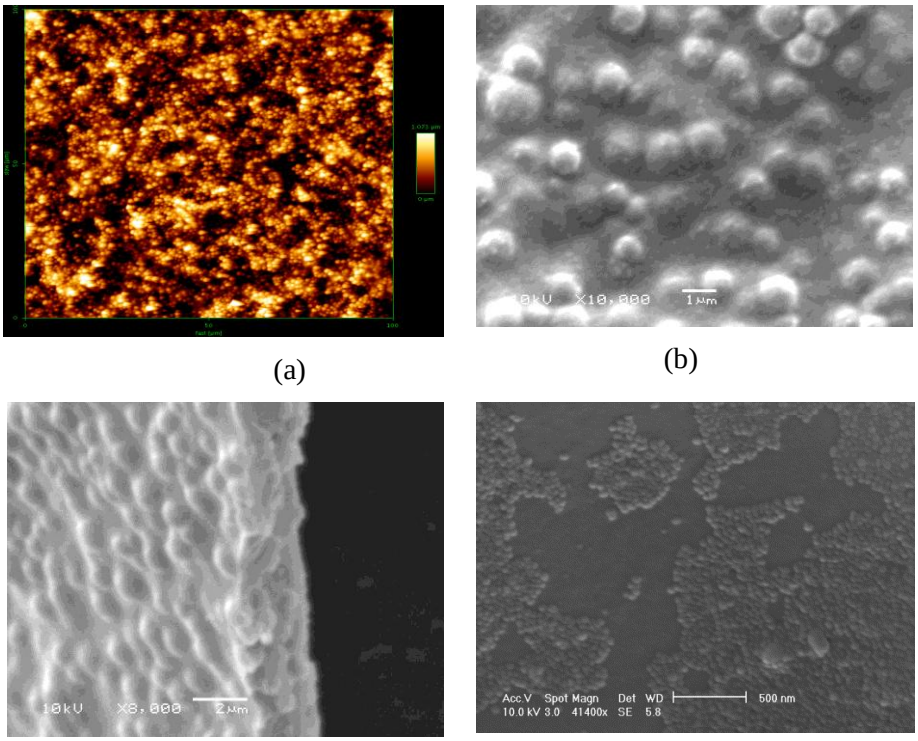

(a) (b)

(c) (d)

Figure 7.2 Surface topography of MF membrane (a) AFM image (RMS roughness: 243.8 nm); (b) SEM image; (c) the thickness of MF membrane by SEM; (d) SEM image of a MF microcapsule.

(2) Friction coefficient results

The static coefficients of friction between a glass sphere and a glass surface, and a glass sphere and a MF membrane in dry conditions were measured and they were 0.44±0.05 and 0.20±0.02 (the mean value ± 1 standard error) respectively. The coefficient of friction between glass surfaces was measured as a control experiment, and the result is comparable with the friction coefficient (0.45) determined from polished glass for dry contact in Belkhir *et al.*'s work (2009). MF microspheres were fabricated and the coefficient of friction between two MF surfaces was about 0.1 by using an ASTM D1884-95 test method (Evert, 2001). The inconsistency was attributed to be the

difference in the surface properties of the glass sphere and the MF sphere. The coefficient of friction was also measured in aqueous solution. However, the MF membrane was swollen and then peeled off from the glass slide. Therefore, no result was obtained. The main reason is that the acryl amide/acrylic acid copolymer was used to formulate the MF membrane and it contains amine and carboxyl groups which led to a hydrophilic nature of the MF membrane.

7.4.2 Particle removal and adhesion based on the simulations of the model of particle removal

7.4.2.1 Particle removal in flow chamber

The minimum size of the microcapsules which can be displaced was calculated according to each motion mechanism as a function of location in the channel (Figure 7.3). The critical radius of the particle that can be displaced from the substrate in a fully developed flow region is dependent on the particle location from the centre of the channel. With the increase of the distance, the critical radius of the particle that can be displaced increases, which indicates that it is easier for smaller particles to be displaced in the area near the central line of the channel. The main reason is the parabolic distribution of the velocity and shear stress in the flow chamber. The critical radius of particle that can be displaced by lift, sliding and rolling is 60 μm, 23 μm and 0.2 μm respectively. In this work, the average radius of microcapsule is 10 μm, therefore microcapsules were most probably displaced by rolling in the flow chamber. However, it can be still displaced by sliding motion if the operation parameters are changed. The influence of parameters including the particle radius, the coefficient of friction, the flow

rate and the particle location will be discussed later. Simulation results here are comparable with the conclusion that the rotation is the main reason causing the onset of removal of micro particles from surfaces suggested by Zoeteweij *et al.* (2009); similar results of the minimum radius for lift, sliding and rolling motion were observed, which is 100 μm, 80 μm and 1.6 μm respectively when they investigated the displacement of glass spheres from glass substrates by air flow by calculating the critical Reynolds numbers.

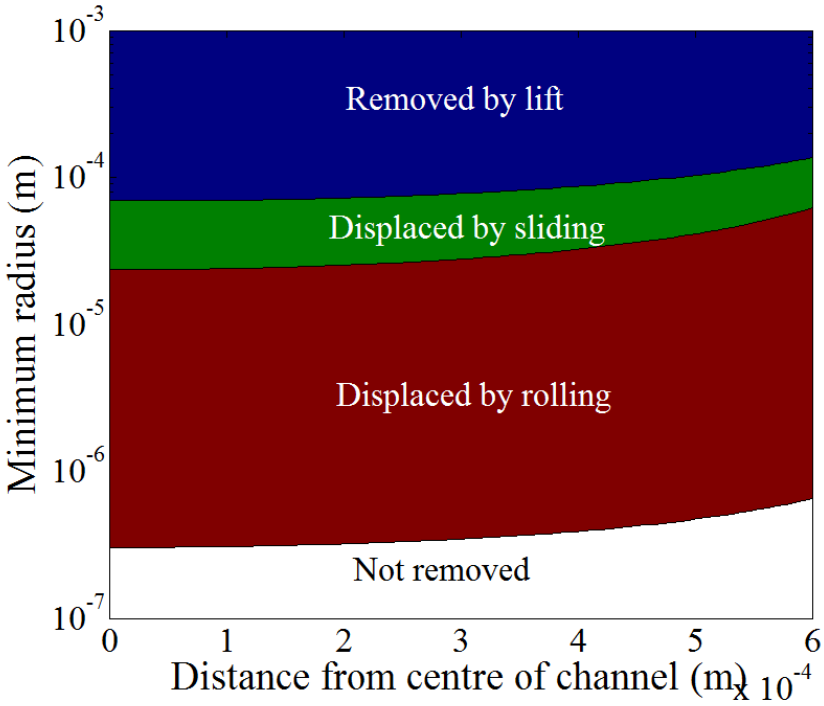

Figure 7.3 The minimum radius of microcapsules that can be removed as a function of location under each motion mechanism. The simulation parameters (flow rate: 50 mL h^{-1}; density of particle: 1050 kg m^{-3}; coefficient of static friction: 0.2 (experimental data); Young's modulus values of particle and glass: 1.8 GPa (Mercade-Prieto *et al.*, 2011) and 70 GPa (Akhtar *et al.*, 2009); Poisson's ratio values of particle and glass: 0.5 (Liu, 2010) and 0.23 (Akhtar *et al.*, 2009), the adhesion energy per unit area 100 μJ m^{-2} (Liu *et al.*, 2002a)).

7.4.2.2 The influence of parameters on adhesion

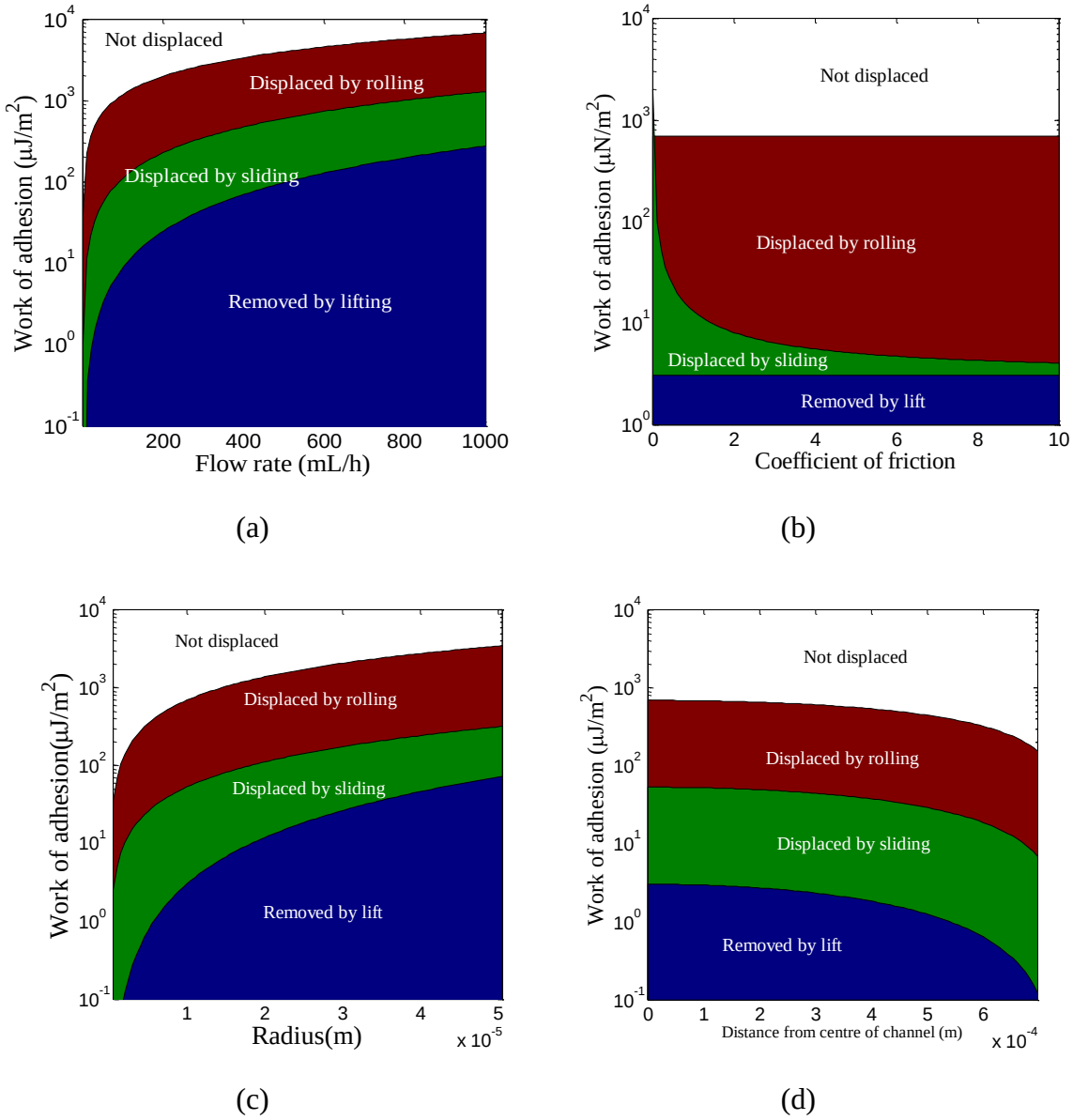

Figure 7.4: The critical interfacial adhesion energy due to each onset of removal motion as a function of the flow rate (a), friction coefficient (b), radius (c), and particle location (d). The simulation parameters (flow rate: 50 mL h^{-1}; density of particle: 1050 kg m^{-3}; coefficient of static friction: 0.2 (experimental data); Young's modulus values of particle and glass: 37.4MPa (experimental data) and 70 GPa (Akhtar *et al.*, 2009); Poisson's ratio values of particle and glass: 0.5 (Liu, 2010) and 0.23 (Akhtar *et al.*, 2009)).

Figure 7.4 illustrates the influence of the flow rate (a), friction coefficient (b), and particle radius (c) and particle location (d) on the critical thermodynamic work of adhesion per unit area according to the three onsets of motions when using a water flow to displace a microcapsule from a glass surface in a flow chamber. The critical thermodynamic work of adhesion needed for each onset of motion is lift < sliding < rolling, which means that microparticles with small adhesion tend to be removed by lift and then sliding and at last rotation as adhesion increases. Additionally, with the increase of the thermodynamic work of adhesion, the critical flow rate needed increases. It is suggested that a higher flow rate will be needed to displace a more adhesive particle. Additionally, a particle with certain thermodynamic work of adhesion can be displaced through different motion mechanism by changing the flow rate. Theoretically, a particle with a thermodynamic work of adhesion which is up to approximate 100 μJ m^{-2} can possibly be displaced by rolling at first and then sliding and at last lift by increasing the flow rate to 1000 mL h^{-1}. In contrast, it is not possible to remove a particle with thermodynamic work of adhesion above 100 μJ m^{-2} by lift with a maximum flow rate of 1000 mL h^{-1}.

The influence of the coefficient of friction on the critical thermodynamic work of adhesion was simulated and the results are presented in Figure 7.4 (b). The work of adhesion is independent of the coefficient of friction for lift and rolling motion but inversely proportional to it for the sliding motion. This is because only sliding motion needs to overcome the resistant force balance in the direction parallel to the substrate. When the friction coefficient is quite small (approximately less than 0.1), the particle with high thermodynamic work of adhesion (approximately up to 1000 μJ m^{-2}) can be displaced by sliding. Additionally, if sliding is the main mechanism when the microparticle is displaced from the surface, the displacement of microparticle from a

surface becomes difficult by increasing the coefficient of friction. The coefficient of friction can be calculated by knowing the thermodynamic work of adhesion for a given system if the particle is displaced by sliding.

The influence of the particle radius on the critical thermodynamic work of adhesion is similar to the flow rate. For a batch of particles with the same thermodynamic work of adhesion up to approximate 60 $\mu J\ m^{-2}$, the smaller ones are possible to displace by rolling and sliding, whilst bigger ones are most likely to be removed by lift. Therefore it is possible to have particles displaced and removed by the three motions in a single experiment if the particle size range is wide enough. Additionally, for a batch of samples with the same particle size, the more adhesive ones could be more possibly displaced by rolling and then sliding, and the less adhesive ones are most likely removed by lift.

The critical thermodynamic work of adhesion is also related to the location of the particle (the distance from the centre line). At the same distance from the centre of the flow chamber channel, the particle will be removed or displaced by lift, sliding and then rolling with the increase of thermodynamic work of adhesion. Additionally, it is possible for particles with a certain thermodynamic work of adhesion to be removed by lift, sliding or sliding and rolling in the same experiment, when they are in different locations.

7.4.3 Calculation of adhesion using the model of particle removal with experimental data

An example of microcapsules deposited on a glass slide under a microscope is given in Figure 7.5 (a). A few microcapsules have been seen and microcapsules in the red circles were not considered because either they are aggregated (in red circles D1, D2, D4, D5) or they are quite close to each other (like the two particles marked as D3). The aggregated microcapsules are not spherical and it is very difficult to determine the contact area and the centre of gravity. Additionally, the flow condition around the particles cannot be assumed to the same as that around a single spherical particle. Therefore, just those isolated microcapsules (in green circles, G1-G4) were recorded for the displacement. Figure 7.5 (b) shows the microcapsule deposition after using a water flow of 18 mL h^{-1} for 3 min. A single microcapsule (G1) in Figure 7.5 (a) was removed.

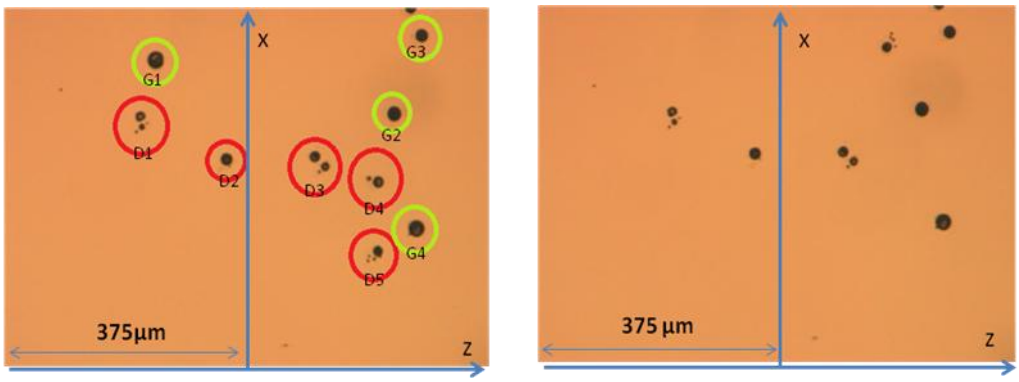

(a) (b)

Figure 7.5 Deposition and removal of microcapsules on a glass slide before (a) and after (b) a water flow through the channel; the horizontal z axis indicates the width of the channel and vertical x axis shows the central line of the channel and the flow direction.

Finally 10 single microcapsules with a radius of 7.5 to 15 μm were recorded to be displaced by the water flow in the flow chamber. 16 single microcapsules were used to measure adhesion by AFM and then the thermodynamic work of adhesion was calculated according to the DMT model (Derjaguin *et al.*, 1975) The adhesion results are illustrated in Figure 7.6 (a). As can be seen, the adhesion for each single microcapsule is scattered, obtained both from the model of particle removal with the flow chamber experimental data and AFM experiments, which is attributed to the effect of surface properties (e.g. surface roughness (Vakarelski *et al.*, 2000, Katainen *et al.*, 2006)). The mean values of adhesion from the model of particle removal with the flow chamber experimental data is 89.1 ± 14.2 nN, and it is more than 10 times larger than the mean value of adhesion measured by AFM, which is 7.5 ± 1.6 nN. The thermodynamic work of adhesion was also calculated according to DMT contact and the results are shown in Figure 7.6 (b). Values of the thermodynamic work of adhesion calculated from the model of particle removal with the flow chamber experimental data and AFM data are 1239 ± 144 μJ m^{-2} and 89 ± 20 μJ m^{-2} respectively. The work of adhesion predicted by the model of particle removal in a flow chamber is much bigger than that of AFM. The inconsistency in the adhesion and the thermodynamic work of adhesion are probably due to that using the DMT model was an over simplication for describing the contact mechanics at the interface of microcapsules and the glass in aqueous solution and it will be further investigated in §7.5.

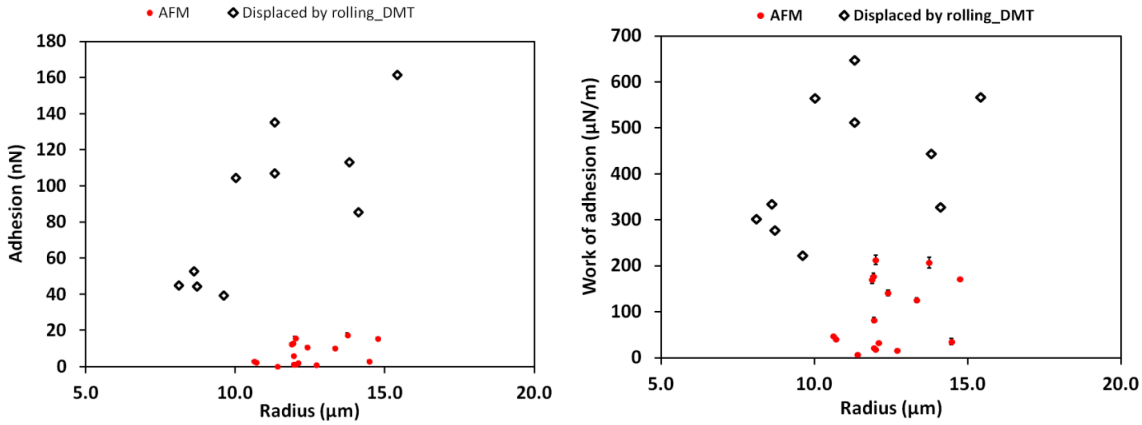

(a) (b)

Figure 7.6 Adhesion (a) and the thermodynamic work of adhesion determined by the model of particle removal with the flow chamber experimental data and AFM (An unpaired samples-T-TEST (O'Rourke *et al.*, 2005) was used to evaluate the equal variances of two groups of adhesion and work of adhesion from (a) and (b) respectively, and both the P values are less than 0.0001).

7.5 Discussion

7.5.1 The contact between the two surfaces in aqueous solution

The model of particle removal proposed in this work is based on a hypothesis of DMT contact between two surfaces. However, the query whether the contact between a microcapsule and a substrate obeys conventional contact models such as the JKR model and DMT model was raised in previous publications (Liu *et al.*, 2002a, Liu *et al.*, 2002b, Elsner *et al.*, 2004). Liu *et al.* (2002b) found that the ratio of contact radius of urea-formaldehyde microcapsules on a glass surface was from about 0.07 to 0.50 for microcapsules with a radius of 10 µm to 80 µm under different buffer concentrations, which is bigger than that determined by JRK and DMT models; the ratio was independent of the particle size but increased with the buffer concentration; microcapsules with a diameter of 10 µm generated a contacted radius of 10% of the

particle radius in water. Elsner *et al.* (2004) also investigated the deformation of polyelectrolyte microcapsules on a substrate in dry conditions and it was found that the contact radius increased with increasing the radii of microcapsules; a microcapsule with a radius of 10 μm generated a contacted radius of 20% of the particle radius. The microcapsule-glass system in this work was similar to the system reported in Liu *et al.* (2002), therefore the contact radius, which is assumed to be equal to 10% of particle radius was used to re-calculate the adhesion and the thermodynamic work of adhesion. Since the deformation of microcapsules on the glass surface in aqueous solution may no longer obey DMT model, the pull-off force cannot be calculated according to DMT model. However, the pull-off force was found to be the same as the expression proposed in DMT model for a thin shell sphere separating from a substrate (Shanahan, 2003). The trend of minimum radius of particle as a function of particle location (distance from the centre line) that can be displaced by lift, sliding and rolling is similar to the results reported in Figure 7.5, and the minimum value at central line is 60 μm, 24 μm and 1.5 μm for lift, sliding and rolling respectively; similarly, the trend of the influence of the flow rate, coefficient of friction, radius and particle location on the critical thermodynamic work of adhesion is similar to the trend in Figure 7.6. The adhesion and thermodynamic work of adhesion recalculated by using a contact radius of 10% of radius is 4.8± 0.8 nN and 67±10 μJ m^{-2}. Based on these value and that determined by AFM, the p-value for an unpaired samples t-test result is 0.21 and 0.29 for the adhesion and thermodynamic work of adhesion respectively. Therefore, it seems that the inconsistency between adhesion and the thermodynamic work of adhesion between microcapsules and a glass surface in § 7.4.3 is mainly due to the contact between microcapsules and a glass surface, which it no longer obeys DMT model. The contact suggested for microcapsules settled on a glass surface in aqueous solution in Liu *et al*'s work (2001) helps to describe the contact mechanics in this work.

Additionally, the work above was based on an assumption that a real contact was achieved between two surfaces. However, the assumption may not be sound for aqueous solution, if the external force applied is not big enough to squeeze the water molecule layer (Vakarelski and Higashitani, 2001, Kendall *et al.*, 2010Rossetto *et al.*, 2012) between two surfaces. The presence of a layer of confined water molecules on the surface in aqueous solution was validated by Vakarelski et.al (2000, 2001), and it was further investigated by Kendall et al (2010) and they found that it is impossible to squeeze the last water monolayer even at a pressure high enough to cause plastic deformation of MgO in contact. Therefore, it was possible that there was a layer of water molecules between the MF microcapsule and the glass surface. The layer of water molecules increased the distance between the two surfaces, which decreased the van der Waals force, and then possibly decreased the contact radius. If the contact radius decreases by 20%, the ratio of contact radius to particle radius is 8%. The adhesion force and thermodynamic work of adhesion calculated by the model of particle removal are 6.0 ± 1.1 nN and 84 ± 13 μJ m^{-2}, and the p-value of equal variance is 0.48 and 0.68 respectively. The better agreement indicates that a layer of water molecules possibly was present at the interface when the microcapsule settled on a glass surface in water. The scattering of the adhesion data from two techniques is another reason for the fitting result of the equal variance. It may be due to the difference in surface roughness of different microcapsules and limited number of microcapsules measured (He *et al.*, 2013).

A further experimental work was conducted to validate the contact issue between a microcapsule and a substrate in water. A 25 μm microcapsule colloidal probe was applied to scan a glass and PET surface and the lateral deflection signal by increasing the compression load was recorded. The results of the lateral deflection as a function of

compression load are shown in Figure 7.7. The lateral deflection was independent of the applied load on the glass surface. However, it increased with the applied load but without passing the base point on PET. The adhesive forces between single microcapsules and glass and PET surfaces in water were 7.5 ± 1.6 nN and 34.9 ± 3.2 nN (experimental result in Chapter 6) respectively. The interaction between the microcapsules and PET surface is much stronger compared with that on glass surface. Therefore it is possible that the microcapsule contacted with the PET surface and then the lateral deflection increased with the applied load. Without a compression load or at a very low compression load, a layer of confined water molecules is present between the two surfaces, causing the curve of lateral deflection vs. applied load does not pass the base point. However, the interaction between microcapsules and the glass surface was quite weak; additionally, as both the glass and microcapsules are negatively charged, the repulsive force may occur between them in water. When the microcapsules approached to the glass surface, it was unlikely for them to penetrate into the water layer and make real contact. Therefore, the microcapsules are always contacted with a water layer by increasing the compression load, which might be the reason for the independence of the lateral deflection on the applied load.

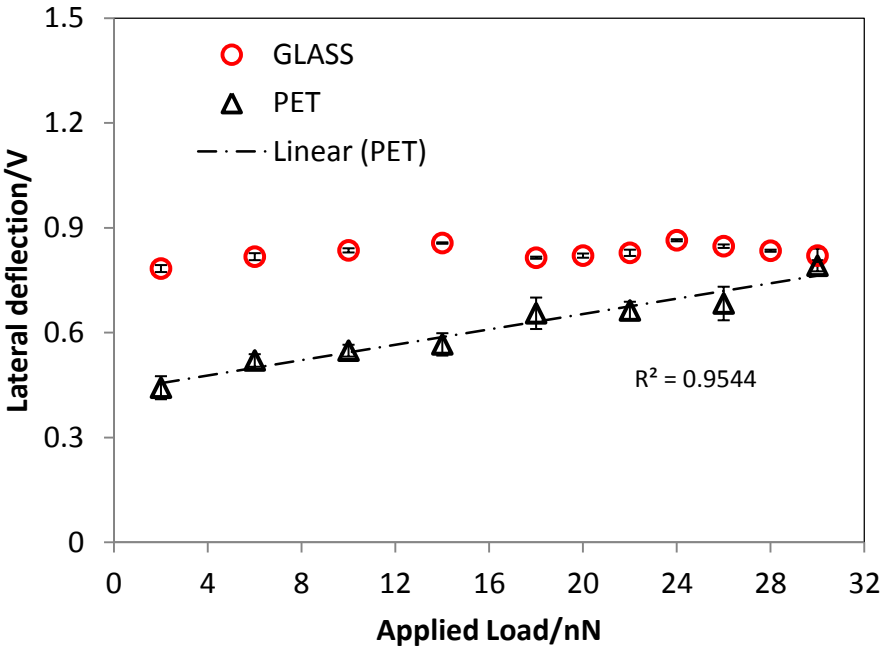

Figure 7.7 The lateral deflection of the microcapsule as a function of the applied load on a glass and PET surface in aqueous solution.

The results of adhesion and thermodynamic work of adhesion from the two techniques after considering the contact issue between microcapsules and a glass surface in aqueous solution are in the same order of magnitude as the adhesion energy calculated in the previous publication (Liu *et al.*, 2002a, Liu *et al.*, 2002b, Elsner *et al.*, 2004). Liu *et al.* (2002a, 2002b) studied the adhesion between urea-formaldehyde microcapsules and a glass substrate as a function of osmosis. They developed a model to calculate adhesion energy by characterization of contact area and osmotic inflation of microcapsule volume. The adhesion energy between the microcapsules and glass surface was from approximately 10 μJ m^{-2} to about 500 μJ m^{-2} under different buffer concentrations for urea-formaldehyde microcapsules (Liu *et al.*, 2002a) and 60 mJ m^{-2} to 257 mJ m^{-2} for another three kinds of microcapsules (Liu *et al.*, 2002b). Elsner *et al.* (2004) studied the adhesion between microcapsules and a glass surface. The adhesion energy was calculated by fitting the shell thickness of microcapsules and the contact

area to a model based on balancing the energy cost of the mechanical deformation and the energy gain due to the work of adhesion. Values of the adhesion energy calculated by the small deformation model were 280 ± 20 μJ m^{-2} (according to radius dependency fit), and 260 ± 70 μJ m^{-2} (according to thickness dependency fit) respectively, the thermodynamic work of adhesion obtained in this work is within the same range as their data and the difference is probably attributed to the difference between the term of "thermodynamic work of adhesion" and "adhesion energy", which was treated as the same in many previous publications. The thermodynamic work of adhesion is the work needed to separate two contact surfaces; while the adhesion energy is the energy between the two contacted surfaces. Additionally, the difference in microcapsules wall material, the wall thickness, the buffer concentration and the contact area can influence the results. Therefore, the model of particle removal can be potentially used to predict the adhesion behaviour of microparticles on a substrate in a flow chamber.

7.5.2 Interpretation of the inconsistency between adhesion and retention between microcapsules and polyester surfaces in Chapter 6.

The model of particle removal predicts that with the increase of the adhesion, a higher flow rate is needed to displace microcapsules from a surface in aqueous solution, and the conclusion is consistent with the experimental results in Chapter 5, of which a higher retention of microcapsules on PE-modified cellulose thin films was found after the adhesion between them was increased.

However, the adhesion of microcapsules was found to decrease to PET surfaces after they were modified with PEs, but the retention of microcapsules on PET surfaces was enhanced after modification with PEs. A conclusion that the attachment of long

molecular chains which are beyond the contact region on the side of the microcapsule wall causes the change on the torque balance and then the gradual breaking of the joints between a microcapsule and single molecules leads to a more difficult displacement of the microcapsule from the modified PET surface was suggested in Chapter 6. A schematic diagram was presented in Figure 6.15 (b) to illustrate the attachment of PE molecules to the side wall of microcapsule and the change in the right position for the torque balance. An attempting of using the model of particle removal to interpret the inconsistency on adhesion and retention are presented here.

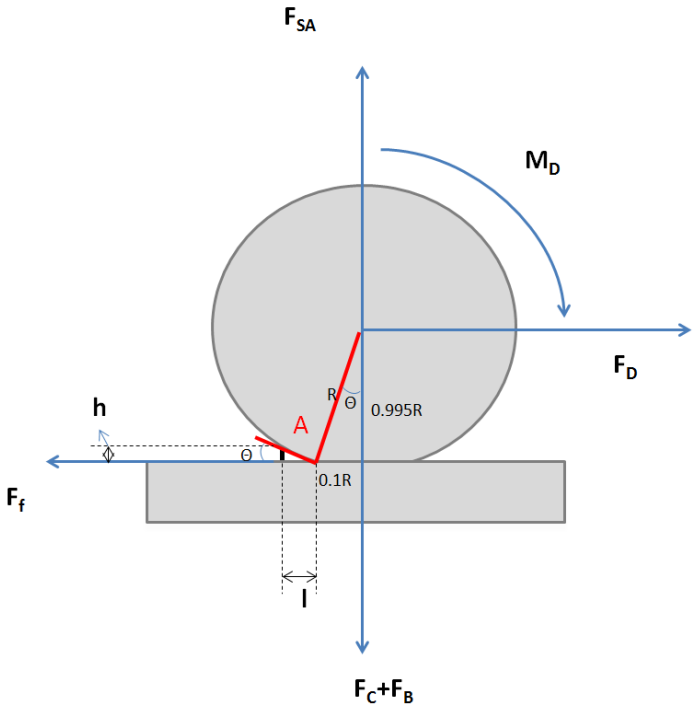

Figure 7.8 Schematic to illustrate a microcapsule in contact with a PET surface and the relationship between Θ, R, h.

The microcapsule is assumed to retain a spherical form, except in the flattened zone in direct contact with the substrate, which subtends an angle of 2 Θ (Shanahan, 2003), as presented in Figure 7.8. The radius of the truncated sphere is considered to be

unchanged ((1-cosΘ) «1). Based on the conclusion in 7.5.1.3, a real contact is suggested to be achieved between a microcapsule and a polyester surface. Therefore, a contact of 10% of radius is used in the model, which leads to cosΘ =0.995 and SinΘ=0.1. Then whenever there is a change in the position for the contact, the torque balance will be changed. The modified toque balance of Equation 7.13 and 7.15 are presented in Equation 7.22 and 7.23,

$$\tau_{\upsilon} = (F_B + F_C - F_{SA})(\alpha + l) \tag{7.22}$$

$$\tau_f = M_D + F_D(R\cos\theta - h) \tag{7.23}$$

and then the expression of torque balance is changed to Equation 7.24

$$F_C \leq \frac{M_D + F_D(R\cos\theta - h)}{\alpha + l} + F_{SA} - F_B \tag{7.24}$$

Where *h* is the vertical distance between the contact point and the surface, and it represents the vertical length of a stretched PE molecule from a PET surface to the side wall of a microcapsule (PE molecules were assumed to contact two surfaces tightly without free length, which is like a straight stick); l is equal to (h/tan(θ)).

The typical Young's modulus and Poisson's ratio of PET are 3 GPa and 0.3 (provided by Goodfellow, UK) respectively. The average radius of microcapsules is 10 μm and their Young's modulus is 1.8 GPa (Mercade-Prieto *et al.*, 2011) and their Poisson's ratio is assumed to be 0.5 (Liu, 2010). A flow rate of 200 mL h^{-1} was used to remove microcapsules from a non-modified PET surface in aqueous solution, as described in Chapter 6. For a non-modified PET surface, there is no PE molecule attached on the

side wall of microcapsules and h is equal to zero. The adhesion and thermodynamic work of adhesion between microcapsule and a PET surface in aqueous solution predicted by the modified model were 34 nN and 542 $\mu J\ m^{-2}$, which agree well with the adhesion results obtained by AFM shown in Chapter 6, which are 35 ± 3 nN and 560 ± 50 $\mu J\ m^{-2}$ by holding single microcapsules to a PET surface for 10s.

Then PET surfaces were modified with PE molecules, which attached on the side wall of the microcapsule. The maximum pull-off force between microcapsules and each PE(PVF/chitosan/PEI)-modified PET surface dropped to 23 ± 6 nN (10 s), 21 ± 4 nN (10 s) and 23 ± 4 nN (10 s) respectively. In order to break the main contact between the microcapsule and the PE-modified PET surface, the thermodynamic work of adhesion needed is 400 ± 100 $\mu J\ m^{-2}$, 340 ± 70 $\mu J\ m^{-2}$ and 360 ± 60 $\mu J\ m^{-2}$ according to Equation 7.21. However, in order to displace a microcapsule from a surface, other than break between the microcapsule and the surface, it still needs to break the joints between PE molecules and the wall of the microcapsule, which needs to overcome the extra thermodynamic work of adhesion between PE molecules and the microcapsule surface. The thermodynamic work of adhesion as a function of the distance from the contact joint of a PE molecule with the wall of microcapsule to the PET surface was investigated in Figure 7.9 (All the contacts are assumed on the parallel plane to the flow direction and past the origin of the sphere; additionally, the molecules are assumed to contact the wall of microcapsule and the surface in the vertical direction stiffly without any free length, which acts like a straight stick between them). When the contact joint is approximately 1000 nm far away from the surface the thermodynamic work of adhesion needed to break the point is 63 $\mu J\ m^{-2}$, and it increases with the decrease of h (the vertical distance between the contact joint and the PET surface). The thermodynamic work of adhesion needed for a microcapsule separating with a PE-modified PET surface

is the sum of the thermodynamic work of adhesion between the PE molecules and the side wall of the microcapsule and the microcapsule and the PET surface. Therefore, only with few PE-microcapsule contact joints on the side wall of the microcapsule, the sum of the thermodynamic work of adhesion can overcome that needed to break the sole microcapsule-PET contact. With the increase of the number of the contact joins, more thermodynamic work of adhesion is needed to displace a microcapsule from a PET surface. Therefore, the stretching of PE molecules to the microcapsule surface and making contact joins is the main reason causing the increase of the sum of the thermodynamic work of adhesion when using a fluid flow to displace the particle and then it will be less easy for the particle to be removed from the PE-modified PET surface as found in Chapter 6. The more contact joints, the longer of the molecules, the higher the sum of thermodynamic work of adhesion. Therefore PE molecules with long linear structures and less steric hindrance can possibly enhance the retention between microparticles and a surface. Other than the adhesion force, the sum of the thermodynamic work of adhesion is the main parameter to interpret the removal of particle from a surface in a flow chamber, which sometime is missed.

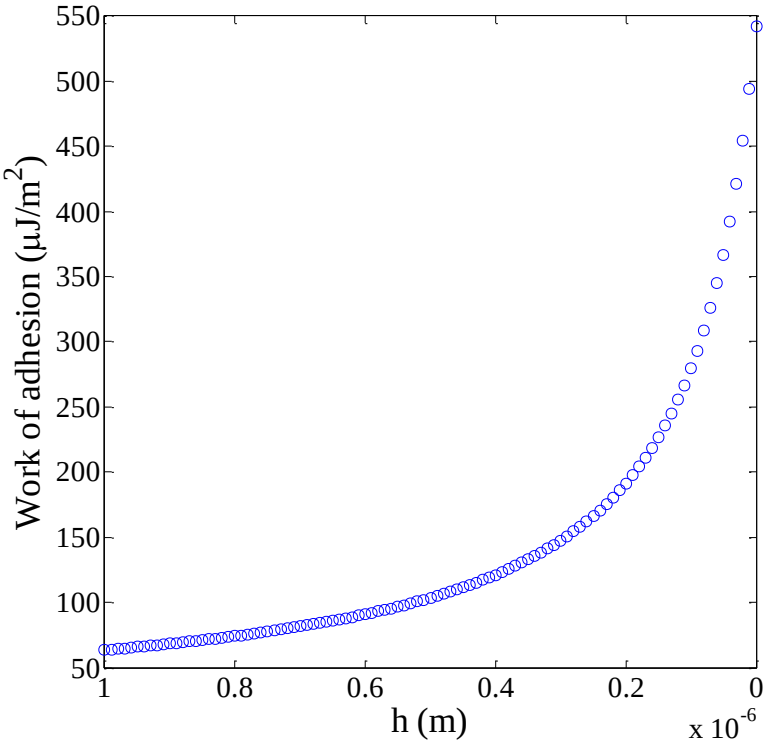

Figure 7.9 The thermodynamic work of adhesion as a function of h. The simulation parameters (flow rate: 200 ml/h; density of particle: 1050 kg m^{-3}; coefficient of static friction: 0.2 (experimental data); Young's modulus values of particle and glass: 1.8 GPa (Mercade-Prieto *et al.*, 2011) and 3 GPa (provided by Goodfellow, UK); Poisson's ratio values of particle and glass: 0.5 (Liu, 2010) and 0.3(provided by Goodfellow, UK), the interfacial adhesion energy per unit area 560 μJ m^{-2} (experimental data)).

7.6 Conclusions

The model of particle removal has been developed, and it predicts that the displacement of microcapsules from a glass surface is possibly due to rotation. The adhesion is related to onset of removal from a substrate by a fluid flow, particle radius, the flow rate, coefficient of friction between the particle and the substrate and the particle location (distance from the centre line). The adhesion and thermodynamic work of adhesion calculated according to the model of particle removal by considering DMT contact mechanic with the flow chamber experimental data is 89 ± 14 nN and 1200 ± 100 μJ m^{-2},

which are much higher than the values of 7.5 ± 1.6 nN and 90 ± 20 μJ m^{-2} obtained by the AFM colloidal probe technique. A better agreement of the adhesion and the thermodynamic work of adhesion results were achieved by considering the possible mechanisms of contact (the contact radius of 10% of particle radius in aqueous solution suggested by Liu *et al.* (2002) and a layer of water molecules present between two surfaces) between microcapsules and a substrate in aqueous solution, which is 6.0 ± 1.1 nN and 84 ± 13 μJ m^{-2}. Additionally, the adhesion and thermodynamic work of adhesion between microcapsules and non-PET surfaces were predicted by the model are 34 nN and 542 μJ m^{-2}. They agree well with the adhesion results determined by AFM in Chapter 6, which are 35 ± 3 nN and 560 ± 50 μJ m^{-2}. The consistent results of the adhesion on glass surfaces and PET surfaces given by the two approaches indicate the model of particle removal developed in this work is promising to predict the adhesion behaviour between microparticles and a substrate in a liquid environment and it may be applicable to predict both thermodynamic work of adhesion and friction coefficient in microparticle –surface systems.

The model reveals that with the increase of the adhesion, a higher flow rate is needed to displace microcapsules from the surface; in other words at a constant flow rate, more particles will remain. The conclusion is consistent with the trend of experimental results in Chapter 5 but contradictory to the results in Chapter 6. The model was further used to predict the sum of the thermodynamic work of adhesion after PE molecules attached on the side wall of microcapsules and it was suggested that other than adhesion, the sum of thermodynamic work of adhesion may be the main parameter to determine the removal of microcapsules from a surface in a flow chamber. The sum of thermodynamic work of adhesion is a function of both adhesion and the properties of the PE molecules acting as bridges at the interface. Therefore, adhesion is the main parameter to determine the

removal of microcapsules from a surface in a flow chamber when the bridging interactions are not the main adhesion mechanism, which can also interpret the data in Chapter 5.

Chapter 8: Overall Conclusions and Recommendations for Future Work

8.1 Overall Conclusions

Perfume microcapsules are intended to be incorporated in household products such as detergents, to provide a pleasant scent to consumers after laundry process. To realise this, it is essential for the microcapsules to deposit on fabric surfaces during the laundry process. Therefore, the main aim of this project was to investigate the adhesion and retention of perfume microcapsules on fabric surfaces and then to propose strategies to enhance the retention of microcapsules onto fabric surfaces during laundry process. The main conclusions are summarised as follows.

(1) Positively charged polyelectrolytes (PEs) polyvinyl formamide (PVF), chitosan enhanced adhesion between microcapsules and cellulose thin films by either modifying the microcapsules or the cellulose thin films (Chapter 4 and Chapter 5). Although both modifications in Chapter 4 and Chapter 5 enhanced adhesion, the adhesion mechanisms were different. Adhesion between non-modified microcapsules and non-modified cellulose thin films was considered mainly due to bridging forces because of the extension of cellulose chains. After modifying microcapsules with PEs, the increase in adhesion between microcapsules and cellulose thin films was concluded to be mainly due to the bridge interactions because of the entanglement of PE molecular chains and cellulose chains. Simultaneously, after the modifications, electrostatic attraction was suggested to

capture the microcapsules to the modified cellulose film and then hydrogen bonds as well as bridging forces played important roles to contribute the adhesion when they were separated. Therefore positively charged polyelectrolytes can be used to enhance adhesion between microcapsules and cellulose thin films either through bridging forces or electrostatic interactions. It can be potentially used to increase adhesion between other particle-substrate systems.

(2) The aggregation of microcapsules was observed after modification of microcapsules with PEs and big variations in the value of adhesion between different microcapsules were observed, as presented in Chapter 4. Bridge interactions because of the entanglement of PE molecular chains were the reason causing aggregation. The limited number of the microcapsules measured in the work and the uneven coverage of PE molecules and the increase of the surface roughness may be the main reasons to cause the adhesion variation between difference microcapsules. Therefore, it is suggested that the aggregation of microcapsules should be avoided and a technique based on analysing a population of microcapsules is needed. Therefore, an alternative protocol to modify model fabric surfaces with polyelectrolytes and then investigation of retention of microcapsules to cellulose thin films by a flow chamber technique has been adopted.

(3) Both retention of microcapsules characterised by the flow chamber technique and the average pull-off force by AFM were found to increase after PEs were applied to modified cellulose thin films, as presented in Chapter 5. It was concluded that the flow chamber technique can be potentially used as a tool for fast screening the

effects of various chemicals on the adhesion of microcapsules on different fabric surfaces.

(4) Both retention and adhesion of microcapsules on PET surfaces (Chapter 6) were greater than those on cellulose thin films (Chapter 5). The main reason was that the PET surface is much more hydrophobic than that of cellulose thin film, and the increase of the adhesion on PET was attributed at least partially to hydrophobic interaction, combined with the bridging interactions caused by the extension of cellulose chains on the cellulose surface. Therefore, the hydrophobic interaction can also be important between surfaces.

(5) Adhesion was found to decrease after PET surfaces were modified with PEs, which seems be inconsistent with the results of the increase in the retention (Chapter 6). The inconsistency could be explained as adhesion is simply measured by AFM based on popping-out a single microcapsule from a substrate in the vertical direction and it is mainly determined by the surface properties (the decrease of the hydrophobic nature and the increase in surface roughness), whilst micro particles are theoretically predicted to be displaced by rolling; without modification, the microcapsules start to rotate by overcoming the torque balance on the centre of the contact region; however, after the modification of the PET surface with PEs, the right position for the torque balance is raised to each contacted point and then the displacement of the microcapsules from the PET surface is not a single motion anymore, which becomes to be a gradual process of breaking joints from the position far away from the substrate to the contact region; the strength and the number of the contact joints become important to influence the displacement; those molecules with longer chains and smaller steric hindrance

tend to form close and long distance contacts with the wall of microcapsule more easily and then it can be less easy for the microcapsules to be removed from the substrate. Therefore, the retention of microcapsules was enhanced even when the adhesion was decreased.

(6) The performance of PVF was better than that of chitosan and then PEI in terms of enhancing retention, as presented Chapter 4, 5 and 6, but no much difference was observed in adhesion by AFM after they were used modify PET surfaces. The main reason may be the difference in the molecule structures: PVF is a molecule with long linear structure, whilst chitosan is formed with spiral planes and PET is highly branched. The difference in structures was also validated by analysis of the protuberances on PE-modified surfaces, the viscosity of PE solution, and the "microcapsule-surface separation distance" observed on AFM force curves from experimental results. It was concluded that long linear molecules with small steric hindrance may be more favourable to enhance adhesion at interface than branched molecules and they can be used to modify either microcapsules or fabric surfaces to enhance the retention of microcapsules on fabric surfaces during laundry processes.

(7) A model was developed based on the displacement of a microcapsule from a substrate in a flow chamber to establish the relationship between the removal of microcapsules exposed to a fluid flow and their adhesion to the substrate. The model predicts that microcapsules were removed by rolling and the thermodynamic work of adhesion between microcapsules and the substrate in the flow chamber was found to be related to the particle radius, flow rate, coefficient of friction and the distance from the centre line before the particle. The

predictions of adhesion and thermodynamic work of adhesion between microcapsules and a glass surface in aqueous solution agree well with the results obtained by AFM by considering a relationship between the contact radius and the radius of microcapsules suggested by Liu (2002) (the contact radius is 10% of particle radius) and a layer of water molecules present between two surfaces in aqueous solution. Additionally, the adhesion and thermodynamic work of adhesion between microcapsules and non-modified PET surfaces were predicted well by the model. The consistent results on adhesion between microcapsules and glass surfaces and PET surfaces given by the two approaches indicate the model of particle removal developed in this work is promising to predict the adhesion behaviour of microparticles on a substrate and it may be applicable to predict both thermodynamic work of adhesion and friction coefficient in microparticle – surface systems.

(8) The model reveals that with the increase of the adhesion, a higher flow rate is needed to displace the microcapsules from the surfaces; in other words with a constant flow rate, more particles will be remaining. The conclusion is consistent with the trend of experimental results in Chapter 5 but contradictory to the results in Chapter 6. The model was further used to predict the sum of the thermodynamic work of adhesion after PE molecules attached on the side wall of microcapsules and it was suggested that other than the adhesion, the sum of thermodynamic work of adhesion, a parameter which is hidden behind adhesion, is also an important parameter to determine the removal of microcapsules from a surface in a flow chamber.

8.2 Future work

(1) Adhesion was found to increase after perfume microcapsules were modified with PEs through bridging forces as presented in Chapter 4. However, entanglement of the long PE molecule chains between microcapsules also caused their aggregation. The presence of the big microcapsule aggregates not only influenced their retention behaviour on fabric surfaces but also affected product image if the microcapsule aggregates can be apparently seen in the product. Therefore, new formulation to prepare microcapsules such as via adding PE molecules to the wall materials or a protocol to modify microcapsules with PE chemicals with no or less aggregation is required.

(2) In the work presented in Chapter 6 and Chapter 7, the retention of microcapsules on a polyester surface was enhanced through bridging interactions by increasing the sum of thermodynamic work of adhesion, and the retention behaviour is related to the PE molecular structures. It is proposed that the flow chamber technique be used for the investigation of the molecular interactions. Such work can be possibly done by introducing a well understood system, and then PE molecules with different concentration can be implanted on one of the surfaces, and then the removal of the particle can be recorded to analyse the sum of the thermodynamic work of adhesion for each concentration. Then a relationship of the sum of thermodynamic work of adhesion with the concentration of PE can be built. The number of the PE molecules is a function of their concentration. Therefore it is possible to calculate the thermodynamic work of adhesion and then adhesion of single molecules.

(3) Adhesion was found to be enhanced through the protocol for modifying the fabric surfaces with PEs as described in Chapter 4, 5 and 6 and the main mechanisms of adhesion enhancement are considered to be caused by either bridging forces or electrostatic attraction. The difference in the performance of enhancing adhesion and retention of microcapsules on fabric surfaces between the three chemicals used in this work was considered to be due to their different structures. However, the molecular weights of the three chemicals are also different. Therefore, it is suggested that one chemical with different molecular weights be used to investigate the influence of the molecular weight on the adhesion and retention of microcapsules on fabric surfaces; then a further understanding of the effect of the molecular weight and structure on the adhesion behaviour can be developed.

(4) The adhesion and thermodynamic work of adhesion of microcapsules on fabric surfaces were validated to be important for the retention of microcapsules on them in a flow chamber device in this work. However, the real laundry process is much more complicated and the friction between microcapsules and fabric surfaces may also influence the detachment of microcapsules. Therefore, the friction between microcapsule and fabric surfaces at molecule level in liquid environments should be further investigated. Currently, the MF membrane which was used to mimic the surface of the MF microcapsule was swollen in aqueous solutions and friction measurements failed by using tribometer. The methodology by AFM proposed in Chapter 7 can be used as a complimentary method to measure frictions between single microcapsules and fabric surfaces after finding a proper calibration grid; the

frication can be also predicted by the model of particle removal combined with experimental results with the flow chamber technique to achieve a better understanding of the retention of microcapsules on fabric surfaces.

(5) Contact between microparticles including microcapsules and a substrate in aqueous solution is a complex issue. The model in Chapter 7 predicts the adhesion values, which are in good agreements with the results obtained by AFM for contact between microcapsules and a substrate by using a ratio of contact radius to particle radius of 0.1 observed in Liu *et al.* (2002). However, no universal understanding of the contact issue between microparticles and a substrate in aqueous solution was provided. Therefore, a further investigation of the contact between microparticles and a substrate in aqueous solution should be carried out. Then an improved model of particle removal in the flow chamber can be developed by introducing the contact mechanics which is applicable in aqueous solution to predict adhesion and the thermodynamic work of adhesion, and the model can be used further to characterize adhesion behaviour between microparticles and substrates in liquid environment widely.

(6) The adhesion was investigated between microcapsules and the flat model fabric surfaces in this work. But real fabric surfaces are rough with network structures and surfactant and other additives are involved. Hence, a more representative system with real fabric and detergent should be investigated. Moreover, the retention caused by the physical entrapment also needs to be investigated; it is suggested that the influence of size of the microcapsules on their physical entrapment by real fabric surfaces be investigated.

(7) The Re number of the fluid in the flow chamber used in this work was calculated based on a straight pipe flow, which indicates it was laminar. However, the configuration of the quarter turnings of the inlet and outlet of the flow chamber may cause turbulent flow at these regions. Therefore future work should include investigation of the flow pattern in the flow chamber. If turbulence is observed, the configuration of the flow chamber should be improved.

(8) In this work the static contact angle was measured to show the hydrophilic and hydrophobic nature of the surface. After the model fabric surface was modified with polyelectrolytes, the surface may be rough and not homogenous and it may be possible to observe contact angle hysteresis; therefore both the advancing contact angle and receding contact angle are suggested to be measured.

Reference

AKHTAR, R., SCHWARZER, N., SHERRATT, M. J., WATSON, R. E. B. & GRAHAM, H. K. 2009. Nanoindentation of Histological Specimens: Mapping the Elastic Properties of Soft Tissues. *Journal of Materials Research,* 24**,** 638-646.

AL-HASHMI, A. R. & LUCKHAM, P. F. 2010. Characterization of the Adsorption of High Molecular Weight Non-ionic and Cationic Polyacrylamide on Glass from Aqueous Solutions Using Modified Atomic Force Microscopy. *Colloids and Surfaces A: Physicochemical and Engineering Aspects,* 358**,** 142-148.

ALTOBELLI, G., LEGRAS, S., POCH, O., CHOUKRALLAH, M. A., BERTIN, I., JOST, B. & DAVIDSON, I. 2010. Cell-specific interaction of retinoic acid receptors with target genes in mouse embryonic fibroblasts and embryonic stem cellsDelacroix L, Moutier E, . *Molecular and Cellular Biology,* 30**,** 231-244.

ARADHYA, S. V., FREI, M., HYBERTSEN, M. S. & VENKATARAMAN, L. 2012. Van der Waals interactions at metal/organic interfaces at the single-molecule level. *Nature Materials,* 11**,** 872-876.

AUTUMN, K., SITTI, M., LIANG, Y. A., PEATTIE, A. M., HANSEN, W. R., SPONBERG, S., KENNY, T. W., FEARING, R., ISRAELACHVILI, J. N. & FULL, R. J. 2002. Evidence for van der Waals adhesion in gecko setae. *Proceedings of the National Academy of Sciences,* 99**,** 12252-12256.

BATCHELOR, G. K. 1967. An Introduction to Fluid Dynamics. *Cambridge University Press.,* ISBN 0-521-66396-2.

BHUSHAN, B. 2003. Adhesion and Stiction: Mechanisms, Measurement Techniques, and Methods for Reduction. *Journal of Vacuum Science & Technology. B,* 21**,** 2262-2296.

BIANCHETTI, G., OTTAVIA, E., MARC FRANCOIS, T., SMETS, J. & GRANDE, G. 2010. Bleaching compositions containing perfume microcapsules. *US 20100180386*.

BIGGS, S. 1996. Steric and bridging forces between surfaces bearing adsorbed polymer: an atomic force microscopy Study. *Langmuir,* 11**,** 156-162.

BINNIG, G., QUATE, C. F. & GERBER, C. 1986. Atomic force microscope. *Physical Review Letters,* 56**,** 930–933.

BORDI, F., SENNATO, S. & TRUZZOLILLO, D. 2009. Polyelectrolyte-induced Aggregation of Liposomes: A New Cluster Phase with Interesting Applications. *Journal of Physics: Condensed Matter* 21**,** 1-27.

BORKOVEC, M. & PAPASTAVROU, G. 2008. Interactions between Solid Surfaces with Adsorbed Polyelectrolytes of Opposite Charge. *Colloid Interface Science,* 13**,** 429-437.

BOURA, C., MENU, P., PAYAN, E., PICART, C., VOEGEL, J. C., MULLER, S. & STOLTZ, J. F. 2003. Endothelial Cells Grown on Thin Polyelectrolyte Mutlilayered Films: an Evaluation of a New Versatile Surface Modification. *Biomaterials,* 24**,** 3521-3530.

BOWEN, J., CHENELER, D., WALLIMAN, D., ARKLESS, S. G., ZHANG, Z., CLWARD, M. & ADAMS, M. J. 2010. On the calibration of rectangular atomic force microscope cantilevers modified by particle attachment and lamination. *Measurement Science and Technology,* 21**,** 106-115.

BOWEN, W. R., FENTON, A. S., LOVITT, R. W. & WRIGHT, C. J. 2002. The measurement of Bacillus mycoides spore adhesion using atomic force microscopy, simple counting methods, and a spinning disk technique. *Biotechnology and Bioengineering,* 79**,** 170-179.

BOWEN, W. R., HILAL, N., LOVITT, R. W. & WRIGHT, C. J. 1998. Direct measurement of interactions between adsorbed protein layers using an atomic force microscope. *Journal of Colloid and Interface Science,* 197**,** 348-52

BOWEN, W. R., LOVITT, R. W. & WRIGHT, C. J. 2001. Atomic force microscopy study of the adhesion of saccharomyces cerevisiae. *Journal of Colloid and Interface Science,* 237**,** 54-61.

BOWLING, R. A. 1985. An analysis of particle adhesion on semiconductor surfaces. *Journal of The Electrochemical Society,* 132**,** 2208-2214.

BROECKX, W., AUGUST, M., DEL, V. & EVA, M. 2004. Microcapsules. *US 7897555*.

BROWN, D. C. & LARSON, R. S. 2001. Improvements to parallel plate flow chambers to reduce reagent and cellular requirements. *BMC Immunology,* 2**,** 9-15.

BROWN, R. W. & BOWMAN, R. P. 1985. Capsule manufacture. *US 4552811*.

BRUNNER, R., TYNDALL, G. W., WALTMAN, R. J. & TALKE, F. E. 2010. Adhesion between surfaces separated by molecularly thin perfluoropolyether films. *Tribology Letters,* 40**,** 41-48.
BRYDSON, J. A. 1999. Plastics Materials. *Butterworth-Heinemann,* 7th edition.
BUTT, H. J. 1991. Measuring electrostatic, van der Waals, and hydration forces in electrolyte solutions with an atomic force microscope. *Biophysical Journal,* 60**,** 1438-1444.
BUTT, H. J., BARNES, W. J. P., CAMPO, A. D., KAPPL, M. & SCHÖNFELD, F. 2010. Capillary forces between soft, elastic spheres *Soft Matter,* 6**,** 5930-5936.
CHE, A. F., LIU, Z. M., HUANG, X. J., WANG, Z. G. & XU, Z. K. 2008. Chitosan-modified poly(acrylonitrile-co-acrylic acid) nanofibrous membranes for the immobilization of concanavalin A. *Biomacromolecules,* 9**,** 3397-3403.
CHEN, A. & MOY, V. T. 2000. Cross-Linking of cell surface receptors enhances cooperativity of molecular adhesion. *Biophysical Journal,* 78**,** 2814-2820.
CHEN, Q., XU, K., ZHANG, W., SONG, C. & WANG, P. 2009a. Preparation and characterization of poly (N-isopropylacrylamide)/polyvinylamine core-shell microgels. *Colloid & Polymer Science,* 287**,** 1339-1346.
CHEN, W., LEUNG, V., KROENER, H. & PELTON, R. 2009b. Polyvinylamine−phenylboronic acid adhesion to cellulose hydrogel. *Langmuir,* 25**,** 6863-6868.
CHEN, W., LU, C. & PELTON, R. 2006. Polyvinylamine Boronate Adhesion to Cellulose Hydrogel. *Biomacromolecules,* 7**,** 701-702.
CHERUKAT, P., MCLAUGHLIN, J. B. & GRAHAM, A. L. 1994. The inertial lift on a rigid sphere translating in a linear shear flow field. *International Journal of Multiphase Flow,* 20**,** 339-353
CHIBOWSKI, S., PATKOWSKI, J. & GRZADKA, E. 2009. Adsorption of Polyethyleneimine and Polymethacrylic Acid onto Synthesized Hematite. *Journal of Colloid and Interface Science,* 329**,** 1-10.
CHRISTENDAT, D., ABRAHAM, T., XU, Z. & MASLIYH, J. 2005. Adhesion forces between functionalized probes and hydrophilic silica surfaces. *Atomic Force Microscopy in Adhesion Studies***,** 65-279.
CLAESSON, P. M., DEDINAITE, A. & ROJAS, O. J. 2003. Polyelectrolytes as adhesion modifiers. *Advances in Colloid and Interface Science,* 104**,** 53-74.
CLAESSON, P. M. & NINHAMI, B. W. 1992. pH-dependent interactions between adsorbed chitosan layers. *Langmuir,* 8**,** 1406-1412.
CLEAVER, J. A. S. & LOOI, L. 2007. AFM study of adhesion between polystyrene particles: the influence of relative humidity and applied load. *Powder Technology,* 174**,** 34-37.
COOPER, K., GUPTA, A. & BEAUDOIN, S. 2001. Simulation of the adhesion of particles to surfaces. *Journal of Colloid and Interface Science,* 234**,** 284-292.
COULSON, C. A. 1961. Valence. *Oxford University Press,* 2nd Edition.
CRICK, C. R. & PARKIN, I. P. 2011. Aerosol Assisted Deposition of Melamine-formaldehyde Resin: Hydrophobic Thin Films from a Hydrophilic Material. *Thin Solid Films,* 519**,** 2181-2186.
DA RÓZ, A. L., LEITE, F. L., PEREIRO, L. V., NASCENTE, P. A. P., ZUCOLOTTO, V., OLIVEIRA JR, O. N. & CARVALHO, A. J. F. 2010. Adsorption of chitosan on spin-coated cellulose films. *Carbohyd Polym.,* 80**,** 65–70.
DADSETAN, M., MIRZADEH, H. & SHARIFI-SANJANI, N. 2000. IR Laser Surface Modification of Polyethylene Terephthalate as a Biomaterial. *Iranian Polymer Journal,* 9**,** 203-209.
DANILATOS, G. 1997. Environmental scanning electron microscopy. In-situ microscopy in materials research. *Kluwer Academic Publishers***,** 14-44.
DECUZZI, P., GENTILE, F., GRANALDI, A., CURCIO, A., CAUSA, F., INDOLFI, C., NETTI, P. & FERRARI, M. 2007. Flow chamber analysis of size effects in the adhesion of spherical particles. *International Journal of Nanomedicine,* 2**,** 689-696.
DERJAGUIN, B. V., MULLER, V. M. & TOPOROV, Y. P. 1975. Effect of contact deformations on the adhesion of particles. Journal of Colloid and Interface Science, 53, 314-326.
DERKSEN, J. J. & LARSEN, R. A. 2011. Drag and lift forces on random assemblies of wall-attached spheres in low-Reynolds-number shear flow. The Journal of Fluid Mechanics, 673, 548-573.
DOUGLAS, J. G., GLORIA, S. O. & RYAN, M. 2008. Adhesion and surface issues in cellulose and nanocellulose. *Journal of Adhesion Science and Technology,* 22**,** 545-567.
DRELICH, J., TORMOEN, G., W. & BEACH, E., R. 2004. Determination of solid surface tension from particle- sbustrate pull-off forces measured with the atomic force microscope. *Journal of Colloid and Interface Science,* 280**,** 484-497.
DUCKER, W. A., SENDEN, T. J. & PASHLEY, R. M. 1992. Measurement of forces in liquid using a force microscope. *Langmuir,* 8**,** 1831-1836.
DURST, F., RAY, S., ÜNSAL, B. & BAYOUMI, O. A. 2005. The Development Lengths of Laminar Pipe and Channel Flows. *Journal of Fluids Engineering,* 127**,** 1154-1160.

EASTMAN, T. & ZHU, D. M. 1996. Adhesion forces between surface-modified AFM tips and a mica surface. *Langmuir,* 12**,** 2859-2862.
EL-HEFIAN, E. A., ELGANNOUDI, E. S., MAINAL, A. & YAHAYA, A. H. 2010. Characterization of Chitosan in Acetic Acid: Rheological and Thermal Studies. *Turkish Journal of Chemistry,* 34**,** 47-56.
ELSNER, N., DUBREUIL, F. & FERY, A. 2004. Tuning of Microcapsule Adhesion by Varying the Capsule-wall Thickness. *Physical Review E,* 69**,** 031802.
ERATH, J., SCHMIDT, S. & FERY, A. 2010. Characterization of Adhesion Phenomena and Contact of Surfaces by Soft Colloidal Probe AFM. *Soft Matter,* 6**,** 1432-1437.
ESLAMI, H. & MÜLLER-PLATHE, F. 2009. Structure and Mobility of Poly(ethylene terephthalate): A Molecular Dynamics Simulation Study. *Macromolecules,* 42**,** 8241-8250.
EVERT, S. 2001. Microspheres of Melamine. *US 6291632 B1*.
FAGHIHNEJAD, A. & ZENG, H. 2012. Hydrophobic interactions between polymer surfaces: Using polystyrene as a model system. *Soft Matter,* 8**,** 2746-2759.
FISCHER, K. E., ALEMÁN, B. J., TAO, S. L., DANIELS, R. H., LI, E. M., BÜNGER, M. D., NAGARAJ, G., SINGH, P., ZETTL, A. & DESAI, T. A. 2009. Biomimetic Nanowire Coatings for Next Generation Adhesive Drug Delivery Systems. *Nano Letters,* 9**,** 716-720.
FRANCA, E. F., FREITAS, L. C. G. & LINS, R. D. 2011. Chitosan molecular structure as a function of N-acetylation. *Biopolymers,* 95**,** 448-460.
FRAS ZEMLJIČ, L., PERŠIN, Z. & STENIUS, P. 2009. Improvement of chitosan adsorption onto cellulosic fabrics by plasma treatment. *Biomacromolecules,* 10**,** 1181-1187.
FU, J., JI, J., YUAN, W. & SHEN, J. 2005. Construction of Anti-adhesive and Antibacterial Multilayer Films via Layer-by-layer Assembly of Heparin and Chitosan. *Biomaterials,* 26**,** 6684-6692.
GALLAGHER, J. O., MCGHEE, K. F., WILKINSON, C. D. W. & RIEHLE, M. O. 2002. Interaction of animal cells with ordered nanotopography. *NanoBioscience, IEEE Transactions on,* 1**,** 24-28.
GAO, J. Y. & DUBIN, P. L. 1999. Binding of proteins to copolymers of varying hydrophobicity. *Biopolymers,* 49**,** 185-193.
GARCíA, R. & PÉREZ, R. 2002. Dynamic atomic force microscopy methods. *Surface Science Reports,* 47**,** 197-301.
GARRETT, T. R., BHAKOO, M. & ZHANG, Z. 2008. Characterisation of bacterial adhesion and removal in a flow chamber by micromanipulation measurements. *Biotechnol Lett.,* 30**,** 427-433.
GHOSH, S. K. 2006. Functional coatings: by polymer microancapsulation. *Wiley_VCH***,** Weinheim
GIESBERSA, M., KLEIJNB, J. M. & STUARTA, M. A. C. 2002. Interactions between acid- and base-functionalized surfaces. *Journal of Colloid and Interface Science,* 252**,** 138-148.
GOLDSTEIN, J., NEWBURY, D. E., JOY, D. C., LYMAN, C. E., ECHLIN, P., LIFSHIN, E., SAWYER, L. & MICHAEL, J. R. 2003. Scanning Electron Microscopy and X-ray Microanalysis. *Springer Science+Business Media, Inc,* Third edition.
GRAF, P., FINKEN, R. & SEIFERT, U. 2006. Adhesion of microcapsules. *Langmuir,* 22**,** 7117-7119.
GRASSO, D., SUBRAMANIAM, K., BUTKUS, M., STREVETT, K. & BERGENDAHL, J. 2002. A review of non-DLVO interactions in environmental colloidal systems. *Environmental Science & Bio/Technology,* 1**,** 17-38.
GROBELNY, J., PRADEEP, N., KIM, D.-I. & YING, Z. C. 2006. Quantification of the meniscus effect in adhesion force measurements. *Applied Physics Letters,* 88**,** 1-3.
GURUMOORTHY, A. V. P. & KHAN, K. H. 2011. Polymers at Interfaces: Biological and Non-biological Applications. *Biosciences and Technology,* 3**,** 80-86.
HAN, J., YEOM, J., MENSING, G., JOE, D., MASEL, R. I. & SHANNON, M. A. 2009. Surface energy approach and AFM verification of the (CF)n treated surface effect and its correlation with adhesion reduction in microvalves. *Journal of Micromechanics and Microengineering,* 19**,** 1-9.
HARIHARAN, P. 2007. *Basics of Interferometry (Second edition).* Burlington: Academic Press.
HARTLEY, P. A., PARFITT, G. D. & POLLACK, L. B. 1985. The role of the van der Waals force in the agglomeration of powders containing submicron particles. *Powder Technology,* 42**,** 35-46.
HAUN, J. B. & HAMMER, D. A. 2008. Quantifying Nanoparticle Adhesion Mediated by Specific Molecular Interactions. *Langmuir,* 24**,** 8821-8832.
HE, Y., BOWEN, J., ANDREW, J. W., SMETS, J. & ZHANG, Z. 2013. Adhesion of Perfume-Filled Microcapsules to Model Fabric Surfaces. *Journal of Microencapsulation,* Submitted.
HECHT, E. 2003. Optics (International Edition). *Pearson,* Fourth Edition
HERMAN, S. J. 2002. Fragrance Applications: A Survival Guide. *Allured Publishing Corporation*.
HERSEL, U., DAHMEN, C. & KESSLER, H. 2003. RGD modified polymers: biomaterials for stimulated cell adhesion and beyond. *Biomaterials,* 24**,** 4385-4415.
HERTZ, H. 1896. Miscellaneous papers. *London: Macmillan***,** 146.

HODGES, C. S., CLEAVER, J. A. S., GHADIRI, M., JONES, R. & POLLOCK, H. M. 2002. Forces between polystyrene particles in water using the AFM: Pull-Off force vs particle size. *Langmuir,* 18**,** 5741–5748.

HODGES, C. S., LOOI, L., CLEAVER, J. A. S. & GHADIRI, M. 2004. Use of the JKR model for calculating adhesion between rough surfaces *Langmuir,* 20**,** 9571–9576.

HOLDER, D. J. & KEYHANI, N. O. 2005. Adhesion of the Entomopathogenic Fungus Beauveria (Cordyceps) bassiana to Substrata. *Applied and Environmental Microbiology,* 71**,** 5260-5266.

HOLMBERG, M., WIGREN, R., ERLANDSSON, R. & CLAESSON, P. M. 1997. Interactions between cellulose and colloidal silica in the presence of polyelectrolytes. *Colloids and Surfaces A: Physicochem. Eng. Aspects,* 129-130**,** 175-183.

HONG, K. & PARK, S. 1999. Melamine resin microcapsules containing fragrant oil: synthesis and characterization. *Materials Chemistry and Physics,* 58**,** 128-131.

HONG, K. & PARK, S. 2000. Preparation of Poly(l-lactide) Microcapsules for Fragrant Fiber and Their Characteristics. *Polymer,* 41**,** 4567-4572.

HSIEH, W. J., WANG, C. H., LAI, S. H., WONG, J. W., SHIH, H. C. & HUANG, T. S. 2006. Cathodoluminescence of fluorine doped amorphous carbon nanoparticles deposited by a filtered cathodic arc plasma system. *Carbon,* 44**,** 107-112.

HU, J., CHE, H.-Q. & ZHANG, Z. 2009. Mechanical properties of melamine formaldehyde microcapsules for self-healing materials *Materials Chemistry and Physics,* 118**,** 63-70.

HU, J., XIAO, Z., ZHOU, R., LI, Z., WANG, M. & MA, S. 2011. Synthesis and characterization of polybutylcyanoacrylate-encapsulated rose fragrance nanocapsule. *Flavour and Fragrance Journal,* 26**,** 162-173.

HUANG, F., LI, K. & KULACHENKO, A. 2009. Measurement of interfiber friction force for pulp fibers by atomic force microscopy. *Journal of Materials Science,* 44**,** 3770-3776.

HUH, M. W., KANG, I.-K., LEE, D. H., KIM, W. S., LEE, D. H., PARK, L. S., MIN, K. E. & SEO, K. H. 2001. Surface Characterization and Antibacterial Activity of Chitosan-grafted Poly(ethylene terephthalate) Prepared by Plasma Glow Discharge. *Journal of Applied Polymer Science,* 81**,** 2769-2778.

HUNTER, R. J. 1981. Zetapotential in collodial science. *Academic Press, New York*.

HUNTER, R. J. 2001. Foundations of colloid science. *Oxford University Press Inc., New York,* second edition.

ISHIDA, N., KUSAKA, Y. & USHIJIMA, H. 2012. Hydrophobic attraction between silanated silica surfaces in the absence of bridging bubbles. *Langmuir,* 28**,** 13952-13959.

ISHIKAWA, H., UEHARA, Y. & TAKENAKE, T. 1971. Am. Perfume. Cosmet. *Am. Perfume. Cosmet.,* 86**,** 42.

ISRAELACHVILI, J. N. 2011. Intermolecular and surface forces. Oxford: Academic press.

ISRAELACHVILI, J. N. & WENNERSTROEM, H. 1990. Hydration or Steric Forces between Amphiphilic Surfaces? *Langmuir,* 6**,** 873-876.

JANHOM, S., WATANESK, R., WATANESK, S., GRIFFITHS, P., ARQUERO, O.-A. & NAKSATA, W. 2006. Comparative study of lac dye adsorption on cotton fibre surface modified by synthetic and natural polymers. *Dyes and Pigments,* 71**,** 188-193.

JELLINEK, J. S. 1975. The use of fragrance in consumer products. *John Wiley& Sons, Inc.*

JOHANSSON, L. S. & CAMPBELL, J. M. 2004. Reproducible XPS on biopolymers: cellulose studies. *Surface and Interface Analysis,* 36**,** 1018-1022.

JOHNSON, K. L. 1985. Contact mechanics *Cambridge University Press*.

JOHNSON, K. L. & GREENWOOD, J. A. 1997. An adhesion map for the contact of elastic spheres, . *Journal of Colloid and Interface Science,* 192**,** 326–333.

JOHNSON, K. L., KENDALL, K. & ROBERTS, A. D. 1971. Surface energy and the contact of elastic solids. *Proceedings of the Royal Society of London A,* 324**,** 301–313.

JONES, R., POLLOCK, H. M., CLEAVER, J. A. S. & HODGES, C. S. 2002. Adhesion forces between glass and silicon surfaces in air studied by AFM: effects of relative humidity, particle size, roughness, and surface treatment. *Langmuir,* 18**,** 8045-8055.

JPK INSTRUMENTS 2009. NanoWizard® AFM Handbook.

KADOLPH, S. J. 2010. Textiles. *Prentice Hall,* 11th edition.

KAPPL, M. & BUTT, H. J. 2002. The colloidal probe technique and its application to adhesion force measurements. *Particle & Particle Systems Characterization,* 19**,** 129-143.

KARNER, S. & URBANETZ, N. A. 2012. Arising of electrostatic charge in the mixing process and its influencing factors. *Powder Technology,* 226**,** 261-268.

KARSA, D. R. & STEPHENSON, R. A. 1993. Encapsulation and controlled release. *The Royal Society of Chemistry*.

KATAINEN, J., PAAJANEN, M., AHTOLA, E., PORE, V. & LAHTINEN, J. 2006. Adhesion as an interplay between particle size and surface roughness. *Journal of Colloid and Interface Science,* 304**,** 524–529.

KENDALL, K., DHIR, A. & YONG, C. W. 2010. Strength by atomic force microscopy (AFM): molecular dynamics of water layer squeezing on magnesium oxide. *Philosophical Magazine,* 90**,** 4117-4128.

KESTIN, J., SOKOLOV, M. & WAKEHAM, W. A. 1978. Viscosity of Liquid Water in the Range -8 ℃ to 150 ℃. *Journal of Physical and Chemical Reference Data,* 7**,** 941-948.

KOCUNA, M., GRANDBOISB, M. & CUCCIA, L. A. 2011. Single molecule atomic force microscopy and force spectroscopy of chitosan. *Colloids and Surfaces B: Biointerfaces,* 82**,** 470-476.

KWOK, D. Y. & NEUMANN, A. W. 1999. Contact angle measurement and contact angle interpretation. *Advances in Colloid and Interface Science,* 81**,** 167-249.

LAM, K. K. & NEWTON, J. M. 1992. Influence of particle size on the adhesion behaviour of powders, after application of an initial press-on force. *Powder Technology,* 73**,** 117-125.

LAMB, K. 1994. Genetics and spearmans's "g" factor. *Mankind Quarterly,* 34**,** 379-391.

LAMPROU, D. A., SMITH, J. R., NEVELL, T. G., BARBU, E., STONE, C., WILLIS, C. R. & TSIBOUKLIS, J. 2010. A comparative study of surface energy data from atomic force microscopy and from contact angle goniometry. *Applied Surface Science,* 256**,** 5082–5087.

LARSEN, R., ESKIN, D. & DERKSEN, J. 2010. Lift and Drag on Agglomerates Attached to Walls. *7th International Conference on Multiphase Flow*.

LI, J. X., WANG, J., SHEN, L. R., XU, Z. J., LI, P., WAN, G. J. & HUANG, N. 2007. The Influence of polyethylene terephthalate surfaces modified by silver ion implantation on bacterial adhesion behavior. *Surface and Coatings Technology,* 201**,** 8155-8159.

LIAO, Q., DOBRYNIN, A. V. & RUBINSTEIN, M. 2003. Molecular Dynamics Simulations of Polyelectrolyte Solutions: Nonuniform Stretching of Chains and Scaling Behavior. *Macromolecules,* 36**,** 3386-3398.

LINS, L. & BRASSEUR, R. 1995. The hydrophobic effect in protein folding. *The FASEB Journal,* 9**,** 535-40.

LIU, J. 2012. Mechanisms for Cellulose-reactive Polyvinylamine Graft-TEMPO Adhesive. *Open Access Dissertations and Theses***,** 7145.

LIU, K. K., CHAN, V. & ZHANG, Z. 2002a. Capsule-substrate contact deformation: determination of adhesion energy. *Medical & Biological Engineering & Computing,* 40**,** 491-495.

LIU, K. K., WANG, H. G., WAN, K. T., LIU, T. & ZHANG, Z. 2002b. Characterizing capsule-substrate adhesion in presence of osmosis. *Colloids and Surfaces B: Biointerfaces,* 25**,** 293-298.

LIU, K. M., PREECE, J. A., YORK, D., BOWEN, J. & ZHANG, Z. 2012. Measurement of the adhesion between single melamine-formaldehyde resin microparticles and a flat fabric surface using AFM. *Journal of Adhesion Science and Technology,* 27**,** 973-987.

LIU, M. 2010. Understanding the mechanical strength of microcapsules and their adhesion on fabric surfaces. PhD Thesis, The University of Birmingham, UK.

LIU, Y., HE, T. & GAO, C. 2005. Surface Modification of Poly(ethylene terephthalate) via Hydrolysis and Layer-by-layer Assembly of Chitosan and Chondroitin Sulfate to Construct Cytocompatible Layer for Human Endothelial Cells. Colloids and Surfaces B: Biointerfaces, 46, 117-126.

LONG, Y., VINCENT, B., YORK, D., ZHANG, Z. & PREECE, J. A. 2010. Organic–inorganic double shell composite microcapsules. *Chemical Communications,* 46**,** 1718-1720.

MALVERN_INSTRUMENTS 2007a. Dynamic Light Scattering: anintroduction in 30 Minutes. *Malvern Instruments Ltd.,* Technical note.

MALVERN_INSTRUMENTS 2007b. Simplifying the measurement of zeta potential using M3-PALS. *Malvern Instruments Ltd.,* Application note.

MALVERN_INSTRUMENTS 2007c. Zeta potential: An introduction in 30 minutes. *Technical Note***,** 1-6.

MARTINES, E., MCGHEE, K., WILKINSON, C. & CURTIS, A. S. G. 2004. A parallel-plate flow chamber to study initial cell adhesion on a nanofeatured surface. *IEEE Trans Nanobioscience,* 3**,** 90-95.

MAUGIS, D. & POLLOCK, H. M. 1984. Surface Forces, Deformation and Adherence at Metal Microcontacts. *Acta Metallurgica,* 32**,** 1323-1334.

MEDENDORP, C. A. 2011. Atomic force microscopy method development for surface energy analysis. PhD Thesis, University of Kentucky, US.

MERCADE-PRIETO, R., NGUYEN, B., ALLEN, R., YORK, D., PREECE, J. A., GOODWIN, T. E. & ZHANG, Z. B. 2011. Determination of the Elastic Properties of Single Microcapsules Using Micromanipulation and Finite Element Modeling. Chemical Engineering Science, 66, 2042-2049.

MERKUS, H. G. 2009. Particle size measurements: fundamentals, practice, quality. *Springer Science+Business Media, Inc*.

MEYER, A. 1992. Perfume Microencapsulation by Complex Coacervation. *CHIMIA International Journal for Chemistry,* 46**,** 101-102.

MEYER, E. E., ROSENBERG, K. J. & ISRAELACHVILI, J. 2006. Recent Progress in Understanding Hydrophobic Interactions. *Proceedings of the National Academy of Sciences,* 103**,** 15739-15746.

MICHAEL, W. R. 1990. Perfume microcapsules for use in granular detergent compositions. *EU 0367385A2*.

MOHAMED, N. H., BAHNERS, T., WEGO, A., GUTMANN, J. S. & ULBRICHT, M. 2012. Surface Modification of Poly(ethylene terephthalate) Fabric via Photo-chemical Reaction of Dimethylaminopropyl Methacrylamide. *Applied Surface Science,* 259**,** 261-269.

MONLLOR, P., CAPABLANCA, L., GISBERT, J., D ÍAZ, P., MONTAVA, I. & BONET, Á. 2010. Improvement of microcapsule adhesion to fabrics. *Textile Research Journal,* 60**,** 631-635.

MYERS, D. 1991. Surfaces, interfaces and colloids: principles and applications. *VCH Publisher, Inc*.

NADER, J. & KARTHIK, L. 2004. A review of atomic force microscopy imaging systems: application to molecular metrology and biological sciences. *Mechatronics,* 14**,** 907-945.

NAVANEETHA, P., K., SELVARAJAN, V., DESHMUKH, R. R. & GAO, C. 2008. Adhesive properties of polypropylene (PP) and polyethylene terephthalate (PET) film surfaces treated by DC glow discharge plasma. *Vacuum,* 83**,** 332-339.

NELSON, G. 2002. Application of microencapsulation in textiles. *International Journal of Pharmaceutics,* 242**,** 55-62.

NIGMATULLIN, R., LOVITT, R., WRIGHT, C., LINDER, M., NAKARI-SETÄLÄ, T. & GAMA, M. 2004. Atomic force microscopy study of cellulose surface interaction controlled by cellulose binding domains. *Colloids and Surfaces B: Biointerfaces,* 35**,** 125–135.

NINA, A., ISHIZAKI, T. & SAITO, N. 2011. Cell adhesion behaviors on polyethylene terephthalate surface modified by surface-wave plasma-initiated graft polymerization. *Nanotechnology,* 1**,** 437-440.

NIVALDO, J. T. 2008. Chemical in focus: a molecular view of our world. *Cengage Learning,* 4th Edition.

NORDGREN, N., LO ¨NNBERG, H., HULT, A., MALMSTROM, E. & RUTLAND, M. W. 2009. Adhesion dynamics for cellulose nanocomposites. *ACS Applied Materials & Interfaces* 1**,** 2098-2103.

NOTLEY, S. M. 2009. Stretching and solvency of charged cellulose chains. *ACS Applied Materials & Interfaces* 1**,** 1218-1223.

NOTLEY, S. M., CHEN, W. & PELTON, R. 2009. Extraordinary adhesion of phenylboronic acid derivatives of polyvinylamine to wet cellulose: A colloidal probe microscopy investigation. *Langmuir,* 25**,** 6898-6904.

NOTLEY, S. M. & WÅGBERG, L. 2005. Morphology of modified regenerated model cellulose II surfaces studied by atomic force microscopy: effect of carboxymethylation and heat treatment. *Biomacromolecules,* 6**,** 1586-1591

O'ROURKE, N., HATCHER, L. & STEPANKSI, E. J. 2005. A Step-by-Step Approach to Using SAS® for Univariate & Multivariate Statistics. *SAS Institute,* Second Edition.

OFORI-KWAKYE, K., FELL, J. T. & KIPO, S. L. 2006. Effects of pH of medium and molecular weight on polyelectrolyte complex formation between pectin and chitosan. *Journal of Science and Technology,* 26**,** 66-73.

OHLOFF, G., PICKENHAGEN, W. & LAWRENCE, B. M. 1994. Scent and fragrances: the fascination of odors and their chemical perspectives. *Springer-Verlag Berlin and Heidelberg GmbH & Co. K*.

OLIVERIA, R. 1997. Understanding adhesion: a means for preventing fouling. *Experimental Thermal and Fluid Science,* 14**,** 316-322.

ONUSSEIT, H., WEFRINGHAUS, R., DREEZEN, G., WICHELHAUS, J., SCHALL, J., THIELE, L. & VAN HALTEREN, A. 2000. Adhesives, 1. General. *Ullmann's Encyclopedia of Industrial Chemistry.* Wiley-VCH Verlag GmbH & Co. KGaA.

ORELMA, H., FILPPONEN, I., JOHANSSON, L.-S., LAINE, J. & ROJAS, O. J. 2011. Modification of cellulose films by adsorption of CMC and chitosan for controlled attachment of biomolecules. *Biomacromolecules,* 12**,** 4311−4318.

OUALI, L. & BENCZEDI, D. 2008. Polyurethane and polyurea microcapsules. *US 20080206291*.

PAKARINEN, O. H., MATIVETSKY, J. M., GULANS, A., PUSKA, M. J., FOSTER, A. S. & GRUTTER, P. 2009. Role of van der Waals forces in the adsorption and diffusion of organic molecules on an insulating surface. *Physical Review B,* 80**,** 1-5.

PAN, X., YORK, D., PREECE, J. A. & ZHANG, Z. 2012. Size and strength distributions of melamine-formaldehyde microcapsules prepared by membrane emulsification. *Powder Technology,* 227**,** 43-50.

PASHLEY, R. M. 1981a. DLVO and hydration forces between mica surfaces in Li^+, Na^+, K^+, and Cs^+ electrolyte solutions: A correlation of double-layer and hydration forces with surface cation exchange properties. *Journal of Colloid and Interface Science,* 83**,** 531-546.

PASHLEY, R. M. 1981b. Hydration forces between mica surfaces in aqueous electrolyte solutions. *Journal of Colloid and Interface Science,* 80**,** 153-162.

PEDRONI, V. I., SCHULZ, P. C., GSCHAIDER, M. E. & ANDREUCETTI, N. 2003. Chitosan Structure in Aqueous Solution. *Colloid & Polymer Science,* 282**,** 100-102.

PINSCHMIDT, R. K. 2010. Polyvinylamine at Last. *Journal of Polymer Science Part A: Polymer Chemistry,* 48**,** 2257-2283.

PODGORNIK, R. & LIČER, M. 2006. Polyelectrolyte bridging interactions between charged macromolecules. *Current Opinion in Colloid & Interface Science,* 11**,** 273-279.

POPTOSHEV, E. & CLAESSON, P. M. 2002. Forces between glass surfaces in aqueous polyethylenimine solutions. *Langmuir,* 18**,** 2590-2594.

RADTCHENKO, I. L., PAPASTAVROU, G. & BORKOVEC, M. 2005. Direct force measurements between cellulose surfaces and colloidal silica particles. *Biomacromolecules,* 6**,** 3057-3066.

REIMER, L. 1998. Scanning Electron Microscopy: Physics of image formation and microanalysis. *Springer Science+Business Media, Inc,* Second edition.

REITSMA, M., CRAIG, V. & BIGGS, S. 2000. Elasto-plastic and visco-elastic deformations of a polymer sphere measured using colloid probe and scanning electron microscopy. *International Journal of Adhesion & Adhesives,* 20**,** 445-448.

REN, Y. L. D., A. M.; ZHANG, Z. B 2007. Investigation of radiation damage to microcapsules in environmental SEM. *Materials Science and Technology,* 23**,** 857-864.

RENSHAW, K. M., ORR, D. E. & BURG, K. J. L. 2005. Design and evaluation of a novel flow chamber for measuring cell adhesion to absorbable polymer films. *Biotechnology Progress,* 21**,** 538-545.

RIMAI, D. S., BROWN, K., ZARETSKY, M. C., LOFFTUS, K., ASLAM, M., FOWLKES, W. Y. & WEISS, D. S. 2010. The role of adhesion in electrophotographic digital printing. *Journal of Adhesion Science and Technology,* 24**,** 583-617.

RODRIGUES, S. N., FERNANDES, I., MARTINS, I. M., MATA, V. G., BARREIRO, F. & RODRIGUES, A. E. 2008. Microencapsulation of limonene for textile application. *Industrial & Engineering Chemistry Research,* 47**,** 4142-4147.

RODRIGUES, S. N., MARTINS, I. M. & FERNANDES, I. P. 2009. Scentfashion®: microencapsulated perfumes for textile application. *Chemical Engineering Journal,* 149**,** 463-472

ROITER, Y. & MINKO, S. 2005. AFM Single Molecule Experiments at the Solid−Liquid Interface: In Situ Conformation of Adsorbed Flexible Polyelectrolyte Chains. *Journal of the American Chemical Society,* 127**,** 15688-15689.

ROSSETTO, H. L., BOWEN, J. & KENDALL, K. 2012. Adhesion of alumina surfaces through confined water layers containing various molecules. *Langmuir* 28**,** 4648-4653.

SAFFMAN, P. G. 1965. The lift on a small sphere in a slow shear flow. *Journal of Fluid Mechanics* 22**,** 385-400.

SANJIT, K. D., SHARMA, M. M. & SCHECHTER, R. S. 1994. Adhesion and hydrodynamic removal of colloid particles from surfaces. *Journal of Colloid and Interface Science,* 164**,** 63-77.

SCZECH, R. & RIEGLER, H. 2006. Molecularly smooth cellulose surfaces for adhesion studies. *Journal of Colloid and Interface Science,* 301**,** 376-385.

SELL, C. S. 2006. The Chemistry of Fragrances. From Perfumer to Consumer (2nd edition). *The Royal Society of Chemistry Publishing,* Cambridge.

SHANAHAN, M. E. R. 2003. Adhesion of a liquid-filled spherical membrane. *The Journal of Adhesion,* 79**,** 881-891.

SHARMA, M. M., CHAMOUN, H., SARMA, D. S. H. S. R. & SCHECHTER, R. S. 1992. Factors controlling the hydrodynamic detachment of particles from surfaces. *Journal of Colloid and Interface Science,* 149**,** 121-134.

SHIN, H., JO, S. & MIKOS, A. G. 2003. Biomimetic materials for tissue engineering. *Biomaterials,* 24**,** 4353-4364.

SJOLLEMA, J. & BUSSCHER, H. J. 1990. Deposition of Polystyrene Particles in a Parallel Plate Flow Cell. 2. Pair Distribution Functions Between Deposited Particles. *Colloids and Surfaces,* 47**,** 337-352.

STEGEMANN, B., BACKHAUS, H., KLOSS, H. & SANTNER, E. 2007. Spherical AFM probes for adhesion force measurements on metal single crystals. *Modern Research and Educational Topics in Microscopy,* 3**,** 820-827.

SUN, G. & ZHANG, Z. 2001. Mechanical properties of melamine-formaldehyde microcapsules. *Journal of Microencapsulation,* 18**,** 593-602.

SUN, G. & ZHANG, Z. 2002. Mechanical strength of microcapsules made of different wall material. *International Journal of Phytoremediation,* 242**,** 307-311.

SURAYA, A. R., LUCKHAM, P. F. & LAWRENCE, C. J. 2005. Interaction Forces Between Polymer-Coated Glass Surfaces. *International Journal of Engineering and Technology,* 2**,** 27-35.

SZE, A., ERICKSON, D., REN, L. & LI, D. 2003. Zeta-potential measurement using the Smoluchowski equation and the slope of the current-time relationship in electroosmotic flow. *Journal of Colloid and Interface Science,* 261**,** 402-410.

TABOR, D. 1977. Surface forces and surface interactions. *Journal of Colloid and Interface Science,* 58**,** 2-13.

TAKKE, V., BEHARY, N., PERWUELZ, A. & CAMPAGNE, C. 2011. Surface and adhesion properties of poly(ethylene glycol) on polyester(polyethylene terephthalate) fabric surface: effect of air-atmospheric plasma treatment. *Journal of Applied Polymer Science,* 122**,** 2621-2629.

THEODOLY, O., OBER, R. & WILLIAMS, C. E. 2001. Adsorption of Hydrophobic Polyelectrolytes at the Air/water Interface: Conformational Effect and History Dependence. *The European Physical Journal E,* 5**,** 51-58.

THORMANN, E., SIMONSEN, A. C., HANSEN, P. L. & MOURITSEN, O. G. 2008. Interactions between a polystyrene particle and hydrophilic and hydrophobic surfaces in aqueous solutions. *Langmuir,* 24**,** 7278-7284.

TOCHA, E., SCHÖNHERR, H. & VANCSO, G. J. 2006. Quantitative Nanotribology by AFM: A Novel Universal Calibration Platform. *Langmuir,* 22**,** 2340-2350.

TORMOEN, G. W. & DRELICH, J. 2005. Deformation of Soft Colloidal Probes during AFM pull-off Force Measurements: Elimination of Nano-roughness Effects. *Journal of Adhesion Science and Technology,* 19**,** 181-198.

TORMOEN, G. W., DRELICH, J. & NALASKOWSKI, J. 2005. A distribution of AFM pull-off forces for glass microspheres on a symmetrically structured rough surface *Journal of Adhesion Science and Technology,* 19**,** 215-234.

ÜZÜM, C., MAKUSKA, R. & VON KLITZING, R. 2012. Effect of Molecular Architecture on the Polyelectrolyte Structuring under Confinement. *Macromolecules,* 45**,** 3168-3176.

VAKARELSKI, I. U. & HIGASHITANI, K. 2001. Dynamic features of short-range interaction force and adhesion in solutions. *Journal of Colloid and Interface Science,* 242**,** 110-120.

VAKARELSKI, I. U., ISHIMURA, K. & HIGASHITANI, K. 2000. Adhesion between silica particle and mica surfaces in water and electrolyte solutions. *Journal of Colloid and Interface Science,* 227**,** 111-118.

VARENBERG, M., ETSION, I. & HALPERIN, G. 2003. An improved wedge calibration method for lateral force in atomic force microscopy. *Review of Scientific Instruments,* 74**,** 3362-3367.

WANG, J., PAN, C. J. & PAN, C. J. 2004. Characteristics and anticoagulation behavior of polyethylene terephthalate modified by C2H2 plasma immersion ion implantation-deposition. *Journal of Vacuum Science & Technology A,* 22**,** 170-176.

WEISENHORN, A. L., HANSMA, P. K., ALBRECHT, T. R. & QUATE, C. F. 1989. Forces in Atomic Force Microscopy in Air and Water. *Applied Physics Letters,* 54**,** 2651-2653.

WYATT, N. B., GUNTHER, C. M. & LIBERATORE, M. W. 2011. Increasing viscosity in entangled polyelectrolyte solutions by the addition of salt. *Polymer,* 52**,** 2437-2444.

WYATT, N. B. & LIBERATORE, M. W. 2009. Rheology and Viscosity Scaling of the Polyelectrolyte Xanthan Gum. *Journal of Applied Polymer Science,* 114**,** 4076-4084.

XU, J., LI, M., ZHAO, Y. & LU, Q. 2007a. Control over the Hydrophobic Behavior of Polystyrene Surface by Annealing Temperature Based on Capillary Template Wetting Method. *Colloids and Surfaces A: Physicochemical and Engineering Aspects,* 302**,** 136-140.

XU, L. C. & SIEDLECKI, C. A. 2009. Atomic Force Microscopy Studies of the Initial Interactions Between Fibrinogen and Surfaces. *Langmuir,* 25**,** 3675-3681.

XU, S., DONG, M., LIU, X., HOWARD, K. A., KJEMS, J. & BESENBACHER, F. 2007b. Direct force measurements between siRNA and chitosan molecules using force spectroscopy. *Biophysical Journal,* 93**,** 952–959.

XU, Z., CHI, R., DIFEO, T. & FINCH, J. A. 2005. Surface Forces between Sphalerite and Silica Particles in Aqueous Solutions. *Atomic Force Microscopy in Adhesion Studies,* 14**,** 1813-1827.

YANG, L., CHEN, J., GUO, Y. & ZHANG, Z. 2009. Surface modification of a biomedical polyethylene terephthalate (PET) by air plasma. *Applied Surface Science,* 255**,** 4446-4451.

YAO, G., ZHENG, J. & CHEN, H. 2011. Preparation and application of VE microcapsules with polyurethane shell for skin-care textiles. *Advanced Materials Research* 311**,** 402-406.

ZAMAN, M., LIU, H., XIAO, H., CHIBANTE, F. & NI, Y. 2013. Hydrophilic Modification of Polyester Fabric by Applying Nanocrystalline Cellulose Containing Surface Finish. *Carbohydrate Polymers,* 91**,** 560-567.

ZANDER, N. E. 2009. Chelating Polymers and Environmental Remediation. *Army research laboratory,* 6**,** 1-22.

ZBIK, M. S. & FROST, R. L. 2010. AFM study of forces between silicon oil and hydrophobic-hydrophilic surfaces in aqueous solutions. *Journal of colloid and interface science,* 349**,** 492-497.

ZHANG, D., THOMPSON, K. L., PELTON, R. & ARMES, S. P. 2010. Controlling deposition and release of polyol-stabilized latex on boronic acid-derivatized cellulose. *Langmuir,* 26**,** 17237-17241.

ZHANG, F. 1999. Submicron particle removal in post chemical mechanical planarization (CMP) cleaning. *Journal of Applied Physics,* A69**,** 437–440.

ZHANG, F., BUSNAINA, A. A., FENG, J. & FURY, M. A. 1999a. Particle adhesion and removal in chemical mechanical polishing (CMP) and post-CMP cleaning. *Journal of The Electrochemical Society,* 146**,** 2665-2690.

ZHANG, R., SEKI, A., ISHIZONE, T. & YOKOYAMA, H. 2008. Reduced Hydrophobic Interaction of Polystyrene Surfaces by Spontaneous Segregation of Block Copolymers with Oligo (Ethylene Glycol) Methyl Ether Methacrylate Blocks: Force Measurements in Water Using Atomic Force Microscope with Hydrophobic Probes. *Langmuir,* 24**,** 5527-5533.

ZHANG, Z., SAUNDERS, R. & THOMAS, C. R. 1999b. Mechanical strength of single microcapsules determined by a novel micromanipulation technique. *J Microencapsul,* 16**,** 117-124.

ZOETEWEIJ, M. L., DONCK, J. C. J. V. D. & VERSLUIS, R. 2009. Particle removal in linear shear flow: model prediction and experimental validation. *J. Adhes. Sci. Technol.,* 23**,** 899–911.

ZOPPE, J. O., OSTERBERG, M., VENDITTI, R. A., LAINE, J. & ROJAS, O. J. 2011. Surface interaction forces of cellulose nanocrystals grafted with thermoresponsive polymer brushes. *Biomacromolecules,* 12**,** 2788–2796.

Appendix

The Matlab code to count the number of microcapsules in an image (The code was written by Dr James M. Andrews)

```
folder='D:\'; % Root directory of the image
pixelareas=4.3403*10^(-12); % Put the area of the pixel here units m^2,
can be changed according to experiments

for indx=1:6
    % Get image
    basefilename=sprintf('%d.jpg',indx); % Filename
    filename=fullfile(folder,basefilename);  %  Full  location  of  the
file
    I1=imread(filename);
    % NB change file name above

    % Image inversion is necessary in this case
    % If your image is not true color comment out the next line
    negImage = rgb2gray(I1) ;  % Convert true colour to grayscale
    negImage=double(negImage); % Convert the image matrix to double

    negImageScale  =  1.0/max(negImage(:));   %  Find  the  max  value  in
array
    negImage = 1 - negImage*negImageScale; % Make negative image
    figure;imshow(negImage);
    %I2=histeq(I1);           % Histogram equalization of a gray-scale
image.
    I2=histeq(negImage);

    % Remove background
    negImage=imtophat(negImage,strel('disk',50));
    negImage = medfilt2(negImage,[3 3]);
    negImage=imclearborder(negImage);
    %bw=edge(negImage,'canny',level,5.5);
    I2=histeq(negImage);
    %level=graythresh(I2)
    level=0.2;

    % Convert to binary image
    bw=im2bw(negImage,level);
    bw=imfill(bw,'holes');

%    figure;imshow(bw);

% Apply a morphological opening routine

    [labels,N]=bwlabel(bw,4);

% NB: N returns the number of objects found
% labels contains information about locations of objects
% The 4 indicates that particles must touch along an edge
```

```
% in order to be considered as an object

    % Extracting the size of each object

    data=regionprops(labels,'basic') %
    areas=[data.Area];
    data1=regionprops(labels,'perimeter');
    perimeter=[data1.Perimeter] % Care in using this ??
    sortareas=sort(areas) % Sorts the areas into ascending areas

    realareas=sortareas.*pixelareas;
    sizedistribution=sqrt(realareas./pi);

    % Store data
    basefilename=sprintf('ParticleShape%d.dat',indx); % Filename
    filename=fullfile(folder,basefilename);  %  Full  location  of  the
file
    fid = fopen(filename, 'w') ;% Open file for writing
    if fid==-1
        error('File is not open')
    end
    fprintf(fid, 'Pixel area (10^(-12) m^2): %f\n\n', pixelareas/10^(-
12));
    fprintf(fid,   'Particle   area   (piexel^2)\tParticle   perimeter
(pixel)\n')
    for i=1:length(areas)
        fprintf(fid, '%e\t\t\t%e\n', areas(i), perimeter(i))
    end
    fclose(fid);
    basefilename=sprintf('ParticleSize%d.dat',indx); % Filename
    filename=fullfile(folder,basefilename);  %  Full  location  of  the
file
    fid = fopen(filename, 'w') ;% Open file for writing
    if fid==-1
        error('File is not open')
    end
    fprintf(fid, 'Particle diameter (10^(-6) m)\n')
    fprintf(fid, '%f\n', sizedistribution/10^(-6))
    fclose(fid)

% Plot the particle diameter in a histogram
     figure
     hist(sizedistribution);
     xlabel('Radius (m)')
     ylabel('Number of particles')
end
```

Conferences and seminar attendance

9th European Congress of Chemical Engineering, Hague, the Netherlands, 2013, oral presentation;

RSC Postgraduate symposium on nanotechnology - Chemical Engineering (RSC Chemical Nanoscience & Nanotechnology Group), Birmingham, UK, 2012, poster presentation;

Postgraduate symposium on nanotechnology - Chemical Engineering (RSC Chemical Nanoscience & Nanotechnology Group), Birmingham, UK, 2012, poster presentation;

Frontier in Chemical Engineering: the fourth Global Chinese Chemical Engineers Symposium;

The Research Poster Conference, Birmingham University, UK, 2012, poster presentation;

The 19th Joint Annual Conference of CSCST-SCI, Reading, UK, 2011, poster presentation;

The 18th Joint Annual Conference of CSCST-SCI, Cambridge, UK, 2011, oral presentation;

The 17th Joint Annual Conference of CSCST-SCI, Oxford, UK, 2011